UNIVERSITY OF LONDON

IMPERIAL COLLEGE OF SCIENCE AND TECHNOLOGY

Physics Department

Biophysics Section

AN INVESTIGATION INTO THE SPECTRAL CHARACTERISTICS OF METACONTRAST PHENOMENA AND OF ADAPTATION EFFECTS IN HUMAN VISION

by

Brian John Nunn

Thesis submitted for the degree of

Doctor of Philosophy of the University of London

1978

The work described in this thesis was performed solely by the author except where it has been made clear in the text that the assistance of other persons was involved.

Brian Nunn

Abstract

In this investigation, psychophysical techniques have been used to investigate several aspects of human colour vision. The introductory chapter contains a review of relevant psychophysical data and electrophysiological studies of the vertebrate visual system. The aims of this thesis are then stated with reference to these previous studies. Apparatus which was built for the experimental work in this thesis is described in the second chapter. The third chapter is devoted to a description of experiments concerning the influence of a masking stimulus on the threshold of a spatially adjacent probe stimulus (the so-called metacontrast effect). It is shown that the cone system modifies threshold detection mediated by the rod system, and the characteristics of this rod-cone interaction were studied. Chapters four and five deal with two different experimental techniques for disturbing colour matches. In chapter four, changes in foveal colour matches following adaptation to spatially and/or temporally modulated stimuli are reported and the characteristics of the effects are described in detail. The second method of disturbing colour matches employs adaptation to very bright monochromatic lights (chapter five) and experiments have been carried out on normal and anomalous trichromatic subjects. It was established that foveal colour matches are subject to larger changes than non-foveal matches, and that red-green anomalous trichromatic and normal subjects all yield similar colour matches under very high illumination levels of adaptation. These results are shown to be compatible with a model of anomalous trichromacy in which normal pigments occur as mixtures in single cones.

"there will be no difficulty in seeing how and (of) what mixtures the colors are made....He, however, who should attempt to verify all this by experiment would forget the difference of the human and the divine nature".

Timaeus, by Plato (c. 380 BC).

Translation by Benjamin Jowett (1871).

INDEX

CHAPTER 5: A STUDY OF ANOMALOUS TRICHROMACY

INTRODUCTION

Eyes are the peripheral sense organs of the visual systems of vertebrates and invertebrates. A portion of the light energy entering the eye is absorbed by pigments encapsulated in a mosaic of specialized receptor cells located at the back of the eye. Conformational changes in the pigment molecules caused by the absorption of photons, result in the propagation of electrical signals along nerve cells connected to these receptors. These electrical signals are modified by the nerve network at the back of the eye, and are then transmitted to the primate brain by a bundle of ganglion nerve cells. The nerve bundle from each eye terminates mainly in a body in the midbrain called the lateral geniculate nucleus (LGN), from whence axons of geniculate relay cells carry the light-evoked signals to the visual cortex at the back of the brain. The axons entering the visual cortex make synaptic contact with cortical neurones, and map the retina receptor mosaic onto the cortical receiving area in a spatially ordered manner.

The visual cortex processes the signals further, and then transmits them to the 'association' areas of the brain. As a result of this process the signals are perceived to originate from self-luminous and light-reflecting objects in the outside world. Attributes of these objects, such as their spatial distribution, colour and brightness, and the temporal rate of variation of these attributes are encoded in the signals transmitted through the visual system.

Investigations of the visual systems of vertebrates and invertebrates can be performed in a variety of ways. Objective

approaches include measurements of the responses of single neurones or groups of neurones, morphological categorization by microscopic examination of stained sections, while approaches such as mathematical modelling and psychophysical techniques are also used. The objective studies almost invariably involve catastrophic entry into some part of the visual system, and are also incapable of measuring the overall response of the system, especially in the case of spatially extensive light images impinging on the receptor mosaic. In the case of electrical recording of neural activity, it is also difficult to correlate the measured responses with the perceptual response. The psychophysical approach usually involves threshold or matching techniques, and is necessarily limited in that the visual system is treated only as a constant-output device. It remains, however, the only way of correlating with certainty the perceived image with the visual stimulus. Any complete description of the human visual system must therefore encompass the results derived from both the direct and indirect approaches.

The investigations reported in this thesis were made using psychophysical techniques, and the design of experiments was based on a portion of the body of knowledge accumulated in the literature on psychophysics. It is attempted to correlate the results obtained, both with earlier psychophysical data and also with results obtained by investigators using objective measuring methods. Few data have been obtained from objective measurements on man, so that the results obtained from studies of other vertebrates were often invoked. Striking similarities exist at all levels between the visual systems of man and animals, especially the other primates, so that their visual systems can

be profitably compared. Before describing the psychophysical experiments of other workers relevant to this thesis, a description is given of the visual system and its functions, mainly as shown by objective investigations.

CHAPTER ONE

A) THE VISUAL SYSTEM: MORPHOLOGY AND ELECTROPHYSIOLOGY

1. The Optical Pathway

A horizontal section of the right human eye is shown in figure 1.1. Light from objects in the external world is refracted at the cornea and focussed by the lens onto the retina, which lines most of the chamber containing the vitreous humour.

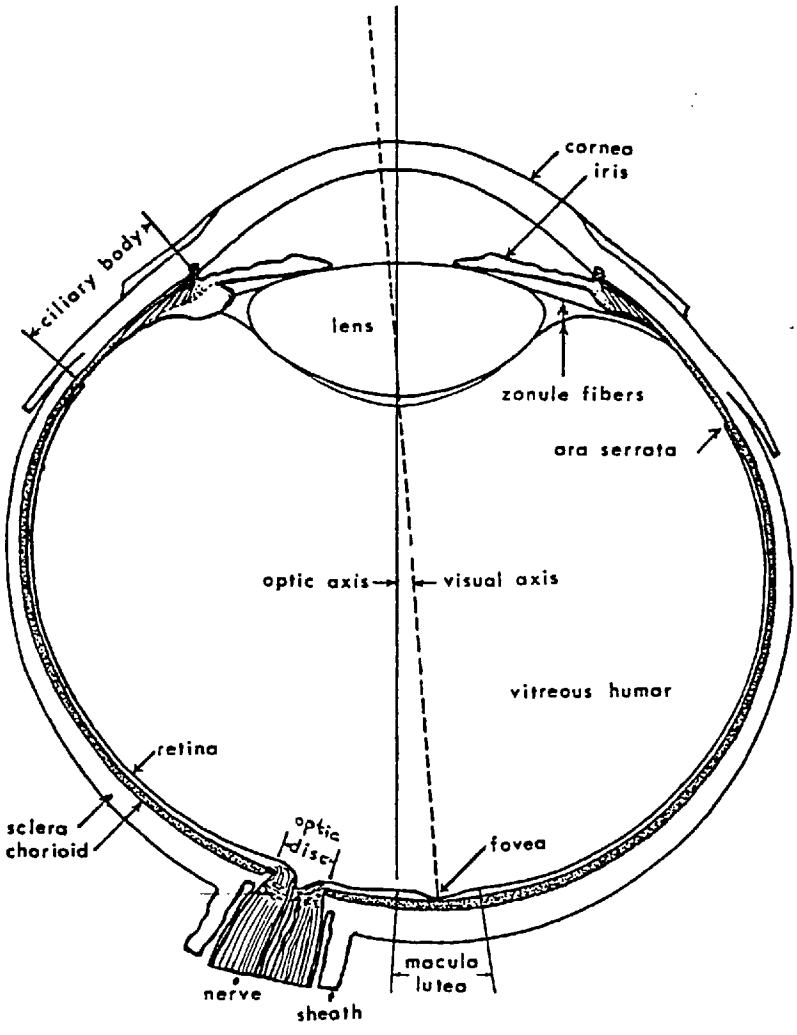

FIGURE 1.1 Horizontal section of the right human eye. (After Walls (1942); originally from Saltzmann (1912)).

The human retina is a thin (0.5 mm) sheet of tissue attached to the choroid, and contains five main types of sensory neuron which are morphologically and functionally distinct: photoreceptor cells which contain the visual pigments, and horizontal, bipolar, amacrine and ganglion cells. These cells are arranged in layers which are ordered perpendicularly to the light rays imaged on them. Their perikarya or cell bodies are arranged in three nuclear layers, and the 'synaptic' contacts between cells of these three layers occur in two interposed 'plexiform' layers. The layer containing the photoreceptors lies closest to the choroid, so that light has to pass through the rest of the retinal cells before being absorbed by the visual pigments. It is the spectral sensitivity of the visual pigments which determines the spectral characteristics of visual responses.

2. The Spectral Sensitivity of Vision

The useful wavelength band of visible light extends from about 400 nm to some 700 nm. Much of the light entering the eye is not absorbed in the photoreceptors. The lens absorbs strongly in the near ultraviolet with a peak absorbance around 365 - 368 nm (Cooper and Robson, 1969). Absorption in the other optical media, and scatter further reduce the efficiency of photon capture, in the manner shown by figure 1.2.

A photochemically inert macular pigment within 6^{o} to 10^{o} of the fovea (q.v.) further reduces the sensitivity of photoreceptors lying in this region of the retina. (The pigment is the xanthophyll lutein, whose absorption spectrum derived by psychophysical methods is shown in figure 1.3).

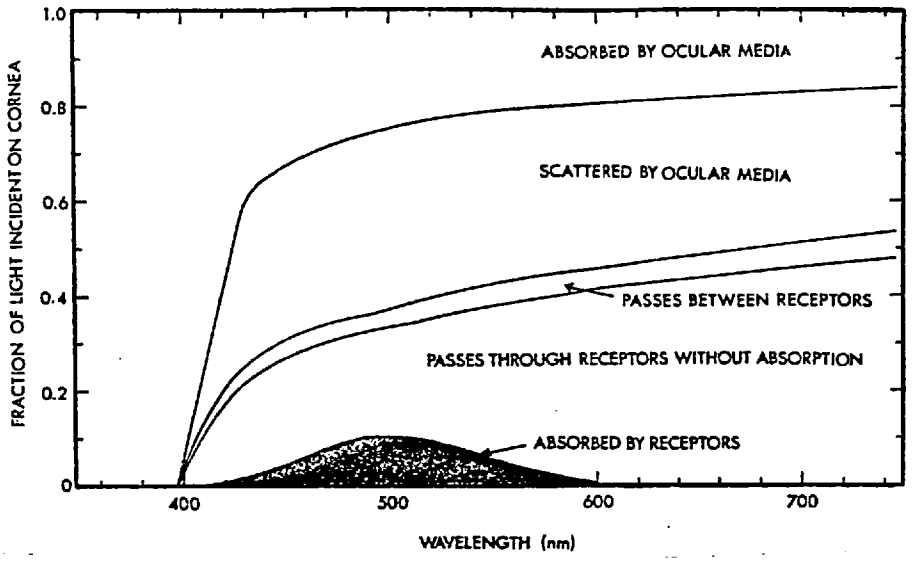

FIGURE 1.2 Fate of light entering the human eye. Based on transmittance data of Boettner (1967) and the assumption that 10% of the 500 nm photons incident on the corneal surface are absorbed by the visual pigment.

The light which passes through the photoreceptor layer without absorption is mostly absorbed by the pigmented epithelium layer sandwiched between the photoreceptors and the choroid. The epithelium layer also provides nutrients to the photoreceptor cells, and phagocytoses discarded retinal tissue.

There are two types of photoreceptor distinguishable in microscopy, shown in figure 1.4a.

Cones derive their name from the tapered outer segments which they have in non-foveal regions. At the fovea, the cone outer segments are cylindrical, and longer than elsewhere and their diameter (2 μm, Polyak, 1941) corresponds to the maximum visual resolution of about 1' of arc.

Rods have cylindrical outer segments and, like the cones, are oriented with their long axis parallel to the incident light and have their outer segments buried in the apical processes of

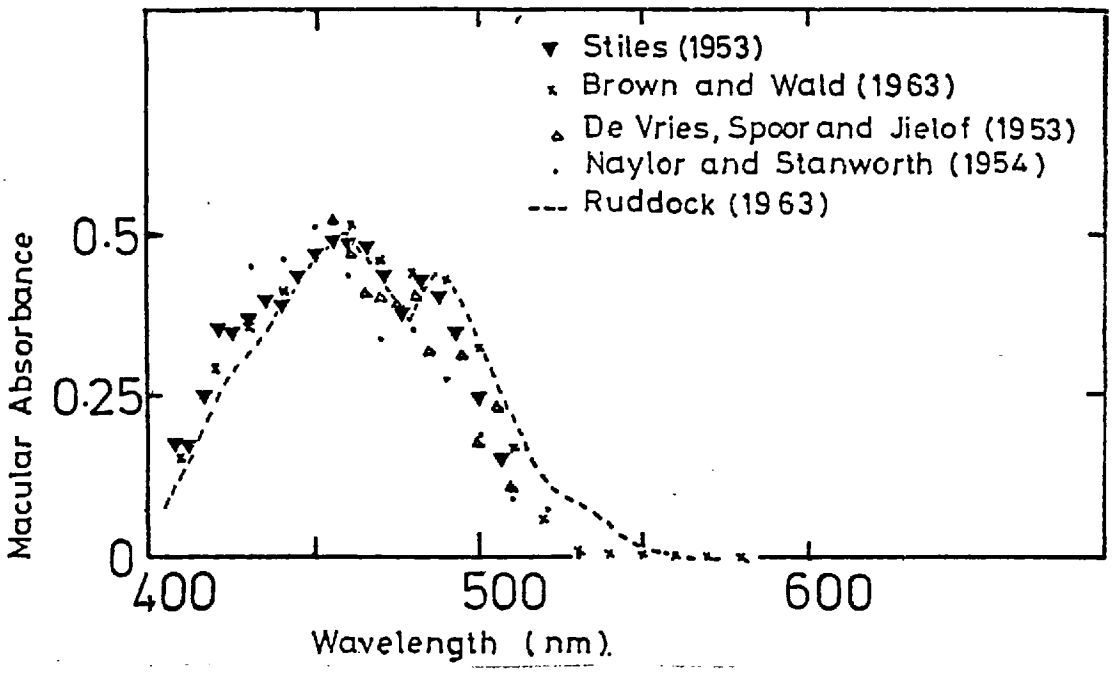

FIGURE 1.3 Absorbance spectrum of macular pigment based on measurements at foveal and extrafoveal locations of the relative visual cone sensitivities (Brown and Wald, 1963; Stiles, 1953) and of colour-matching properties (Ruddock, 1963); and measurements on Haidinger brushes (De Vries, Spoor and Jielof, 1953; Naylor and Stanworth, 1954). For comparison, the peak absorbances have been adjusted to about 0.5.

the retinal epithelium. The outer segments of rods and cones are filled by a lamellar membrane oriented perpendicular to the photoreceptor axis. The lamellae are formed by infoldings of the outer segment envelope in cones: they comprise separate 'discs' in rod outer segments. The lamellar spacing is 30 - 40 μm, and the visual pigment units, 4 - 5 nm in size, form a liquid-like array across the membrane (Blasie, Worthington and Dewey, 1969; Blasie and Worthington, 1969).

The existence of one visual pigment in rods and of three more visual pigments in the cones of man was first indicated by psychophysical experiments (q.v.). Several optical methods

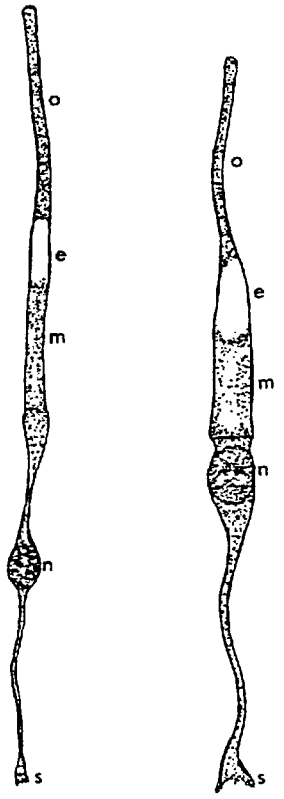

FIGURE 1.4a Scale drawings of (a) a human rod, and (b) a human cone. Abbreviations: o, outer segment; e, ellipsoid; m, myoid; n, nucleus; s, synaptic body. (From Young, 1969).

have been used to determine the spectral sensitivities of the visual pigments. Rushton and Weale used fundus reflectometry to measure the difference spectra of human visual pigments (e.g. Rushton, 1956, 1965a; Weale, 1962a,b, 1967). The absorption peak of rhodopsin obtained in this way was shifted 10 - 15 nm towards longer wavelengths compared to that obtained by Crescitelli and Dartnall (1953), who determined the difference spectrum of a digitonin extract of rhodopsin. The shift found by Rushton and by Weale was dependent on the bleaching period, being maximum for bleaches of short duration. Weale (1967) attributed the shift to the formation of a transient intermediate in the bleaching process. He concluded that the intermediate was pararhodopsin, which absorbs visible light, and also that it was photolabile, regenerating to native pigment on exposure to light.

The presence of a red-senstive (λ_{max}, 565 nm) and a green-sensitive pigment (λ_{max}, 535 nm) was shown for small foveal regions of the human retina by Brown and Wald (1963), who used a method of transillumination and selective bleaching. These measurements agreed with measurements made by Rushton on deuteranopes and protanopes. Rushton found, by the method of partial bleaching,

that the foveae of protanopes contain a single (green-sensitive) photopigment with a peak absorption between 530 - 550 nm (Rushton, 1958, 1963a,b,c), and that the foveae of deuteranopes contain one (red-sensitive) photopigment with a peak absorption at 570 nm (Rushton, 1965a,b,c).

Microspectrophotometry of single human rods has revealed one visual pigment with a peak absorbance at a wavelength of 500 nm (Brown and Wald, 1963, 1964). The two types of cone pigment found by reflectance methods, as well as a third, have been demonstrated by microspectrophotometry of single human cones. The wavelengths of peak absorption of these pigments were 440 - 450 nm, 525 - 530 nm and 555 - 570 nm (Brown and Wald, 1964; Wald and Brown, 1965). The three pigments discovered in single cones of other primates have peak absorbances close in wavelength to those of humans (Brown and Wald, 1964; Marks, Dobelle and MacNichol, 1964; Liebman, 1972). The absorbances measured by Marks et al., are shown in figure 1.4b.

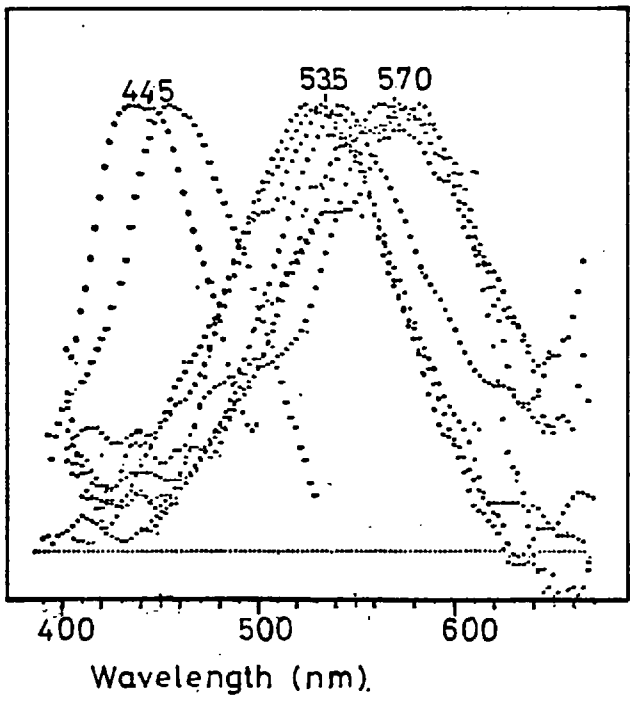

FIGURE 1.4b Difference spectra recorded from ten primate parafoveal cones (from Marks, Dobelle and MacNichol, 1964).

The rod pigment unit contained in the rod outer segments, rhodopsin, appears to be a lipoprotein complex consisting of a single retinal chromophore 1.2 nm long which is attached to a moeity known as opsin, consisting of protein phospholipid and a single oligosaccharide (Rodieck, 1973, page 20). The pigments contained in the cones have not been isolated. Brown and Wald (1963) showed however that the prosthetic group of the pigments of the red- and green-sensitive cones and of rods is the same, by demonstrating regeneration of these two cone photopigments upon the addition of 11-cis retinal to the bleached retina.

3. Optical Constraints on Vision

Constraints are imposed on the sharpness of visual images by several factors. First, chromatic aberrations result in imperfect optical images. This effect is imperceptible, which fact Hartridge (1947) attributed to neural suppression. Second, diffraction limits visual acuity, which varies with pupil diameter and is maximum for a pupil diameter of 2.4 mm. Third, light entering the eye from the edge of the pupil is less efficient at stimulating receptors than light along the optical axis. This is known as the Stiles-Crawford effect, and it has been proposed that it is due to light funnelling by receptors. It has been demonstrated psychophysically (Stiles and Crawford, 1933; Pirenne, 1962; Stiles, 1962; Enoch, 1963) and by fundus reflectometry (Ripps and Weale, 1964, 1965; Coble and Rushton, 1971). The rods are the least directionally-sensitive receptors, and their directional sensitivity is almost exactly balanced by the lens pigmentation at some wavelengths (Stiles, 1939; Flamant and Stiles, 1948; Weale, 1961). The cones

are more sensitive to the angle of incident light, and the 'green' cones are more directionally sensitive than are the 'red' cones (Enoch and Stiles, 1961; Ripps and Weale, 1964, 1965). The perceived image is further determined by the spatial distribution of receptors.

The distribution of rods and cones in the human retina is approximately symmetric about the foveal pit, apart from the optic disc (figure 1.1), which is free from photoreceptors and constitutes the 'blind spot'. The cones number about 6×10^6 and are most densely packed in the foveal region, while the 10^8 rods are most densely packed at eccentricities of 15 - 25° from the fovea (figure 1.5). The central 0.7° of the fovea lacks rod receptors entirely, and earlier psychophysical evidence indicated that blue-sensitive cones are absent within 10' of the central portion of the fovea (König, 1894; Willmer and Wright, 1945; Willmer, 1946), although there is now strong evidence against this (McCree, 1960; Burton and Ruddock, 1972).

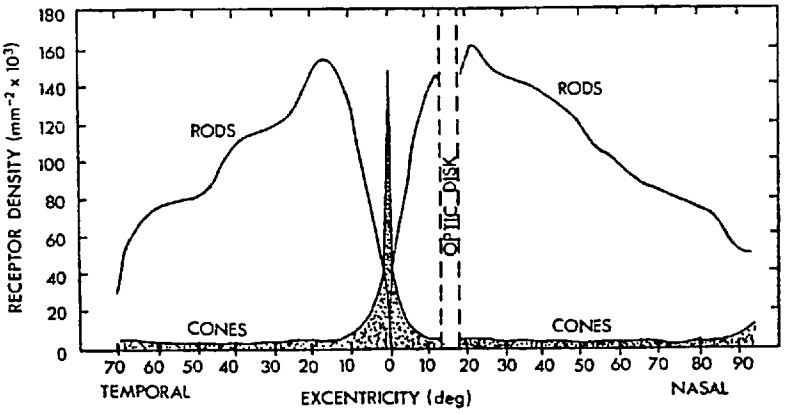

FIGURE 1.5 Density of rods and cones in the human retina. (After Pirenne (1967); original data from Østerberg (1935)).

4. Neural Architecture of the Visual System

The pattern of neural connectivity between the receptors and the higher visual centres determines further the limits of visual sensation elicited by light stimulation. This pattern has been revealed in part by neural atrophy, following intentional lesions induced in animals (Talbot and Marshall, 1941; Daniel and Whitteridge, 1961; Hubel and Wiesel, 1969), and following accidental brain damage in man (Holmes, 1918; Spalding, 1952a,b; Teuber, Battersby and Bender, 1960). Atrophy propagates from one cell to the next across synapses in some cases (e.g. Penman, 1934; Le Gros Clarke, 1959). Microscopy combined with tissue staining techniques has revealed the fine structure of the visual system. Electron microscopy has been used to study the system in great detail, and synaptic structure revealed by this technique allows the direction of information flow across synapses to be inferred. Further information has been deduced from electrical recording of the responses to light and electrical stimulation in primates and man, and from the analysis of visual images evoked by the electrical stimulation of the brain of man (Geschwind, 1965a,b; McCulloch, 1965; Brindley and Lewin, 1968).

These techniques mostly require skill for successful implementation, and a great deal of experience and art is involved in their interpretation. However, a general 'picture' of the neural architecture of the visual system has emerged.

4a. The Retina

The direction of primary information flow in the retina is from the photoreceptors, through the bipolar cells, to the ganglion

cells, the axons of which pass out of the eyeball and form the optic nerve fibres. The horizontal cells transmit signals in directions perpendicular to the direction of primary information flow, at the level of the photoreceptor-bipolar synapses; this is shown schematically in figure 1.6.

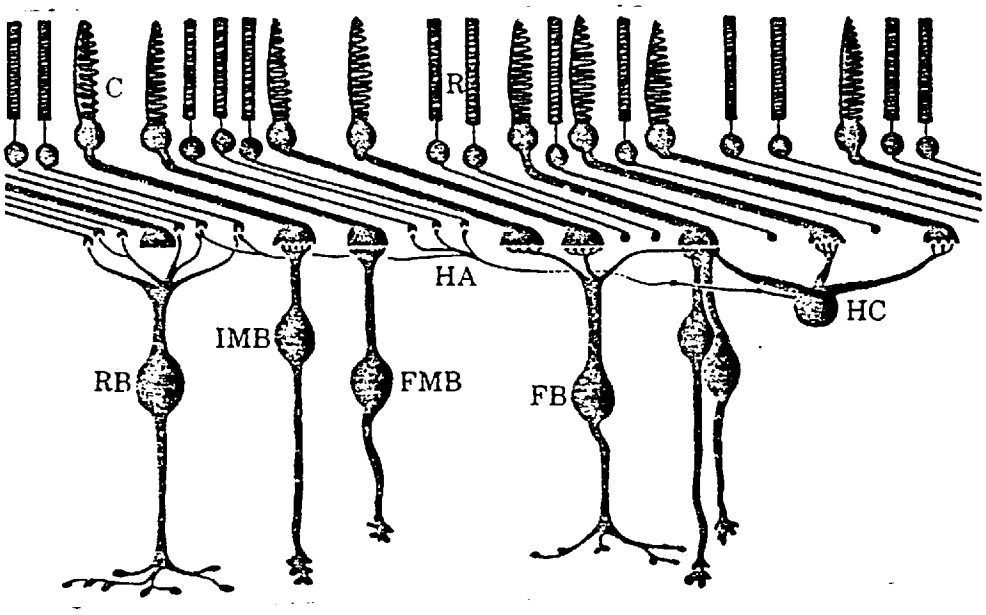

FIGURE 1.6 Schematic summary diagram of the different nerve cells and the types of connections that they make with the receptors in the outer plexiform layer of the primate retina, close to the fovea. The cones (C) and rods (R) are shown feeding into the different bipolar cells (RB, IMB, FMB & FB) and the horizontal cell (HC). The horizontal cell axon (HA) is represented as a broken line because the direct evidence for the axon terminals being connected to the horizontal cell is not yet available (from Kolb, 1970).

The amacrine cells also transmit information laterally, at the level of the bipolar-ganglion cell synapses (Dowling and Werblin, 1969). These two types of interneuron apparently receive information from cells immediately preceding them in the primary information pathway, and can transmit back to cells of this type, to neighbouring interneurones (of the same type), and to cells immediately succeeding them in the visual pathway (Werblin, 1973). The input dendritic

fields of bipolar and ganglion cells generally show varying amounts of overlap and mixing, depending on cell type and eccentricity of location in the retina. At the retina location represented in figure 1.6, the rod bipolars are exclusive to rods and contact 30 to 50 of them, whereas the diffuse flat cone bipolars (FB) each contact 6 - 7 cones. The high resolution of the fovea is achieved by the linking path, between the individual cones and single midget ganglion cells, provided by the single midget bipolar cells (IMB and FMB in figure 1.6).

4b. The Optic Nerve and the Lateral Geniculate Body

Each primate optic nerve contains about 1.0 - 1.4 x 10^6 fibres (Ogden and Miller, 1966; Potts et al., 1972a,b) of which 3.5 x 10^4 carry signals from foveal cones (Gose, 1969). Some optic nerve fibres project to the 'superior colliculus', but the majority terminate in the lateral geniculate nucleus (LGN). The optic nerves from the nasal and temporal hemi-retinae decussate at the optic chiasma in the manner illustrated schematically in figure 1.7. (This diagram emphasizes the ordered way in which the two-dimensional receptor mosaic is mapped serially onto further two-dimensional sheets of neural tissue, although in reality the topological distribution of these sheets is complicated by foldings and fissures of the brain). Thus the two halves of the light image, if it is divided vertically at the fixation point, are represented in different halves of the normal brain. (Decussation is more complete in albinos.) The retina area corresponding to about 2^o of visual field about the fixation point may be represented in both projections (Teuber, Battersby and Bender, 1960).

The information from the two eyes still remains separate at the

level of the LGN, each eye output feeding into three neural sheets (figure 1.7; Minkowski, 1920; Le Gros Clarke and Penman, 1934; Glees, 1961). There is a virtual point-to-point representation of the retina in the LGN, and a single corresponding point on both retinae maps onto spatially adjacent points in the six LGN layers (Le Gros Clarke and Penman, 1934; Walls, 1953; Le Gros Clarke, 1959). Interaction between the two visual half-fields does not occur before the visual cortex, which receives its input from the LGN via the geniculo-calcarine tract.

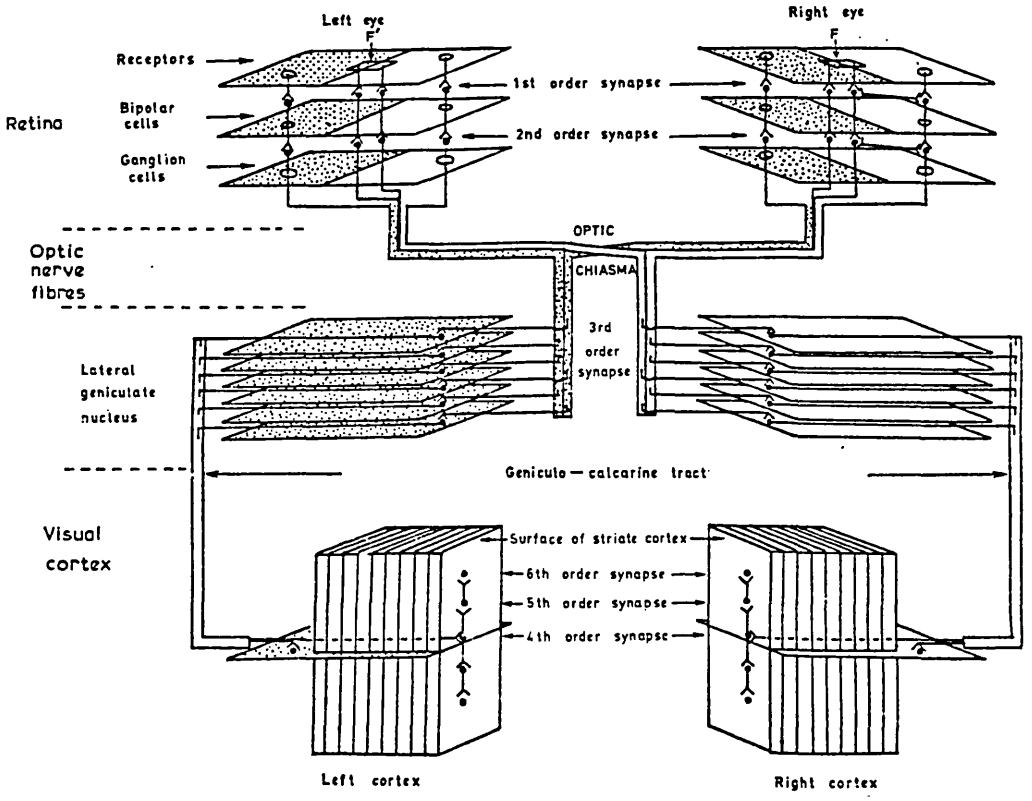

FIGURE 1.7 Diagram showing the ordering of synaptic contacts in the primate visual system. Note that the left half field is completely represented in the left striate cortex and vice versa. The small squares surrounding the foveal receptor regions (F and F') are represented by the area of the cortex built up into parallel sheets, i.e. there is a large magnification of the central area of the retina in the cortical map. The sheets represent the columnar or sheet-like organisation of neurones in the striate cortex. From Ruddock (1975). The symbols —≺ and •— indicate the transmitting and receiving ends of a synapse, respectively.

4c. The Visual Cortex

The input from the LGN maps directly onto the striate primary visual area (area 17, Hubel and Wiesel, 1965, 1968), which sends fibres to the parastriate visual association areas (areas 18 and 19). The projection of the foveal retina area on the cortex is disproportionately large (figure 1.7).

The cells of the cortex are arranged in columns perpendicular to its surface, and also in distinct layers parallel to its surface (Hubel and Wiesel, 1962). The fourth-order synapse (figure 1.7) occurs in the middle layer of the cortex, and higher-order synapses are made away from this level along columns. Two striate cortical layers project to layers 18 and 19, while one projects to a non-cortical area (Gilbert and Kelly, 1975).

The inputs from the two eyes have been shown to be separated in the columns of layer IV in area 17 (Levay, Hubel and Wiesel, 1975; Wiesel, Hubel and Lam, 1974). The activity in the two hemispheres is integrated in area 18 by means of connecting fibres in the corpus callosum; area 18 is also associated with temporal lobe activity (Bonin, Garol and McColloch, 1942; Choudhury, Whitteridge and Wilson, 1965).

The pathway and function of the primary visual system beyond areas 17, 18 and 19 are poorly understood. Some outputs from the cortex have been described for the macaque monkey by Jones and Powell (1970), and Zeki (1976). One of these links the primate striate cortex and superior colliculus. It is thought that the visual cortex and the superior colliculus act in concert to guide eye movements (Schiller, Stryker, Cynander and Berman, 1974; Finlay, Schiller and Volman, 1976; Mohler and Wurtz, 1976, 1977).

5. Electrophysiology of the Visual Pathways

5a The Retina: Electrophysiology

If electrical recordings are made from a neural cell in the visual system, it is seen to respond to light stimuli presented anywhere within the retina region known as the receptive field of the cell. Werblin (1973) has proposed a functional model of the vertebrate retina, mostly on the basis of electrical recordings which revealed the receptive field properties of the mudpuppy retina cells (Werblin and Dowling, 1969; Werblin, 1970). In this model, illustrated in figure 1.8, the average background luminance on the retina affects photochemical reactions in the receptor cells. The large receptive fields of horizontal cells enable them to influence the signals at the receptor-bipolar synapse in a manner which depends on the illumination in surrounding regions (simulated by the annulus in figure 1.8). The extended receptive-fields of the amacrine cells are thought to respond only to changes in stimuli (in this case provided by the rotating windmill pattern), and to modify the bipolar-ganglion cell synapse activity. The ganglion cells thus carry signals relating to steady or changing luminance at local regions; these signals are modified by activity in areas surrounding the local

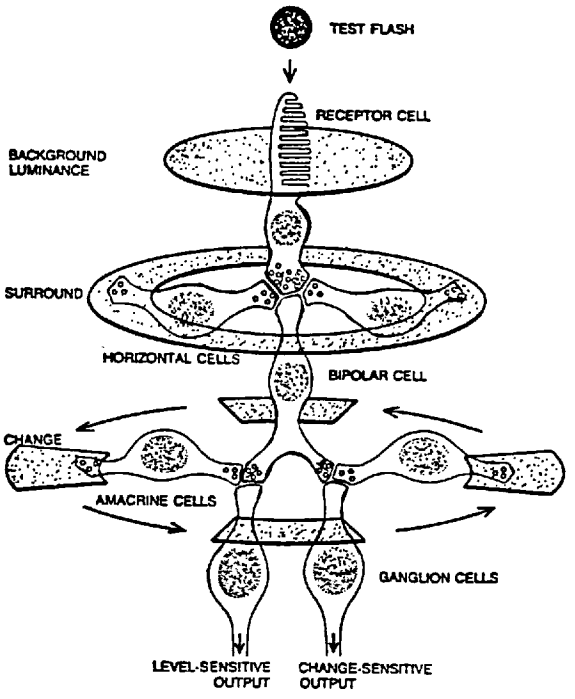

FIGURE 1.8 Diagram illustrating a functional model of the retina (after Werblin, 1973).

regions (Copenhagen, 1975).

Few data exist of the intracellular activity of cells in the primate retina. Most of the data presented in the following section relates to other vertebrate retinas, and can only be used to infer the likely activity of primate retinas, on the strength of morphological and extracellular cell response similarities amongst vertebrates.

The electrical responses of photoreceptors, horizontal cells and bipolar cells have graded amplitude-modulated waveforms. Electrical 'spikes', up to 20 ms in duration, are superimposed on graded potentials in the amacrine cells, and frequency-modulated spike trains are the only way in which information is transmitted to the higher centres.

Intracellular recordings from photoreceptors have only been made from cells with large inner and/or outer segments (e.g. Bortoff, 1964; Tomita, 1965; Toyoda, Nosaki and Tomita, 1969; Baylor and Fuortes, 1970). Schwartz (1975a,b) showed that turtle rod photoreceptor activity is influenced by that of neighbouring cones as well as rods, and deduced that these interactions were not mediated by horizontal cells. The measured receptive fields of turtle cones are 40 µm, several cone widths (Baylor, Fuortes and O'Bryan, 1971). The spectral sensitivity of the electrical response corresponds with data obtained by microspectrophotometry for the carp (Tomita, Kaneko, Murakami and Pautler, 1967; Marks, 1965).

Two classes of horizontal cell response (or S-potential) have been recorded from fish retinae (Svaetichin and MacNicol, 1958; Kaneko, 1970). Only one of these, the 'L-type' S-potential, has been demonstrated for higher vertebrates (Grüsser, 1960; Rodieck, 1973). The action spectrum of this L-type response corresponds to

that of single pigments, but is sometimes broader than that of single pigments (Orlov and Maksimova, 1965).

The L-type S-potentials in cat, and maybe in primates, receive mixed contributions from cones and rods (Brown and Murakami, 1968; Steinberg, 1969a,b,c; Kolb, 1970). Kolb (1970, and figure 1.6) found anatomically that the primate horizontal cell body contacts with cones via the short dendrites, and that the terminal arborization synapses with rods. The same architecture holds for cat horizontal cells (Nelson, Lutzow, Kölb and Gouras, 1975). Niemeyer and Gouras (1973) recorded from such cells and demonstrated that rod and cone responses showed independence when their mixed S-potentials were recorded in single cells.

Naka and Rushton (1966a) showed that the receptor-horizontal cell synapse is linear. They showed too (Naka and Rushton, 1967) that fish S-potentials arising from receptors in the extensive receptive field summate in a linear manner; this has also been proved for turtle receptors by Lamb (1976). Naka and Rushton (1966a,b) also inferred the spectral sensitivities of the three basic photoreceptor types driving the horizontal cells in goldfish, in agreement with micro-spectrophotometry and single-cone recordings. Their discovery by this method of a fourth receptor type remains unconfirmed by other methods.

Bipolar cells have a receptive field consisting of two concentric and antagonistic regions (Werblin and Dowling, 1969; Kaneko, 1970; Naka, 1977). The central region, which is 350 μm in diameter for the mudpuppy, is probably driven by local receptors connected directly to the bipolar cell, and the antagonistic surround is probably mediated by the integrating action of horizontal cells. This view of Werblin and Dowling (1969) was suggested by the fact that the

response latency of the central zone was shorter than that of the antagonistic surround. Naka (1977) found two types of bipolar cell in the catfish which were functionally independent; the on-centre and the off-centre types.

Concentric organization of the receptive field is also evident for amacrine cells, which are probably driven by a limited number of bipolar cells with spatially coincident receptive fields (Werblin, 1970). There are two types in the mudpuppy: the on-centre unit which responds to light with a transient depolarization, both when a light is turned on in its central region, and when a light is turned off in its surround; the off-centre variety responds similarly but is organised spatially in the opposite manner. Chan and Naka (1976) have identified two types of morphologically and electrically distinct 'amacrine' cells in the amacrine cell layer of the catfish. Ruddock and Djamgoz (in print, and private communications) have shown that amacrine cells receive mixed rod-cone input in Cyprinid fish.

The receptive fields of the majority of monkey ganglion cells are concentrically arranged (Hubel and Wiesel, 1960; Gouras, 1969), and are also colour opponent, that is, the centre and the surround regions are driven by different receptor types (Gouras, 1968; Marrocco, 1972; De Monasterio, Gouras and Tolhurst, 1975a,b). De Monasterio and Gouras (1975a) identified three functionally distinct classes in a sample of 460 ganglion cells of the rhesus monkey. The first class had concentrically organized receptive fields, and sustained colour-opponent responses which were mediated by one cone mechanism in the centre and one or two in the antagonistic surround. A few cells of this class had co-extensive receptive field organisation. The second (broad-band) class had transient

responses and concentric antagonistic receptive fields. Two cone mechanisms usually mediated the centre response and the surround had the same spectral sensitivity as the centre; in some cells the surround had a different spectral sensitivity (colour-opponent). The third, non-concentric, class of ganglion cell contained one group with extremely phasic on-, off- or on-off- responses and no spontaneous activity, while another group had regular spontaneous activity and was responsive only to moving stimuli. Figure 1.9 shows

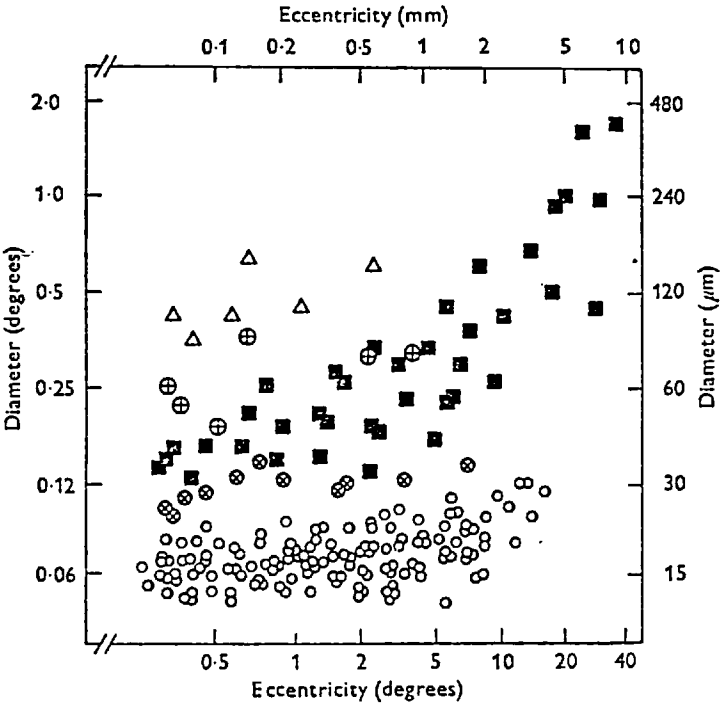

FIGURE 1.9 Distribution of receptive-field centres or activating areas in relation to retinal eccentricity. ○: data from concentric colour-opponent cells, receiving input from one cone mechanism to the centre. ⊗: data from concentric colour-opponent cells, receiving input from two cone mechanisms to the centre. ⊕: data from non-concentric colour-opponent cells. ■: data from broad-band cells (both varieties). △: data from non-concentric cells with phasic responses. (From De Monasterio and Gouras, 1975).

the receptive field size of the cell types in relation to their position on the retina. The fraction of colour-opponent cells decreases from 0.8 at the fovea to 0.3 beyond 10^{o}, that of the

broad-band cell increases from 0.1 at the fovea to 0.6 beyond 10^{o} and the fraction of non-concentric cells is almost invariant at around 0.1.

In a study of 211 colour-opponent cells in the parafoveal region of the rhesus monkey, De Monasterio, Gouras and Tolhurst (1975a) found that 24% were driven by all three cone types. In the majority of these the blue-sensitive cones opposed the red- and green-sensitive ones, and all of the cells receiving blue-sensitive cone input were trichromatic. All of the ganglion cells studies in the macaque monkey by Gouras and Link (1966), and Gouras (1967) were driven by both the rods and cones. The rod response latency was longer, rod responses occurring 50 ms after the light stimulus. Interaction of rod- and cone-initiated responses has not been demonstrated in primate ganglion cells, although Rodieck and Rushton (1976a,b) have shown this for the cat.

Ogden and Miller (1966) found that primate optic nerve fibres with diameters around 1.2 μm were most numerous. Axons of these small dimensions are least accessible to microelectrode recording techniques, so that the studies noted above are probably not fully representative.

5b. Electrophysiology: The Lateral Geniculate Nucleus

Reports on electrical recordings from retinal ganglion cells and from LGN cells suggest that they might have the same functional organisation except for those cells which project to the superior colliculus. Earlier recordings from monkey ganglion cells (Hubel and Wiesel, 1960; Gouras, 1968) failed to show as many response-types as were found in the LGN by Wiesel and Hubel (1966) and De Valois and co-workers (De Valois, 1965). The first two classes of ganglion

cell found by De Monasterio and Gouras (1975) however, encompass all the response types found in the LGN by Wiesel and Hubel (1966). There is little evidence for reorganisation of visual information in the LGN, other than resegregation of cell types: cells of the first class (colour-opponent) terminate in the parvocellular layers (inner layers) only and most cells of the second class (broad band) terminate in the magnocellular (outer) layers of the LGN (from Dreher, Fukada and Rodieck, 1976).

The cells in the LGN can be classified in terms of the latency of their response to visual stimuli (Marrocco, 1976). The cells in the parvocellular layer are all driven by slowly-conducting (tonic) ganglion cells, and include off-centre colour-opponent (class 2) responses besides those of class 1. The cells in the magnocellular layer are driven by fast-conducting (phasic) ganglion cells. Padmos and Norren (1973) found that 6 of the 85 primate LGN cells which they studied were trichromatic, but they studied only 10 colour-opponent cells fully.

The third class of ganglion cell response has not been found in the primate LGN. The responses of this class of ganglion cell however, correspond well with those found in the superior colliculus of the macaque (Schiller and Koerner, 1971; Goldberg and Wurtz, 1972), and might be the cells which Schiller, Stryker, Cynander and Berman (1974) found, anatomically, linking the retina and the colliculus.

5c. Electrophysiology of the Visual Cortex

Hubel and Wiesel (1968) classified cells in area 17 of the primate visual cortex as circular-concentric, simple, complex and hyper-complex. (Other more detailed classifications have recently been introduced (Schiller, Finlay and Volman, 1976a,b,c)). Bartlett

and Doty (1974) found in addition that 40% of cortical cells of the squirrel monkey responded to steady light over periods in excess of a minute. 44% of these 'luxotonic' units had no definite receptive field.

Units with circular-concentric responses may be geniculo-calcarine fibres (Brindley, 1970). The other types of cortical response are associated with elongated receptive fields. The simple cells of Hubel and Wiesel are otherwise similar to retinal ganglion cells: linear stimuli are more effective at stimulating these cells when they mostly fill the on-centre and not the off-surround area of the receptive field, and vice versa. Complex cells respond uniformly to an appropriately oriented bright or dark line or boundary over a fairly large receptive area (3^{o}), and to moving linear stimuli. Hypercomplex cells occur in areas 18 and 19 as well, and respond maximally if an appropriately oriented line terminates or bends within the receptive field, at one or both ends. The simple cells correspond mainly to stellate cells, with spherical dendritic fields, and the complex and hypercomplex cells correspond mainly to pyramidal cells which have elongated dendritic fields (Van Essen and Kelly, 1973a,b; Kelly and Van Essen, 1974). A further cell type has been reported, comprising 40% of the cells in area 18 of primates (Hubel and Wiesel, 1970), which is binocularly driven and probably subserves stereoscopic depth perception. These cells respond optimally if the visual image on the two retinae are at some specific angular disparity (Barlow, Blakemore and Pettigrew, 1967; Nikara, Bishop and Pettigrew, 1968).

Hubel and Wiesel (1962, 1965, 1968) found that the visual cortex was divisible into 'columns' according to the ocular dominance of the cells, and according to the receptive field axis orientation of

the cells. The preferred orientations of these receptive fields change, usually in a continuous fashion, along tracks parallel to the cortical surface.

The proportion of colour-opponent cells in the cortex depends on their cortical location and the location of their receptive fields on the retina. One quarter of the simple cells with parafoveal receptive fields are colour-opponent, and 7% of the corresponding complex and hypercomplex cells are colour-opponent (Hubel and Wiesel, 1968). When mainly cells with foveal receptive fields are investigated, this proportion is 28 - 30% (Boles, 1971; Gouras, 1972, 1974; Dow and Gouras, 1973; Yates, 1974). In a study of 52 cells of the visual cortex, Yates found in addition 7 pure-hue cells responding to spatially optimal stimuli within wavelength ranges of only 40 nm. Dow (1974) found that many colour cells not in the middle layer of the visual cortex have input from all three cone types, and that some respond to chromatic contrast regardless of wavelength and are actively inhibited by luminous contrast.

Graded potentials representing gross neural responses have been recorded from the surface of the foveal striate cortex of primates, and they also showed trichromatic (cone) response (Padmos and Norren, 1973; Gouras and Padmos, 1974), which correlated with the behavioural data of Sperling and Harwerth (1971). Similar graded responses recorded from the occipital scalp of man yielded spectral sensitivities of cones and rods comparable with those obtained from psychophysical measurements (Estevez, Spekreijse, van den Berg and Cavonius, 1975; Regan, 1975).

B) PSYCHOPHYSICAL INVESTIGATIONS OF HUMAN VISION

It was mentioned earlier that some results of psychophysical

experiments have been confirmed by direct measurements, such as the trichromatic basis of vision and the presence of a macular pigment (section IA.2). It was also seen that other sensory measurements have yielded results not yet tested directly, such as the presence or absence of blue-sensitive cones in the central fovea (section IA.3b). Many observable phenomena have not been linked completely with the physiology and electrical activity of the visual system. Among the most interesting of these is colour vision. The spectral sensitivities of the 'channels' subserving colour vision have been studies by means of colour matching, threshold and flicker experiments.

1. Colour Vision and Colour Matches

Extensive work has shown that foveal colour- and intensity-matches can be established between two neighbouring fields of about 1^{o} in extent with mixtures of only four colours, provided no two of these can be mixed separately to match a third (König and Dieterici, 1886; Abney, 1913; Wright, 1929; Guild, 1931; Stiles, 1955). This empirical finding of trichromacy extends to extra-foveal colour matching, even though the rods are participating in the match (Wright, 1946; Gilbert, 1950; Moreland and Cruz, 1959; Clarke, 1963). The direct evidence mentioned before (in section IA.2) for three types of cone pigment has led to the belief that trichromacy is established by these pigments. This leads to the conclusion that colour matches between non-identical lights cannot be disturbed by adaptation to spatially uniform fields, provided it does not alter the pigment spectral sensitivity (Brindley, 1957). Wright (1936) and Brindley (1953) found that such matches were disturbed by adaptation to very bright lights. Brindley attributed

these shifts to the relatively small narrowing of pigment spectral sensitivities, which is caused by the bleaching dilution of the pigments (Dartnall, 1957).

The Wright system of colour matching (Wright, 1946) involves the mixing of variable amounts of monochromatic red (650 nm), green (530 nm) and blue (460 nm) stimuli to match a fourth colour stimulus of fixed radiance. The colours are represented by, respectively, R, G, B and C, and the amounts of these needed for a match by say, r_1, g_1, b_1 and c_1. The match is commonly represented by the identity

$$cC = rR + gG + bB, \qquad (1.1)$$

where $c = c_1/(r_1 + g_1 + b_1)$, etc. When 'c' is taken to be 1, the identity is known as the unit trichromatic equation. This equation is a function of two variables (since r + g + b = 1) and is plotted on a 'chromaticity diagram', the orthogonal axes of which are usually used as the r and g axes. In the Wright (WDW) system the amounts of red and green needed to match a yellow (582.5 nm) are equated, as are the amounts of green and blue needed in the match against a blue (494.0 nm) test colour. These two matches made by an observer are used to normalize all other trichromatic equations to be plotted on the WDW diagram for that observer.

2. Spectral Sensitivities

2a. Threshold and Dark-adaptation

Threshold measurements outside the fovea readily yield the spectral sensitivity of the rods (if the absorption of the optical

media of the eye is ignored), since in the dark-adapted state the rod sensitivity exceeds that of the cones over most of the visible spectrum. The time constant for regeneration of rhodopsin is 270 s (Gosline, MacLeod and Rushton, 1976), and that of the cones is 120 s (Rushton and Henry, 1968). Graphs of the temporal course of threshold recovery following light adaptation of non-foveal regions thus usually comprise two decaying exponential curves, reflecting the early recovery of cone sensitivity, and the slower recovery of the more sensitive rods. Precise determinations of absolute threshold are confounded by the rhythmic variations of threshold level (with periods of 5 - 10 minutes) which may exceed 0.4 log units for some observers (Lee, Finch and Pounds, 1945; Bornschein, 1951; Swets, 1973). Also, prolonged adaptation in a sunlight environment can delay dark-adaptation noticeably for many hours (Clarke, Johnson and Dreher, 1946; Hecht, Hendley, Ross and Richmond, 1948).

Threshold measurements of the dark-adapted foveas of colour-normal individuals (q.v.) yield spectral sensitivity functions similar to the standard 'V_λ' curve of the C.I.E. Other methods used for finding spectral sensitivity functions include brightness matching between two differently-coloured half-fields (heterochromatic brightness matching), and flicker matches in which a field is illuminated alternately by two dissimilar lights, the relative intensities of which are altered to reduce the perceptual brightness flicker to a minimum. These methods are more difficult to interpret, however, and yield slightly different sensitivity curves from threshold measures.

2b. Threshold and Chromatic Bleaching or Adapting Backgrounds

Separation of the three cone sensitivities can be accomplished

by selective chromatic bleaching, in which only two cone pigments are strongly bleached, followed by threshold measurements (Brindley, 1953; Auerbach and Wald, 1954). This method yields sensitivity functions in agreement with those obtained from threshold measurements of dichromats (Pitt, 1935). The measurements are more precise than those of direct methods, and agree with the results of the latter, and of colour-matching methods within experimental error.

Stiles (1939, 1949, 1953, 1959) introduced a further method for isolating chromatic mechanisms. In his two-colour threshold method, the threshold of a probe field is measured in the presence of a steady adapting field. The wavelengths of these two fields, and the luminance of the background field are chosen to isolate a particular mechanism. Stiles found five separate cone-mediated mechanisms using this technique, besides the rod mechanism which he labelled π_0. The mechanisms which he called π_1, π_2 and π_3 have peak sensitivities around 440 nm and are mediated primarily by the 'blue' cones. The long-wavelength portion of the π_1 mechanism has been shown to result from the action of the 'green' cones with possibly some contribution from the 'red' cones as well (Pugh, 1976). The π_2 mechanism probably receives contributions from all cone types (Rodieck, 1973). The spectral sensitivity of the π_4 mechanism peaks at 540 nm, and that of the π_5 mechanism at 575 nm. The π_4 mechanism reflects the properties of the green cones under most conditions, and the π_5 mechanism receives contributions from red and green cones. The spectral sensitivities of π_4 and π_5 change shape at high intensities; Stiles labelled the high-intensity forms π_4' and π_5'. The mechanisms have different temporal and spatial resolutions and are independent under greatly varying conditions, but Boynton, Das and Gardiner (1966) have shown minor exceptions to this.

3. Temporal and Spatial Properties of the π-mechanisms

The critical duration over which complete temporal summation of spatially coincident stimuli occurs, and the relative latent period measured by reaction time to a visual stimulus, increase with eccentricity and with decreasing intensity (Arden and Weale, 1954; Krauskopf and Mollen, 1971; Mollen and Krauskopf, 1973). These measures vary independently according to the sensitivity of the colour mechanism concerned, and are least for the red (π_5) and green (π_4) mechanisms and longest for the rod mechanisms (Ueno, 1976). The critical duration varies between 25 ms and 200 ms depending on stimulus conditions, and reaction time is about 200 ms longer under the same conditions. Also, the maximum frequency of flicker which can be discerned is about 55 Hz for the π_4 and π_5 mechanisms and about 20 Hz for the rod and blue (π_1) mechanisms (Brindley, Du Croz and Rushton, 1966). Conner and MacLeod (1977) showed that the rod mechanism responds to flicker up to 28 Hz at high intensities, although Gouras has expressed reservations about this result (private communication).

The maximum resolution of the fovea, 1' of arc, is mediated by the red (π_5) and green (π_4) mechanisms. The maximum resolution of the blue-sensitive mechanism is several times coarser than that of the red- and green-sensitive mechanisms (Stiles, 1949; Green, 1968) and is slightly higher than that of the rod mechanism (Brindley, 1954). The resolution of each cone mechanism decreases with increasing eccentricity because of increasing spatial summation, which is probably mediated by the increasing size of the dendritic fields of the bipolar cells (Green, 1970). The summation areas of the cone and rod mechanisms over which the threshold is independent of the spatial distribution of light energy, also

increase with eccentricity. The diameter of the summation area of the foveal blue (π_1 and π_3) mechanisms is 13' of arc, and that of the π_4 and π_5 mechanisms is 2' - 6' of arc (Brindley, 1970).

Area summation is an example of interaction of signals arising from images on spatially adjacent areas on the retina. Westheimer (1965, 1967) and Shchadrin and Bougard (1971) showed that the energy threshold of a small probe test spot, presented in the middle of a circular background of variable size, increased to a maximum and then decreased, as the diameter of the background was progressively increased. This indicated that interactions can be inhibitory as well as excitatory, consistent with physiological findings mentioned earlier. Similar results indicating antagonistic organisation of receptive fields have been shown for test stimuli with straight edges (Fiorentini and Mazzantini, 1966; Thomas, Padilla and Rourke, 1969; Bagrash, Kerr and Thomas, 1971).

The energy threshold of a circular probe determined in the presence of steady or transient annular surrounds is thus very sensitive to spatial parameters (Teller and Lindsey, 1970; Teller, Matter and Phillips, 1970; Teller, Matter, Phillips and Alexander, 1971; Sturr and Teller, 1973; Alexander, 1974). McKee and Westheimer (1970) and Westheimer (1970) showed that the interaction between signals from the annular sensitizing zone and the non-overlapping circular test-flash area is determined independently by the cone red (π_5) and green (π_4) mechanisms, and by the rod mechanism. Lennie and MacLeod (1973) however demonstrated rod-cone interaction in this area sensitization effect, for probes superimposed on a circular background.

The 'metacontrast' phenomenon has been used to study the interactions of signals evoked by spatially adjacent and non-

overlapping stimuli of short duration (Stigler, 1910; Alpern, 1952, 1953; Weisstein, 1972). The effect is commonly demonstrated by presenting a circular probe stimulus inside a concentric annular 'mask' stimulus. The effect of the mask stimulus is to decrease the apparent brightness of the probe under suitable conditions. This effect is measured by recording the changes in energy level of the probe, or of the mask, which are necessary to maintain the probe flash either at a constant brightness or at its threshold. When the constant brightness criterion is used and the two stimuli are of the same order of brightness, the maximum reduction in brightness of the probe occurs when its onset occurs about 100 ms to 50 ms before the onset of the mask (Kahneman, 1968; Lefton, 1973). When the probe is much dimmer than the mask or at threshold, the maximum masking effect occurs when the two stimulus onsets coincide, and the effect decreases monotonically as the onset of the mask is advanced temporally with respect to the onset of the probe ('forward masking'), or retarded ('backward masking'). Weisstein (1972) explained the masking in terms of lateral inhibitory interactions between neural signals.

The rod mechanism and each cone π mechanism have been shown to act independently in the metacontrast interactions when the mask onset occurs about 50 ms before the probe onset (Alpern, 1965; Alpern and Rushton, 1965, 1967; Alpern, Rushton and Torii, 1969, 1970 a,b,c,d). Independence of the rod and cone mechanisms is not ubiquitous however, and interaction between them has been shown in many psychophysical phenomena. Rod-cone interaction has also recently been demonstrated using metacontrast both monoptically (Foster, 1976; Yellott and Wandell, 1976) and dichoptically (Foster and Mason, 1977).

The magnitude of masking in the metacontrast effect is strongly

dependent on the spatial arrangement of the stimuli and their edge luminance profiles (Kolers and Rosner, 1960; Battersby and Wagman, 1962; Schiller and Wiener, 1963; Schiller, 1965; Sekuler, 1965; Growney, 1976), and metacontrast interferes with visual acuity (Westheimer and Hauska, 1975). Studies of metacontrast in which structured probe stimuli were flanked or surrounded by similarly structured masks have indicated a high degree of form specificity in the interaction (Werner, 1935; Sekuler, 1965; Uttal, 1970; White and Lorber, 1976). However the accounts given by Werner and Uttal are only qualitative, and all of the data on the form-specificity could be explained by the change of lateral interaction resulting from variations of the stimulus edge separation, as opposed to the interaction of central form-specific mechanisms.

In the present investigation, the metacontrast effect has been utilised to study the lateral interactions of rod- and cone-initiated signals in the dark-adapted state. The results of this study are reported in Chapter 3.

4. Adaptation to Spatially Structured and Coloured Stimuli

Spatially structured stimuli can adapt the visual system in a way which differs markedly from the adaptation produced by uniform fields of the same average illumination flux levels. Grating patterns consisting of parallel dark and light bars of equal width are commonly used to study the effect of spatial structure in adaptation stimuli. Gilinsky (1968), Pantle and Sekuler (1968) and Blakemore and Campbell (1968, 1969) showed that the contrast threshold of a probe grating could be raised, by an adaptation grating field, above that obtained with a uniform adaptation stimulus of the same average illumination flux level. The effect was specific to

the spatial frequency and orientations of the gratings, and a maximum elevation of contrast threshold was obtained when the widths of the bars were equal, and when their orientations were the same. The effect is attributed to adaptation effects associated with detection mechanisms specific to the bar-widths of the adaptation and probe gratings (De Valois, 1973, 1977; Burton, Naghshineh and Ruddock, in print). The colour-selectivity of these shape-specific adaptation mechanisms is, however, a matter of some dispute, there being no specificity when the probe and adaptation gratings are presented to different eyes (Maudarbocus and Ruddock, 1973a), but there is some evidence of selectivity when they are presented to the same eye (May, 1972; Maudarbocus and Ruddock, 1974; but see Timney, Gentry, Skowbo and Morant, 1976).

Burton, Naghshineh and Ruddock (in print, and private communication) found that the spatially structured adaptation stimuli introduced brightness and colour changes in supra-threshold test stimuli, compared to the stimulus appearance following adaptation to a uniform field of the same average illuminance. These colour changes have been investigated as part of the present study and the results obtained are presented in Chapter 4.

5. Red-Green Anomalous Trichromacy

Colour-matching characteristics associated with the perception of red, yellow and green stimuli are usually classified in terms of a colour match established between a yellow comparison stimulus and a mixture of red and green matching stimuli. This colour match is known as the Rayleigh match, and the measure employed for the purposes of classification is the ratio of the red and green stimuli, R/G, which the subject uses to establish the match.

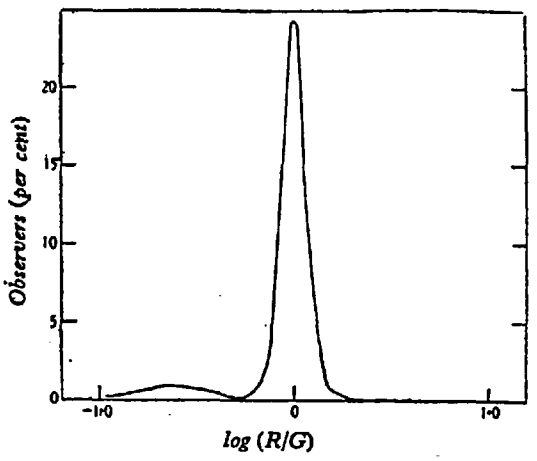

FIGURE 1.10 Distribution of matches on Nagel anomaloscope. Number of observers plotted in each 0.1 of abscissa scale. (From Wright, 1946).

The distribution of the log R/G values amongst Caucasians comprises a sharp central peak together with a smaller peak at low log R/G values (figure 1.10; Nelson, 1938). Most trichromatic observers accept each other's Rayleigh matches and these constitute the group possessing normal colour vision. Two percent of the Caucasian males (and 0.04% of the females) are unable to differentiate hues in the red-green part of the visible spectrum, and are dichromatic for other wavelengths. Such observers are known as red-green dichromats, of which there are two kinds: protanopes and deuteranopes. Protanopes need more red light than deuteranopes in a match between red and green stimuli. About 6% of the trichromats make Rayleigh matches which are unacceptable to colour-normal observers. Of these anomalous trichromats, 1% make matches which appear too red to the normal, and 5% make matches which appear too green: these observers are termed protanomalous and deuteranomalous respectively. Protanomalous and deuteranomalous observers do not in general accept colour-matches of other observers in the same category, or those of colour-normal observers. The spectral sensitivity functions of dichromats and anomalous trichromats differ from those of colour normals. The protanopes and protanomals have reduced sensitivity to red light, and the deuteranopes and deuteranomals have a reduction in sensitivity to green and blue light. The red-green dichromats and

anomalous trichromats have a characteristic loss of wavelength-discrimination in the red-green spectral region.

Differences between the spectral sensitivity curves of red-green defective colour vision and those of normal colour vision can be explained by changes in the relative sensitivity of the colour mechanisms caused by, for example, changes in the relative numbers of the different spectral classes of receptor. The differences in spectral sensitivity could also be explained by changes in the shape of the absorption spectrum of one or more of the colour mechanisms or by changes in pre-receptoral absorption of light. Now trichromacy is established at the receptor level (Brown and Wald, 1964; Marks, Dobelle and MacNicol, 1964), so that differences in the colour-matching properties amongst observers is independent of the relative numbers of different spectral classes of photoreceptor and can only be explained by differences of the absorption spectrum shape of at least one of the colour-mechanisms, or by pre-receptoral absorption. In fact, colour-matching differences do occur because of differing absorption in the optical media and macular pigment (Ruddock, 1963), but these differences are most significant in the blue part of the spectrum. Absorption by these media cannot alone account for the variation in colour matching properties, in spectral sensitivity curves and in hue-discrimination for the different observers, especially in the red-green part of the spectrum.

It has been shown by densitometry and colour-matching that deuteranopes and protanopes lack one of the two long-wavelength photopigments of normal colour vision (Rushton, 1963a,b, 1965a,b; Mitchell and Rushton, 1971a,b). The presence of the π_4 and π_5 mechanisms has been reported in protanopes and deuteranopes

respectively, together with a functional loss of the π_5 mechanism in protanopes and the π_4 mechanism in deuteranopes (Das, 1964; Watkins, 1969a,b). The π_4 mechanism appears normal in the protanomals and the π_5 mechanism is normal in deuteranomals (Mitchell and Rushton, 1971b; Rushton, Powell and White, 1973). Watkins (1969a,b) showed that the other long-wavelength mechanisms in these classes of observer appeared abnormal, and the peaks of the π_4 and π_5 mechanisms occurred at longer and shorter wavelengths in deuteranomals and protanomals respectively. Since the Rayleigh matches of protanomals differ from each other, as do those of deuteranomals, there must exist a range of abnormal photopigments in each case. Indeed, in general the average R/G ratio differs even for normal observers (figure 1.10), so that the visual pigment absorption curves differ amongst normals, although these differences are less than in the case of anomalous trichromacy.

Anomalous trichromacy is the subject of the investigations reported in Chapter 5.

Ic.1 Summary of Chapter One

A review has been presented of some aspects of the visual system as revealed by objective and by sensory experiments. It was shown that objective methods could be used to trace the course of events following the onset of a light stimulus, from the formation of an optical image on the retina to the disappearance of the modified light-evoked signals into the white matter of the brain. The description of this sequence was given preference to facilitate correlations of experimental results with anatomy. Then a brief description of some psychological experiments and their results

served as an introduction to the data which will be presented in subsequent chapters.

Ic.2 Aims of the Investigation

The aims of the experiments which were undertaken are outlined below, headed by the number of the chapter in which the results appear.

Chapter 3

In this chapter, results are presented of experiments performed using the metacontrast masking technique, and some threshold measurements are also included. Preliminary experiments were first conducted to establish a suitable stimulus configuration for the masking experiments. The masking of a circular probe stimulus by an annular mask stimulus was measured as a function of mask-stimulus wavelength, probe size, and of the time-interval between the stimuli. The aim of the experiment was to establish that rod-cone interaction occurs, and to seek the possible location of this interaction.

Chapter 4

An investigation was made of the colour-shift found by Burton, Naghshineh and Ruddock (private communication) which results from the introduction of spatial structure into adaptation fields. Monoptic and dichoptic measurements were made using colour-matching techniques. The aim of these experiments was to characterize, and explain, the cause of the colour shifts.

Chapter 5

Anomalous trichromacy was the subject of experimental investigations reported in this chapter. The experiments involved the measurement of the spectral sensitivitiy curves and of the colour-matching properties of anomalous trichromats and colour normal observers. These experiments were performed under various illumination levels of adapting light, which was sufficiently intense to cause measurable pigment bleaching. The changes in the colour matches caused by the pigment bleaching were compared quantitively with those predicted by a model of anomalous trichromacy in which normal red- and green-sensitive visual photopigments are mixed in one class of cone (Ruddock and Naghshineh, 1974).

Chapter 2

The metacontrast experiments (Chapter 3) were performed using equipment built by the author; and the photometric and colour-matching experiments (Chapters 4 and 5) were performed on the Wright colorimeter which was suitably modified by the author. The metacontrast equipment and the modifications to the Wright colorimeter are described in Chapter 2.

CHAPTER TWO

In this chapter, the equipment used in the investigations of metacontrast and of normal and anomalous trichromatic colour vision are described. The equipment used in the metacontrast study was constructed by the author and the Wright colorimeter (Wright, 1946) was modifed in certain respects for the colour vision studies. The stimulus configurations used in these studies are shown, and the methods used to control and calibrate light levels are discussed.

METACONTRAST APPARATUS

The apparatus shown in figure 2.1 was constructed for the presentation of stimuli in the study of the metacontrast effect, and was mounted on a cast-iron 'optical table'. Observers were seated at one end of this table and viewed stimuli through eyepieces E1 and E2. The single light source S (Atlas 24 V type A1/216) situated at the far end of the table from the observer was powered by a constant voltage power supply. Three lenses L1, L2 and L4 focussed images of the lamp filament onto the apertures P1, P2 and P3 respectively. These apertures were made slightly smaller than the respective filament images, and were placed immediately in front of the electromagnetic shutters SH1, SH2 and SH3 (Vickers Instruments type M03 1000) used for controlling the light beams. The achromatic collimating lenses L3, L5 and L6 produced three near-parallel beams of light. The half-silvered mirrors M7, M10 and M4 split each of the three beams into two separate beams, and the other aluminised mirrors M_i were used to reflect these beams. The beams were combined by the beam-splitters B1 and B2, and by the half-silvered mirrors M17 and M18. The achromatic lenses L7, L8, L9 and L10 produced further

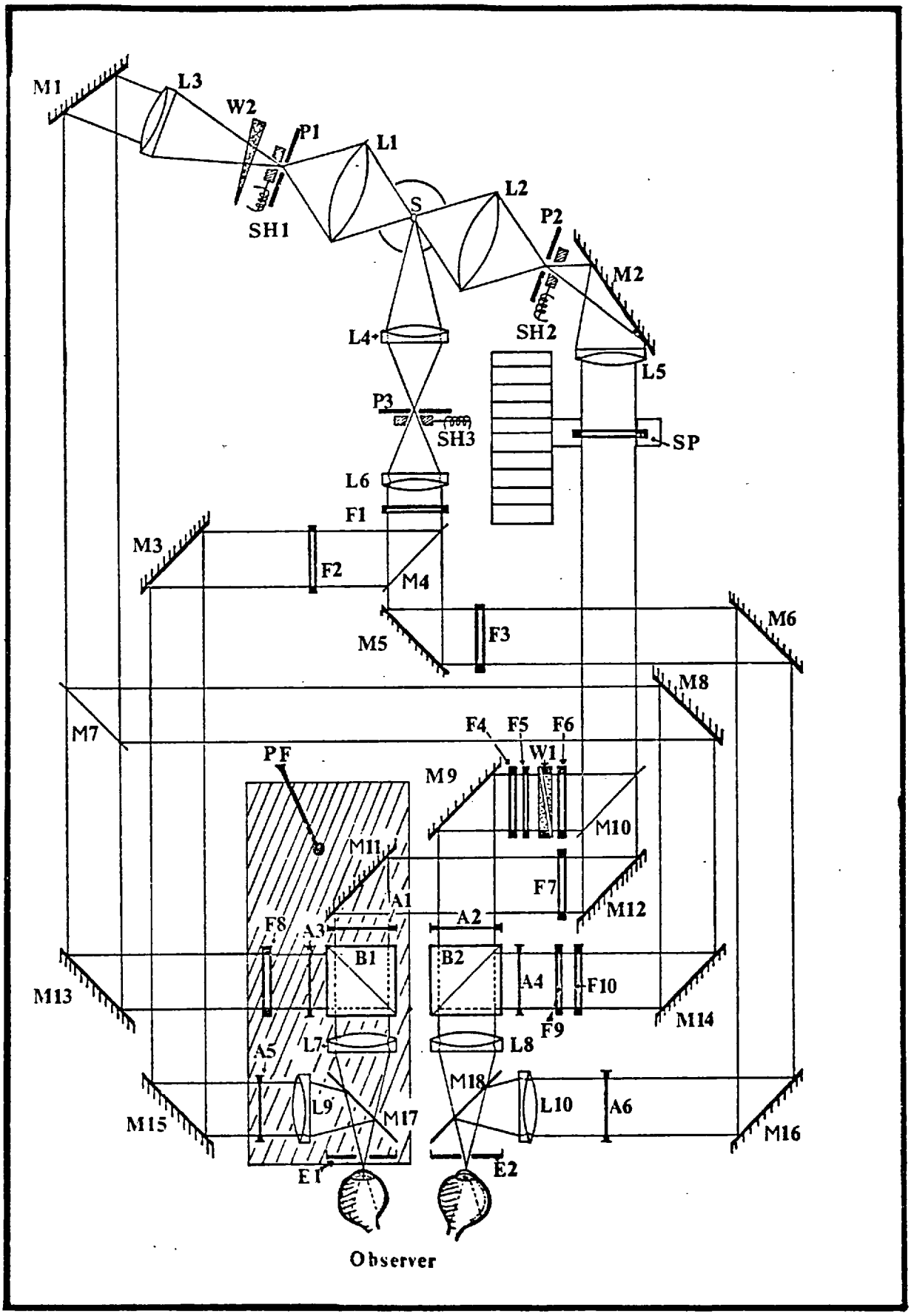

FIGURE 2.1 Schematic diagram of the apparatus built for studying the metacontrast effect.

images of the lamp filament in the pupil plane of the observer's eyes, a few millimeters beyond the 2 mm diameter exit pupils in E1 and E2.

The six stimulus apertures A1 to A6 were seen by the observer in Maxwellian view through the exit pupils. The stimulus patterns were produced photographically and mounted in 35 mm slideholders. The filter-holders F1 - F3 and F6 - F9 were placed in the parallel light beams, and could each hold up to seven neutral-density and colour filters. The neutral-density optical wedges W1 and W2 were used to control the intensity of the light beams illuminating the stimulus patterns at A2, and at A3 and A4 respectively. The illumination level of the light over these apertures was made uniform by placing a stationary compensating wedge at W1, and by positioning the wedge W2 close to the focal plane at P1. Both of the wedges could be controlled by the seated observer by means of knobs linked through suitable rods and gears to the wedge mounts. The filter-change-over unit SP was adapted from an automatic slide projector (Federal model SGDG) to enable interference filters to be positioned in the light beam following the lens L5, in a predetermined sequence. The filters were stored in a slide-cassette with thirty-six compartments, and could be selected by means of a remote-control switch. Five interference filters were too thick to fit into the cassette, and were stacked vertically above each other in the filter-holder F5. The observer could slide this filter-holder vertically to position any of these five interference filters in the light beam. The filter-holder F4 held four neutral density filters of increasing optical density, also stacked vertically. F4 could be slid vertically, and was used as a stepped wedge. The filter-holder F10 held one neutral density filter, and could be slid into, or withdrawn from the beam illuminating the aperture A4.

The platform PF could be traversed horizontally, in a direction perpendicular to the observer line-of-sight, to allow for different interocular separations. The collimated beams reflected from mirrors M13, M15 and M12 to the components mounted on PF were parallel to its direction of traverse, ensuring unaltered viewing conditions for different lateral positions of the platform.

Lamp Power Supply

The D.C. power supply built for the lamp S incorporated current-limiting and precision voltage stabilization.

Sudden current transients in the lamp were avoided by incorporating an automatic, slow turn-on/fade circuit into the power supply. This circuit ensured that the voltage applied to the lamp at turn-on rose gradually, at a rate determined by a resistor-capacitor combination, to a steady value of 23.000 ± 0.003 V within five minutes. The voltage decreased at the same rate when the supply was switched off. (The circuit diagram of the power supply appears in Appendix A together with a more detailed description of its operation).

Shutter Control Unit

The three shutters SH1, SH2 and SH3 (figure 2.1) were operated by a shutter control unit, which was designed to operate up to four shutters in a predetermined timing sequence. The duration for which each shutter was open, the time interval between opening of the shutters, and the sequence of their opening were controlled independently. There was a delay between the onset of the voltage applied to the shutters and their opening, due to mechanical inertia and back-emfs created in their coil windings. This delay was compensated by further adjustable timing circuitry. A timer

circuit was also incorporated to prevent observers from operating the control unit at greater than a preset rate. The duration for which the shutters SH1 and SH2 were open was usually set at 20 ± 1 ms, and the time interval between their opening could be varied continuously, or in precisely-set 10 ms steps between 0 ms and 500 ms. The shutter timing was monitored continuously by means of photodiodes, positioned permanently in the light beams near the apertures A1 - A6 and connected to a calibrated dual-beam oscilloscope.

The timing elements in the circuit were Texas Instruments circuits type SN 72555, and power was supplied to these by a precision 12 V regulator. The output voltages of the timing elements were used to drive the shutters, via Darlington amplifier circuits of the type shown in figure 2.2. This circuit was designed to

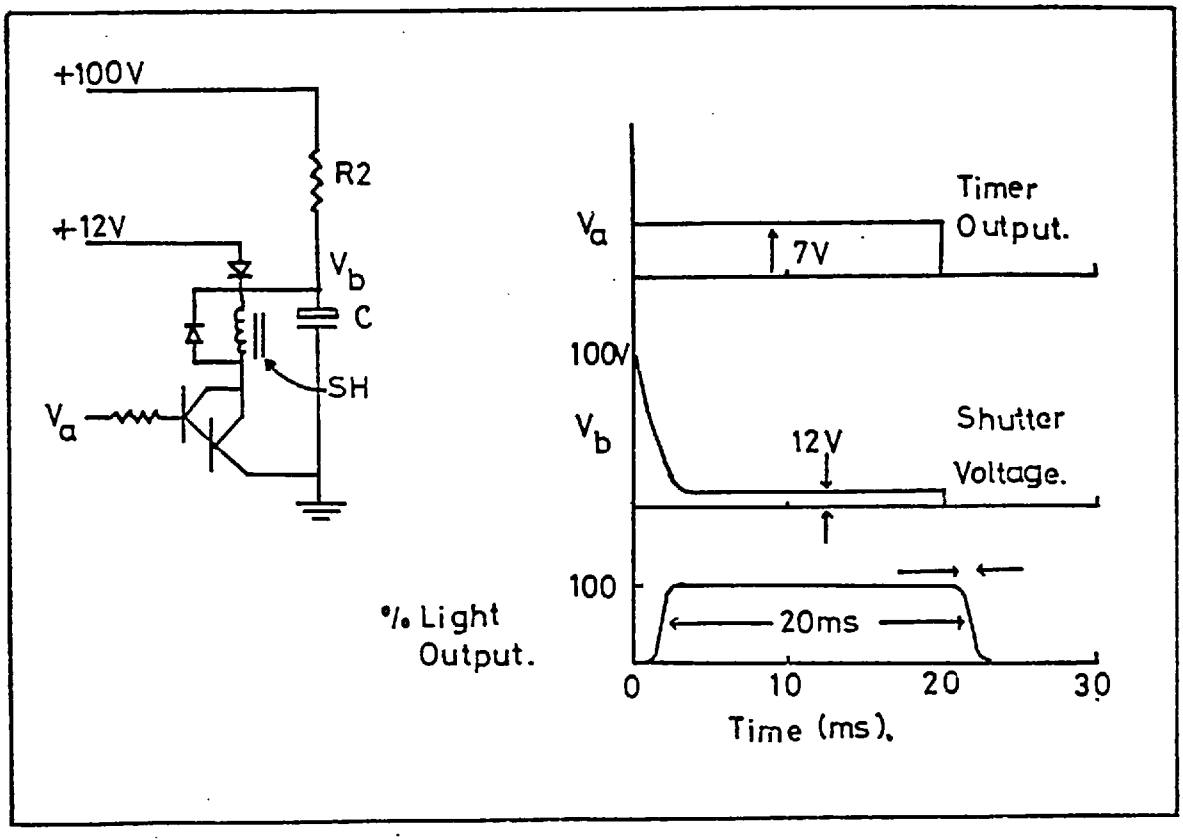

FIGURE 2.2 Circuit of Darlington amplifier used to drive shutters, and graph of shutter timing.

provide a 100 V pulse to the shutters to open them rapidly (as shown to the right of figure 2.2), followed by a continuous potential difference (of 12 V) sufficiently large to hold the shutters open. The low holding voltage reduced back-emf effects at shutter turn-off and also reduced electrical heating of the shutter coils, which is turn made shutter timing more reproducible.

The observer held a control box on which was mounted two switches: the one switch initiated the timing sequence, while the other allowed one of the two shutters SH1 and SH2 to be operated alone.

Data Recording

The position of the movable wedge W1 was initially recorded on a Bryans X-Y potentiometric recorder (model 24 000 A4). A constant reference voltage was supplied to a ten-turn potentiometer connected tightly by gears to the wedge; the output voltage at the middle tap of the potentiometer was connected to the Y-axis amplifier of the recorder. The voltage to the X-axis amplifier could be incremented in 120 equal steps. The position of the wedge W2 was monitored by means of a vernier scale attached to it.

Data collection was later simplified by the acquisition of a digital voltmeter (Dana model 3800B) and a digital printer (Credshire, model DP100). Figure 2.3 shows how the voltage was fed from the potentiometer connected to the wedge W1, to the printer via the digital voltmeter. The position of the stepped wedge F4 (figure 2.1) was monitored by means of a photo-Darlington sensor array and a binary-coded-decimal (BCD) strip attached to this wedge. The sensor-array output was fed both to the printer, and to a single seven-segment display via a BCD-to-seven-segment code converter.

The display was mounted in a metal box (shown as the dotted rectangle in figure 2.3) together with two printer control switches. Depression of the one switch initiated a single print sequence, and the other switch caused red or black numerals to be printed. Provision was made for entering real-time information into the printer from a digital clock. The current positions of the two wedges and the time information were printed in one row on depression of the 'print' switch in the appropriate column.

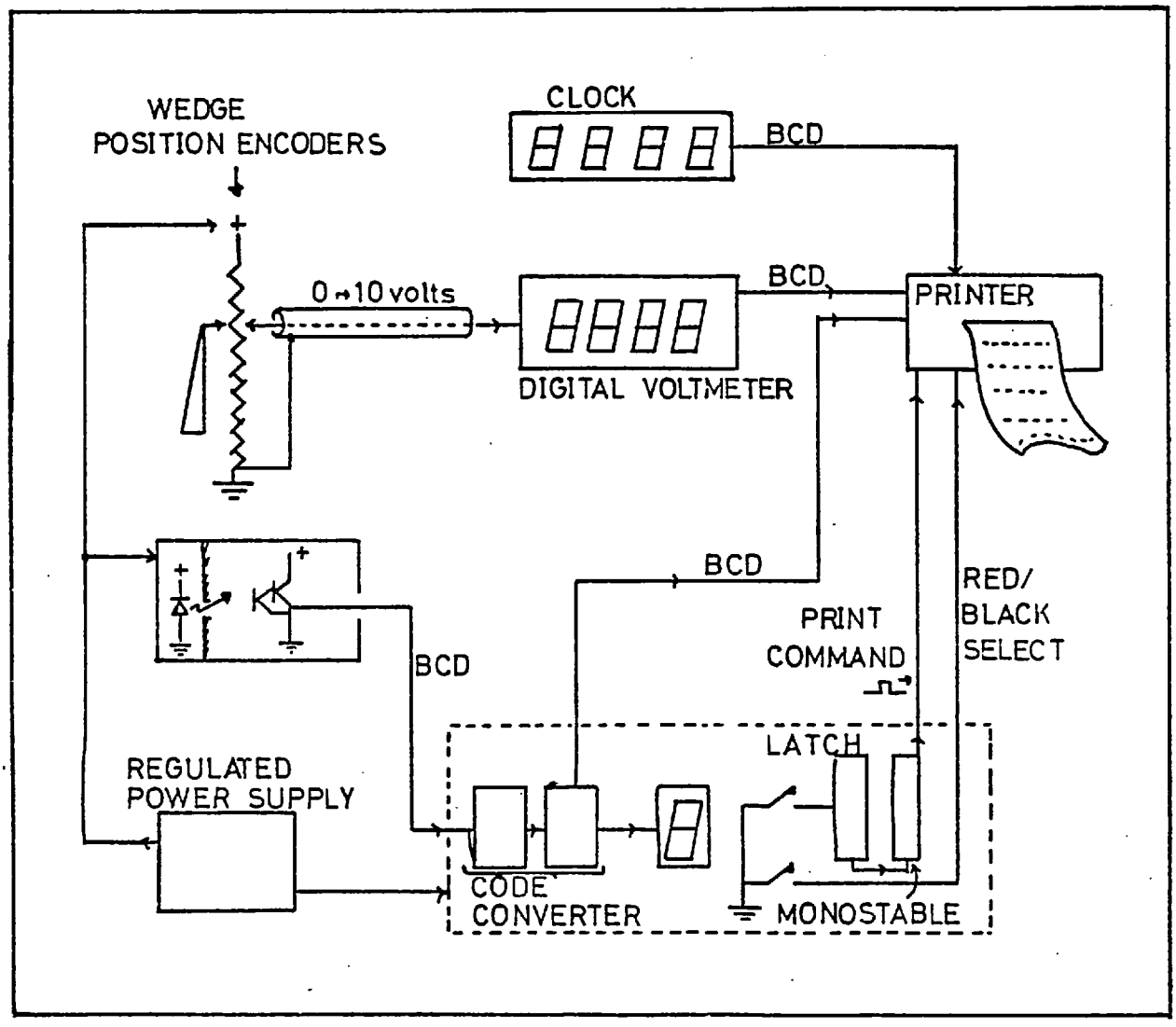

FIGURE 2.3 Block circuit diagram of electronics used for recording data from Metacontrast apparatus

The whole apparatus was enclosed by a metal 'Dexian' framework covered with hardboard which was painted matt black. The observer sat in a

light-tight cubicle, made of black curtaining and hardboard, in which were mounted cooling and extractor fans.

Component Mounting and Calibration Procedure

The fully-aluminised and half-aluminised mirrors were made by vacuum deposition of aluminium on the front surfaces of clean 2.5" x 2.5" x 0.06" glass sheets. The aberrations of these mirrors, once attached to their mounts, were measured with a Twyman-Green interferometer, and found to be less than 15 wavelengths of green light over the whole surface. The mirror mounts could be accurately adjusted about two axes by two screws. The beam-splitter, aperture, lens and eyepiece mounts were designed to be adjustable in all the dimensions necessary for easy alignment of the equipment.

Eighteen neutral-density filters (Wratten gelatin, type 1A) were glued between squares of neutral (optical quality) glass. Spectral selection of the light stimuli was achieved with some 20 Balzers types B20 and B40 interference filters. The spectral transmission coefficients for the interference filters were measured with a Beckman recording spectrophotometer (model DK2), and the relative energy transmission through the filters was calibrated *in situ* with an EMI photomultiplier (type 9558) of known spectral sensitivity. The photomultiplier was calibrated, in terms of absolute energy for a stimulus wavelength of 551 nm, against an energy/power meter (Quantronix type 504, using the energy sensor model 500, and the power sensor model 502). The relative sensitivity at other wavelengths was determined from comparison with an NPL calibrated Hilger-Schwartz thermopile. The energy calibration of the narrow wave-band stimuli provided by the interference filters

was repeated at least weekly, as it was found that the effective black-body temperature of the lamp decreased slowly with age. This also ensured that the slow accumulation of dust on optical surfaces was taken into account. The neutral-density filters and the wedges W1, W2 and F4 were calibrated *in situ* in combination with each of the interference filters. The optical densities of the neutral filters were checked with the Beckman spectrophotometer. The continuous wedges W1 and W2 were calibrated at between 20 and 30 positions along their length at each wavelength, at intervals of roughly 0.1 log units in optical density. The measurements were all checked several times over the course of the experiments, and were found to be stable, to within 0.01 log units of absorption.

It was found that the logarithm of the optical density varied linearly with the displacement of both wedges W1 and W2, at all wavelengths.

A typical calibration curve of the wedge W1 is shown in figure 2.4a for a wavelength of 405 nm. The voltage along the abscissa was recorded from the wedge position encoder (figure 2.3). Figure 2.4b shows a plot of the slope of the calibration curves for the wedge W1, at each of the wavelengths at which it was calibrated.

The energy and optical-density calibration data were fed into a Tektronix programmable calculator (model 31). A programme was written for the calculator to evaluate the number of quanta incident on the observer's corneal surface per second, using as input the wavelength and wedge positions - recorded by the digital printer - and the integrated time of opening of the shutters (normally 20 ms). The programme also evaluated the average and standard deviation for a number of determinations of one datum point. The programme and calibration data were stored on a magnetic tape cartridge: the energy data were updated weekly after each calibration (Appendix E),

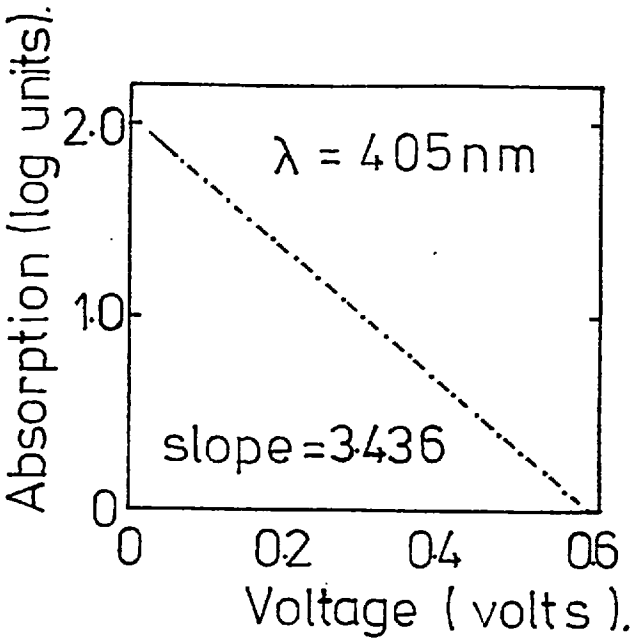

FIGURE 2.4a Plot of wedge absorption versus the voltage of the wedge-position encoder (the potentiometer in figure 2.3).

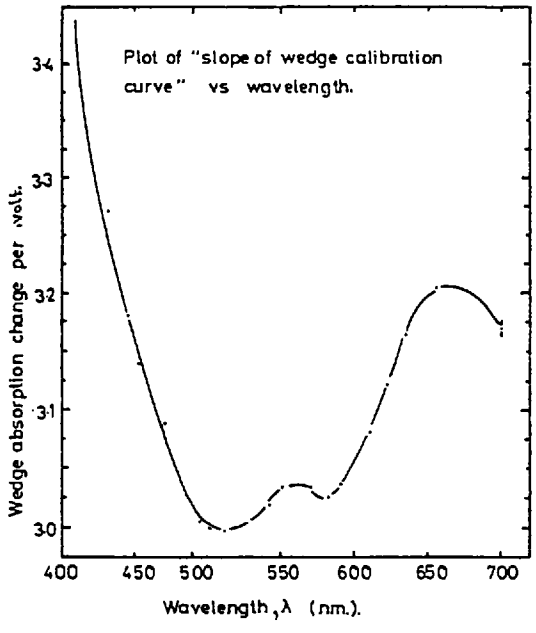

FIGURE 2.4b Plot of the slope of the calibration curves of wedge W1 for a number of wavelengths.

Metacontrast Stimuli

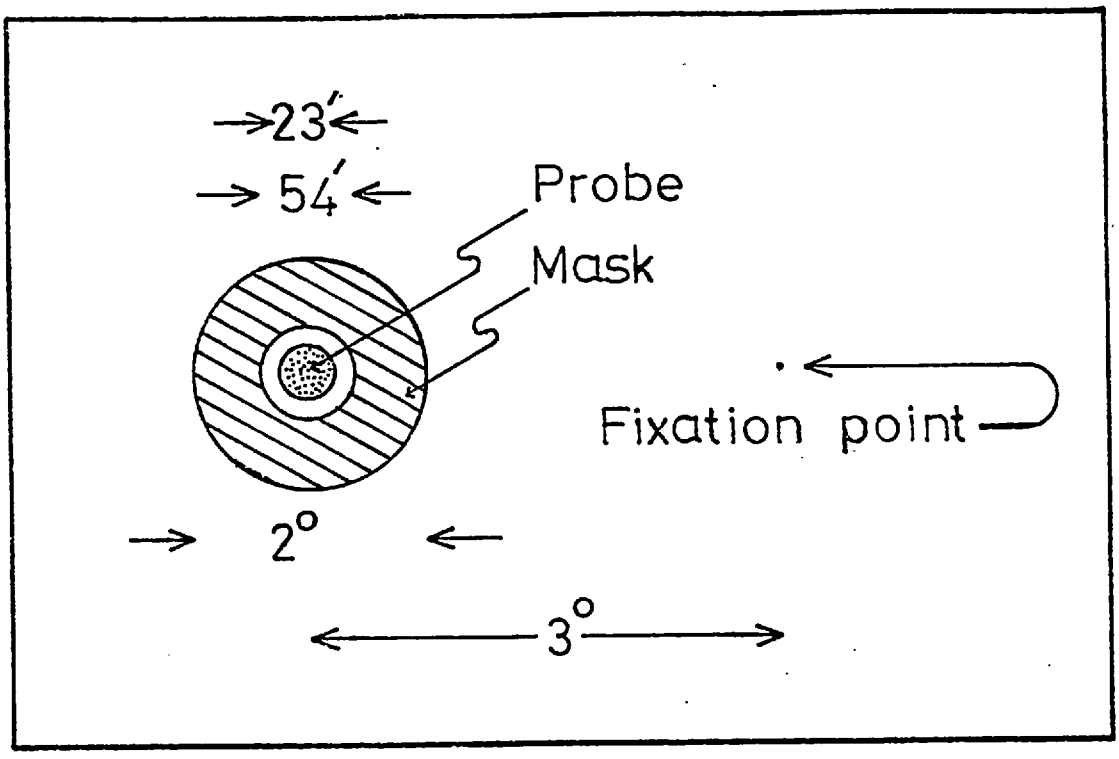

FIGURE 2.5 Typical metacontrast stimulus configuration.

A typical stimulus pattern used in the study of metacontrast is shown in figure 2.5. The red fixation point and the mask stimulus were always presented to the right eye. The probe could be presented, as required, either to the right eye or to the left eye, together with a second fixation point. The mask and probe stimuli were normally presented for durations of 20 ms (± 1 ms).

The Wright Colorimeter

The Wright colorimeter (Wright 1927-28, 1946) was modified for the studies of the effects of adaptation on colour matching, which will be described in Chapters 3 and 4. The modifications are illustrated by figures 2.6 and 2.7. As in the original design, light from the 100 V quartz-halogen lamp at S3 is focussed by lens L4 onto the adjustable vertical entrance slit. Light emerging from this

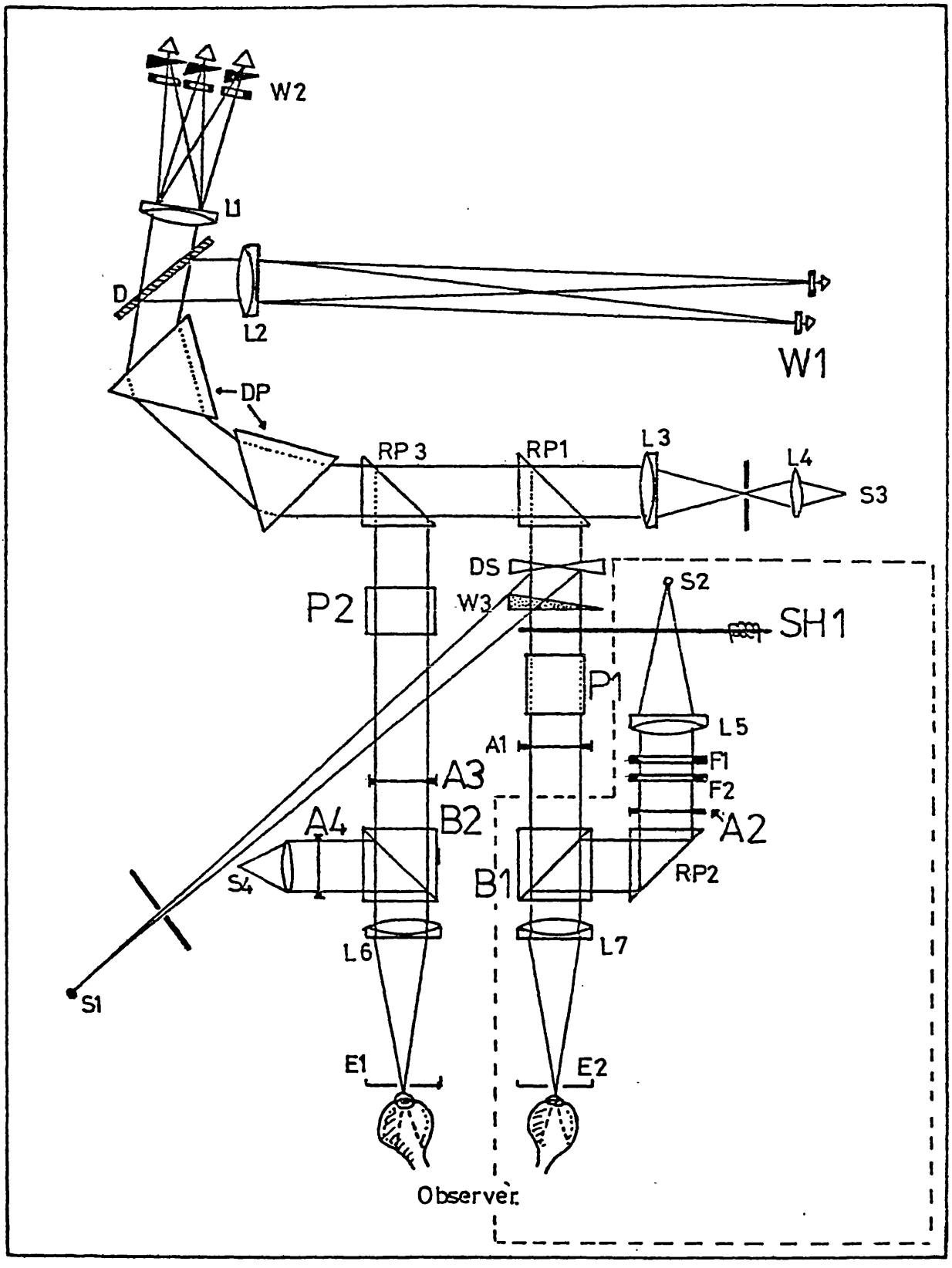

FIGURE 2.6 Schematic diagram of modified Wright colorimeter (see text).

slit is collimated by lens L3, and the collimated light beam passes over the reflecting prisms RP1 and RP3, and is dispersed by prisms DP. The mirror D is cut away to divide the dispersed beam into two, and lenses L1 and L2 provide focussed spectra from these beams at W2 and W1 respectively. The roof-prisms shown at W1 and W2 reflect small-bandwidth portions of these spectra back, immediately below their former paths. The roof-prisms invert the images of the returning light, which is redispersed by DP. In the absence of the reflecting prism RP3, this light is reflected by the prism RP1 into the modified portion of the colorimeter incorporating the Maxwellian image viewing lens L7. The neutral-density optical wedges, in front of the prisms at W2, allow the relative energies of the different spectral components of the reflected beams to be adjusted. Neutral-density filters could be placed in front of all of the roof prisms to provide additional filtering.

The beam from W2 is displaced vertically downward from that reflected by W1. The wedge W3 controls the intensity of the upper W1 beam. The aperture A1 contains two rectangles, one above the other, and the prism P1 raises the beam from W2 to the level of the upper rectangle, while allowing the beam from W1 to pass through the lower one.

Modifications to the Wright Colorimeter

The source S2 (figure 2.6; Phillips 6 V, 100 W strip-filament lamp) provided adaptation stimuli for the experiments. Light from S2 was collimated by lens L5, filtered by colour and neutral-density filters at F1 and F2, and reflected by RP2 and B1 into lens L7. The observer saw images of apertures A1 and A2 in Maxwellian view

through the exit pupil at E2. Source S1 (12 V, 100 W quartz-halogen) was used during flicker photometry experiments to illuminate a magnesium oxide-coated 90^{o} double-sector disc DS. The light scattered by the disc provided the comparison stimulus for the flicker photometric measurements. Flicker presentation was achieved by rotation of the 90^{o} double-sector disc DS, which allowed alternate presentation of the comparison white light beam and the test beams, derived from the spectra at W1 and W2, as it rotated.

Binocular presentation of the test and matching stimuli was achieved by reflection of light into the left-eye channel via the prism RP3. When placed in position this prism could reflect light from the W2 spectrum, or from both spectra, into the lens L6 via the lifting prism P2 and the aperture A3 (figure 2.6). A light-emitting diode source S4 was used to illuminate the aperture A4, which contained the image of a fixation point or fixation line. The light from the apertures A3 and A4 was focussed onto the observer's left eye through the eyepiece E1.

The modification shown in figure 2.7 was added to provide further channels of illumination. (The broken lines in figure 2.6 outline the location where the modification of figure 2.7 was positioned). The top half of the collimated beam of light from lens L8 passed above the reflector RP4; this reflector directed the lower half of the beam to the prism RP5. The two beams were focussed by lenses L9 and L11, and recollimated by lenses L10 and L12. The beamsplitters B4 and B3 allowed the beams to be combined with light from source S2. The light from these channels entered the eyepiece E2 via the beamsplitter B1 and lens L7, and the apertures A5, A6 and A7 were seen in Maxwellian view. An infrared absorbing filter H1 was used to protect the short focal length lens L8, and neutral density and

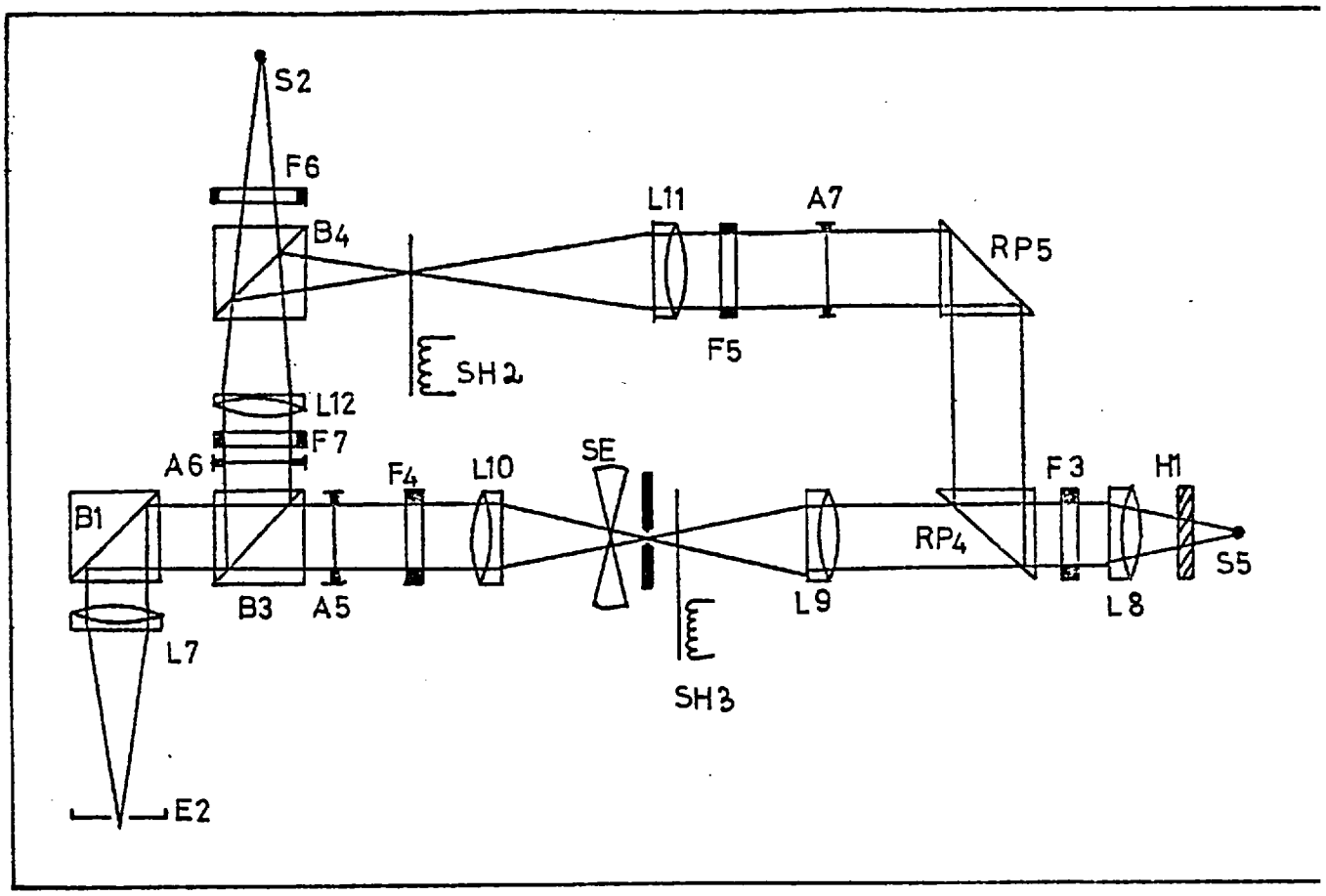

FIGURE 2.7 Modification to adaptation channel of the Wright colorimeter.

interference filters were placed in the holders F3 - F7. A rotating multi-vane sector SE was placed alongside the shutter SH3, near the pinhole aperture at the focus of lenses L9 and L10, to provide flickering light at aperture A5.

The speed of the motor attached to the sector SE (in figure 2.7) was controlled by an adjustable thyristor circuit. All the shutters were controlled by a Digitimer (model 3840), and a power driver unit designed and built for the purpose. The shutter timer could be actuated by a foot-operated switch. Sources S1, S2, S4 and S5 (S5 was an Atlas 150 W lamp type A1/216) were all powered by regulated power supplies, and S3 was powered by a 100 V battery source. Light levels were set daily with a light-dependent resistor powered by a

precision voltage regulator. A galvanometer was used to measure the current through the light-dependent resistor. The light-dependent resistor was permanently located beyond the eyepieces E1 and E2 to the left of the observer's position: light was deflected onto it from the eyepieces by a right-angle prism during calibrations.

Stimulus Configurations

Two different investigations employing colour matching methods have been carried out, and the stimulus patterns required for these investigations are now described.

i) Colour Matching under Adaptation to Spatially Structured or Temporally Flickering Fields

In these experiments, the state of adaptation imposed on the visual system by spatially structured or by flickering light stimuli was determined by colour matching methods. The bipartite matching probe fields used in these experiments are illustrated in figure 2.8. The matching probe field which was used in the first experiments is shown in figure 2.8a. This was presented to the observer's right eye, and the lower and upper halves of this field were provided by light beams from the roof prisms located in the spectra W1 and W2 respectively (figure 2.6). The lower rectangular half-field of the probe stimulus consisted of a near-monochromatic test stimulus, to which a near-monochromatic desaturating stimulus could be added as necessary, and the upper rectangular half-field consisted of a mixture of near-monochromatic red (650 nm), green (530 nm) and blue (460 nm) stimuli. The illumination levels of each of the three lights in the upper half-field could be controlled by the observer in order to establish a colour match between the two halves of the probe field.

Two crossed lines were provided between the two half-fields by the aperture stop: the crossing-point of these lines served as a fixation point (figure 2.8a). During binocular colour matching, the upper half of the probe field was presented to the left eye and the lower half to the right eye (figure 2.8b). A pair of crossed fixation lines was presented to each eye (figure 2.8b) so that stereoscopic fusion of these fixation crosses ensured that the two half-fields appeared vertically aligned as in figure 2.8a. The last experiments to be described in Chapter 4 were performed monocularly with the right eye, and involved the use of identical square-wave 'grating' patterns in the two halves of the probe field (figure 2.8c). The 'grating' patterns consisted of bright vertical bars parallel to each other and separated by a distance equal to their width.

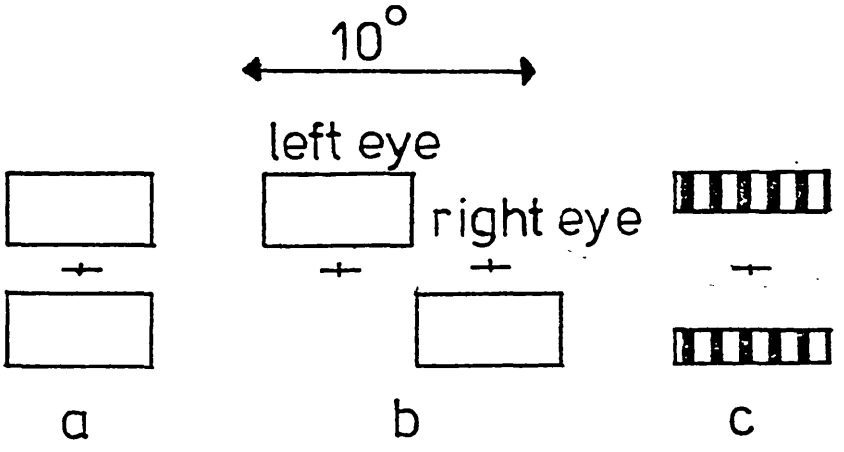

FIGURE 2.8a,b,c Matching fields (scale indicated by 10° arrow at the top of the figure).

The adaptation stimuli used in this study are illustrated in figure 2.9. The upper half of each adaptation stimulus field was uniform, and the space- and time-averaged illumination levels of the upper and lower half-fields were always equal. The lower half-field was either spatially uniform (figure 2.9a) or consisted of

a square-wave grating pattern (figure 2.9b). In some experiments, the lower half of the adaptation stimulus was flickered. The adaptation field of figure 2.9a will be referred to as the 'uniform' adaptation field and that of figure 2.9b will be called the 'grating' adaptation field.

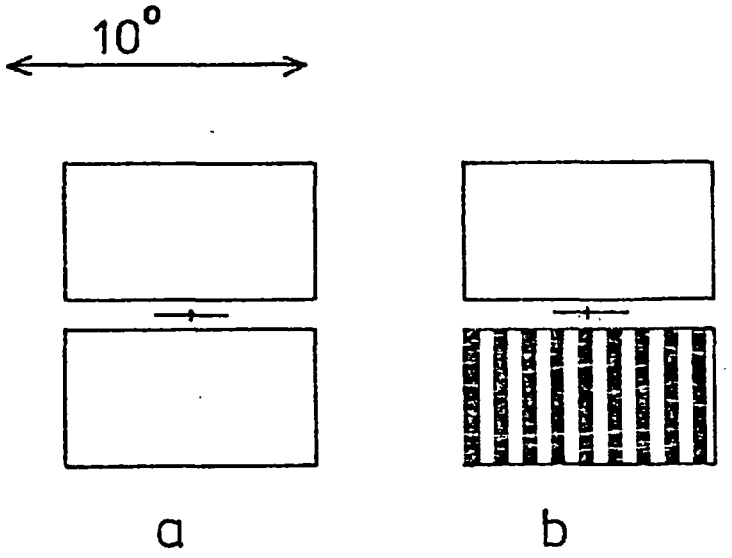

FIGURE 2.9a,b 'Uniform' and 'grating' adaptation fields (to scale: the scale is indicated by the 10° arrow).

ii) Stimuli used in the Study of Anomalous Trichromacy, Chapter 5

In these experiments the colour matching properties of anomalous trichromats were established under various conditions of adaptation. The stimuli used for most of the experiments are shown in figure 2.10: the lower half of the $2^{\circ} \times 2^{\circ}$ probe field (the 'test' stimulus) was illuminated by near-monochromatic yellow (582 nm) light, and the upper half (the 'matching' stimulus) was illuminated by a mixture of red (650 nm) and green (530 nm) lights. The 10° adaptation field was illuminated by near-monochromatic light provided by source S5 (figure 2.7) and an interference filter placed at F3. The off-axis fixation light was provided by a red light-emitting diode. The sequence of presentation of these stimuli is also illustrated in

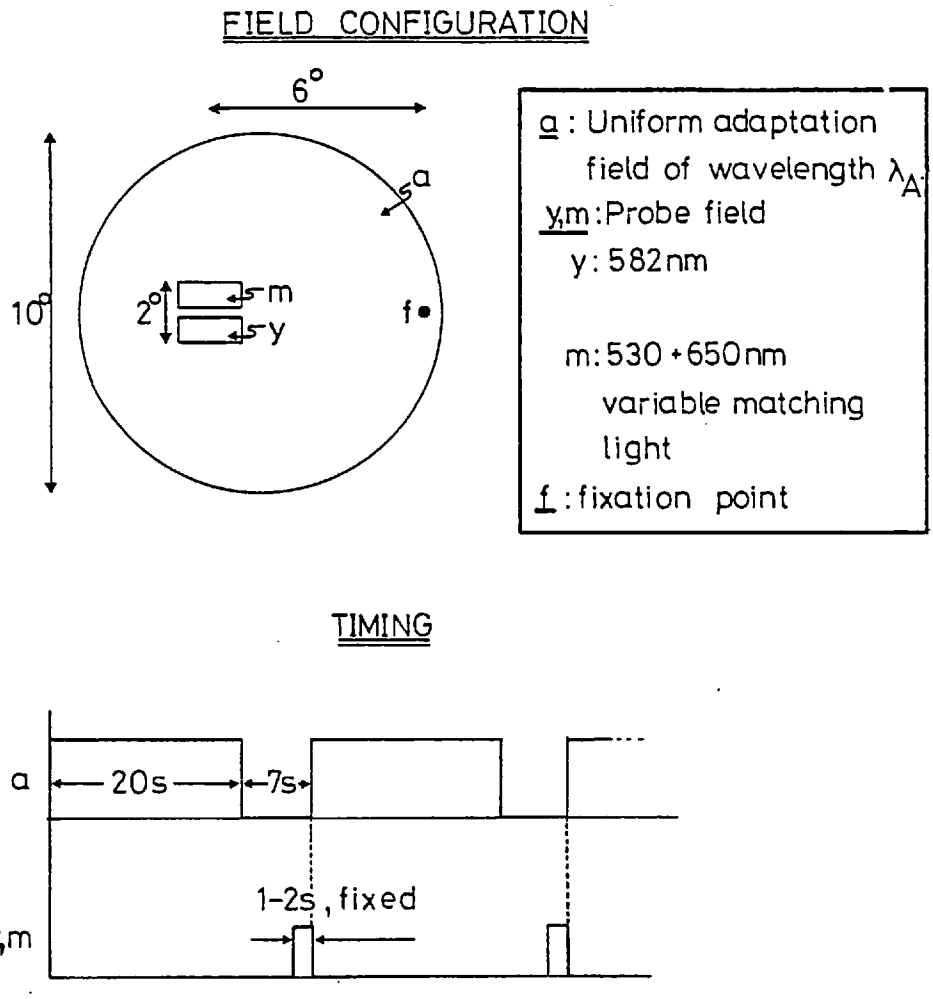

FIGURE 2.10 Field configuration and timing diagram for the study of anomalous trichromacy.

figure 2.10. During measurements the adaptation field was presented for 20 second periods followed by 7 seconds of darkness. The probe field appeared for 1 - 2 seconds at the end of the dark period.

A further experiment was performed with anomalous trichromats in order to determine their parafoveal colour matching properties at low illumination levels. For this experiment the bipartite probe matching and test half-fields were each 2^{o} square, and they were separated vertically by 4^{o}.

Calibration Procedure

Filter Calibrations:

The neutral density filters and optical wedges were calibrated in situ, at all wavelengths at which they were used, by means of a photomultiplier (EMI type 9558) located at the observing position (figure 2.6). The linearity of the photomultiplier was checked by alternating the colorimeter beam with sector shutters located at DS. The sectors were rotated at high speed and provided neutral-density light filtering. The photomultiplier calibrations of the wedges were checked using the brightness matching technique described by Wright (1946, pages 64 - 66). Figure 2.11 shows the best-line fits for some of the wavelengths at which wedge W3 was calibrated.

Relative Energy Measurement:

The relative energies of the monochromatic lights reflected by the prisms at the spectra W1 and W2 were calibrated frequently using the calibrated EMI photomultiplier, in order to correct for slow deterioration of the lamp S3. Figure 2.12 shows one such calibration for the stimulus provided by spectrum W1. The energies

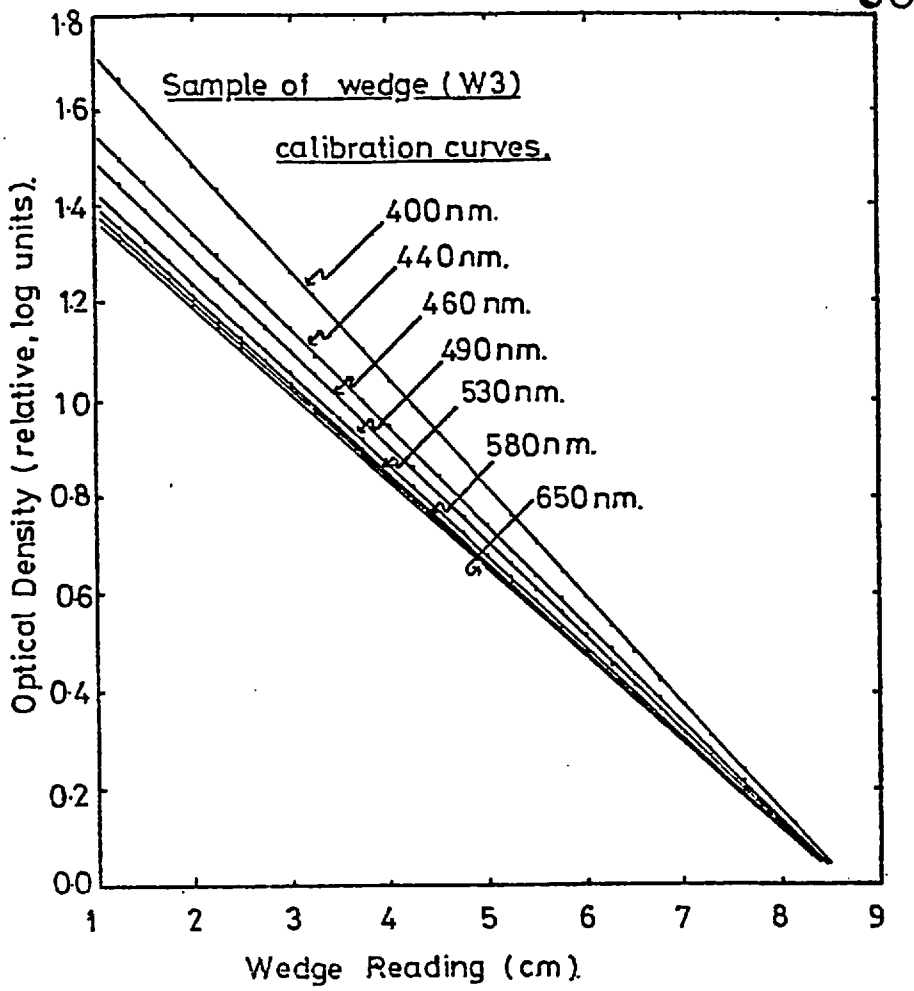

FIGURE 2.11 Calculated best-line fits, and data points resulting from calibration of the wedge W3, for seven wavelengths.

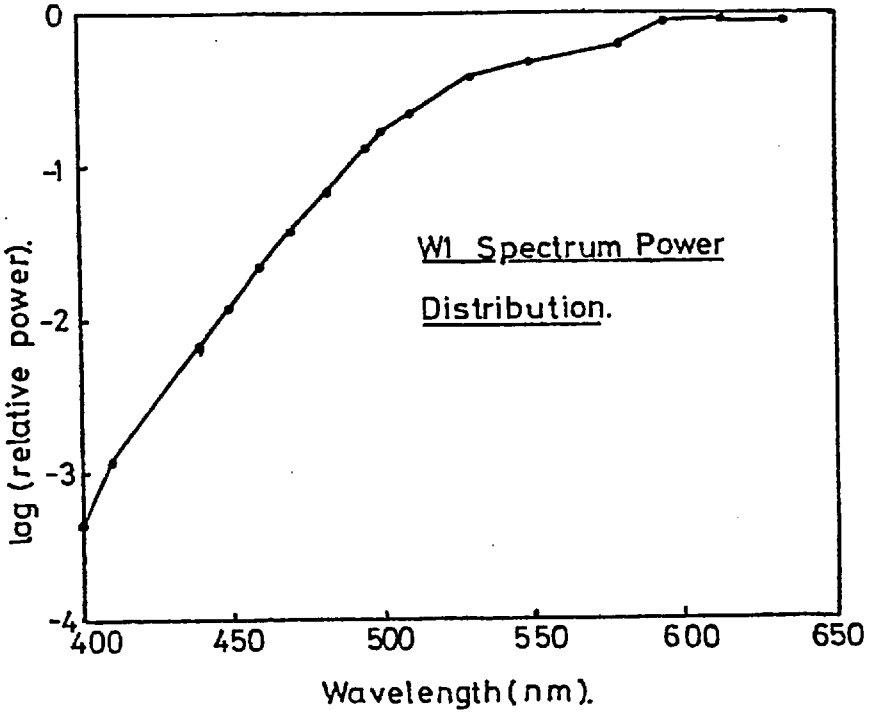

FIGURE 2.12 Energy distribution for test prism in focal plane W2 (shown in figure 2.6).

of the monochromatic lights provided by interference filters placed in other channels were also calibrated regularly.

The time- and space-averaged illumination levels of the two adaptation half-fields (figures 2.9a,b) were equated as follows, using the light-dependent resistor (LDR) mounted beyond the right eyepiece. (A galvanometer was used to monitor current through the LDR.) Light illuminating the LDR from either half of the adaptation stimulus was diffused using a sheet of ground glass, so that the space-averaged illumination levels of the two half-fields could be equated. The rate of flicker of the light, which was used to provide flickering adaptation stimuli, was increased to well above the flicker-response of the galvanometer so that the time-averaged illumination levels of the light from the two halves of the adaptation field could be equated.

Measurement of Retinal Illuminance

The retinal illuminance of the stimuli were measured as follows. A pressed magnesium-oxide tablet with one flat side was placed beyond the eyepiece E2 (figures 2.6 and 2.7) such that the flat surface was parallel to the plane of the eyepiece. A Holophane lumeter (type 48A) was used to measure the luminance of the surface of the tablet when it was illuminated by one of the stimuli. It was assumed for this measurement that the surface of the MgO tablet was perfectly diffusing and that its reflectance was unity.

If the distance from the exit pupil E2 (figure 2.6) to the tablet was d m and the luminance of the surface of the tablet was B ml, then the imaginary source of light in the plane of the exit pupil had an intensity of 10 Bd^2 cd and it produced a retinal illuminance of

$$E(\text{trolands}) = 10^7\ Bd^2 \qquad (2.1)$$

(Westheimer, 1966).

Wavelength Calibration

The wavelength scales of the W1 and W2 spectra were calibrated by substituting a line source (Phillips mixed gas spectral source, type Hg-Zn-Cd 0.9A B7) for the colorimeter source S1. The roof prisms at the spectra W1 and W2 were moved individually until one of the spectral lines was reflected into the exit pupil (E2, figure 2.6). The Cauchy equation was used to interpolate between the lines to obtain a continuous calibration.

Measurement of Shutter Durations and Shutter Rates

The frequency of flicker of light passing through the two rotating sectors (DS, figure 2.6 and SE, figure 2.7) and the shutter-durations (of shutters SH1, figure 2.6 and SH2, SH3, figure 2.7) were monitored on a calibrated oscilloscope connected to photodiodes mounted in the appropriate light beams.

General Experimental Precautions

Both the metacontrast apparatus and the colorimeter were adequately shielded against stray light using matt black card and curtaining. Observers were always required to dark-adapt for at least 15 minutes before any measurements were taken, and for at least 30 minutes before threshold measures were attempted. Observers sat on chairs which could be adjusted in height. Steady head positioning was maintained by the use of dental bites. The diameter of the artificial eye-pupils used was 2 mm unless otherwise stated.

Computer programs which were written for producing stimulus patterns and for evaluating data are described briefly in Appendix E.

CHAPTER THREE

AN INVESTIGATION OF INTERACTIONS OF ROD AND CONE SYSTEMS

3.1 Introduction

Electrophysiological data obtained from vertebrate retinae together with the retinal morphology of primates discussed in Chapter 1 indicate the existence of lateral rod-rod interactions, and the possibility of interactions between signals from adjacent rods and cones. In the experiments described in this chapter interactions between signals arising from stimuli falling on spatially adjacent areas of the retina have been investigated; those interactions which occur between signals arising entirely in the rod or cone systems are designated rod-rod or cone-cone interactions respectively, and those between signals arising in the rod and cone systems are designated rod-cone interactions.

Interaction between the rod and cone systems has been shown in the processing of colour in mesopic vision (Stiles and Burch, 1959; Clarke, 1960; McCann and Benton, 1969; Trezona, 1970; McCann, 1972; Stabell and Stabell, 1973, 1974, 1975a,b 1976a,b), in experiments involving threshold measurements (Maudarbocus, 1973; Lennie and MacLeod, 1973; Makous and Boothe, 1974; Blick and MacLeod, 1974; Frumkes and Temme, 1977; Temme and Frumkes, 1977; Latch and Lennie, 1977) and involving flicker and stimulus motion (Walters, 1971; MacLeod, 1972; Von Grunau, 1976; Ingling, Lewis, Loose and Myers, 1977). The reports mentioned in Chapter 1, which demonstrated rod-cone interaction in metacontrast, were published after the bulk of the measurements in this chapter were recorded. Further to showing rod-cone interactions, the data in this chapter show

the form of the rod-rod and rod-cone signal interaction in relation to spatial, temporal and colour attributes of the stimuli. An attempt was also made to identify the sites of interaction.

The relative stimulation of the rod and cone systems depends on the size of the stimulus and its position in the visual field. Wald (1945) determined the foveal cone and parafoveal rod spectral sensitivities using threshold measurements, and also the threshold illumination level of the cone plateau during dark-adaptation. The three sensitivity curves which he measured are shown in figure 3.1. The relative parafoveal cone and rod sensitivities can be measured at any wavelength from a plot of this nature. The difference between the rod and cone thresholds, and between foveal and extrafoveal cone thresholds is least for small stimuli, and these differences increase with increasing stimulus size (e.g. Arden and Weale, 1954). These facts were taken into account in choosing the stimulus configurations for this study.

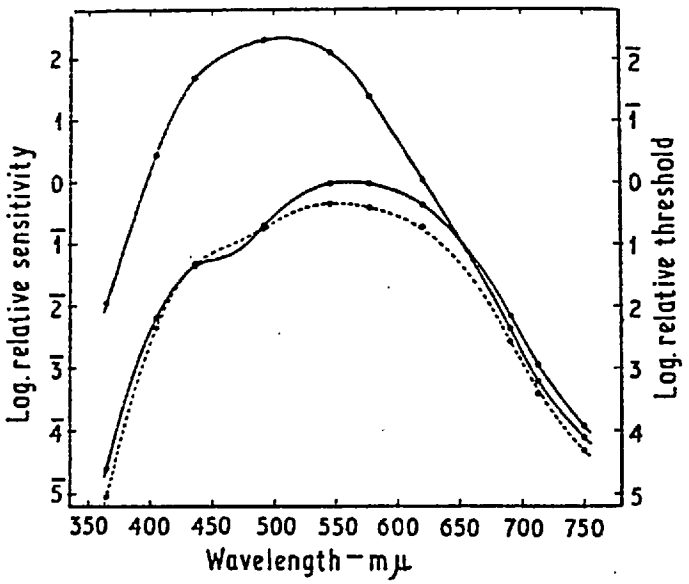

FIGURE 3.1 Sensitivity curves for foveal and peripheral cones compared with that for rods. Top curve: rods. Bottom curves: cones. The broken line refers to peripheral cones. (After Wald, Science).

The metacontrast masking effect discussed earlier (section 1.B.3) was chosen for the study of rod-rod and cone-rod interactions. A concentric disc-annulus stimulus pattern was adopted (figure 2.5), in which the probe stimulus disc field was masked by the non-overlapping

annular mask field surrounding it. The probe field was chosen such that it stimulated only rods, and the radiance of the annular stimulus required to mask this rod-stimulating field was the variable determined in the experiments. The masking effect was measured in this way for a number of wavelengths of the masking field, so that an action spectrum of masking could be plotted in terms of the radiance required for masking, versus wavelength. Since the probe field stimulated only rods, it should be expected that the masking action spectrum would be determined by the spectral sensitivity of the rod system if the masking interaction were purely rod-rod. The Stiles π_o field spectral sensitivity curve closely follows the spectral sensitivity of the rod system for the average observer, so that the extent to which the masking action spectra deviated from the π_o shape would provide a measure of cone-rod interaction. In the experiments, the probe and mask stimuli were presented for short durations (20 ms). The time-difference between the onsets of these two stimuli (ΔT) and the stimulus spatial conditions were varied, in order to establish their influence on the masking action spectrum.

A preliminary investigation was performed to find a stimulus location in the visual field suitable for studying the masking effects, and to ascertain that the probe fields stimulated only rods. It was necessary to establish a reliable criterion by which observers could judge the threshold of the probe stimulus in the presence of the masking field. A calculation of the effects of scattered light is also given.

The following criteria were used in selecting the stimulus location for the study of metacontrast effects. First, it was required that the probe stimulus should be clearly visible in the

absence of a masking field and that, at least for some stimulus wavelengths, it did not stimulate the cones. Second, spatial resolution had to be as high as possible to facilitate spatial discrimination between the probe and masking stimuli. Last, the threshold of the mask stimulus had to be determined by rods at some wavelengths and by cones at others, so that a study could be made of both rod-rod and cone-rod signal interaction.

In the first preliminary experiment the threshold spectral sensitivity of a 1.2' probe stimulus was determined for presentation of the stimulus at the fovea and at eccentricities of 3^{o}, 6^{o} and 20^{o} of visual angle from the fixation point along the nasal horizontal meridian. The small stimulus size was selected to minimize the difference between the rod and cone threshold illumination levels at any given retinal location (Arden and Weale, 1954). The results of this experiment were used to choose the stimulus position and wavelength which together satisfied the three criteria stated above. The experiment was repeated for a larger stimulus in order to investigate the resulting changes in shape of the threshold spectral sensitivity curves. In a second preliminary experiment, the difference between the rod and cone threshold illumination levels was determined at 495 nm from dark-adaptation threshold curves for various sizes of probe stimulus. These determinations allowed the illumination levels of the probe stimuli to be chosen such that these stimuli were presented well above the rod threshold illumination level for easy visibility, but below that of the cones. The third preliminary experiment was undertaken to establish a masking threshold criterion which yielded repeatable measurements for a number of observers. Finally, the amount of light scattered by the annular mask stimulus was calculated (Appendix C).

The masking experiments which comprised the principal experimental investigation are listed below, and the aims of the experiments are stated.

i) Masking action spectra were measured for B.N. The variable was ΔT, the separation in time between the onsets of the probe and mask stimuli. The probe field stimulated only rods and changes in the masking action spectrum with changes in ΔT were obtained.

ii) The above experiment was repeated for three further observers, one of whom was a deuteranope, for two values of ΔT for each observer. These experiments were also performed with a rod-stimulating probe field, and were designed to determine the general applicability of the data of experiment (i) obtained for the author, B.N.

iii) The probe stimulus wavelength was changed to red so that it stimulated only or mainly cones, in order to study the masking of cone signals.

In the remaining experiments, the probe stimulus was chosen to stimulate only the rod mechanism.

iv) The probe stimulus was varied in diameter to see whether the masking action spectrum changed in shape.

v) The stimuli were presented dichoptically to ascertain whether the metacontrast masking which was obtained monoptically was due to interactions in the retina or beyond the optic chiasm.

vi) The mask stimulus was changed to a uniform disc so that the effects of uniform and annular masking fields could be compared.

vii) The masking experiment was repeated in the presence of a steady

red background circular disc or an annulus. Such stimuli preferentially suppress the long-wavelength cone sensitivity over restricted regions of the visual field, and were used to provide further information about the form of the rod-cone interaction.

viii) The value of ΔT was varied for red and green annular mask patterns in order to study the time-course of masking.

ix) The mask stimulus was changed to an annular windmill pattern and was presented for 3 second periods. The windmill pattern could be rotated, and different rates of rotation could be used to stimulate preferentially either the rods or the cones. The probe stimulus was presented at the centre of the annular windmill pattern, and the masking effect of the windmill was measured.

In the discussion the effect of scattered light is considered, and it is shown that the masking effects cannot be explained by scattered light. It will be argued that the masking results can therefore only be explained by assuming that under some experimental conditions rod-cone interaction occurs in metacontrast. The contributions of the different cone mechanisms to the experimentally determined action spectra are considered. The rod-cone interaction is discussed in relation to the masking data. An important result concerning rod-rod summation interaction is deduced from the dark-adaptation data (of preliminary experiment 1). The results are compared with those of other psychophysical investigations and are examined in relation to neurophysiological data.

3.2 Procedure

The metacontrast experiments were designed to study mainly cone-rod signal interaction. The cone threshold is very sensitive

to lateral and vertical changes in the eye-position at the exit-pupil of Maxwellian viewing systems (because of the Stiles-Crawford effect, Stiles and Crawford, 1933), whereas the rod threshold is almost independent of eye-position providing there is no vignetting of the stimulus beam. It was therefore necessary to align the observer's eye position accurately and repeatably at the start of each session, to ensure that the relative cone and rod threshold energies remained constant from one session to the next. This was accomplished by making use of the chromatic fringes which can be seen when a mixture of stimulus wavelengths is focussed through a non-central point in the pupil. The chromatic aberration effect was eliminated by adjusting the observer's head position such that light entered the eye axially, in the following way. The disc and annular stimuli (figure 2.5), both of wavelength 656 nm, were first presented to the right eye, and the mask stimulus was moved until it was concentric with the disc stimulus. This process was independent of eye-position, since the wavelengths of the lights illuminating both stimuli were the same. The disc stimulus wavelength was changed to 435 nm, and the observer used fine-position controls on the dental clamp support to move his eye-position to realign the blue disc and red annulus concentrically. Pilot measurements established that this eye-positioning was repeatable to within 0.5 mm, and that changes in foveal threshold resulting from movements in head-position of this magnitude were negligible. Following alignment the observer was dark-adapted for at least 30 minutes to allow full recovery of rod sensitivity. Measurements then commenced, and each session lasted at most 3 hours.

3.3 Preliminary Measurements

1. Threshold spectral sensitivity curves were recorded at the fovea and at three locations away from the fovea for the author, B.N. Most of the measurements were made for two circular probe stimuli with diameters of 1.2' (0.02°) and 23' (0.38°) of arc, the stimulus duration was 20 ms and measurements were made for each of 18 near-monochromatic wavelengths. The visibility threshold was approached by reduction from suprathreshold illumination levels and the illumination level of the probe stimulus was decreased during successive presentations until the probe stimulus was invisible for three consecutive presentations. The order of presentation of the probe wavelengths was randomized. Four separate determinations were made of the masking action spectrum on different days for each stimulus. The observer dark-adapted for at least 45 minutes before each experimental session.

2. Parafoveal and foveal dark-adaptation curves were obtained for the author, B.N., in the following way. The author adapted to a circular field of white light (correlated colour temperature 3000° K) of diameter 5° located foveally or 6° from a dim red fixation point along the nasal horizontal meridian. The illumination level of the adapting light exceeded 6.4 log trolands and the field was presented for 120 seconds. The radiance required for threshold visibility during the time following its offset was determined for circular probe stimuli of various diameters, which were presented concentrically with the patch of adapted retina. The visibility threshold of the probe stimulus was again determined by reducing the radiance of the probe stimulus during successive presentations, until the probe was no longer visible. The probe stimuli were of wavelength 495 nm or

656 nm and of duration 20 ms. The threshold radiance levels were measured over a period of between 30 and 40 minutes following cessation of adaptation, and the average threshold radiances were again determined after three hours of total darkness. Foveal determinations were made using a fixation stimulus consisting of four dim red spots, placed on the corners of an imaginary square of arc length 30' (this fixation stimulus was also used for foveal threshold determinations made in the next preliminary experiment).

The average radiances during the rod and cone plateaus of the dark-adaptation curves were determined for each parafoveal probe stimulus. The differences between these values gave a measure of the differences between the rod and cone threshold radiance levels.

3. The masking effect of an annular stimulus was measured for three observers using a circular concentric probe stimulus. This preliminary experiment was performed to establish a reliable threshold criterion for measuring masking effects.

The stimulus configuration used is shown in figure 2.5; both the probe and the annular mask stimuli were presented for 20 ms. The wavelength of the probe stimulus was 495 nm, and the 18 wavelength values of the masking stimulus were used. The probe stimulus was presented at 0.5 log units above visibility threshold. The visibility threshold of the probe stimulus was determined by reducing its radiance until it was invisible for three consecutive presentations. A 0.5 log unit filter was then removed from the probe stimulus channel, so that this stimulus appeared at 0.5 log units above visibility threshold during the following presentations. When both the annular mask and circular probe stimuli were presented, there was a fixed time delay (ΔT, which could be chosen positive or negative) between their onsets. The radiance of the mask stimulus was initially set at

the minimum instrumental setting, and the observer increased it after each presentation, thereby reducing the visibility of the probe stimulus. The visibility threshold of the probe stimulus in the presence of the masking field was judged by one of two criteria:

(a) when the disappearance criterion was used to judge the visibility threshold of the probe stimulus, the radiance of the annular masking field was slowly raised until the probe was no longer visible;

(b) when observers used the null criterion, they inhibited the action of the shutter controlling the presentation of the probe (SH1, figure 2.1) during alternate presentations, so that the annulus appeared alone for alternate flashes. The position of the wedge controlling the mask radiance was recorded when the observer could no longer distinguish between successive presentations (with or without the probe).

The onset time of the mask stimulus was measured with respect to that of the probe stimulus. The time difference between the onsets of the two stimuli, ΔT, was positive when the onset of the probe stimulus preceded that of the mask stimulus. The order of presentation of the mask stimulus wavelengths was randomized before each session, and ΔT was kept constant while the wavelength of the mask stimulus was varied. Three observers took part in the preliminary masking experiment and values of ΔT equal to +50 ms and +150 ms were used. All three observers had normal colour vision, and one (D.H.F.) used a corrective lens (+2 diopters) in front of the right eyepiece. Four or five determinations were made of the masking field radiance for each mask stimulus wavelength.

The experimental data were plotted as action spectra with the radiance of the annular mask field required to bring the probe stimulus to threshold plotted against wavelength. The data points are the mean values of the radiance determinations at each wavelength,

expressed as the number of quanta per second contained within a cone of solid angle of 0.25 arc. min^2 in object space. A solid angle of 0.25 arc. min^2 corresponds to the angular area of cross-section of an 'average' rod in the parafovea at 10^o from the fovea (Westheimer, 1966), so that the radiance measure used gives an approximate idea of the number of quanta incident per second on each rod. Absorption by, and scatter from the optical media of the eye were ignored in the calculation of the data, which thus refer to the number of quanta, contained in a field area of 0.25 arc. min^{-2}, incident on the cornea per second. The lengths of the lines which were drawn through the points are twice the standard deviation of the mean values.

3.4 Results of Preliminary Experiments

1. Threshold Action Spectrum Curves

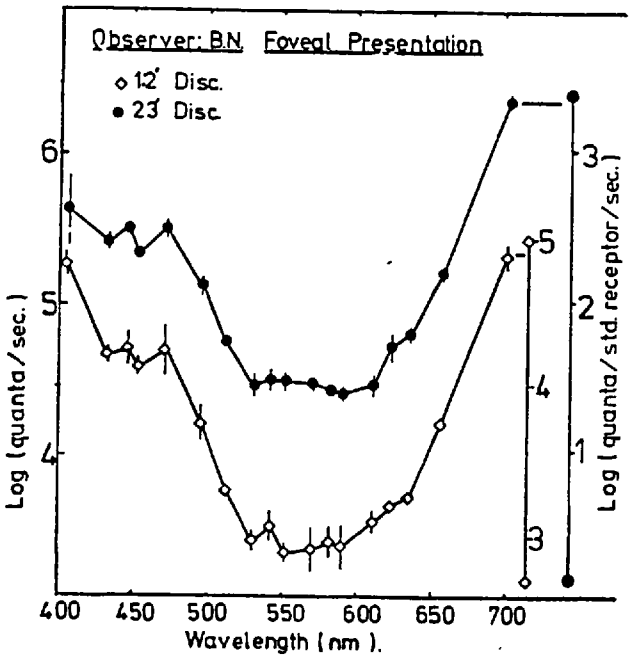

FIGURE 3.2 Threshold radiant flux levels of probes presented foveally for 20 ms.

The average threshold action spectra determined for probe stimuli of different sizes (1.2' and 23' in diameter) and for varying locations on the retina (0^o, 3^o, 6^o and 20^o nasally from the fixation point along the horizontal meridian) are shown in figures 3.2 to 3.5. The radiances for threshold detection of the probe stimulus are plotted in log quanta per second present in a cone of solid angle 0.25

arc min^{-2} (incident on the cornea, right-hand ordinate scales), and also in log quanta per second present in the whole probe stimulus (left-hand ordinate scale).

The rod (π_o) action spectrum is plotted on the graphs of the extrafoveal sensitivity curves (dotted curves, figures 3.3 to 3.5).

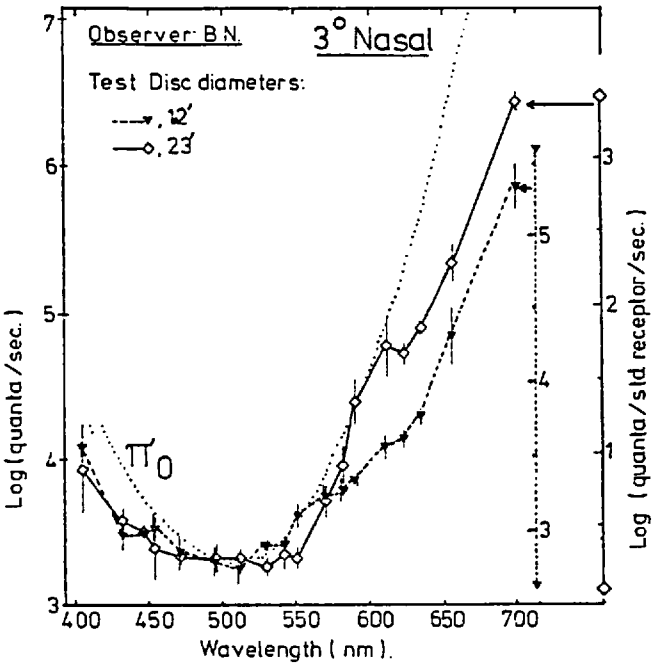

FIGURE 3.3 Threshold sensitivity 3° from the fovea.

It is seen that the extrafoveal threshold sensitivity coincides with the π_o curve at wavelengths around the peak threshold sensitivity. The wavelength range over which the threshold sensitivity is determined by the rod (π_o) sensitivity can be seen to increase with the eccentricity of any one stimulus (from 3° to 20° away from the fovea), and also, for a given retinal location, with the stimulus size. The differences between the shapes of the π_o curve and the threshold action spectra at short wavelengths might be explained by absorption of the optical media and/or the action of the π_1 mechanism. The absorption of the optical media at long wavelengths is constant over a wide wavelength range (figure 1.2), so that the differences from the π_o curve at long wavelengths must result from the cone threshold sensitivity exceeding that of the rods.

The threshold action spectra obtained for the 1.2' and 23' probe stimuli at 3° and 6° from the fixation point deviate from the shape of the π_o action spectrum at wavelengths greater than

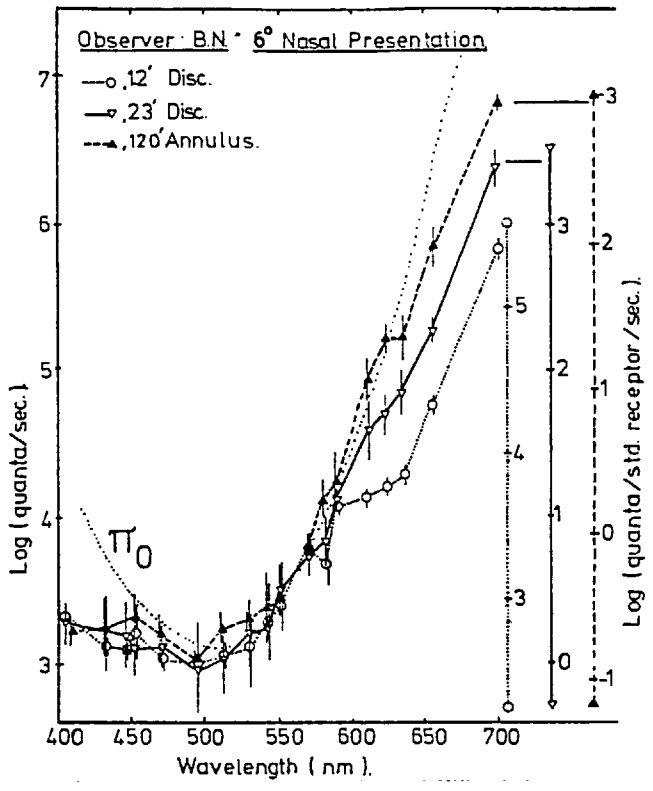

FIGURE 3.4 Threshold radiant flux versus wavelength at 6° from the fovea.

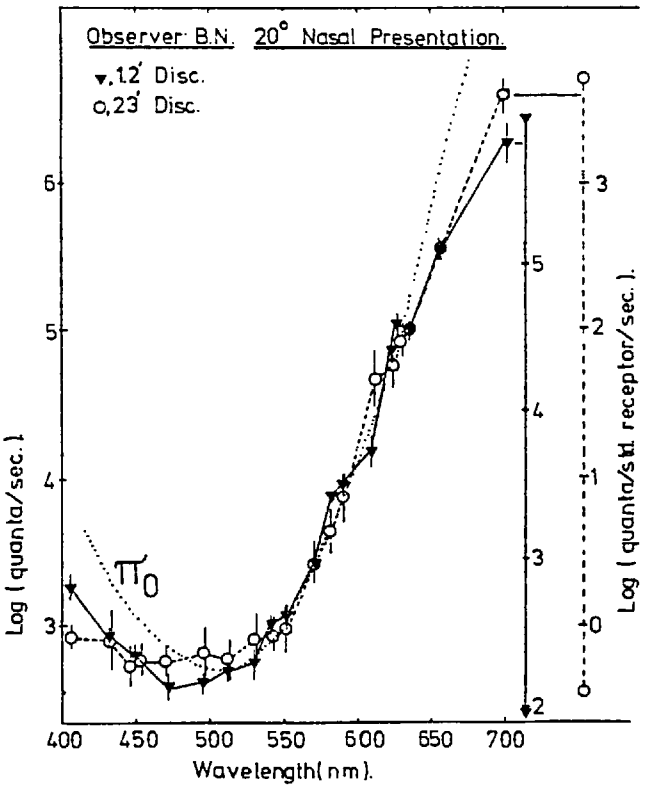

FIGURE 3.5 Radiant flux action spectrum at threshold measured at 20° on the nasal side of the fixation point.

about 600 nm (figures 3.3 and 3.4) and the threshold action spectra obtained at an eccentricity of 20° follow the π_0 action spectrum to about 660 nm (figure 3.5). It was mentioned in the introduction that one criterion for the choice of eccentricity was that stimuli should excite cones at some wavelengths and rods at others. Therefore a position of 20° from the fixation point was unsuitable, as the threshold of stimuli at this eccentricity is determined by rods for most wavelengths. The positions of 3° and 6° from the fixation point were both considered suitable, since at these locations the thresholds of red stimuli (above about 600 nm in wavelength) are determined by cones. Also, the space between the probe and mask stimuli of figure 2.5 could

be resolved at both of these locations, so that visual acuity at these eccentricities was sufficient for the masking studies. Both positions (3° and 6° from the fixation point) were used in the course of the metacontrast experiments.

2. Dark-Adaptation Data

The dark-adaptation curves obtained for five sizes of probe stimulus are shown in figures 3.6 and 3.7. The curves all show a rapid initial recovery of sensitivity following adaptation to a white light source. For the 495 nm stimuli this is followed after about the twelfth minute by a recovery of sensitivity having a longer time-constant. The parafoveal sensitivity curves obtained during the first and second threshold-level plateaus of dark-adaptation are determined by the cone and rod systems respectively (Hecht, Haig and Chase, 1937; Wald, 1945). If the threshold radiance of the cone systems remains unchanged after the absolute

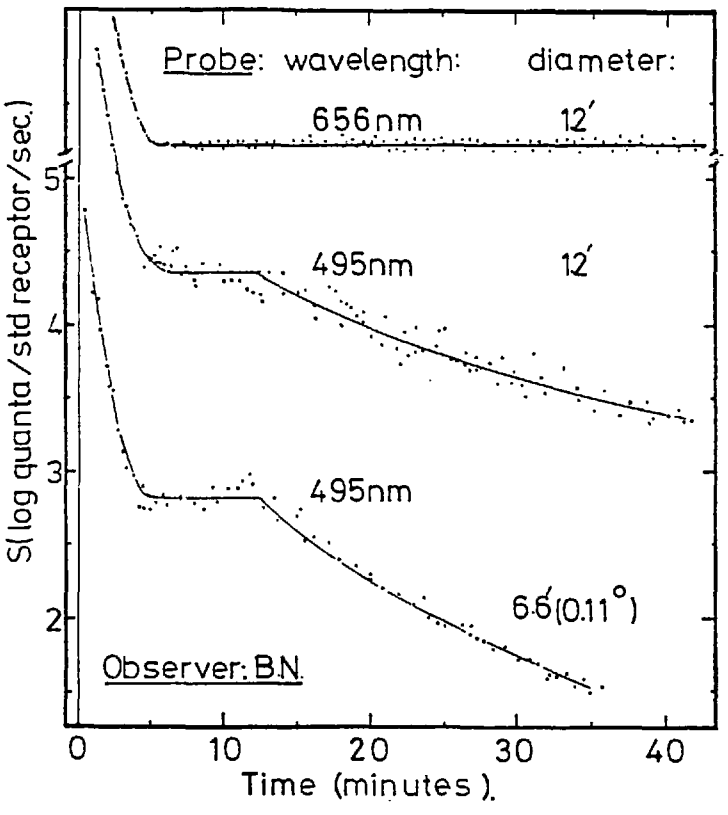

FIGURE 3.6 Log of the threshold radiance (measured in quanta/sec/ standard receptor area) following the offset of a white adaptation light. Presentation was 6° nasal.

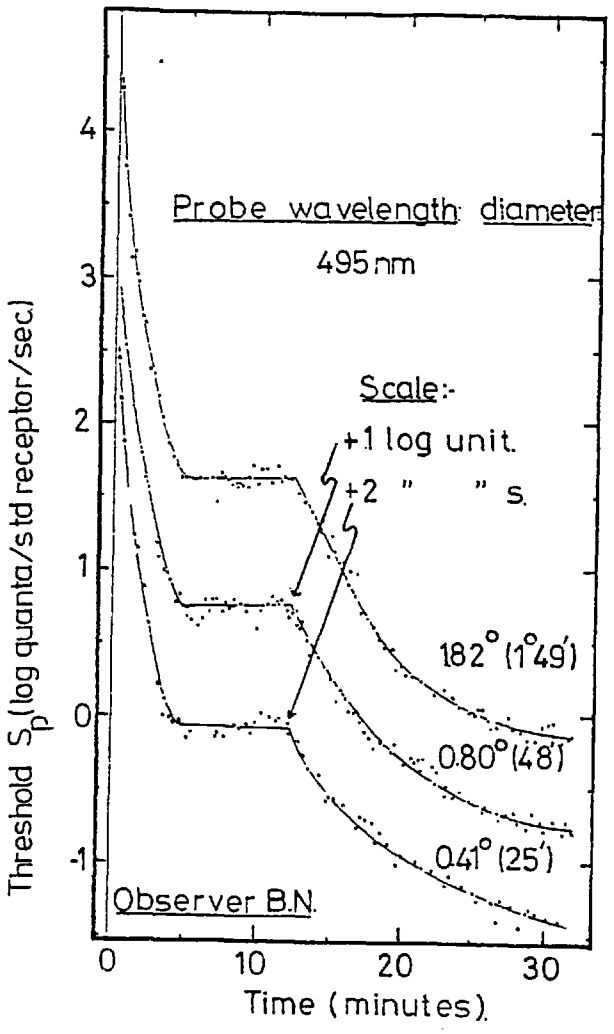

FIGURE 3.7 As in figure 3.6, for larger probe stimuli.

threshold has fallen below the cone plateau, then the difference in threshold radiance between the two plateaus should give a measure of the difference in threshold radiance between the two systems for any particular probe stimulus. It has been suggested however that the cone plateau might decrease slowly during the period when the absolute sensitivity is determined by the rods (e.g. Makous and Boothe, 1974). This possibility was investigated as follows. The threshold radiance of a 1.2' probe stimulus was determined during dark adaptation at a wavelength of 656 nm, and the relative visibility threshold curve is shown as the upper trace in figure 3.6. The threshold remained constant during the portion of the plateau shown, and was the same on average two, and again three hours after the bleach. At the dark-adapted threshold for the eye the 656 nm stimulus should stimulate the π_5 mechanism while the cone threshold plateau observed with a probe stimulus at 495 nm should correspond to that of the π_4 system. It could still be argued that although the π_5 mechanism

threshold remains constant after 12 minutes following the bleach, the π_4 mechanism threshold decreases gradually. However, it was found that the threshold of the 1.2' probe, when it was presented foveally with a wavelength of 495 nm, followed the same time-course of recovery as that of the red stimulus of figure 3.6, and the plateau remained at constant radiance-level for three hours. Thus it is unlikely that the threshold of the cone system most sensitive to 495 nm stimuli, presented 6° from the fovea, changes during the phase of recovery of rod sensitivity.

The averages of the threshold radiances for different probe sizes were evaluated for the cone plateaus between the sixth and eleventh minutes. The average values are plotted against the diameter of the probe field as the filled circles in figure 3.8. The average rod sensitivities following three hours of sensitivity recovery are plotted as open diamonds on the same figure.

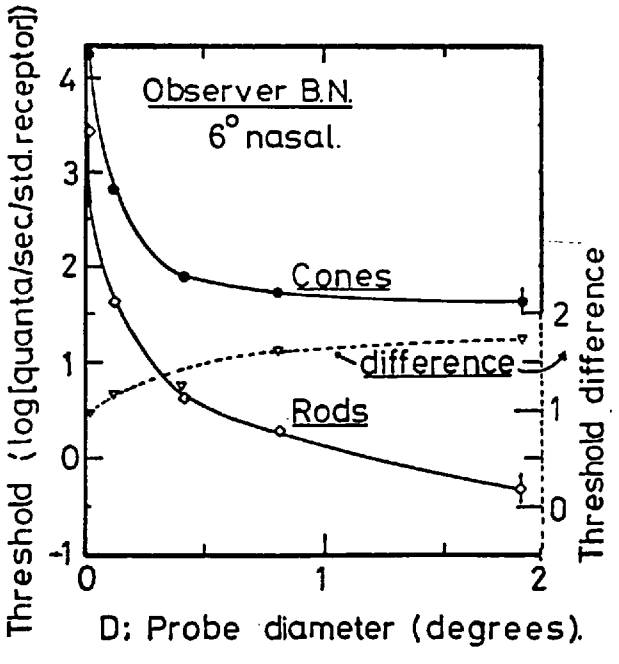

FIGURE 3.8 Relative radiance thresholds of the rod and cone plateaus for various probe diameters. The cone-rod threshold difference is shown by the broken line (right-hand ordinate).

The differences between the cone and rod threshold radiances are indicated by the broken line (right hand ordinate). It can be seen that the difference is never less than 1 log unit. It was decided on the basis of these results to present the probe stimuli at 0.5 log units above absolute threshold during the masking experiments. The illumination levels of the probe stimuli would

therefore be at least 0.5 log units below the cone threshold (figure 3.8), so that the detection of these stimuli would be determined entirely by the rod mechanism. The data of figure 3.8 were obtained at an eccentricity of 6^{o}. Masking measurements were also made at an eccentricity of 3^{o} using a 23' diameter probe stimulus: the average difference in the threshold radiance between the cone and rod plateaus for this stimulus was 1.1 log units, so that this stimulus could also be presented at 0.5 log units above absolute threshold without stimulating the cones.

3. Results of Experiment to Establish a Reliable Threshold Criterion

This metacontrast masking experiment was performed using the stimulus configuration shown in figure 2.5.

The data which were obtained for DHF, using both the disappearance and the null criteria to judge the threshold of the probe stimulus, are shown in figure 3.9 with ΔT = 50 ms. The masking field masks the probe more easily at short wavelengths when the disappearance criterion is used. Comparable data for ΔT = +150 ms are shown in figure 3.10 (for observer MRI), and in this case the differences between the curves obtained by the two methods are even greater than for observer DHF. Further results for observer BN, which reflect

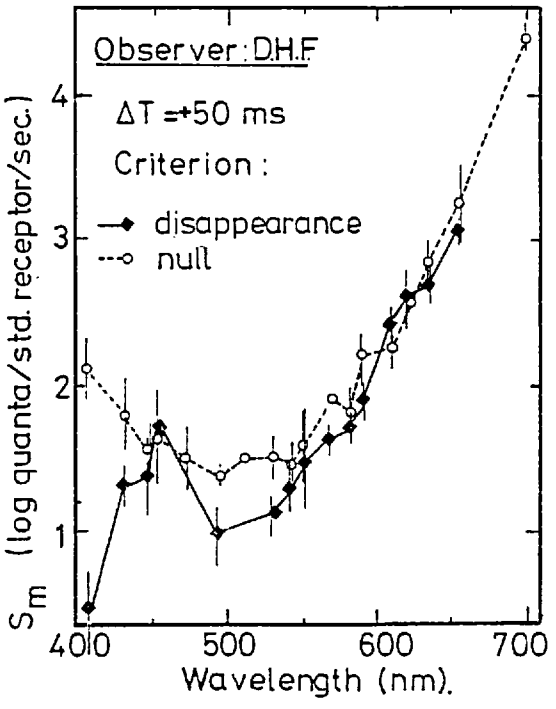

FIGURE 3.9 Plot of masking radiant flux (Δm, log quanta/standard receptor/second) versus wavelength, for two threshold criteria.

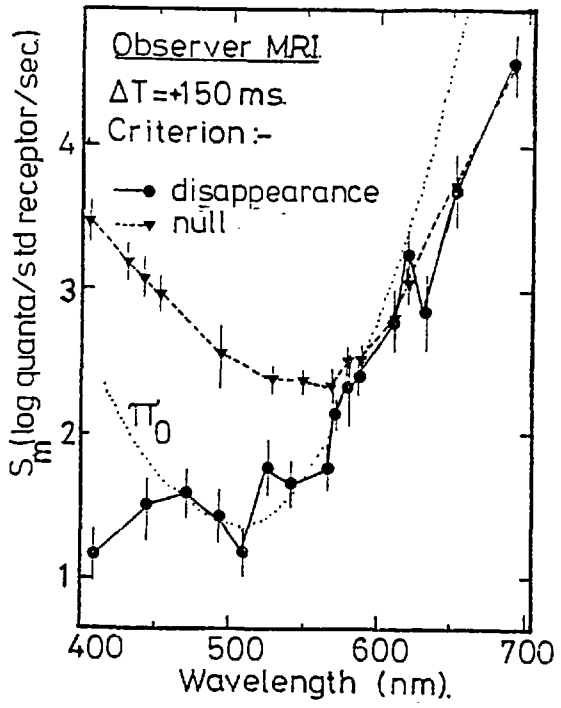

FIGURE 3.10 Masking action spectra obtained using the two criteria (observer MRI).

the differences between the two criteria, are shown in figure 3.11 (ΔT = +150 ms). Care was taken during the determination of these data to focus the annulus precisely for each wavelength of light in turn. Thus the results cannot be explained by the chromatic adaptation resulting from defocussing of the mask stimulus. It is concluded that the sensitivity of masking by the annular mask stimulus is highly dependent on the criterion by which the disappearance of the probe is judged, especially for short-wavelength masking stimuli (e.g. figure 3.11). All observers found that it was more difficult to judge the disappearance of the probe stimuli for short wavelength masking stimuli and easier for long wavelengths. When the annulus was reddish, its inner edge appeared sharp and the centre appeared black when the probe threshold was reached. The detection of the probe just above its threshold was facilitated by the colour

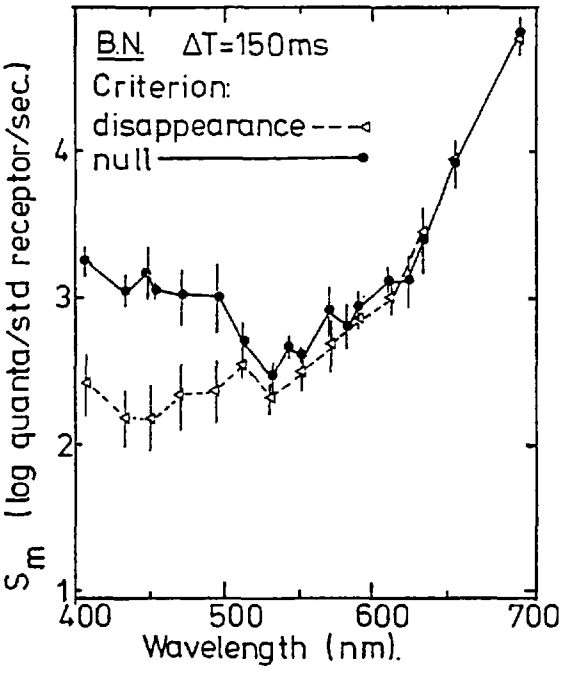

FIGURE 3.11 Masking data for BN.

difference between the red mask and the whitish probe. On the other hand, for masking stimuli of wavelength below about 550 nm, the edges were ill-defined, and the annulus hole appeared to be filled with scattered light. When presented at supra-threshold radiant flux levels, the probe stimulus was seen indistinctly against this 'scattered' light. Similar difficulties associated with short wavelength masking stimuli have been noted by Alpern (private communication).

It was found that even for a single value of ΔT, the action spectra obtained using the disappearance criterion varied from week to week for inexperienced observers, and there appeared to be no correlation between the data for different observers, especially at short wavelengths. The null criterion yielded highly reproducible results however. This can be seen from the low standard deviations obtained by DHF using the null criterion: the data points of figure 3.9 shown as open circles were obtained over a period of five months. The null criterion was consequently adopted for determining the threshold of the probe stimulus for further masking experiments.

3.5 Study of the Masking of Rod-Stimulating Probe Fields: Procedure

For the following nine experiments, the general experimental method and graphical representation of data in the introduction, Section 3.1, were used. In the experiments the null criterion was adopted for judging the threshold of the probe stimulus in the presence of the masking field, as the third preliminary experiment (experiment 3, Section 3.4) had revealed that this criterion yields reproducible results. The procedure used for each of these nine experiments is given below.

(i) Action spectra of metacontrast masking were measured for observer BN for eight values of ΔT between ΔT = -100 ms and +150 ms. Each action spectrum was determined for 18 wavelengths of masking light using the null criterion to judge the disappearance of the probe stimulus. The probe stimulus was set at 0.5 log units above visibility threshold with no background before each measurement of masking, and the arrangement of the fixation point and the probe and annular masking stimuli is shown in figure 2.5. Each determination of the masking effect was the average of four measurements, and 32 separate sessions were performed in order to obtain the data. In any one session, the variable was the wavelength of the masking stimulus, and ΔT was changed between sessions. The order of presentation of the mask stimulus wavelengths were chosen randomly for the first session. The order for subsequent sessions was calculated so as to reduce to a minimum the number of times any one wavelength was preceded or followed by any other wavelength. The eight values of ΔT were each used four times, and the ΔT value for each session was chosen randomly. The observer dark-adapted for at least 30 minutes before each session after aligning himself comfortably by the method described earlier. The maximum rate at which stimuli could be presented was reduced electronically to once every 3 seconds.

(ii) A limited number of masking action spectra were obtained for a further three male observers using the procedures described in (i) above. The observers are listed below, together with their approximate ages, colour vision characteristics and the values of ΔT which they used:

DHF: 30 years, normal colour vision, ΔT = +50 ms, +250 ms.

MRI: 25 years, normal colour vision, ΔT = +50 ms, +150 ms.

NS: 21 years, deuteranope, ΔT = 0 ms, +150 ms.

The remainder of the experimental measurements were obtained for observer BN.

(iii) The masking of a red probe stimulus was measured. The annular masking field is shown in figure 2.5; it had inner and outer diameters of 54' and 2^{o} respectively, and was presented 6^{o} nasally from the fixation point along the horizontal meridian. The 23' probe field appeared concentrically with it, and was illuminated by light from a Wratten long-wavelength-pass filter (no. 609) with a cut-off wavelength of 690 nm. The red probe stimulus was also set at 0.5 log units above visibility threshold before each measurement, and so stimulated only or mainly cone mechanisms. Stimuli were presented only every ten seconds or at longer intervals and the action spectrum of masking was measured as before.

(iv) The annular mask stimulus was again presented 6^{o} nasally, and four circular probe stimuli with diameters of 1.2', 6.4', 12' and 23' were presented at the centre of the annulus. In this experiment, the wavelength of the probe stimuli was 495 nm. The measurements were made by BN using a value of ΔT = +100 ms for the three larger stimuli and four values of ΔT for the 1.2' probe.

(v) The metacontrast masking effect was measured dichoptically for BN. Dim red fixation points were presented to each eye in relative positions that allowed them to be fused easily when viewed binocularly. The mask and probe stimuli were presented 6^{o} nasally in the right eye

and left eye respectively, and had the dimensions shown in figure 2.5. The right eye was aligned so that stimuli entered it axially, and the left eye-piece was adjusted for comfortable viewing. Binocular rivalry was obtained, and so an attempt was made to induce preferential dominance of either eye by presenting a larger, brighter or flickering fixatio stimulus to one eye. However this introduced difficulties associated with fusion, so the masking was measured with small steady fixation points. In order to overcome false results arising from binocular rivalry, the threshold criterion was changed to one for which each of five pairs of presentation could not be distinguished, when each pair consisted of one presentation with the probe stimulus and one without. It was decided that the presentation of five pairs of stimuli would take longer than the time for which one eye dominates the visual responses. The action spectra were obtained for ΔT = -50 ms and +50 ms.

(vi) The masking effect was again measured using a 23', 495 nm probe stimulus located 3^{o} nasally. The mask stimulus for this experiment was a circular disc of diameter 23' or 2^{o} which was presented concentrically with the probe stimulus. The masking was measured, using the null criterion to judge the threshold of the probe stimulus, both monoptically and dichoptically. The experiment was repeated monoptically using a 5^{o} circular masking field, and eight diameters of probe stimulus were used for a value of ΔT = 0 ms.

(vii) In this experiment the magnitude of metacontrast masking was studied in the presence of red background fields which were circular discs or annuli (figure 3.12). These background discs or annuli were presented concentrically with the metacontrast stimuli

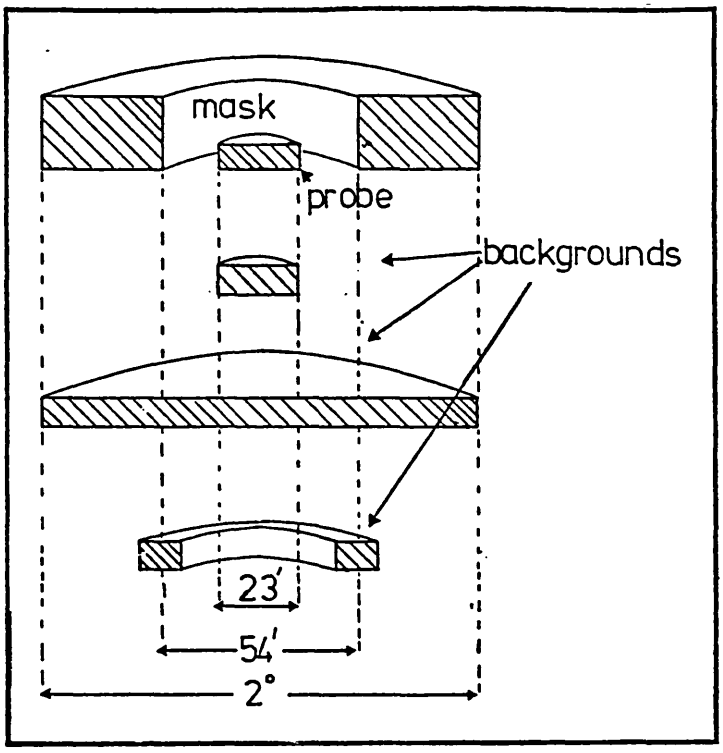

FIGURE 3.12 Cross-section of stimuli.

for three second periods. The stimuli were located 6° nasally from the fixation point. A Wratten infra-red filter was used to provide the red light - this filter has a negligible transmission below 700 nm (<0.5% transmission at 680 nm). The metacontrast stimuli were presented 1.5 seconds after the onset of the three second red background fields (figure 3.13). The probe field diameter was 23' of arc, and the inner and outer diameters of the mask field were 54' and 2° respectively (figure 3.12). Two background discs and one annulus were used. The background disc diameters were 23' (the size of the probe field) and 2° (equal to the mask outer diameter). The average diameter of the background annulus was 54', and its width was 10' so that it covered the inner edge of the masking annulus but did not overlap with the probe field. The time between the onsets of the probe and mask

stimuli, ΔT, was either 0 ms or +100 ms.

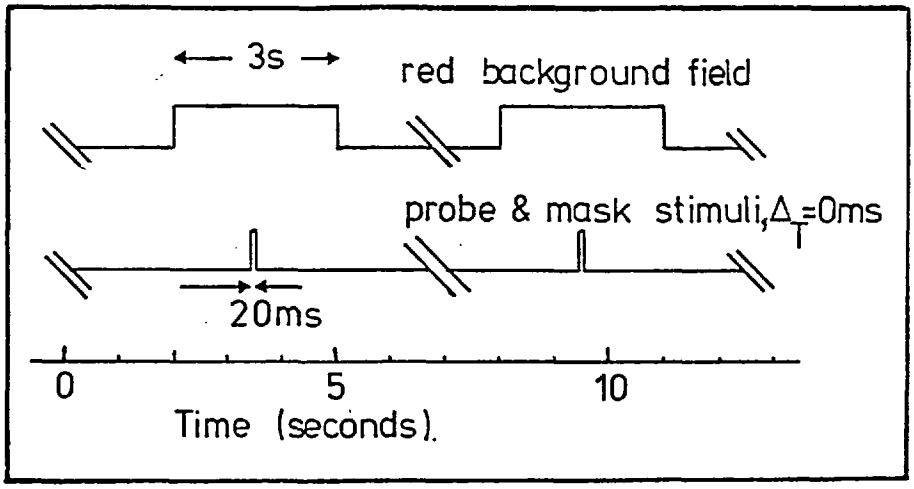

FIGURE 3.13 Timing diagram of red background fields.

(viii) The magnitude of the metacontrast masking effect was measured for the probe and mask stimuli of different sizes centred 6^{o} nasally (figure 3.14). In this case the variable was ΔT, the difference in time between the stimulus onsets (defined in section 3.38). The wavelength of the probe stimulus was 495 nm, and two masking stimulus wavelengths were investigated - 495 nm and 611 nm. The data were again measured in terms of the radiance of the masking stimulus, and these values were plotted against ΔT.

(ix) In this experiment the masking effects of an annular windmill masking stimulus (figure 3.14) was measured. The windmill pattern could be rotated at different speeds. The rotation speeds of the annular windmill were measured as the rate at which sectors passed a stationary point on the annulus, in cycles per second. The light illuminating the masking stimulus was switched on for 3 second presentations, during which time steady fixation was maintained. It was noticed that the windmill mask, when rotated

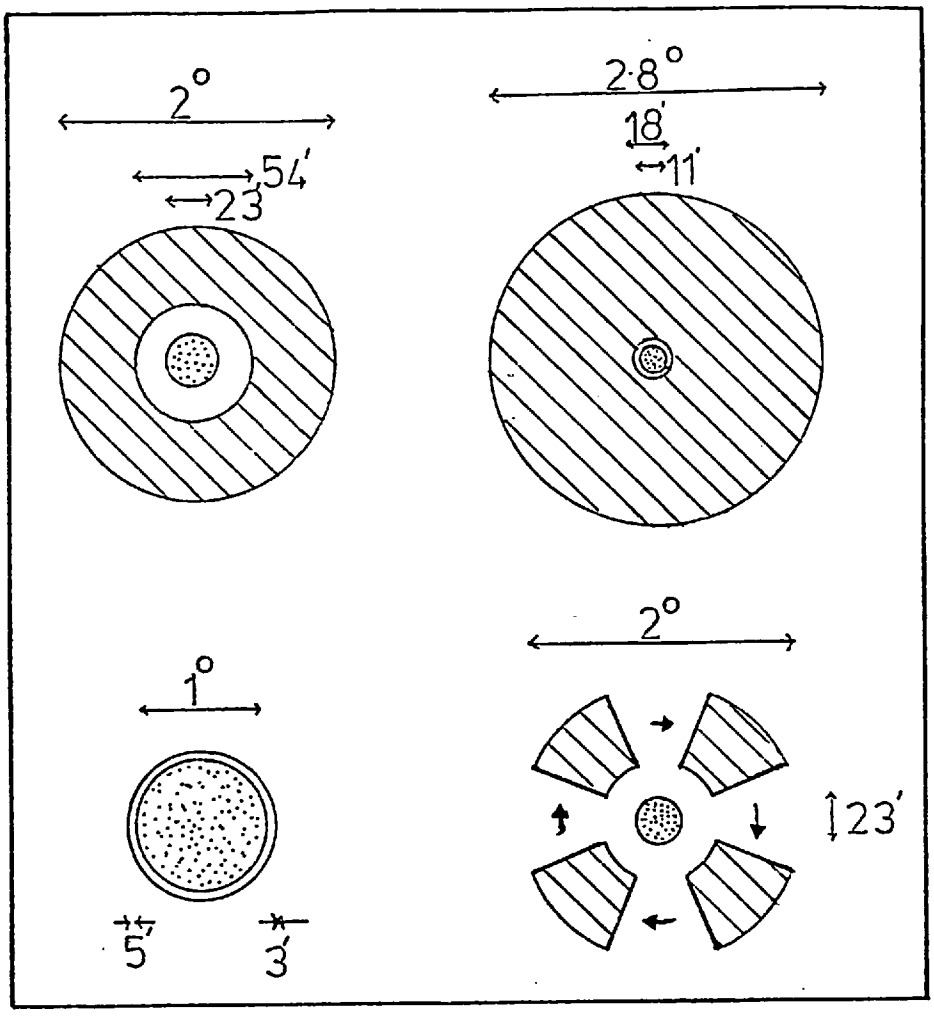

FIGURE 3.14 Mask and probe stimuli.

slowly, appeared to slow down and stop, and the windmill fans appeared to 'spiral' inwards, during the 3 second presentations. The slowing-down is similar to the 'beating' phenomenon described by Foster (1968). The probe was presented 1.5 seconds after the mask onset, and the energy of the mask was increased from a low value until successive presentations, with and without the probe, could no longer be distinguished (the null criterion). The masking action spectrum was obtained for four speeds of rotation of the windmill pattern and at 18 wavelength. The masking effect was measured four times for each condition in separate sessions and the average value was determined.

3.6 Results of Masking Experiments

(i) The masking action spectra for the stimulus configuration shown in figure 2.5, with the probe stimulus wavelength equal to 495 nm, were determined using the null threshold criterion for observer BN. The results are shown in figures 3.15 to 3.19. The action spectra appear together in 3.20, with their ordinate values adjusted so that they coincide at a wavelength of 495 nm. The curves become progressively broader in shape as ΔT increases from -100 ms to +150 ms (positive ΔT values indicate that the onset of the probe stimulus precedes that of the mask stimulus). The π_o action spectrum is drawn alongside these curves, for ΔT = -100 ms, +50 ms and +150 ms (figures 3.15, 3.19 and 3.20), in such a way that the π_o and masking action spectra coincide at around the

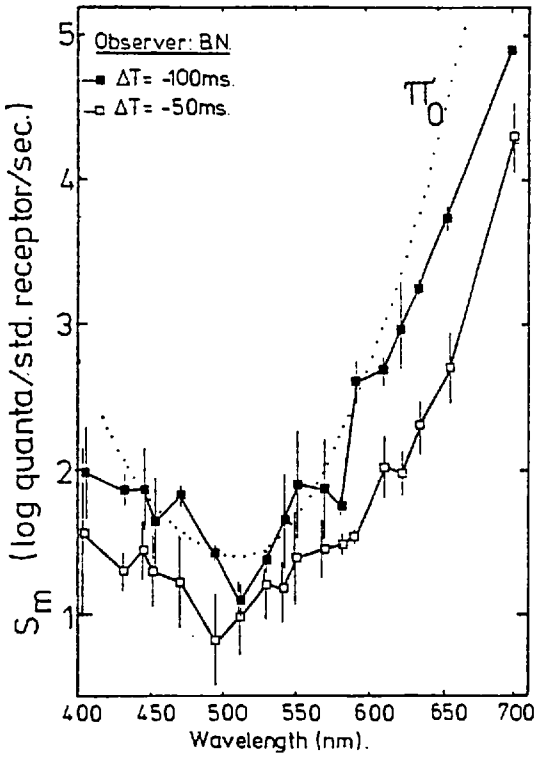

FIGURE 3.15

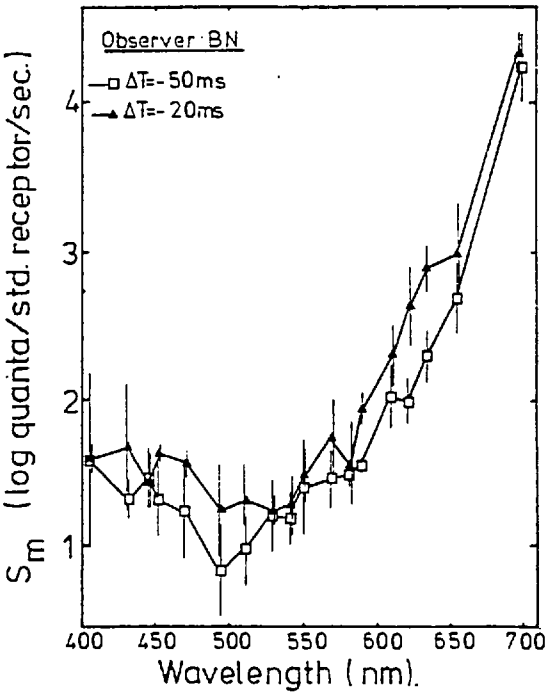

FIGURE 3.16

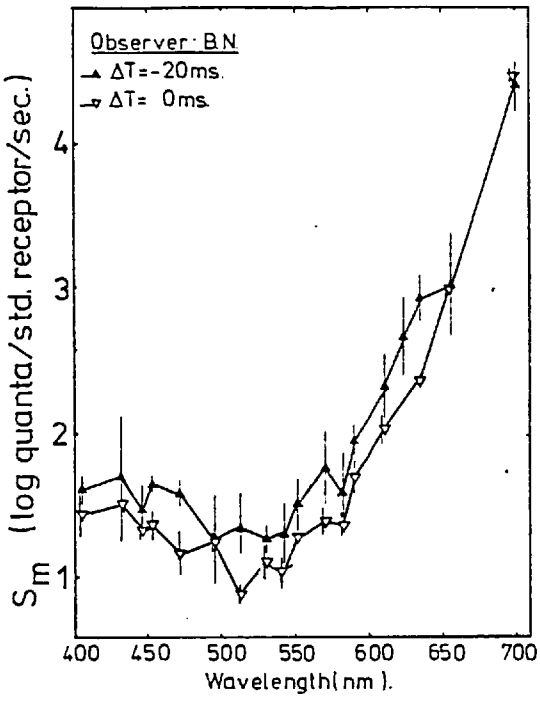

FIGURE 3.17

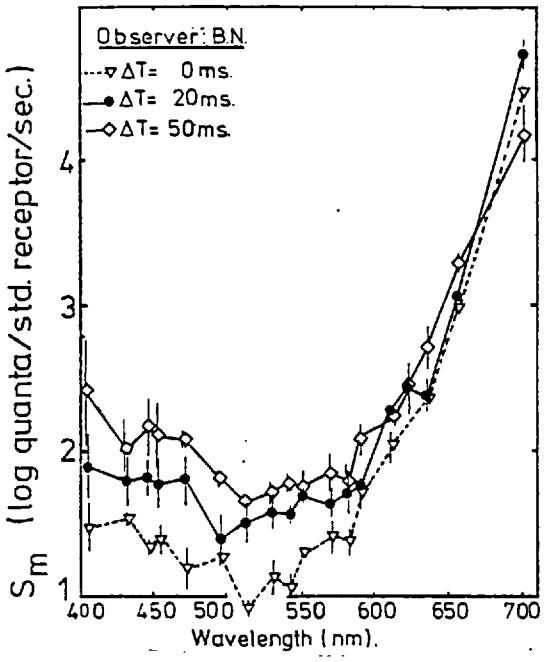

FIGURE 3.18

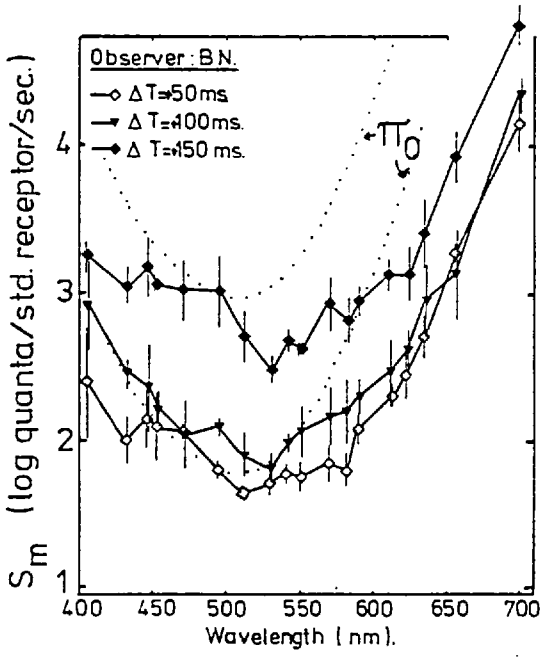

FIGURE 3.19

FIGURES 3.15 - 3.19 Masking action spectra for BN for values of ΔT between -100 ms and +150 ms.

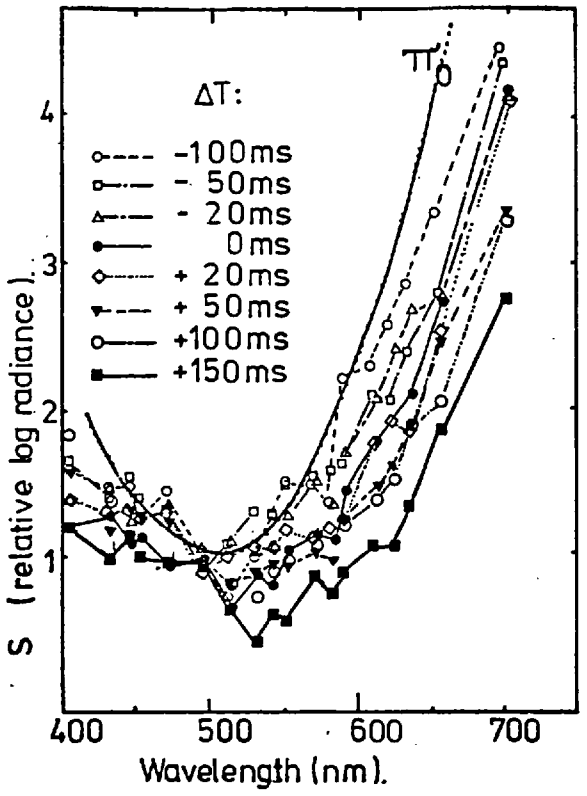

FIGURE 3.20

minimum in the π_o curve. The action spectrum of masking at ΔT = -100 ms coincides with the π_o curve over a large range of wavelengths. The wavelength range over which the π_o curve fits the masking action spectrum decreases progressively with increasing ΔT values (e.g. figure 3.20), and this wavelength range is small for ΔT = +150 ms. Masking action spectra were obtained for the other observers for ΔT = +50 ms and ΔT ⩾ +150 ms: it can be seen from figure 3.19 that the sensitivity to masking for BN was everywhere higher for ΔT = +50 ms than at ΔT = +150 ms.

(ii) The action spectra of masking for DHF are shown in figure 3.21 for ΔT = +50 ms and +250 ms, and those for MRI appear in figure 3.22 for ΔT = +50 ms and +150 ms. The π_o spectral sentivitity curve is again shown with these data, and it is seen that the wavelength range over which the π_o and masking action spectra coincide is greater at ΔT = +50 ms than it is for the larger ΔT value. Also the masking sensivitity is greater at the lower ΔT value (ΔT = +50 ms). These data are therefore in agreement with the pattern of results obtained for observer BN.

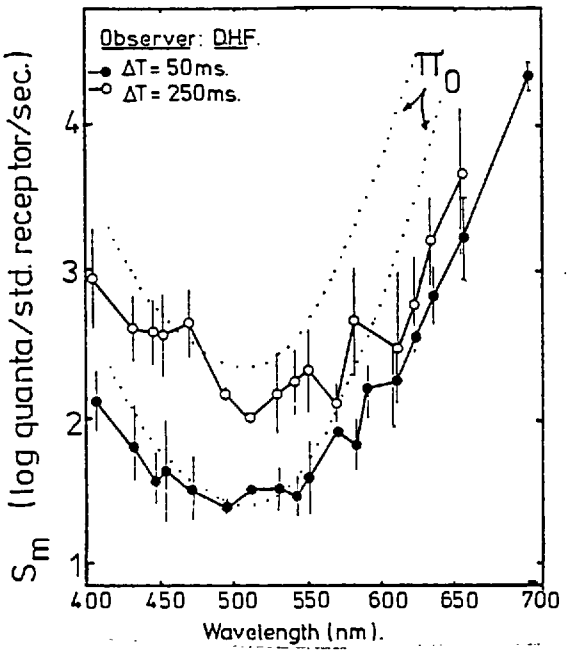

FIGURE 3.21 Masking action spectra for DHF.

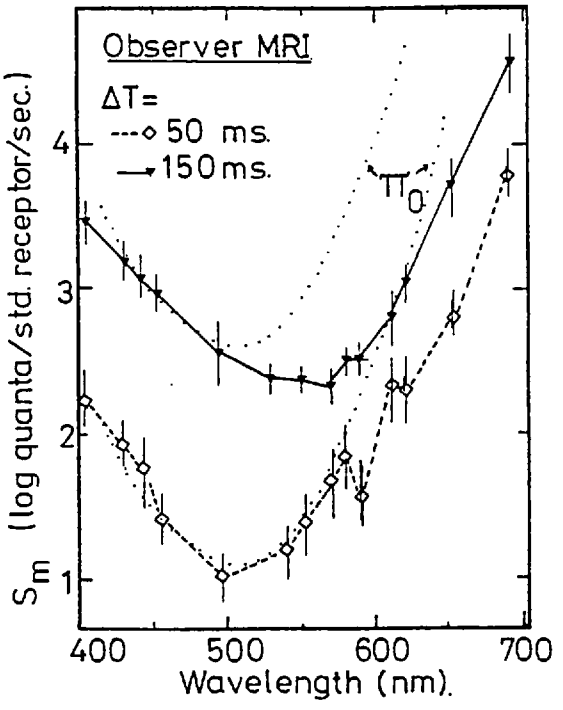

FIGURE 3.22 Masking action spectra for MRI.

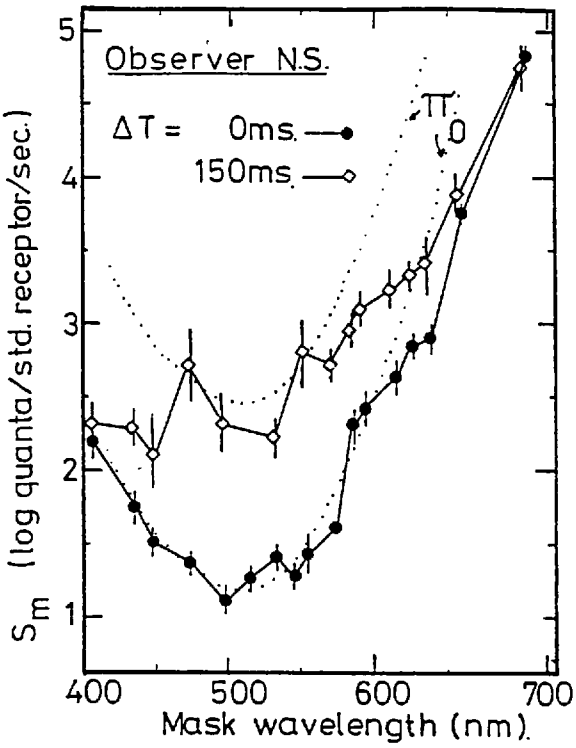

FIGURE 2.23a Action spectra of masking for deuteranope NS.

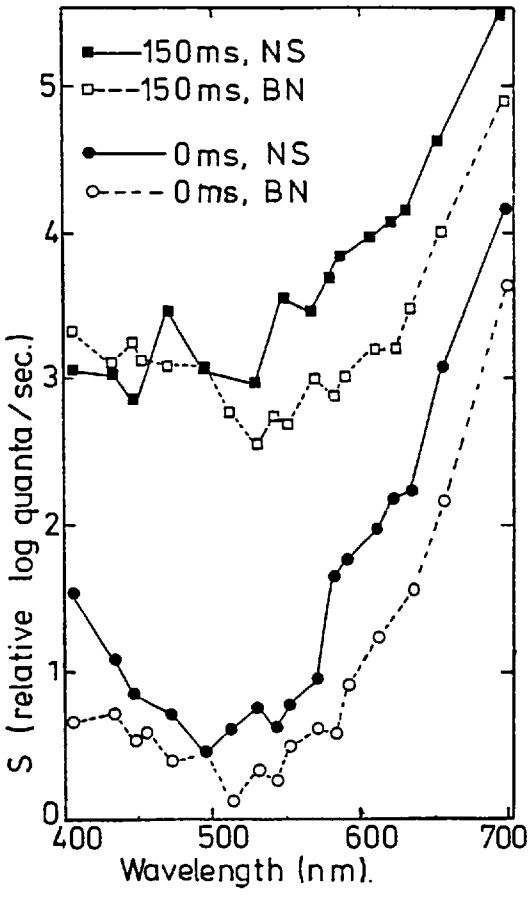

FIGURE 3.23b Action spectra of masking for NS and BN equated at 495 nm.

The masking action spectra for the deuteranope NS are shown in figure 3.23 for ΔT values of 0 ms and +150 ms, together with the π_o action spectrum. The data are qualitatively similar to those of the colour-normal observers, in that the wavelength range over which the π_o and masking action spectra coincide is greater for ΔT = 0 ms, and sensitivity to masking is greater than for ΔT = +150 ms. The data for NS and the colour-normal observer, BN, are plotted together in figure 3.23. The curves for ΔT = 0 ms and +150 ms were moved vertically so as to coincide at a wavelength of 495 nm. It can be seen that the masking action spectrum obtained for BN at ΔT = 150 ms is broader than that of the deuteranope NS for the same value of ΔT.

(iii) Masking for a Red, Cone-Stimulating Probe Field

The action spectrum of masking for a red probe stimulus is shown in figure 3.24 for ΔT = -80 ms and 0 ms. These curves both differ markedly from the π_o action spectrum in shape (dotted, figure 3.24), and it can be seen by inspection that they also differ in shape from the masking action spectra obtained for ΔT = 0 ms for the 495 nm rod-stimulating probe field (for BN, figures 3.15 to 3.17). The two curves of figure 3.24 differ most at short wavelengths, where the sensitivity to masking is greatest at ΔT = -80 ms.

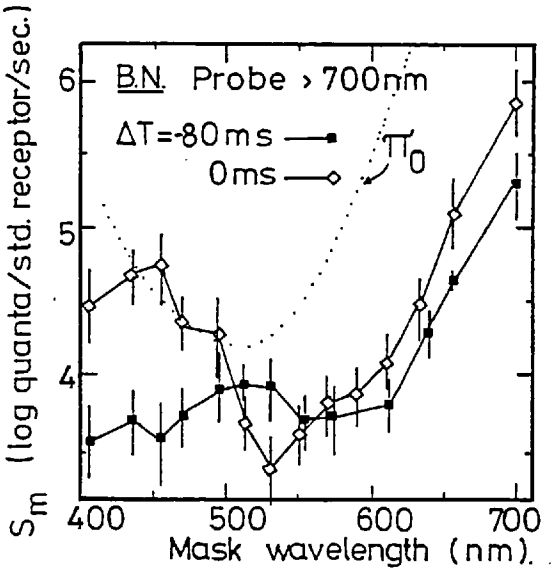

FIGURE 3.24 Masking action spectra for red probe stimulus.

(iv) Variation of the Probe Stimulus Diameter

Masking action spectra are shown in figure 3.25 for a 1.2' probe stimulus for four values of ΔT. When presented at 0.5 log units above absolute threshold, the 1.2' probe stimulus appeared on occasion very small and blue. This suggested that the probe stimulus was, on occasion, exciting a cone mechanism. To check this, the eye was displaced a few millimeters to the right. The masking action spectrum obtained at ΔT = +100 ms for non-axial entry of light is shown in figure 3.26 for the 1.2' probe stimulus. Comparison of these data with the corresponding data for axial entry of light into the eye (dotted line, figure 3.26) shows that at

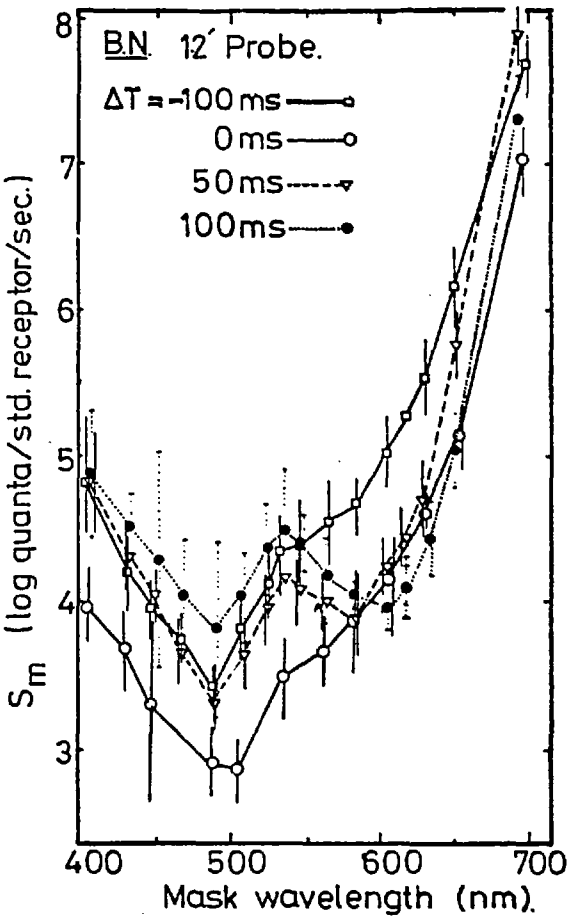

FIGURE 3.25 Masking action spectra for 1.2' probe stimulus.

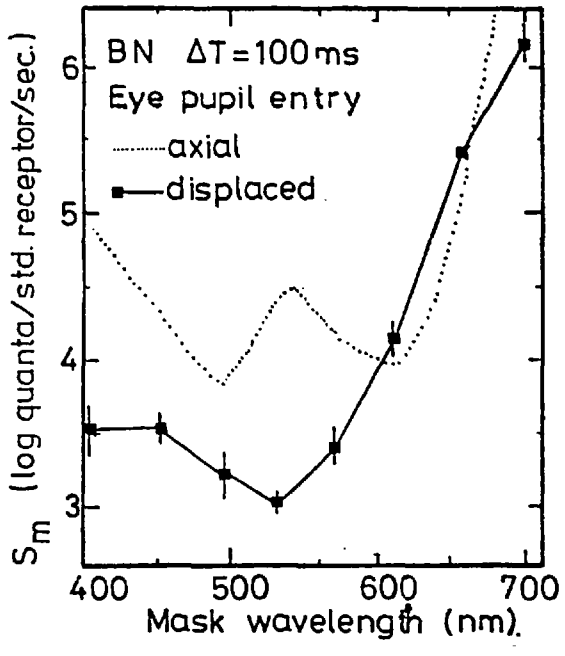

FIGURE 3.26 Masking of probe stimulus for axial and non-axial entry of light into the eye.

short wavelengths there is a large difference in masking radiance.

In a further experiment, the threshold dark-adaptation curve was measured for the 1.2' probe stimulus for the displaced eye-position, using the method outlined in Section 3.3, part 2. The dark-adaptation curve, shown together with the one obtained for axial entry of light (solid curve) in figure 3.27 demonstrates that the cone threshold was raised by the eye-displacement by at least 0.4 log units (the Stiles-Crawford effect), while the rod threshold remained unchanged. Thus since the masking action spectra for the two eye-positions were different (figure 3.26), the data for axial beam entry through the pupil (figures 3.25, 3.26) probably resulted in

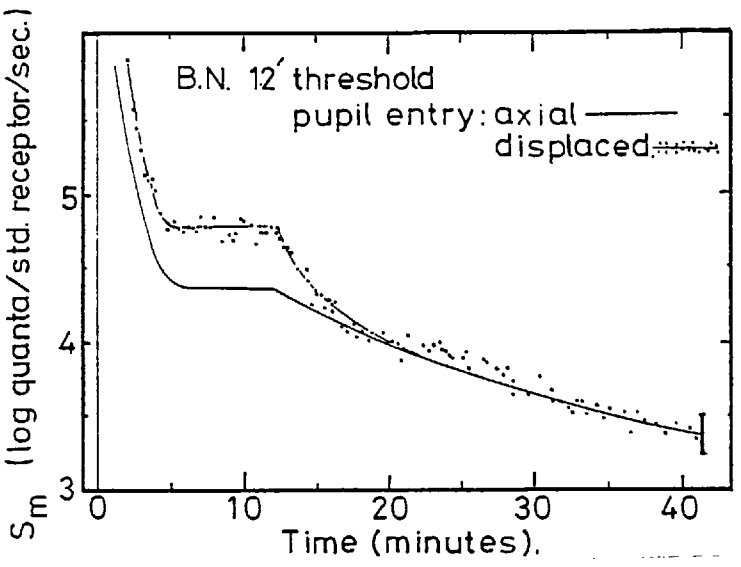

FIGURE 3.27

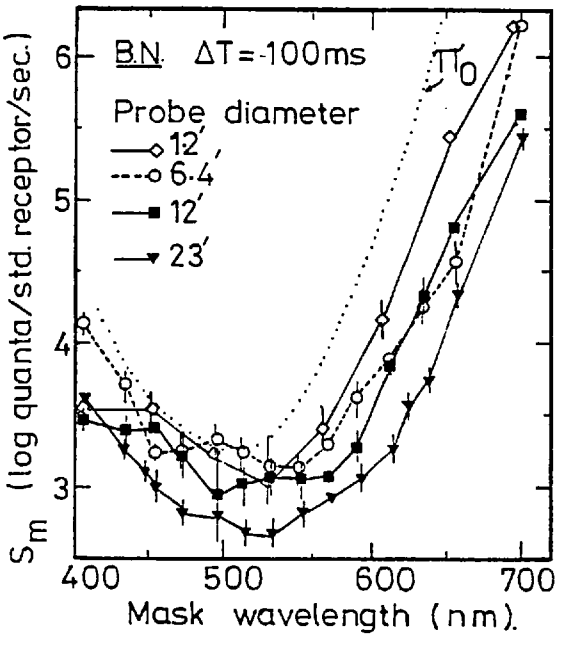

FIGURE 3.28

part from stimulation of the cones by the probe stimulus.

The data obtained for non-axial entry of light from the 1.2' probe stimulus is replotted in figure 3.28. The action spectra of masking of three other probe stimuli of different diameters are also shown in this figure, for ΔT = +100 ms. These action spectra all have similar shapes, but the sensitivity of the probe stimulus to masking increases as the probe field size increases.

(v) Dichoptic Masking Data

The action spectra obtained when the probe and masking stimuli were presented to the dark-adapted left and right eyes respectively are shown in figure 3.29, for ΔT = -50 ms and +50 ms.

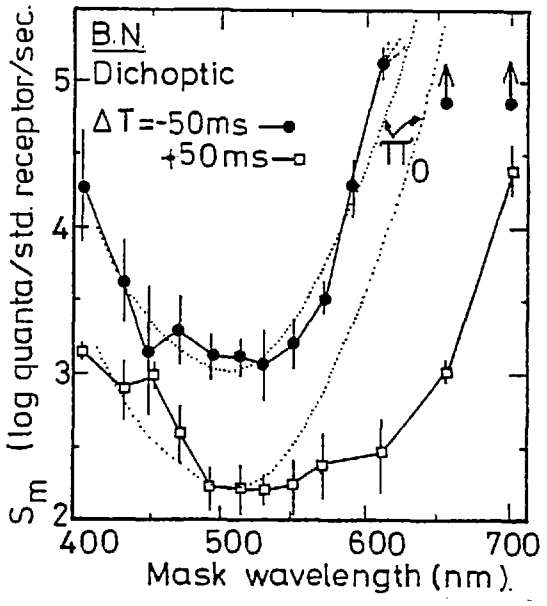

FIGURE 3.29 Dichoptic masking action spectra.

The action spectrum obtained for dichoptic masking at ΔT equal to -50 ms clearly follows the rod (π_o) sensitivity curve (dotted, figure 3.29) while that at ΔT = +50 ms does so over a very restricted wavelength range. Thus, as in the monocular case, the masking action spectrum is closer to the π_o sensitivity at the low ΔT values (-50 ms) than at ΔT = +50 ms (see figures 3.15 and 3.19). However, the wavelength range over which the π_o and masking action spectra coincide at ΔT = +50 ms is less for dichoptic than for monoptic presentation of the probe and mask patterns. Also, the sensitivity to masking at ΔT = -50 ms is lower than that at ΔT = +50 ms in the dichoptic masking (figure 3.29), whereas the reverse is true for monoptic masking (figures 3.16 and 3.19). Therefore the monoptic and dichoptic masking are not entirely equivalent to each other.

(vi) Masking by Uniform Circular Stimuli

No metacontrast masking could be obtained for dichoptic presentation of a spatially uniform 3^o mask field and the 23' probe stimulus. This was found to be true for the 20 ms presentation times used in the experiments, for five masking wavelengths, for ΔT values between -300 ms and +300 ms, and for mask illumination levels of up

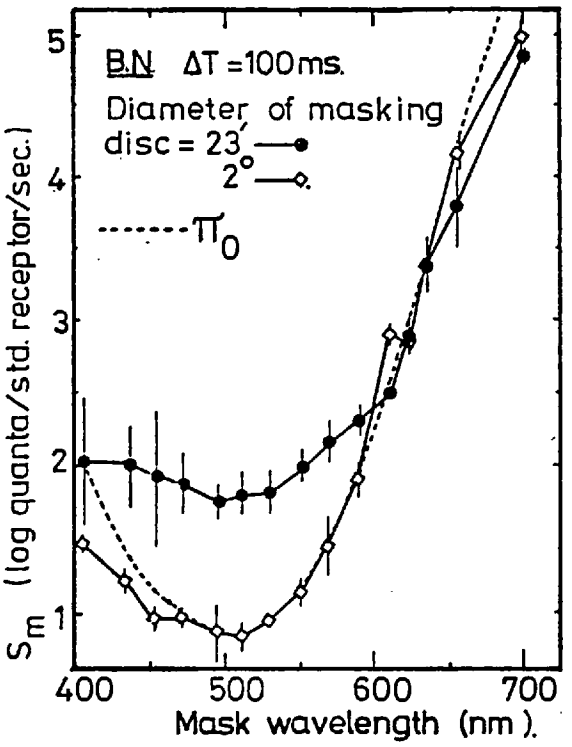

FIGURE 3.30

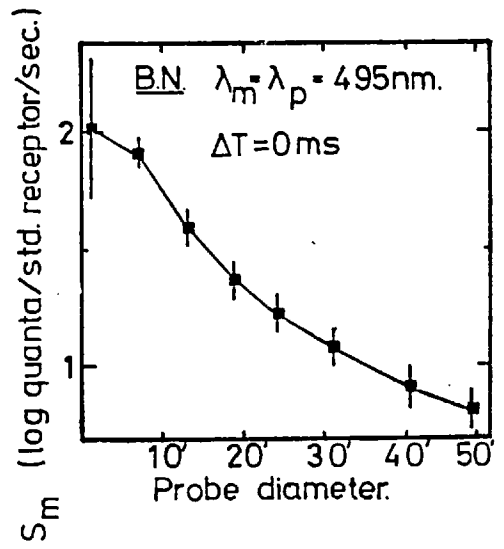

FIGURE 3.31

to 4 log quanta/standard receptor/second. Interaction between uniform circular stimuli presented to the same eye is readily demonstrated, however. This is shown in figure 3.30 for masking stimuli 2° and 23' in diameter (the probe stimulus diameter was 23'), and for ΔT = +100 ms. Note that for both masking stimuli, the masking action spectra are almost identical at wavelengths longer than 600 nm.

The masking sensitivity increases at shorter wavelengths for the larger mask stimulus, and the action spectrum for the larger circular mask is almost the same as that of the π_o mechanism.

The masking by a 495 nm circular mask stimulus, of diameter 5°, is plotted against the diameter of a 495 nm probe stimulus in figure 3.31 (ΔT = 0 ms). All the probes were presented at 0.5 log units above absolute

threshold. It can be seen that the radiant flux level of the mask stimulus which was necessary to veil the probe decreased monotonically with the diameter of the probe.

(vii) Masking in the Presence of Red Background Fields

The masking action spectra shown in figures 3.32 and 3.33 were all obtained using the stimuli illustrated in figure 2.5 located 6^{o} parafoveally along the nasal horizontal meridian. The curves comprising widely-spaced dots were obtained without any background field, but the other data were measured in the presence of circular red fields presented for three seconds (figures 3.12, 3.13) concentrically with the probe and masking stimuli. The two curves in figure 3.32 outlined by rectangles were obtained in the presence of a 3 second red disc which had the same diameter as the probe stimulus (23', figures 3.12, 3.13), for ΔT = 0 ms and +100 ms (shown on diagram). The curve on this diagram marked by circles was obtained with a red background disc 2^{o} in diameter, which thus covered both metacontrast stimuli (figure 3.13 , the value of ΔT for this curve was +100 ms).

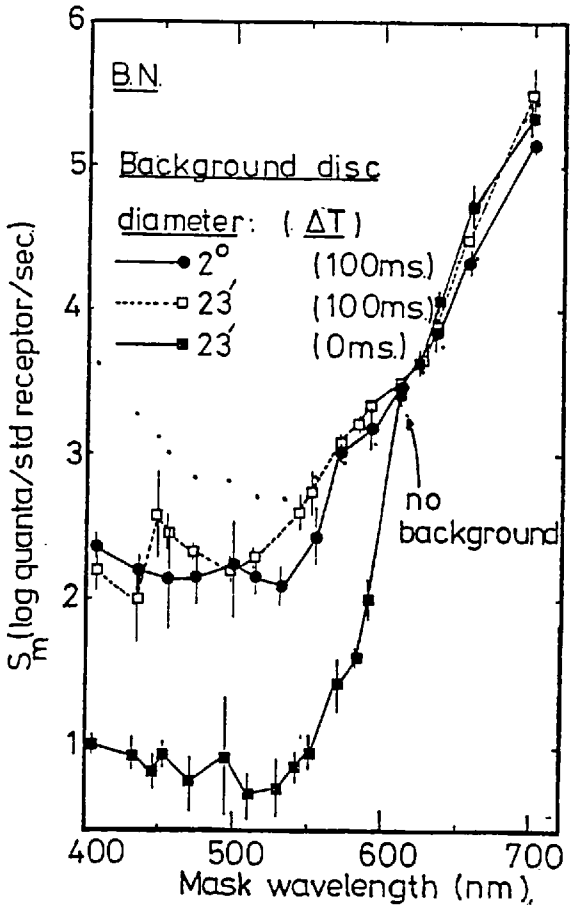

FIGURE 3.32

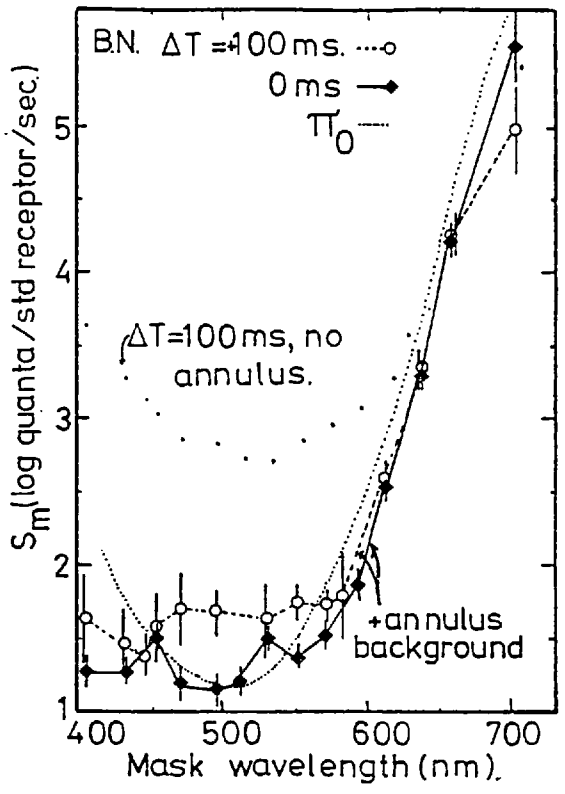

FIGURE 3.33 Masking action spectra in the presence of a red annular background field (figure 3.12).

The data of figure 3.33 were obtained in the presence of a steady red annulus, the average diameter of which was 54' (figure 3.12). The steady (3 second) red annulus had a width of 10' so that it covered the inner edge of the annular masking stimulus (diameter 54'), but did not cover any part of the probe stimulus (figure 3.12). The data of figures 3.32 and 3.33 show several interesting features.

(a) All of the masking spectra obtained for ΔT = +100 ms (with and without red background) in figures 3.32 and 3.33 coincide above 620 nm.

(b) The curves obtained at ΔT = +100 ms with red background discs (figure 3.32) show greater masking sensitivity at short wavelengths than the curve obtained without a background (dotted). The curve of figure 3.33 obtained at ΔT = +100 ms showsthat, in the presence of the red annulus, there are similar, but larger, increases of masking sensitivity at wavelengths below 600 nm. The masking action spectra for ΔT = +100 ms and 0 ms are not very different from the π_o sensitivity curve, in the presence of the annulus (dotted, figure 3.33).

Now when measured in the presence of each of the red background

fields in turn, the threshold radiant flux level required for detection of the probe stimulus did not change from its dark-adapted value by more than 0.07 log units. Thus the changes in masking efficiency at wavelengths shorter than 600 nm are not due simply to a threshold elevation of the probe stimulus by the red background.

(c) The two curves obtained with the small (23') and large (2^{o}) background discs are almost the same when ΔT = +100 ms (figure 3.32). It is therefore unlikely that the interactions are of the centre-surround type found by Westheimer (1966), since these are highly dependent on the diameter of the background disc.

It was noticed that if the probe stimulus was presented alone following several presentations of the red discs it appeared distinctly blue, whereas normally it appeared whitish. This shows that the rods can evoke different chromatic sensations, a phenomenon which has been previously reported by Stabell and Stabell (1973, 1975a,b).

(viii) The Time-Course of Metacontrast Masking

The masking radiant flux levels were measured as a function of ΔT for wavelengths of the mask stimulus equal to 495 nm and 611 nm. The data are expressed in terms of the radiance of each mask stimulus required to mask the probe field, plotted against ΔT. These data are shown in figures 3.34 to 3.37 for various sizes of the probe and masking fields - the stimulus configurations are shown to scale with each figure. The filled circles and the inverted triangles in each case denote the masking radiances for mask stimulus wavelengths of 495 nm and 611 nm respectively. The curves for the 495 nm mask stimuli are also plotted (open circles) after

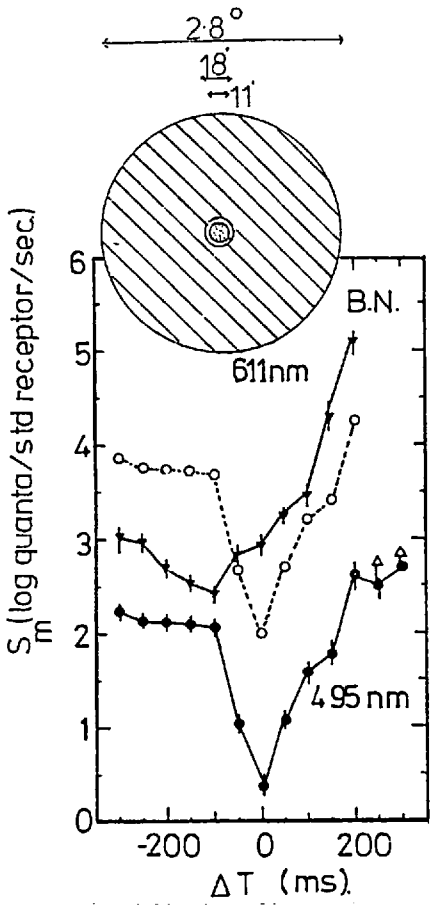

FIGURE 3.34

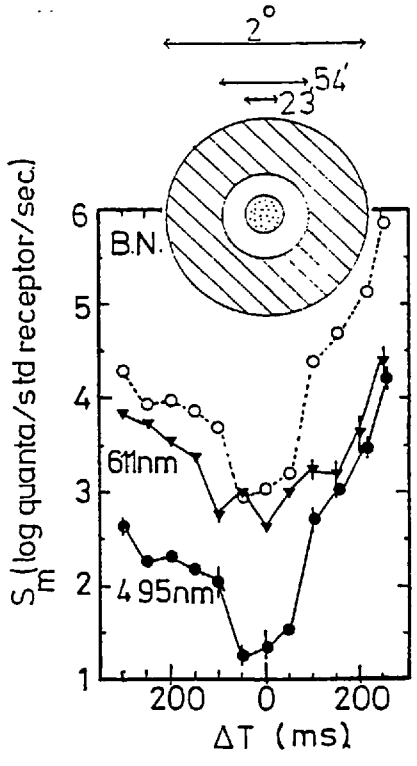

FIGURE 3.35

being displaced upward in radiance by an amount equal to the difference between the scotopic sensitivities for stimulus wavelengths of 495 nm and 611 nm. The broken lines correspond to these shifted curves. Assuming that the effect of the 495 nm masking field is due to rods for all values of ΔT, these broken lines define the masking curve which would be obtained for a 611 nm mask stimulus for pure rod-rod masking.

The data of figures 3.34 to 3.36 were obtained monoptically, and those of figure 3.37 dichoptically. These time-course curves exhibit some important features:

(a) A minimum in the masking radiance-versus-ΔT curve corresponds to a maximum in the sensitivity to masking by the annular stimuli. The data of figures 3.34 to 3.36, which were obtained monoptically, show that the maximum sensitivity to masking by a 495 nm stimulus occurs at about ΔT = -50 ms for probe stimulus diameters of 23' (figure 3.35) and 60' (figure 3.35). The ΔT value at

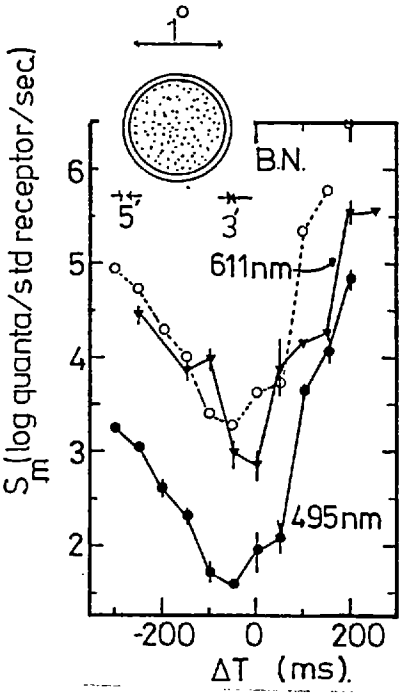

FIGURE 3.36

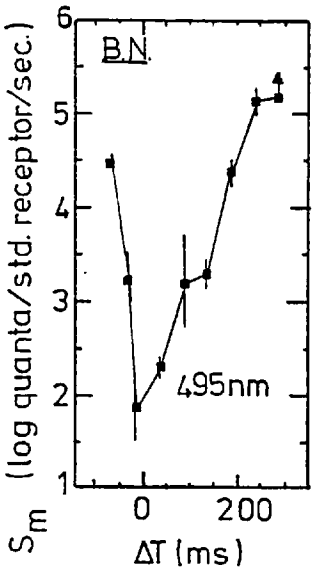

FIGURE 3.37

which maximum masking occurs for the 11' probe stimulus is close to 0 ms (figure 3.34), so that the masking in this case could be caused by scattered light. The masking data for the 23' diameter probe stimulus, obtained dichoptically for a 495 nm mask stimulus (figure 3.37), has a minimum at ΔT = 0 ms. This zero value of ΔT cannot, however, be attributed to light scattered by the mask stimulus, since no masking was obtained dichoptically when a spatially uniform mask stimulus was used (experiment V, Section 3.6).

(b) The width of the 'valley' in the curve obtained monoptically for the 495 nm mask stimulus and the 11' probe stimulus (figure 3.34) is less than those for the larger probe stimuli (figures 3.35 and 3.36). The width of the valley for dichoptic masking (figure 3.37) is narrower than the curve obtained monocularly with the same stimuli (figure 3.35).

(c) The dashed curves of figures 3.34 to 3.36 correspond to the masking curves which would be obtained for a 611 nm

mask stimulus under conditions of pure rod-rod masking. The extent to which the measured curves (inverted triangles in the figures) deviate from the dashed curves is a measure of the deviation from pure rod-rod masking. The dashed curve for the 11' probe stimulus lies below the measured curve for the 611 nm mask stimulus for $\Delta T \geq -50$ ms (figure 3.34), and this indicates that the action spectrum of masking is narrower than the π_o action spectrum for $\Delta T \geq -50$ ms. The dashed curves for the larger probe stimuli lie mostly above the measured data (figures 3.35 and 3.36), and so the masking action spectrum is mostly broader than that of the π_o mechanism for these probe stimuli.

Delay between Rod and Cone Responses

For cone-rod metacontrast masking, the variation of the magnitude of the masking effect with ΔT will depend on the relative time of arrival of rod- and cone-elicited signals at the site of interaction. The delay between rod and cone responses for the author was measured by Barbur (private communication). The measure employed was the reaction time to a 30 ms stimulus flashed at random intervals in the dark-adapted right eye. The stimulus was either a red (629 nm) or blue (439 nm) disc 1° in diameter, which was presented at an illumination level of 0.5 log units above threshold. The stimulus was presented for 30 ms, 6° from the fovea, along the horizontal meridian. Dark-adaptation data showed that the blue stimulus excited only the rod system. The observer pressed a switch as soon as each stimulus was perceived, and the reaction time was measured as the delay between the stimulus onset and the depression of the switch. Four hundred measurements were made for each stimulus wavelength, and the results are plotted in figure 3.38 as the number of responses

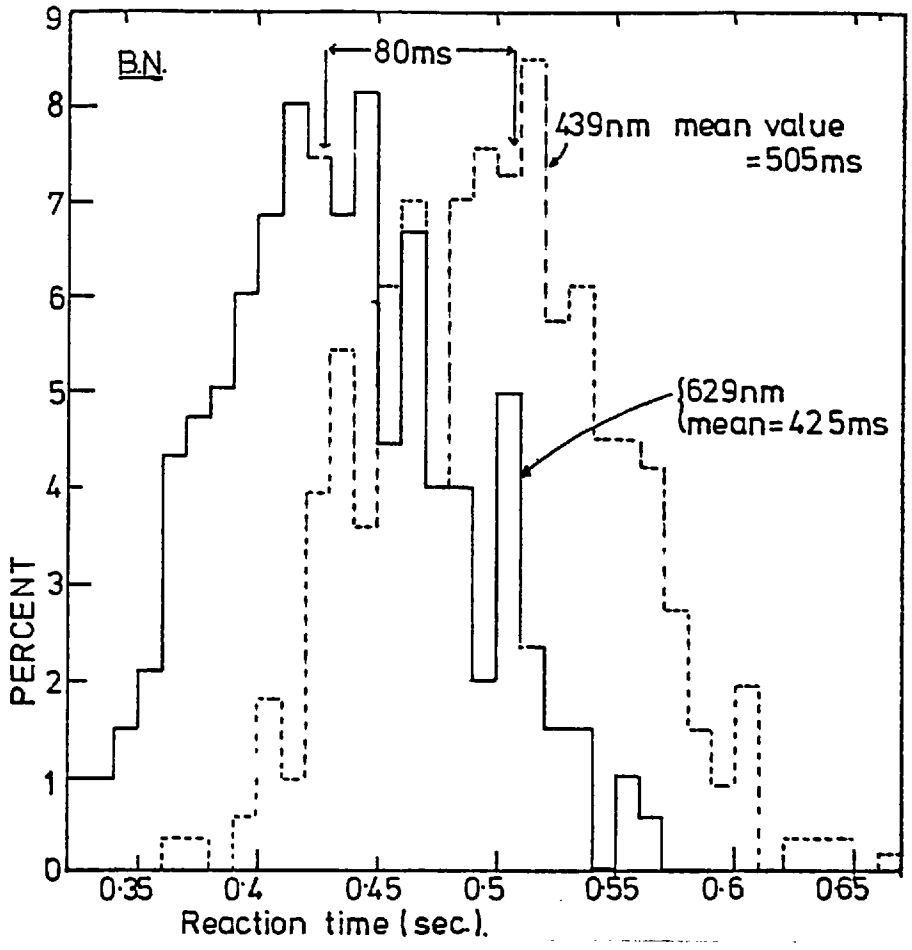

FIGURE 3.38 Reaction time histogram.

against reaction time. The average reaction time for the rod-stimulating blue field was 80 ms longer than that for the cone-stimulating red stimulus. This fact will be taken into account when the time-course of metacontrast masking and the spectral sensitivity of masking are discussed.

(ix) Masking by Windmill-Shaped Stimuli

The masking radiant flux levels measured for annular windmill mask stimuli are shown in figure 3.39 as a function of the masking wavelength, for four frequencies of the windmill stimulus (indicated on the diagram). The sensitivity to masking is greatest at 4Hz,

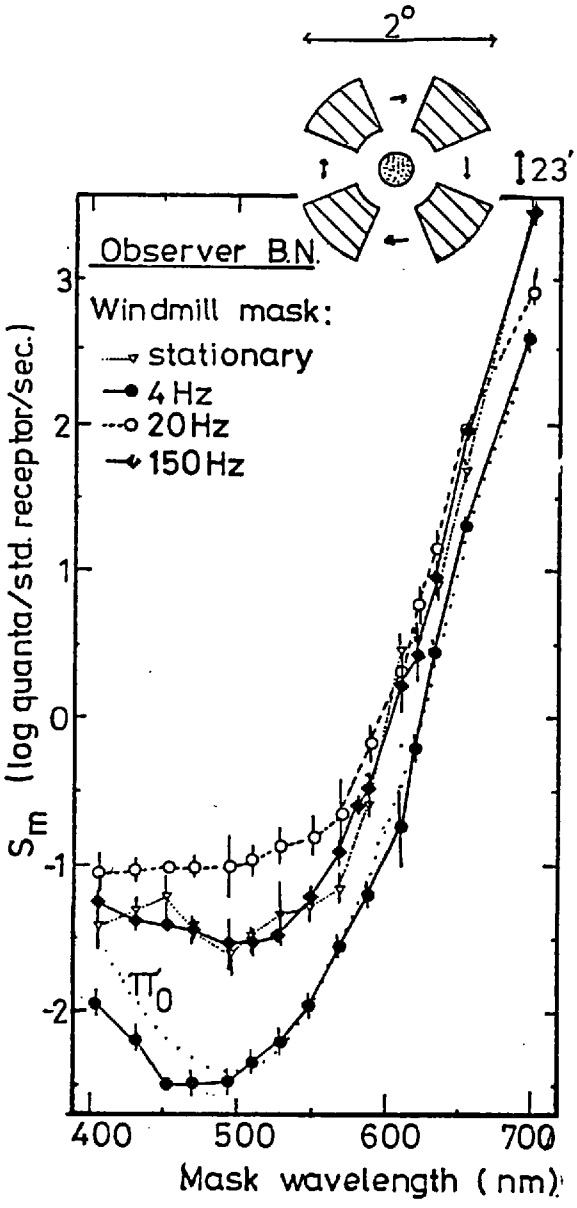

FIGURE 3.39

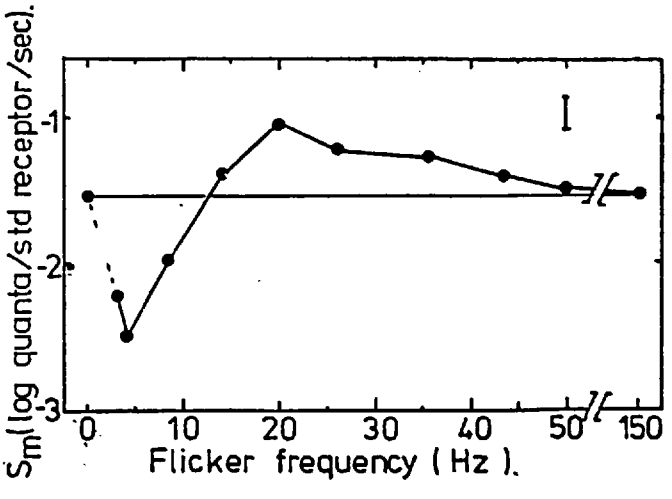

FIGURE 3.40

and the masking action spectrum is close to the π_o curve for this frequency of rotation. For wavelengths shorter than about 580 nm, the masking sensitivity is least for a rotation frequency of 20 Hz. Masking was measured as a function of the rotation frequency for a single masking wavelength of 495 nm (figure 3.40). It was found that a windmill flicker rate of 4 Hz gave the greatest masking effect while one of 20 Hz yielded the least sensitivity to masking.

The masking spectral sensitivity is the same for the stationary windmill and that rotated at 150 Hz. The maximum critical fusion frequency of vision is less than 100 Hz (Brindley, 1970), so that the pattern producing flicker at 150 Hz

is probably equivalent to a uniform annular stimulus. Thus the stationary annular windmill and a uniform annulus with the same space-averaged radiant flux levels have the same masking effect. This result is in agreement with that of Alpern, Rushton and Torii (1970a,b), who used similar annular windmill mask stimuli in metacontrast, and found for different angles of the windmill sectors that the masking magnitude was the same for the same space-averaged illumination levels.

Discussion

3.7 Scattered Light

Before any conclusions can be reached about the nature of the masking which gives the experimental data in the previous section, the effect of light scattered by the ocular media must be evaluated. Scattered light can affect the conclusions drawn from the data in two ways. First, if the radiance of the light scattered from the annular stimuli is sufficient to stimulate receptors at the centres of the annuli, then the masking effects which are measured might be due to the scattered light rather than to lateral neural interactions. Second, if scattered light stimulated cones at the centres of the annuli, differences between the shape of the action spectrum of masking and that of the π_o action spectrum could be attributed entirely to the excitation of cone receptors by scattered light at the centres of the annuli. Conversely, if the radiance of the scattered light was insufficient to stimulate cone receptors at the centres of the masking annuli, deviations of the masking action spectrum from the π_o action spectrum shape could only be interpreted by rod-cone interaction, since the probe stimuli excited only the

rod mechanism.

Three instances of masking will be examined in order to deduce the effect of scattered light.

(a) If scattered light were the cause of the masking, it should be expected that the maximum masking would occur at ΔT = 0 ms. However, the peak masking effect for a masking wavelength of 495 nm occurs at negative ΔT values for the curves shown in figures 3.37 and 3.38, so that the masking for these conditions cannot be explained by scattered light.

(b) The view that the masking action spectra measured in the metacontrast experiments are due to scattered light is inconsistent with the effect of the red background fields on the metacontrast sensitivity (figures 3.32 and 3.33). The results show that over much of the visible spectrum addition of background light increases the sensitivity to masking of the probe stimulus, even though the probe stimulus threshold level was itself unaffected by the red background fields. (This point is discussed further in Section 3.10(1)).

(c) It is established in Appendix C (equation C.4) that the illumination level of scattered light at the centre of the annular pattern shown in figure 2.5 is about 1.6 log units less than the illumination level of the annular stimulus. Thus, according to the calculation of Appendix C, a 23' masking disc, presented at the same location as the probe stimulus, would simulate an annular masking field of retinal illumination level some 1.6 log units greater than that of the probe itself, if scatter from the annular field were the cause of masking. Now, a masking stimulus consisting of a 23' diameter disc pattern was used to simulate the effects of scattered light on the 23' probe stimulus (fig. 3.30).

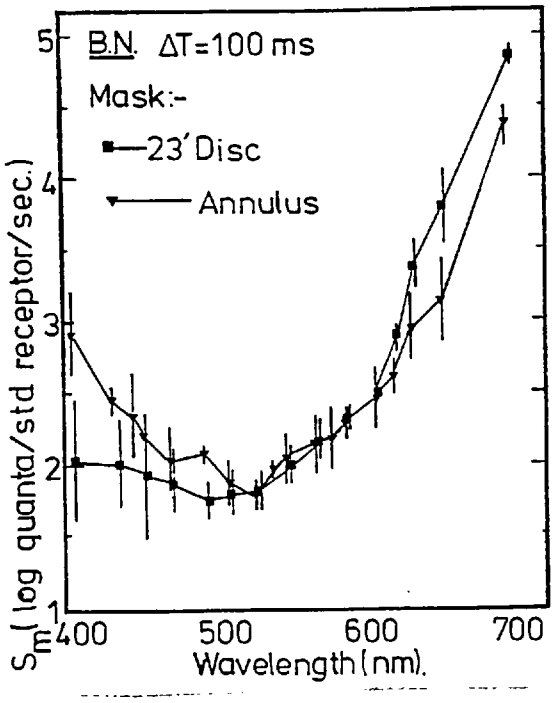

FIGURE 3.41

The masking action spectrum obtained 3° from the fovea, for the 23' disc masking field (figure 2.5) and for ΔT = +100 ms (figure 3.30) is replotted in figure 3.41 (filled squares). The masking curve determined for the annular mask field (fig. 3.19) is also plotte in figure 3.41. Two features of the results are noteworthy. First, the masking functions for the disc and annular masking fields are similar in absolute value, i.e. approximately the same number of quanta per unit area per second are required for both the annular mask and the disc mask to suppress detection of the probe stimulus. Calculation shows, however, (Appendix C) that the scattered light from the annulus gives a retinal illumination level at the centre of the field about 1½ log units less than that of the annulus itself. It should be noted that in order to produce the same illumination level at the centre of the annulus as at the annulus itself, the scatter would have to be uniformly diffused over the retina. In practice, the annulus could usually be clearly resolved by the observers, indicating that scatter is relatively small. The second point to

note is that the absorption spectrum for masking by the disc differs significantly from that for masking by the annulus. It is concluded, therefore, that masking effects associated with the annulus cannot be attributed to scattered light.

The above arguments indicate that masking of the probe stimulus by the surrounding annular masking field (figure 2.5) cannot be attributed to background field light associated with light scatter. Neither the illumination levels nor the temporal characteristics of scatter are consistent with the observed masking. Thus, in the case that probe fields were chosen so as to excite only the rod mechanism, deviations of masking action spectra from the π_o action spectrum shape are caused by interactions between the rod and cone mechanisms. Deviations of the shape of the masking action spectra from that of the π_o-mechanism action spectrum were seen to occur in the metacontrast data presented above. These data are summarized below.

3.8 Summary of Masking Data

1. The masking action spectra obtained for $-100 \text{ ms} \leq \Delta T \leq +150 \text{ ms}$ for BN, for $\Delta T = +50$ ms and +150 ms or +250 ms for the two other colour normals, DHF and MRI, and at $\Delta T = 0$ ms and +150 ms for the deuteranope NS, all deviate from the π_o mechanism curve in shape for long wavelength masking stimuli (figures 3.15 to 3.20 (BN), 3.21 (DHF), 3.22 (MRI), and 3.23a (NS)). The action spectra curves become broader in shape as the value of ΔT is increased (figures 3.20 to 3.23a). The masking action spectra for the deuteranope NS are narrower at long wavelengths than the corresponding curves for the colour-normal BN (figure 3.23b).

2. The action spectrum of masking of a red, cone-stimulating

probe field is very different in shape from the π_o action spectrum (figure 3.24) for ΔT = -80 ms and 0 ms.

3. The shape of the action spectrum of masking remains unaltered as the diameter of the rod-stimulating probe field increases from 1.2' to 23' (figure 3.28), but the sensitivity to masking increases as the probe field diameter is increased. When the probe stimulus is small (1.2' in diameter) and light enters the eye axially, the probe stimulus was presented close to or at the cone-threshold radiance (figure 3.27), and this resulted in dramatic changes in the shapes of the masking action spectra (figures 3.25 and 3.26).

4. The masking action spectrum obtained dichoptically at ΔT = -50 ms follows the π_o curve (figure 3.29), whereas the masking curve is wider than that of the π_o mechanism when measured monoptically at ΔT = -50 ms (figure 3.15). The action spectrum of masking measured dichoptically for ΔT = +50 ms is wider than the π_o mechanism curve at wavelengths above 510 nm (figure 3.29).

5. Masking of a 23' probe stimulus by uniform stimuli presented in the same eye is readily demonstrated (figure 3.30), and the sensitivity to masking by 495 nm stimuli increases with the diameter of the probe field (figure 3.31). No masking was obtained dichoptically using a spatially uniform 3^o masking field and a 23' probe field (results, (vi)).

6. The sensitivity to masking of a rod-stimulating probe field increased at short wavelengths in the presence of red background fields presented for three seconds (figures 3.32, 3.33). The increases in masking activity occurred only for masking wavelengths shorter than about 600 nm, and the increase in sensitivity was

greatest for the steady red annulus (figure 3.33), even though this annulus did not overlap the probe stimulus spatially, and covered only the inside edge of the annular mask stimulus (figure 3.12).

7. The sensitivity to masking follows different time-courses in monoptic and dichoptic masking (figures 3.35 and 3.37). The peak masking sensitivity occurs at ΔT = -50 ms for large probe fields presented monoptically with the mask stimulus, and at ΔT = 0 ms for a small probe field, again presented monoptically (figures 3.34 to 3.36). The peak sensitivity to masking occurs at ΔT = 0 ms in dichoptic masking (figure 3.37).

8. The sensitivity to masking by 495 nm rotating annular masking stimuli was greatest at rotation frequencies of 4 Hz and least at 20 Hz (figure 3.40). The action spectrum of masking followed the π_o curve closely when the windmill was rotated at 4 Hz (figure 3.39). The sensitivity to masking decreased at wavelengths below 600 nm for a rotation frequency of 20 Hz, and was unchanged above 600 nm for this rotation frequency.

3.9 Rod-Cone Interaction

The results of the first three experiments (point 1 in the above summary) show that, in general, the action spectra of metacontrast masking obtained using the stimulus configuration of figure 2.5 do not follow the action spectrum of the π_o mechanism. The probe field in the first three experiments stimulated the rod mechanism only, and it has been argued (Section 3.7) that scattered light from the annulus does not stimulate receptors at the centre of the annulus pattern. It is concluded, therefore, that the

masking is due to lateral interactions which are not specific to a single π-mechanism and appear to involve rod-cone as well as rod-rod masking.

The masking action spectra are all broader than the π_o mechanism curve, and they become broader at long wavelengths as the value of ΔT is increased (figure 3.20). Hence the relative contribution of long-wavelength cones to the masking increases as ΔT increases.

Contributions by the different Stiles π-Mechanisms to Rod-Cone Interactions Observed in Metacontrast

The 495 nm probe stimuli excited only the rod (π_o) mechanism, but it is possible that the mask stimuli excited a number of mechanisms at any one wavelength, and the relative degree of stimulation of the different mechanisms would depend on the wavelength of the masking annulus. Interactions may occur between the different components of the masking stimulus signals or between the signals from the mask and probe stimuli. For the purposes of this subsection, it is assumed that the mask stimulus excites only the π_1, π_4 and π_5 cone mechanisms at any wavelength, and the rod mechanism. It is further assumed that the action spectra of masking are determined by

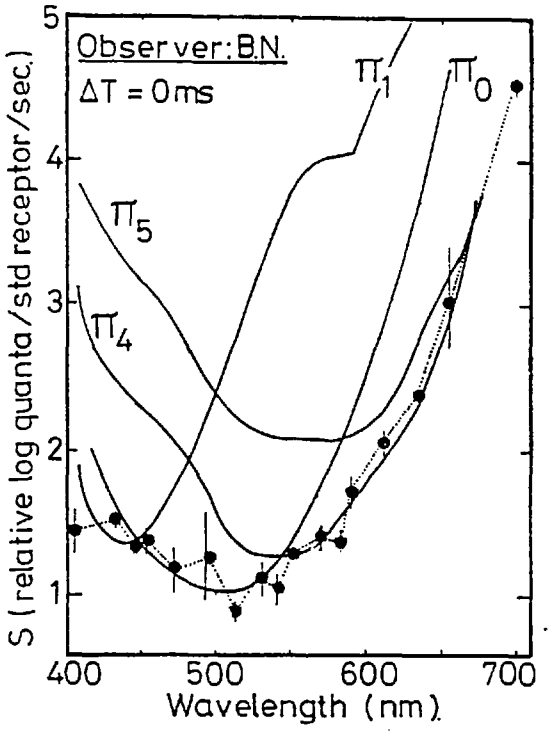

FIGURE 3.42 Method of fitting the π-mechanism curves to the action spectra. The dotted curve is from figure 3.17.

these mechanisms, so that the action spectra of the π-mechanisms can be fitted to the masking action spectra over some portion of the visible spectrum. The method of curve-fitting is illustrated in figure 3.42 for the case of simultaneous presentation of the probe and mask stimuli at an eccentricity of 3^{o} for observer BN (from figure 3.17). The maximum sensitivity of the π-mechanisms was assumed such that for all wavelengths the π-mechanism curves at most equalled, and never exceeded the masking action spectra in sensitivity. The average π-mechanism field sensitivities measured by Stiles were used (Stiles, 1953, 1959; Wyszecki and Stiles, 1967, page 579).

Figure 3.43 illustrates the curve-fitting for ΔT = +150 ms (observer BN). Comparison of figures 3.42 and 3.43 reveals that the broadening of the masking action spectrum for ΔT = +150 ms relative to that for ΔT = 0 ms is caused by an increased sensitivity to masking by the long-wavelength π_4 and π_5 mechanisms, relative to the sensitivity to masking by the π_o mechanism. The method of curve-fitting shows that the masking interaction is not mechanism-specific, since the probe stimulus excited only the π_o mechanism, yet the action spectrum of masking was determined

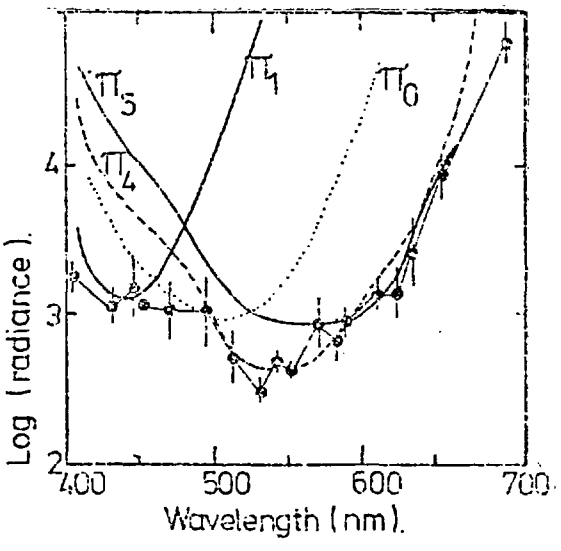

FIGURE 3.43

by the π_4 and π_5 mechanisms at long wavelengths. Also, the curve-fitting procedure shows that the relative contribution of the π_4 and π_5 mechanisms increases with ΔT (figures 3.20, 3.42 and 3.43). The method of curve fitting was applied to two further sets of data.

(i) The action spectra of the deuteranope NS (figure 3.23a) are replotted in figure 3.44, together with the π_o, π_1 and π_5 action spectra. These three π-mechanism curves are sufficient to fit the masking action spectra at all wavelengths, although it was necessary to use the π_4 mechanism curve to fit the long-wavelength portions of the action spectra for the colour-normal BN (figures 3.42, 3.43). Thus it is not required to include a contribution from the π_4 mechanism in order to fit the masking curves for the deuteranope, in agreement with the finding of Watkins (1969a) that the π_4 mechanism is absent in deuteranopes.

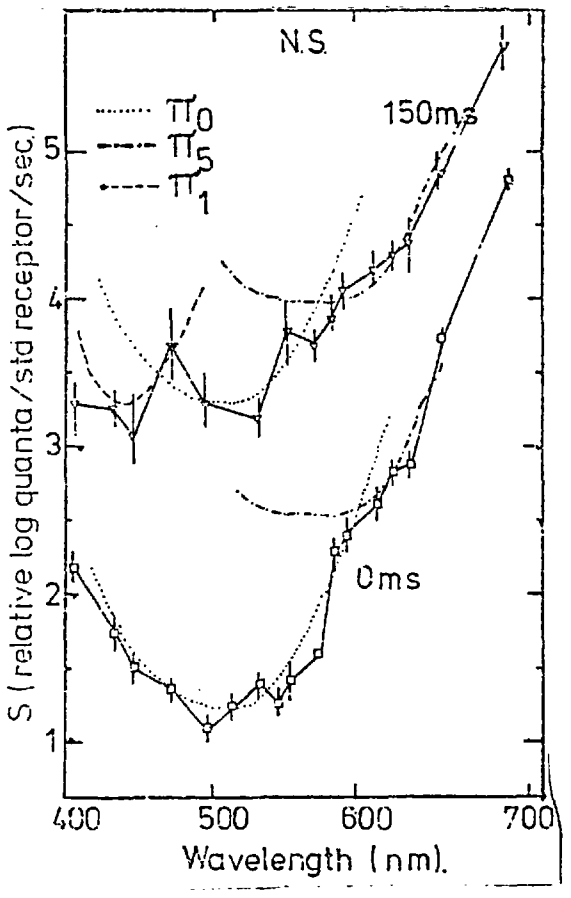

FIGURE 3.44 Action spectra of NS masking data and of π-mechanisms.

(ii) The Stiles π-mechanism curves were also fitted to the masking curves obtained with a red probe stimulus (figure 3.24); this is shown in figure 3.45. From these curves, it can be seen that the π_1, π_4 and π_5 curves suffice to fit the masking curve at all wavelengths, and that it is not necessary to include a contribution

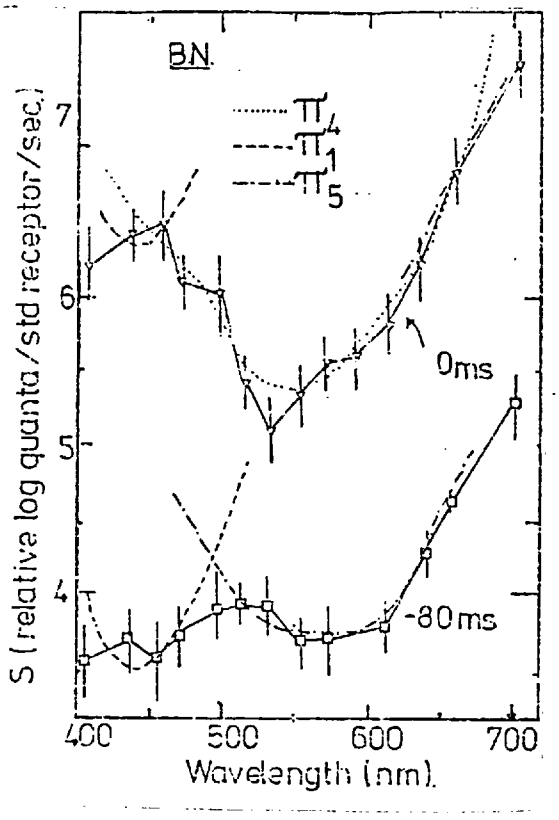

FIGURE 3.45 Masking action spectra for red probe stimulus

from the π_0 mechanism in order to reproduce the masking action spectrum for the red probe stimulus. Therefore masking of a red, cone-stimulating probe field is dominated by cone-cone interaction: it is not necessary to postulate rod-cone masking in this case.

It may be assumed that the red probe field stimulated only the π_4 and π_5 cone mechanisms. Since there is a clear contribution to the masking action spectrum from the π_1 mechanism for ΔT = -80 msec (figure 3.45), ~~the cone-cone interactions in this experiment are also not mechanism specific.~~ one kind of cone can affect another kind of cone

It has been shown that the relative contributions of the rod and the different cone mechanisms to the masking action spectra change with ΔT (figures 3.20 and 3.45). This implies different temporal response properties of the various mechanisms. Reaction time measurements (figure 3.38) showed that signals elicited from the rods lag by some 80 ms those elicited by the same stimulus from the long-wavelength cone mechanisms. Therefore, with ΔT = -100 ms, the mask-elicited cone signals will reach their maximum amplitude at a minimum of 100 ms, and up to 180 ms before the probe-elicited rod signals do, depending on the level of the visual system at which masking interactions occur. Thus there will be little overlap of rod and cone signals evoked by the 20 ms stimuli. The temporal

overlap of rod and cone signals elicited by the two stimuli increases with increasing values of ΔT, and this is consistent with the observation that the sensitivity to masking at long wavelengths (which is governed by cone-rod interactions) increases with increasing values of ΔT (figure 3.20).

The relative sensitivity to masking of the red probe stimulus by a short-wavelength mask stimulus was greater for ΔT = -80 ms than for ΔT = 0 ms (figure 3.45). It has been shown that the response latency of the π_1 mechanism is greater than those of the π_4 and π_5 mechanisms (Krauskopf and Mollen, 1971), so that the overlap in time of the π_1 signals from the mask stimulus with π_4 and π_5 signals from the red probe stimulus is greater for a negative value of ΔT. Thus the ΔT dependence for the red probe stimulus is consistent with the properties of the different classes of receptor.

3.10 A Model for the Metacontrast Rod-Cone Interactions

The results of experiments (vii) and (ix) (summarized under points 6 and 8 above) show that the use of red backgrounds presented for three second periods or of rotation windmill masking stimuli resulted in changes in the masking action spectra, primarily for wavelengths around 500 nm, which is near the wavelength of the maximum sensitivity of the rod (π_o) mechanism. The effect of the red backgrounds and the rotating windmill stimuli on the rod and cone mechanisms is considered below.

1. The Effect of Red Background Stimuli

The increment threshold curve was determined for a 23' diameter 700 nm stimulus (lasting 3 sec) which was superimposed on a continuously-presented 700 nm uniform background field of

diameter 3^{o}. The results are shown in figure 3.46. The slope of the increment threshold curve varied continuously with the illumination level of the background field for illumination levels of the probe stimulus up to 1.2 log units above its threshold on zero background. Therefore the 700 nm probe stimulus excited only one mechanism at illumination levels up to 1.2 log units above absolute threshold (e.g. Stiles, 1959). Hence the 700 nm background stimuli used in the metacontrast experiments had no influence on the rod mechanism, as they were presented at an illumination level of only 0.5 log units above absolute threshold.

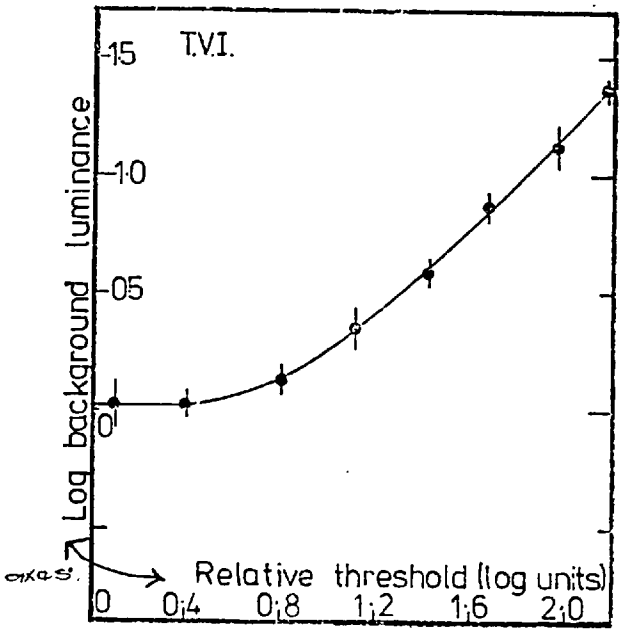

FIGURE 3.46

The effect of the red background stimuli used in the metacontrast experiments is to reduce the response magnitude of the long-wavelength cone mechanism. The effect of this on the masking action spectrum was to make it closer to the π_{o} action spectrum in shape (figures 3.32 and 3.33), which could be attributed simply to suppression of the masking cone signals. However, if this were the case, the masking sensitivity should <u>fall</u> for <u>long</u> wavelength annuli in the presence of the red background relative to that measured without the background.

This is not observed (figures 3.32 and 3.33), and, experimentally, an increase of masking sensitivity is observed for wavelengths around 500 nm, with sensitivity remaining approximately constant for long wavelength stimuli. Thus the effect of the red background is to facilitate rod-rod masking. As the background field does not stimulate rods directly, it appears probable that its effect on rod sensitivity is to remove cone inhibition of the rod system.

2. The Effect of Rotating Windmill-shaped Masks

When rotated at 20 Hz, the windmill stimulus is presented at a flicker rate above the critical fusion frequency for the rod mechanism (which is 15 - 18 Hz, Brindley, du Croz and Rushton, 1966), and it is thus equivalent to a stationary annulus in its effect on the rod mechanism. When the windmill is rotated at 150 Hz, the rate of the flicker is comfortably above the critical fusion frequency for all cone mechanisms (Dzn, 1954, 1958; Brindley, 1970), and is in this case equivalent to a stationary annulus for all response mechanisms. Differences between the masking action spectra which resulted when the windmill stimulus was rotated at 20 Hz and at 150 Hz are therefore due to differences in the cone response. The observed effect was that the sensitivity to masking is reduced for wavelengths below 600 nm for the windmill rotated at 20 Hz relative to that rotated at 150 Hz (figure 3.39). This again shows that the changes in the masking action spectrum at wavelengths around 500 nm are due to changes in cone input, as implied in part 1 above. In order that the conclusions remain consistent with that of part 1, this suggests that stimuli flickered at 20 Hz give increased cone signals, relative to steadily presented stimuli, thus reducing the masking sensitivity at wavelengths around 500 nm.

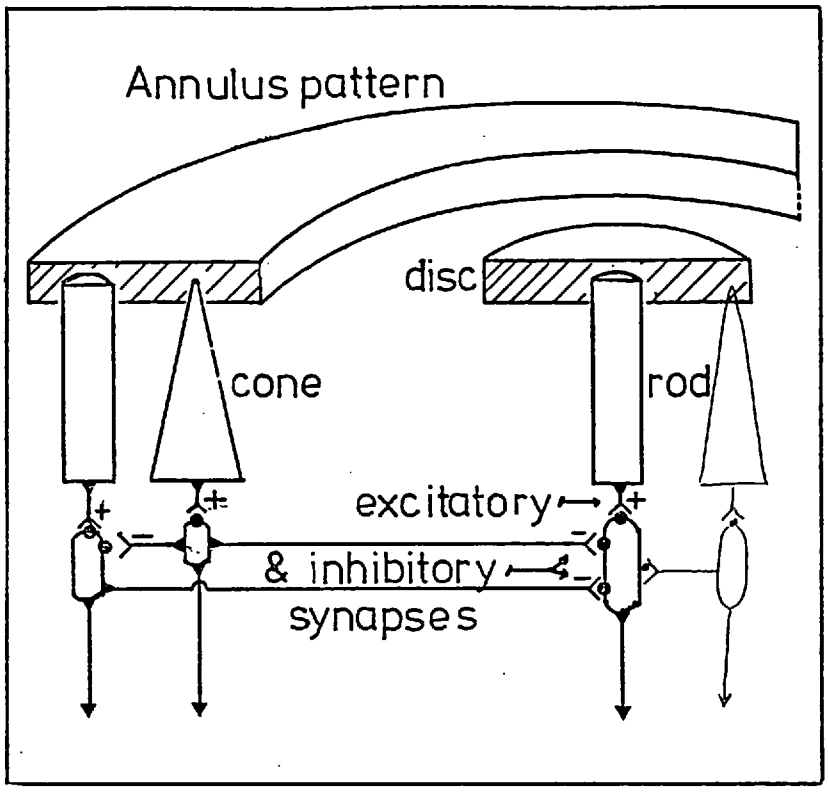

FIGURE 3.47 Model which accounts for metacontrast rod-cone interactions

A model of rod-cone interaction consistent with the above observations is given in figure 3.47. In this model lateral interactions are shown to occur at the level of the horizontal cell layer. (It will be shown in the next section that this cannot be the only site of lateral interaction, but the location of the interaction is not relevant for the purposes of the present discussion.)

It is proposed that the rod signals evoked by both the probe and the masking stimuli are masked by the cone signals evoked by the masking stimulus, via lateral inhibitory synapses (figure 3.47), and also that the rod signals elicited by the masking field mask the probe-elicited rod signals. According to this model, reduction by red background fields of the cone signals elicited by the mask

stimulus leads to a decrease of inhibition of the rod signals elicited by the mask stimulus. Consequently the masking of the probe signals by mask-elicited rod signals increases, and there is a relative increase in the sensitivity to masking at short wavelengths (increased rod-rod masking).

The fact that the masking sensitivity was affected by background stimuli which fell on the retinal area occupied by the probe stimulus, or on the area covered by both metacontrast stimuli, or on the inner edge of the mask stimulus (figure 3.12a), suggests that the inhibition of the masking cone signals by the red background fields occurs across relatively large distances.

3.11 The Sites of the Masking Interactions

In proposing the schematic model of figure 3.47 in the previous section, it was mentioned that it was not the intention to identify the site of the masking interacitons in that section. The question of the site of the interactions is examined in this section.

The action spectra of metacontrast masking differ for monoptic and dichoptic presentation of the same probe and masking stimuli (figures 3.15, 3.17 and 3.29 for $\Delta T = \pm 50$ ms; point 4, section 3.8, above). The masking action spectrum obtained dichoptically at $\Delta T = -50$ ms follows the π_o curve (figure 3.29) and occurs at a higher level of radiance than the corresponding curve measured for $\Delta T = +50$ ms. The masking action spectrum obtained monoptically at $\Delta T = -50$ ms is broader than the π_o curve (figure 3.15) and occurs at about the same level of masking radiance as the monoptic curve for $\Delta T = +50$ ms (figures 3.15 and 3.17). Again the time-courses of monoptic and dichoptic masking differ (figures 3.35 and 3.37): the peak masking sensitivities occur at $\Delta T = -50$ ms and 0 ms respectively for the

two cases, and the "valley" in the time-course curve is narrowest for dichoptic masking.

These differences suggest that the monoptic and dichoptic masking do not occur entirely at the same location in the visual system. Dichoptic masking must occur after the optic chiasma, whereas there is an opportunity for interactions within the retina in monoptic masking. Thus, it is possible that there are two sites at which masking occurs, which are differently organised, one of which is central and one peripheral. Further evidence about the organisation of these sites of interaction may be deduced from the other masking data.

The data of figure 3.28 establish that the sensitivity to monoptic masking increases with the size of the probe stimulus, and that the shape of the action spectrum of masking does not change greatly in shape for the probe sizes used. Now the threshold illumination level falls with increasing probe size because of summation within the rod mechanism (e.g. figure 3.8). The increase in sensitivity to masking by annular (figure 3.28) and spatially uniform stimuli (figure 3.31) may be attributed in part to the summation properties of the rod mechanism, but the increasing sensitivity to masking by the annular pattern with the increasing probe stimulus size may also be due to the decreasing separation of the edge of the probe pattern and the inner edge of the mask pattern (Battersby and Wagman, 1962; Sekuler, 1965), which in turn leads to increased masking in central units (Kolers and Rosner, 1960; Growney, 1976). Masking by a spatially uniform mask stimulus could not be induced dichoptically (results vi above), whereas it was easily demonstrated monoptically (figures 3.30 and 3.31), so that masking in central units is highly pattern-specific, whereas

peripheral masking occurs for annular or spatially uniform masking patterns. Again, this is indicative that the peripheral and central mechanisms are functionally different in organization.

The demonstration of rod-cone interactions has recently been confirmed for monoptic presentation of metacontrast stimuli (Foster, 1976; Yellott and Wandell, 1976) and for dichoptic presentation (Foster and Mason, 1977).

The failure of Alpern (1965) to find rod-cone interactions in metacontrast masking can be attributed to the stimulus conditions which were designed specifically to isolate rod responses: he used a large red adapting background field (which suppresses the measured rod-cone interactions, figures 3.32 and 3.33). Also his measurements were made at only one value of ΔT (ΔT = 50 ms), and the amount of rod-cone interaction depends strongly on the value of ΔT (figures 3.20, 3.34 - 3.36).

3.12 Correlations of the Masking Data with Neurophysiology

Numerous instances of rod-cone interaction have been cited in the psychophysical literature, of which some were quoted in the introduction (section 3.1).

Physiologically, mixed rod-cone input has been measured in single cells at all stages of the vertebrate visual system. Hammond (1971, 1972) demonstrated this for the visual cortex and LGN of the cat. He and Andrews also showed mixed rod-cone signals in single optic-tract nerves of the cat (Andrews and Hammond, 1970a,b), a finding which has been confirmed for the cat by Enroth-Cugell, Hertz and Lennie (1977) and Rodieck and Rushton (1976a) and the monkey by Gouras and Link (1966). Mixed rod and cone signals have also been recorded in the amacrine cells of cyprinid fish (Ruddock

and Djamgoz, in print: private communication), in cat horizontal cells (Steinberg, 1969a,b; Niemeyer and Gouras, 1973; Nelson, Kolb, Famiglietti and Gouras, 1976) and in the photoreceptors of mudpuppy (Fain, 1975), turtle (Schwartz, 1975b) and cat (Nelson, 1977). Whitten and Brown (1973a,b) recorded extracellular responses from the receptor layer of the intact macaque monkey eye and showed that the rod receptor potential was suppressed by cone-initiated lateral inhibition. This provides a strong reason for supposing that at least some cone-rod signal inhibition occurs at the receptor level. This hypothesis is given further support by the fact that horizontal cells are thought to receive input mainly via cones in the cat (Nelson, Lützow, Kolb and Gouras, 1975), since the long axons connecting the rods and horizontal cells (figure 1.6) do not conduct sufficiently to account for the rod responses recorded from horizontal cells. Anatomical evidence indicates that such rod-cone interactions can occur via direct rod-cone gap junctions (Raviola and Giula, 1973).

There are several models to account for the data of threshold and suprathreshold metacontrast masking. Most of these models are unrelated to primate physiology (e.g. Kahneman, 1967; Uttal, 1970; Turvey, 1973), and in the neurosensory models it is assumed that the masking occurs centrally (Weisstein, 1966, 1968, 1972; Bridgeman, 1971). In fact, inhibition of signals evoked by a probe stimulus by those of an adjacent mask stimulus has been demonstrated for the cat in ganglion cells by Poggio et al. (1969) and Bridgeman (1975), and by the latter author in the cat LGN and cortex.

It was shown earlier that dichoptic metacontrast masking is highly dependent on the shape of the mask stimulus. Such behaviour could be explained by masking at the level of simple cortical cells, which have circular symmetry but whose responses depend strongly

on the stimulus pattern and size (Hubel and Wiesel, 1968).

3.13 Spatial Summation during Dark Adaptation

It was found that the dark-adaptation curves of figures 3.9 and 3.10 changed in a regular fashion with the diameter of the probe stimulus. This is demonstrated in this subsidiary section.

The dark-adaptation curves of figures 3.9 and 3.10 obtained during the first ten minutes following bleaching could be superimposed exactly by sliding the curves vertically. None of the curves obtained for 495 nm stimuli followed the same time-course of recovery after the rod-cone break, however, indicating that the rate of threshold recovery of the rod system depends on the area of the probe flash, even though the bleaching conditions were identical. The time-course of recovery of rod threshold was exponential for all probe sizes, and a measure of the recovery rates was obtained by replotting the natural logarithm of the ordinate values in figures 3.9 and 3.10 against the abscissa values. The replotted data appear in figure

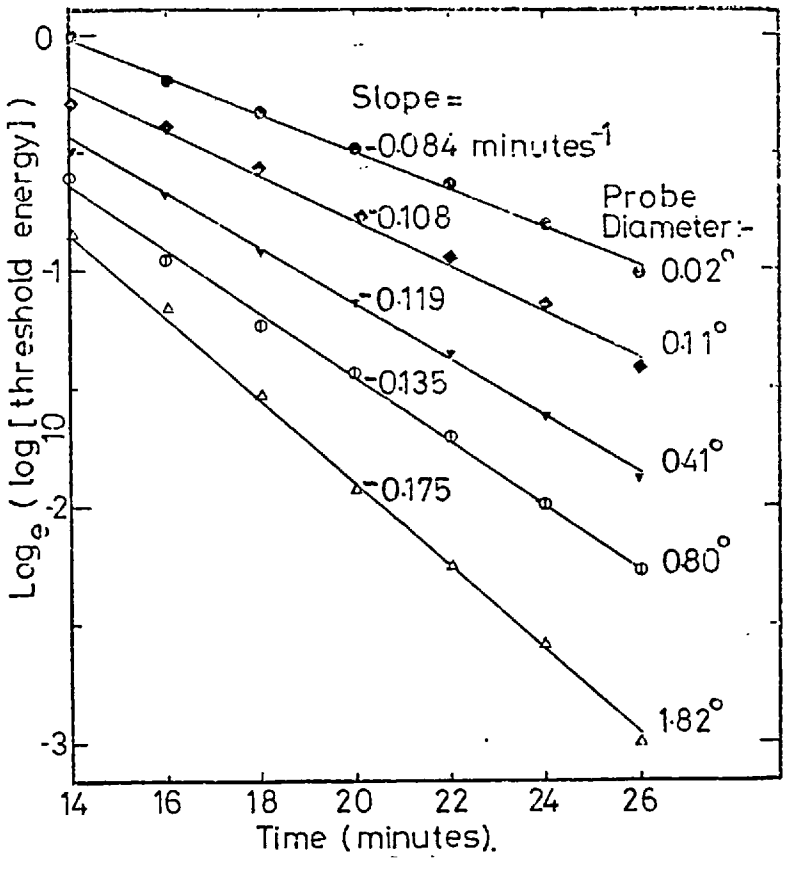

FIGURE 3.48 Log_{10} of the values of figures 3.9 and 3.10 replotted.

3.48, and it can be seen that the slopes of the curves decrease monotonically with the probe diameter.

The value of the slope of each line in figure 3.48 is the inverse of the time taken for the threshold of the corresponding probe stimulus to decay to 1/e of its value during recovery of the rod system. The characteristic times, or time constants, varied linearly with e^{-D}, where D is the probe diameter. This is illustrated in figure 3.49. The data point given by the open circle is the recovery time constant measured for the rod system by Gosline, MacLeod and Rushton [1976] using a probe diameter of 7^{o}.

It has been known for a long time that the rate of dark-adaptation is enhanced by increasing the size of the probe stimulus [Hecht, Haig and Chase, 1937; Craik and Vernon, 1941; Rushton and Cohen, 1954; Arden and Weale, 1954], and the above data indicate that the rate of dark-adaptation of the rod mechanism depends in a predictable manner on the probe stimulus diameter. Attempts have been made to explain the fact that the threshold of the rod mechanism is not dependent solely on the amount of rhodopsin bleached, both by psychophysical methods [Rushton and Westheimer, 1962; Rushton, Fulton and

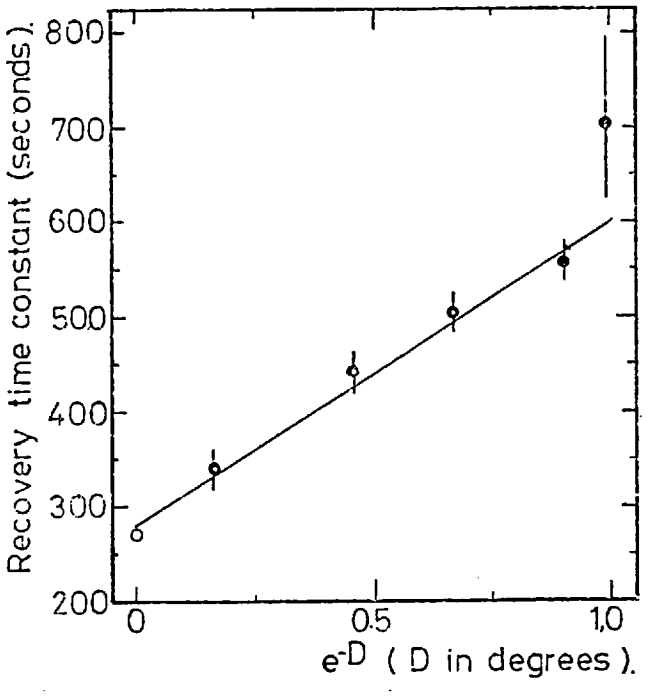

FIGURE 3.49 Recovery time constant versus probe diameter.

Baker, 1969; Rushton and Powell, 1971, 1972; Barlow and Andrews, 1973), and using electrophysiological techniques (Dowling, 1963; Steinberg, 1969c, Grabowski, Pinto and Pak, 1972; Schwartz, 1973, 1975a; Copenhagen and Owen, 1976; Lennie, Hertz and Enroth-Cugell, 1976). Dowling (1963) attributed the effect of probe area on the dark-adaptation rate to 'neural adaptation'. The site of the interaction is uncertain, but it could be due to a membrane recovery process (Steinberg, 1969c; Grabowski et al., 1972).

The recovery time constant, which must depend on the recovery of rhodopsin and of the putative membrane process, depends in a regular manner on the probe diameter. This might be explained by a model of the type proposed by Naka and Rushton (1967) and Lamb (1976) for the horizontal cell layer, in which the threshold voltage at the centre of a stimulus is determined in a predictable manner by the membrane resistance of the horizontal cell layer, and by the size of the probe stimulus.

3.14 Conclusion

The investigations described in this chapter have demonstrated that rod-cone interactions occur in metacontrast masking. A model which accounts for the data assumes that cone-rod interaction occurs between signals elicited by the mask stimulus, and that cone-rod and rod-rod masking occurs between the probe and masking signals (figure 3.47). The increasing relative contribution of cone-rod masking at increasing values of ΔT, the time between the stimulus onsets, was attributed to the slower temporal response of the rod (π_o) mechanism (section 3.9). Cone-cone metacontrast masking was also shown not to be mechanism specific (figure 3.45). Rod-rod and cone-rod masking were demonstrated monoptically and dichoptically.

The dichoptic masking results from interactions in central units and, unlike the monoptic results, were highly dependent on the differences between the patterns of the probe and mask stimuli. Possible reasons for the failure of Alpern (1965) to find rod-cone interactions in metacontrast masking are proposed (section 3.11). Numerous instances of rod-cone interaction measured psychophysically and electrophysiologically support the conclusions drawn from present data, which demonstrate that rod and cone signals share common pathways. Finally, data from a preliminary dark-adaptation experiment are analysed, and it is shown that the rate of dark-adaptation varies in a functionally related way with the probe stimulus diameter.

Chapter 4

Modification of Colour Matches Induced by Adaptation to Spatially or Temporally Structured Periodic Stimuli

4.1 Introduction

It is known that the contrast threshold illumination level of a test grating is influenced by adaptation to a grating stimulus and that the effect is dependent on the spatial properties of the adaptation stimulus (Gilinsky, 1968; Pantle and Sekuler, 1968; Blakemore and Campbell, 1968, 1969). In the study described in this chapter, colour matches were established between the two halves of a colorimeter probe field following adaptation to an asymmetric stimulus. The upper half of the asymmetric adaptation field was always uniform and the lower half was either uniform or contained a grating structure (figure 2.9a,b). The observer fixated on the centre line between the two halves of the adaptation field and this procedure results in differential adaptation by the two half-fields. The average illumination levels of the two halves of the adaptation field were always equated, but as will be shown, the grating structure in the lower adaptation half-field gave rise to changes in the colour matches compared to those established when both halves of the adaptation field were uniform. The hue shifts were observed at illumination levels of the adaptation stimuli well below the minimum level (10^4 trolands) at which spatially uniform adaptation stimuli disturb colour matches (Wright, 1936; Brindley, 1953).

The aim of the experiments reported in this chapter was to investigate the colour shifts associated with grating adaptation, and to determine how the colour matches depend on the wavelengths

of the test and adaptation fields, and on the spatial frequencies and illumination levels of the grating adaptation field. Experiments were also performed with flickering adaptation stimuli in order to assess the relative importance of temporal effects associated with involuntary or voluntary scanning of the grating adaptation stimulus.

The author BN, an emmetropic male aged 24 with normal colour vision, was the principal observer for the experiments. Some experiments were repeated with a female subject TP, aged 21 who also possesses normal colour vision. A correction of -1.5 D was required for this subject, who was mildly myopic. An account of this work is in press for publication (Nunn, 1977).

4.2 Procedure

During each period in which an adaptation stimulus was visible, the observer moved his point of fixation continuously along the central fixation line (figure 2.9) in order to minimise local retinal adaptation (Jones and Tulunay-Keesey, 1975). At the start of each colour-matching sequence, the initial adaptation process lasted for at least two minutes, after which the adaptation field was occluded for 0.5 seconds every 10 seconds. The probe field was presented during the 0.5 second interruptions. The illumination levels of the red, green and blue component stimuli of the matching half of the probe field were adjusted during the ten second readaptation periods, in order to obtain a match between the matching and test halves of the probe field (figure 2.8a). The relative illumination levels of the red, green and blue stimuli required for the match were recorded from the W2 wedge scales (figure 2.6).

Representation of Experimental Data

The relative illumination levels of the matching stimuli were used to calculate, in the WDW system (Wright, 1946), the red and green chromaticity coordinates (r and g respectively) for the match, and these values were plotted in the WDW chromaticity diagram (appendix E).

The uniform adaptation field (figure 2.9a) was used as a reference adaptation stimulus. For each colour match established following adaptation to the grating stimulus (figure 2.9b), a reference colour match was also obtained for a uniform adaptation field with the same colour and average illumination level. (A similar procedure was also adopted for matches established when the lower half of the adaptation field was flickered, i.e. for temporal as opposed to spatial modulation of the lower half of the adaptation stimulus). At least four matches were made for each combination of adaptation- and probe-field conditions, and any change between the average colour matches established under the reference (uniform) adaptation field and that established under the grating adaptation field gives rise to a shift in the chromaticity co-ordinates. The changes in colour-matches are recorded on the WDW chromaticity diagram by means of arrows (e.g. figure 4.1a). The tail of each arrow corresponds to the matches made under conditions of spatially uniform and temporally steady adaptation, and the head of each arrow corresponds to the matches made under adaptation to the grating stimuli. The magnitudes of the standard deviations of the mean of the red and green chromaticity co-ordinates were evaluated for each colour-match determination. The larger of the two standard deviations, obtained for the red chromaticity values at either end of each arrow, is drawn alongside that arrow as a horizontal line: the length of each

line represents twice the standard deviation. Similarly, the vertical line alongside each arrow represents twice the magnitude of the larger of the standard deviations for the two green chromaticities.

The wavelength of the test stimulus (i.e. the lower half of the probe field) was varied between 440 nm and 680 nm, and sufficient desaturation was added to the test stimulus whenever necessary, so that it could be matched by a mixture of the three matching stimuli. The chromaticity co-ordinates of all test stimuli which were used lay within the triangle whose vertices are defined by the chromaticity points of the green (530 nm), blue (460 nm) and red (650 nm) matching stimuli ((r,g) = (0,1), (0,0) and (1,0) respectively). The effects of the desaturating stimuli used were not subtracted during the calculations of the chromaticity co-ordinates so that no assumption was made regarding the additivity of the parafoveal region under study. In the first set of experiments, the adaptation condition was defined by a particular combination of wavelength and illumination level. For each adaptation condition,a number of desaturated, near-monochromatic test stimuli with wavelengths covering the visible spectrum were investigated. The desaturated test stimuli will be referred to as 'monochromatic test stimuli', or simply 'test stimuli'. The matches established for each of these test stimuli, under the two adaptation conditions (figures 2.9a, 2.9b), were plotted on the same chromaticity diagram. Separate chromaticity diagrams were constructed for each adaptation wavelength condition. Note that the resulting chromaticity diagrams pertain only to the parafoveal retinal regions stimulated by the probe field. In the first set of experiments, the retinal illumination level of the two adaptation fields was set at 1500 td at 530 nm and that of the

test stimulus was set at 140 trolands at 500 nm. The adaptation fields were set at the same radiant flux level for all wavelengths ('constant radiance input'), rather than at a constant photometric level, e.g. at constant troland level. Similarly, test stimuli of different wavelengths were also, as far as possible, set at the same radiant flux level. Test stimuli of wavelengths less than 470 nm were set at the maximum available flux levels, these being lower than that of the 500 nm test stimulus. The following experiments were performed.

1. Colour matches were established under adaptation to both adaptation stimuli (figures 2.9a,b) for a number of wavelengths of the adaptation and test stimuli. The spatial periodicity of the grating adaptation field (figure 2.9b) was 1.69 cycles deg^{-1}. Seven adaptation wavelengths were used between 405 nm and 694 nm, and about 8 wavelengths of the test stimulus were used for each adaptation stimulus. The observations were repeated for a second observer, TP, for one test field wavelength and for each of five adaptation wavelengths.

2. The effect on the colour matches of changing the periodicity of the grating pattern in the lower half of the second adaptation field was determined and the intensity of the adaptation field was also varied in order to study its effect on the colour matches. The way in which the effect varied, after the adaptation field was occluded following five minutes of adaptation, was also measured.

3. The hue shifts were measured using a grating probe stimulus. Stimuli were again presented monocularly. At first, the probe field shown in figure 2.8a was used, with an identical grating pattern in each half-field. However, the field appeared vertically

non-uniformly coloured following adaptation. This non-uniformity was reduced considerably by presenting the probe field shown in figure 2.8c. The length of the vertical bars of the two half fields of the probe stimulus in figure 2.8c is less than the vertical height of the fields in figure 2.8a. The presentation sequence of the adaptation and probe stimuli which was described earlier was used in this experiment. The variable parameter in this experiment was the periodicity of the adaptation grating. The periodicity of the probe field structure was constant and equal to 5.63 cycles deg^{-1}.

4. The hue-shifts induced by flickering stimuli were first studied using binocular colour-matching. The adaptation stimuli were presented to the right eye, and the adaptation wavelength was 656 nm. The test and desaturating wavelengths were 630 nm and 490 nm. The lower, test half of the probe field was presented to the (light-adapted) right eye, and the upper matching half to the dark-adapted left eye (figure 2.8c). Red fixation lines were presented in each eye to allow correct fusion of the fields. Both eyes were fully dark-adapted at the start of the measurements. The left eye was kept in the dark-adapted state during the course of measurements, and the illumination level of the adaptation field in the right eye was increased progressively from the lowest value.

The experiment with flickering adaptation stimuli was repeated using monocular colour-matching. The probe field used is shown in figure 2.8a. Either the spatially uniform or the grating adaptation stimuli was used, with the lower half either steady or flickered. For each adaptation wavelength and grating spatial frequency, the flicker frequency of the lower half was varied and the effect of this variation measured. The cycle of presentation of the probe

and adaptation stimuli was as described above (at the start of 'Procedure').

4.3 Results

1. Disturbances of Colour Matches made with Spatially Uniform Matching Stimuli

The chromaticity co-ordinates obtained for the various test and adaptation wavelengths are shown in figures 4.1 - 4.7. The chromaticity co-ordinates for each test stimulus, obtained for adaptation to a uniform and to a grating stimulus (figures 2.9a,b) are connected by arrows in the chromaticity charts. The tail of each arrow is located at the chromaticity point (r,g) corresponding to the match made by the observer while adapted to the uniform field, while the head of each arrow plots the match made under adaptation to the grating field. The spatial frequency of the vertical bars of the grating half of the adaptation field was 1.69 cycles deg^{-1} for the results plotted in figures 4.1 - 4.7, and each of these figures refers to a single adaptation wavelength. The average of four readings was taken for each chromaticity point, and the standard deviations of the r and g values were determined for the two chromaticity points at either end of each arrow. The pair of crossed horizontal and vertical bars alongside each arrow in the WDW diagrams indicate the magnitude of the larger of the two standard deviations of the r and of the g coordinates, respectively. The ringed cross in each diagram corresponds to the colour match established with the dark adapted eye for a near-monochromatic test stimulus of wavelength equal to that of the adaptation stimulus. The results are plotted on the WDW chromaticity

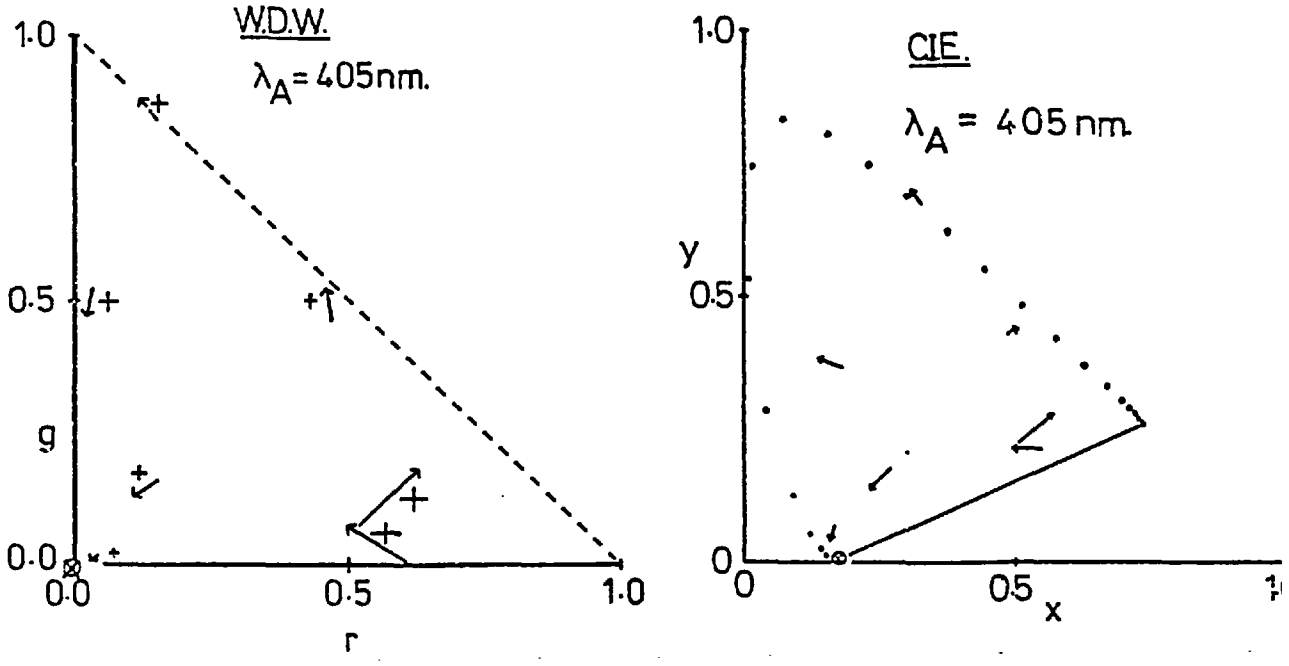

FIGURE 4.1 WDW and CIE chromaticity diagrams showing chromaticity shifts obtained following the introduction of a grating structure into the lower half of a 405 nm adaptation stimulus.

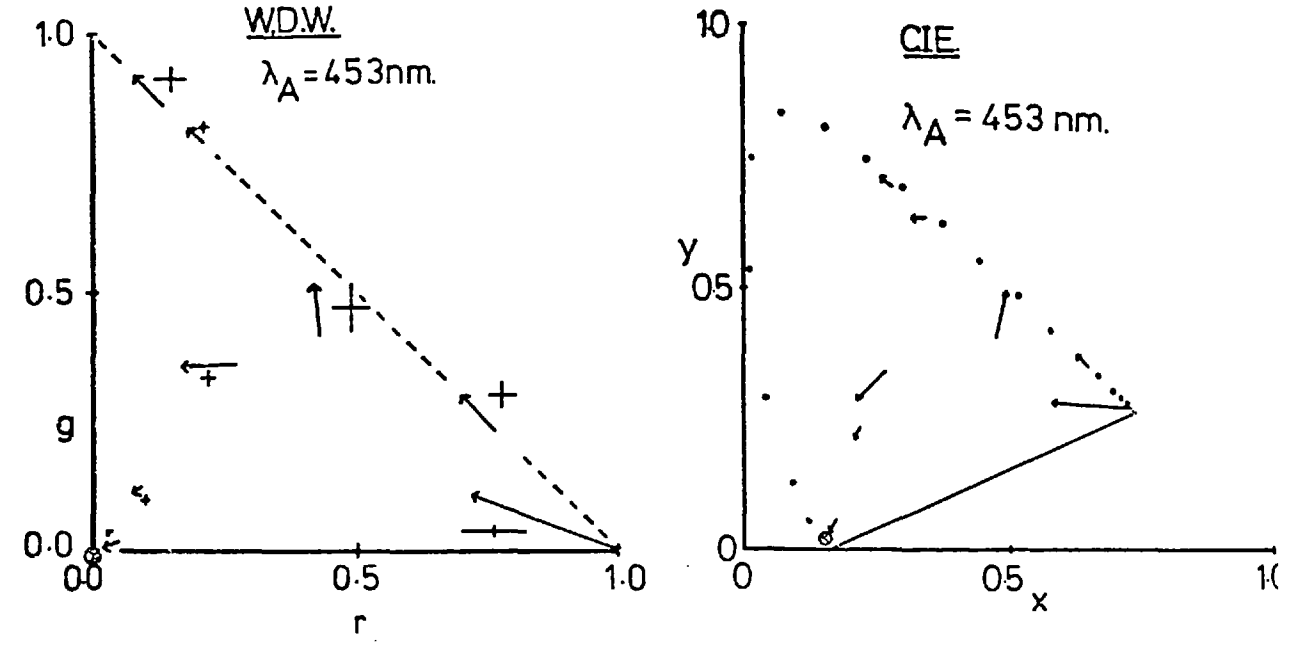

FIGURE 4.2 (As above, for an adaptation wavelength of 453 nm).

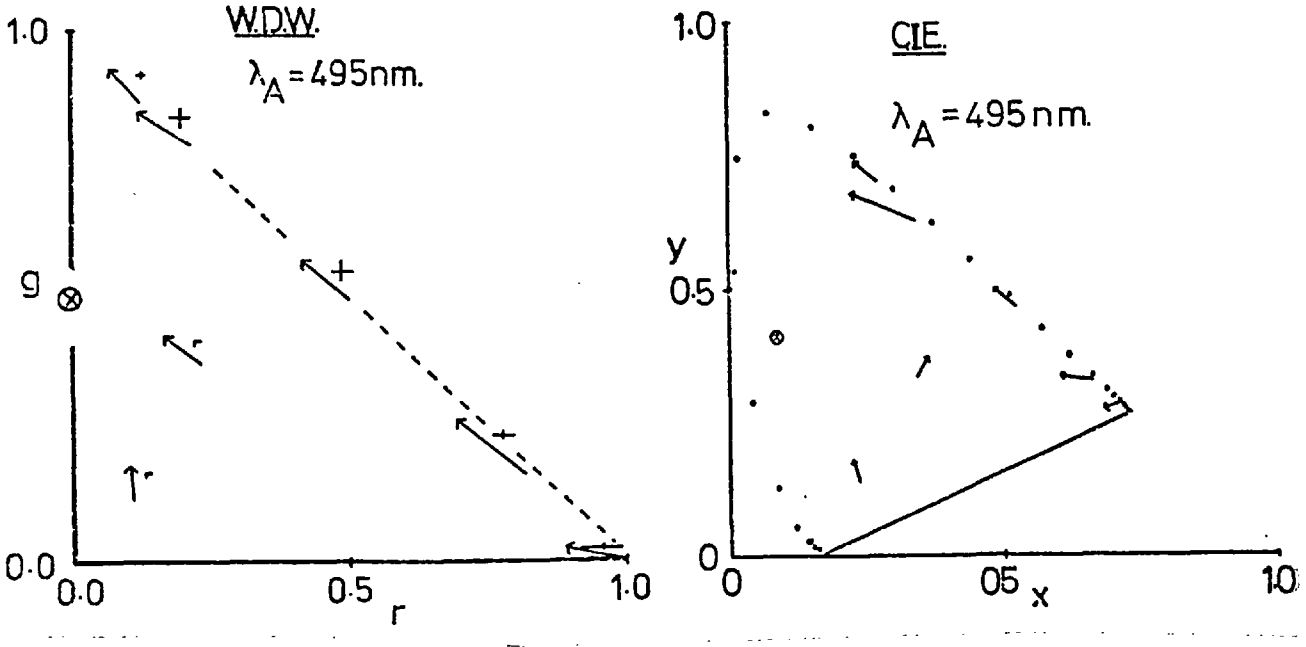

FIGURE 4.3

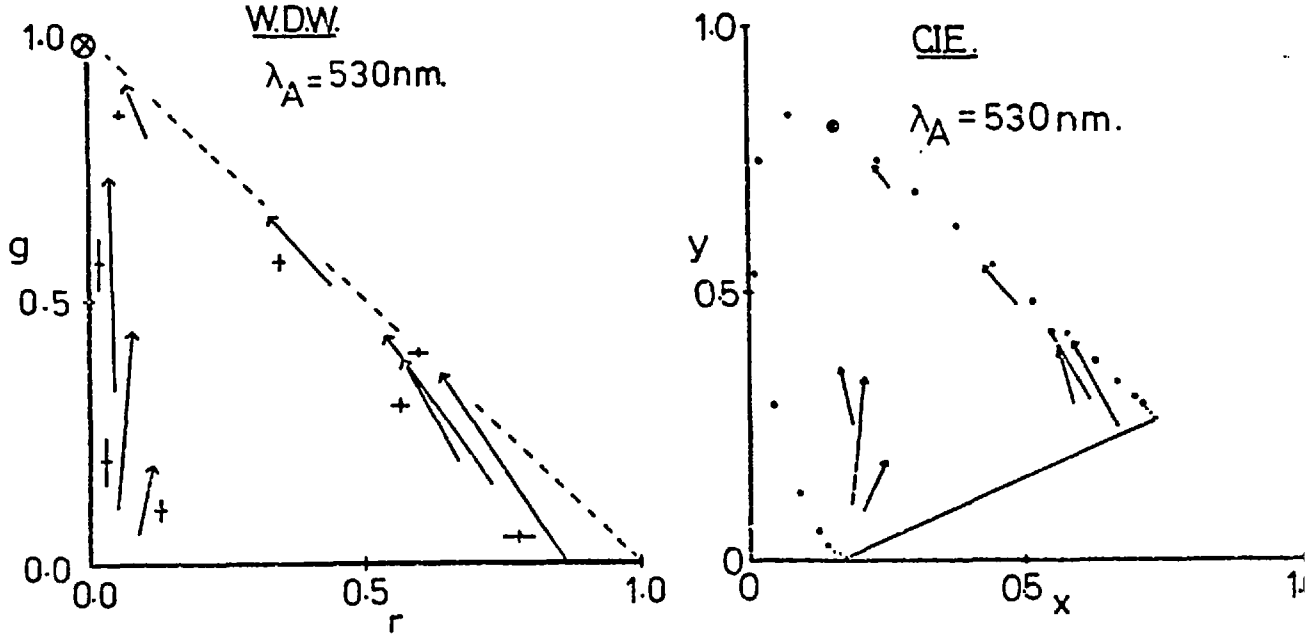

FIGURE 4.4

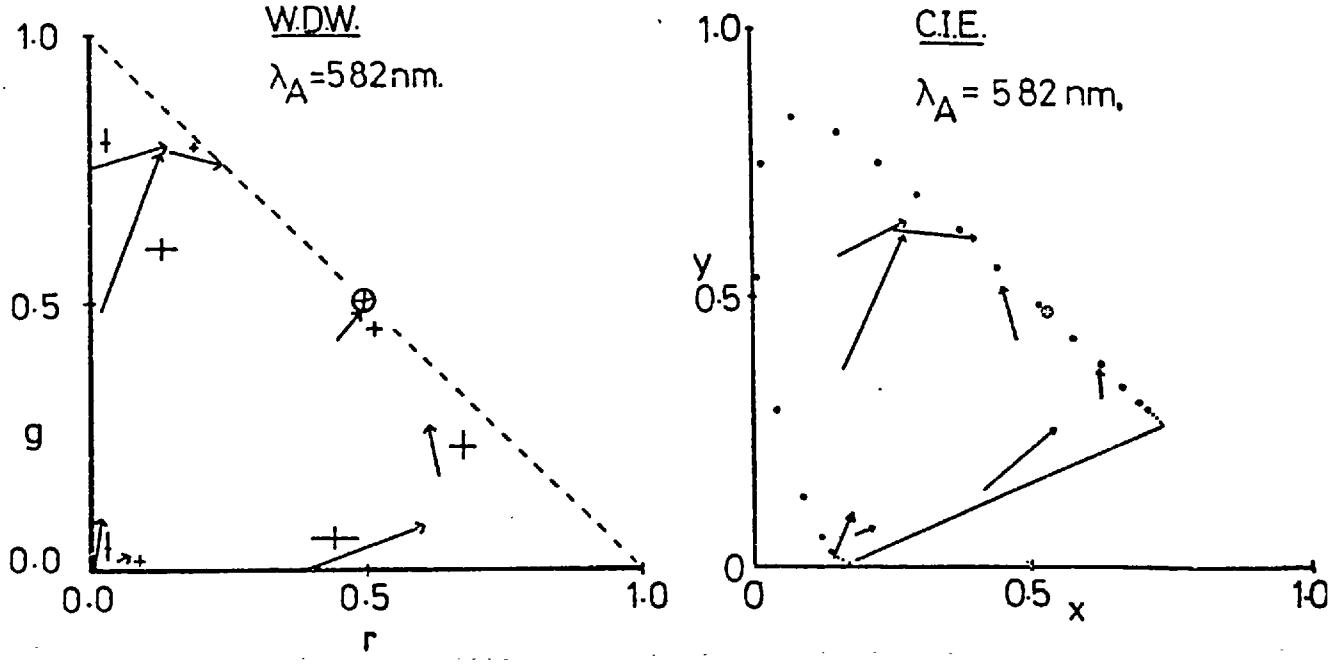

FIGURE 4.5

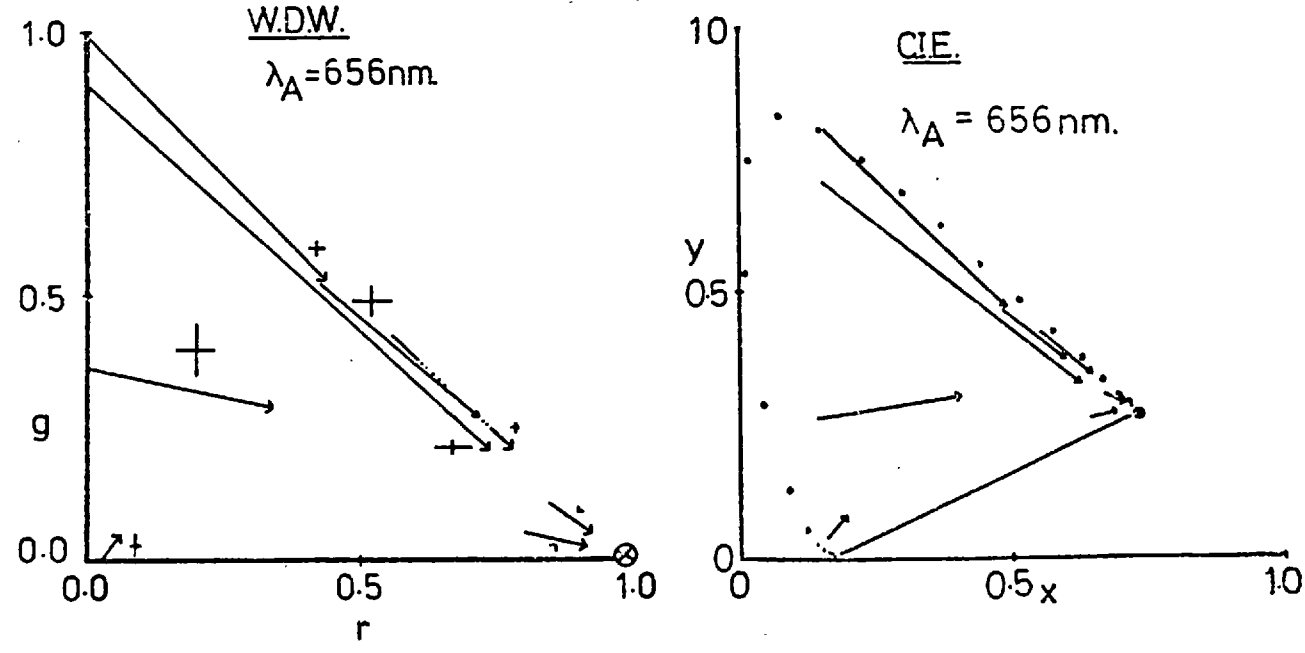

FIGURE 4.6

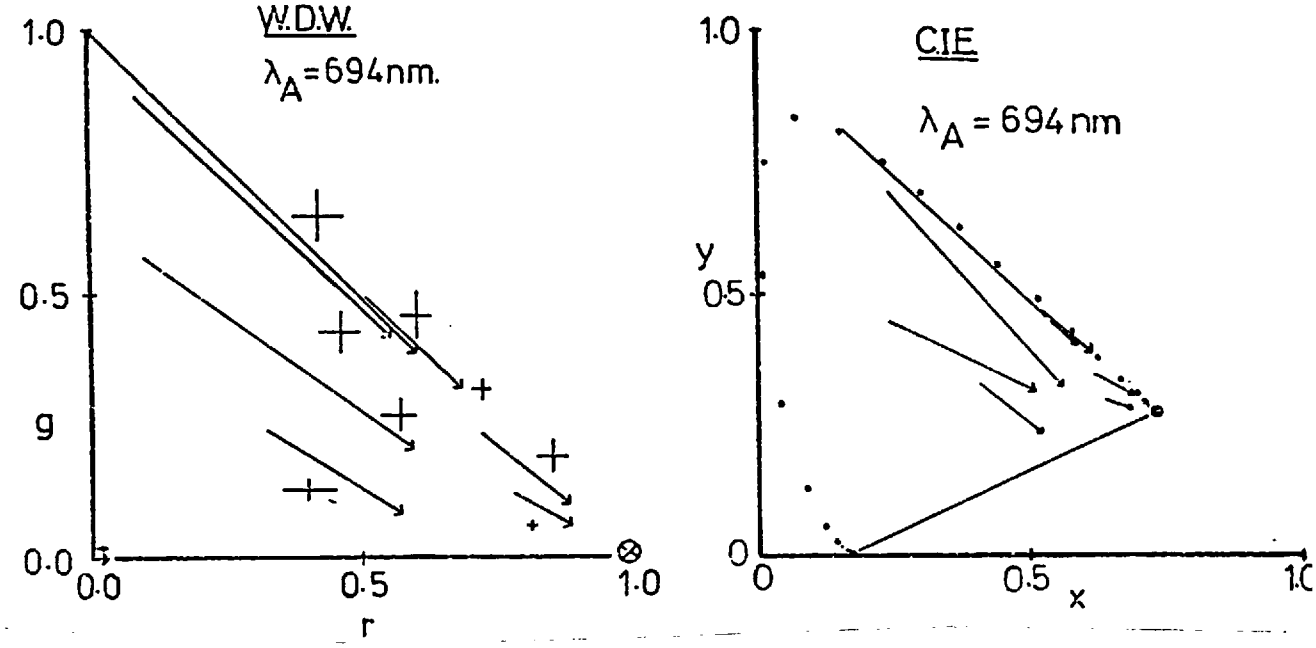

FIGURE 4.7

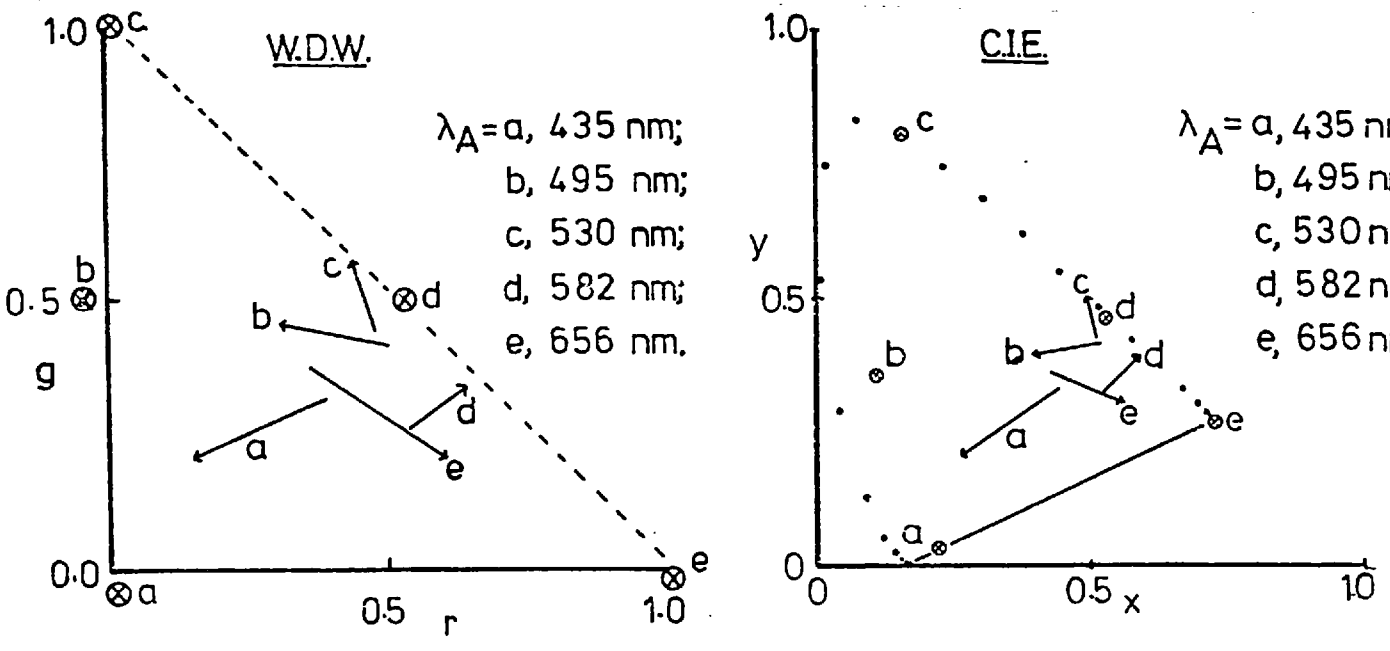

FIGURE 4.8

diagram for all adaptation wavelengths (λ_A), and are also plotted on the CIE chromaticity diagram for comparison. (The transformation from the WDW to the CIE co-ordinates is given in Appendix B.)

It can be seen that for green (530 nm), and red (650 nm and 694 nm) adaptation stimuli, all the arrows point in the direction of the chromaticity point corresponding to the adaptation wavelength. Adaptation to blue (405 nm and 453 nm), blue-green (495 nm) and yellow (582 nm) stimuli resulted in several directions of shift. For these adaptation colours, test colours whose chromaticity points were close to the adaptation field chromaticity point were shifted towards this point under conditions of grating adaptation, whilst those that were further away were shifted more towards the red (650 nm) or the green (530 nm) chromaticity points.

A limited set of data obtained for observer TP is presented in figure 4.8, and it can be seen that these data show similar trends to those noted above for observer BN.

The periodicity of a 656 nm adaptation grating stimulus was varied, and the effect of this variation was measured for a single observer, BN, using a 530 nm test stimulus with an added 460 nm desaturating stimulus. The direction of the colour shift on the chromaticity diagram was the same for all spatial periodicities, and the lengths of the arrows for the various grating spatial periodicities were taken as a qualitative measure of the shift magnitude. These relative shift magnitudes are plotted in figure 4.9a: the arrow in the WDW chromaticity diagram inset represents the maximum shift obtained. It can be seen that the effect falls off with increasing spatial periodicity and reaches zero just above 20 cycles deg^{-1}, consistent with the parafoveal

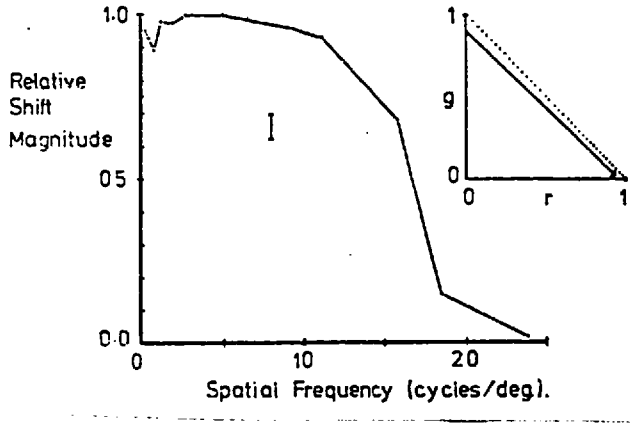

FIGURE 4.9a Plot of the relative shift magnitude versus the spatial frequency of the adaptation grating.

grating acuity limit of 25 cycles deg^{-1}, which was measured experimentally for observer BN. The chromaticity points resulting from adaptation to different grating spatial periodicities (figure 4.9a) were replotted on the 1960 CIE-UCS chromaticity diagram, for which there is an approximately uniform scaling of chromaticity (Wyszecki and Stiles, 1967, p. 456). The replotted data are shown on the CIE-UCS diagram in figure 4.9b, and the relative shift magnitudes for this diagram appear in figure 4.9c. Comparison of figures 4.9a and 4.9c shows that the shift magnitude varies qualitatively in the same manner for the two

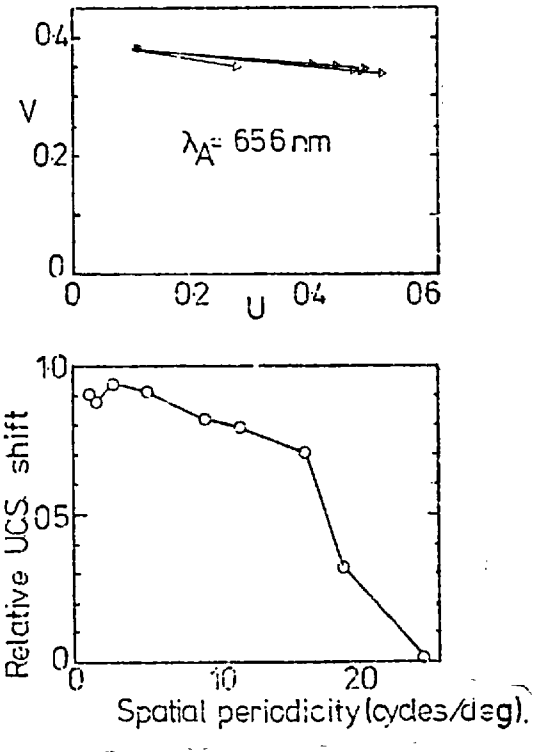

FIGURES 4.9b & c Data of fig. 4.9a replotted for CIE-UCS diagram.

chromaticity diagrams.

An interesting effect, which does not show on the chromaticity plot, is illustrated in figure 4.10. In this diagram the logarithm of the relative amounts of the red, green and blue matching stimuli required to match the test stimulus after adaptation are plotted as a function of the grating spatial frequency. The zero on the ordinate scale corresponds to the amounts of red, green and blue stimuli needed to match the test stimulus following adaptation to a uniform adaptation stimulus. The significant point about these data is that the relative amount of the blue stimulus (460 nm) needed in the match, following grating adaptation, falls to a minimum at around 0.7 cycles deg^{-1}, and the relative amount of green (530 nm) stimulus falls to a broad minimum at higher spatial periodicities. The change in the red stimulus (650 nm) is much larger than those of the blue and green, however, so that these effects are not significant when plotted on the chromaticity diagram.

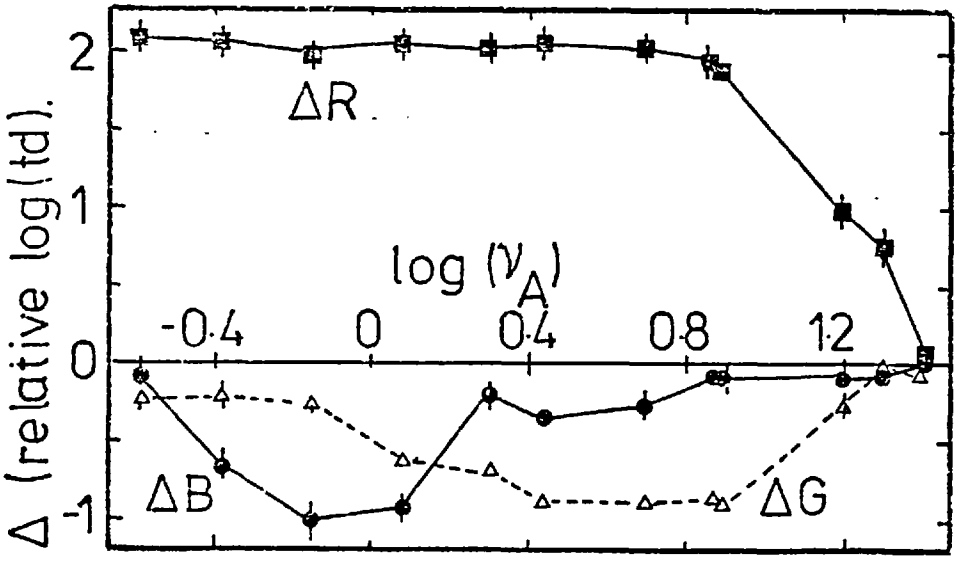

FIGURE 4.10 Values of log ΔR, log ΔG and ΔB versus spatial periodicity (log ν_A).

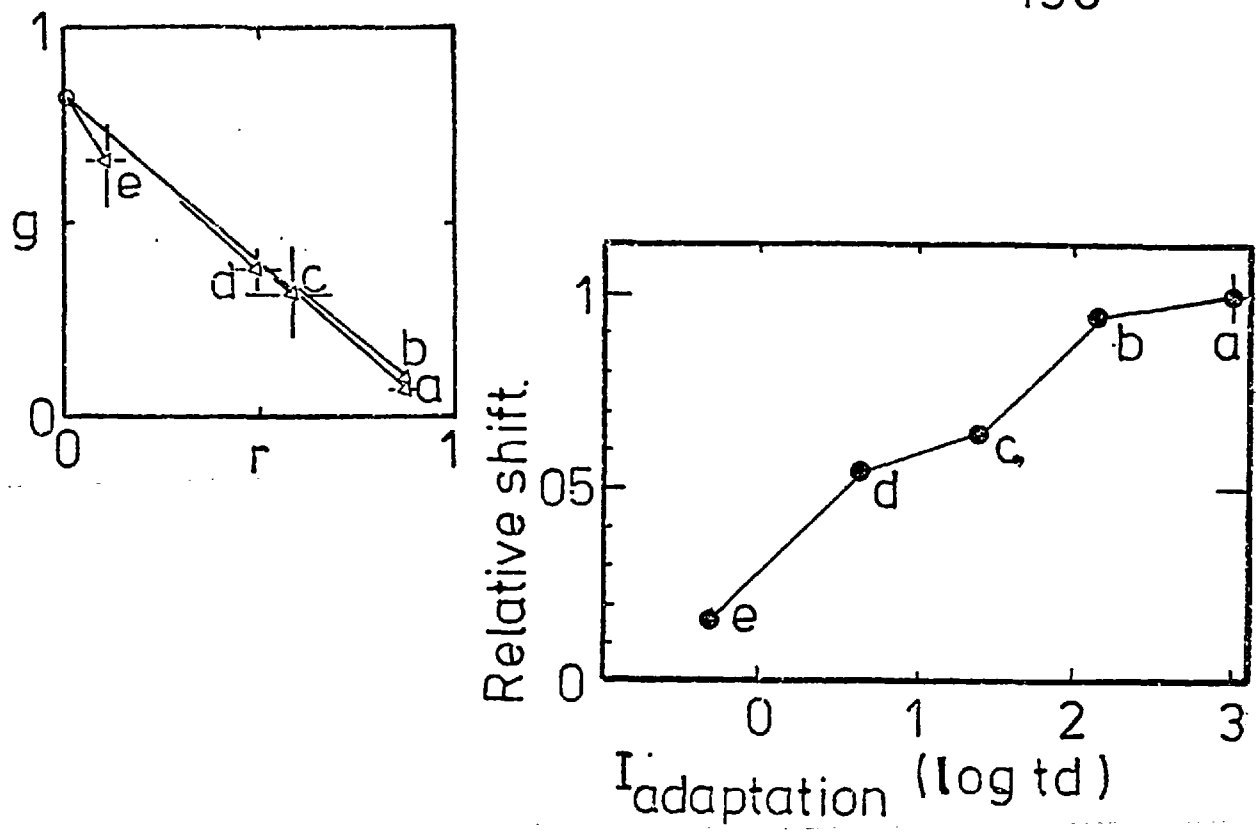

FIGURE 4.11 Colour shifts obtained for various adaptation illumination levels - the illumination levels for the points a - e in figure 4.11a are shown in figure 4.11b.

Results for various illumination levels of the adaptation fields (figures 2.9a,b) are presented in figure 4.11. These data were obtained with an adaptation wavelength of 656 nm and with a spatial periodicity of 5.1 cycles deg^{-1}, and the comparison (or lower) half of the probe field was again composed of a mixture of lights of wavelengths 650 nm, 530 nm and 460 nm. The shifts obtained for the various adaptation illumination levels are shown in figure 4.11a, where the adaptation illumination levels are indicated in decreasing value by a, b, c, d and e alongside the arrowheads. The shift direction again remained almost constant for all five illumination levels of the adaptation stimulus, and the length of the arrows representing the shifts were again taken as a measure of the relative shift magnitude. These relative shift magnitudes are plotted in figure 4.11b for the various illumination levels, and it is seen that they increase monotonically with increasing intensity.

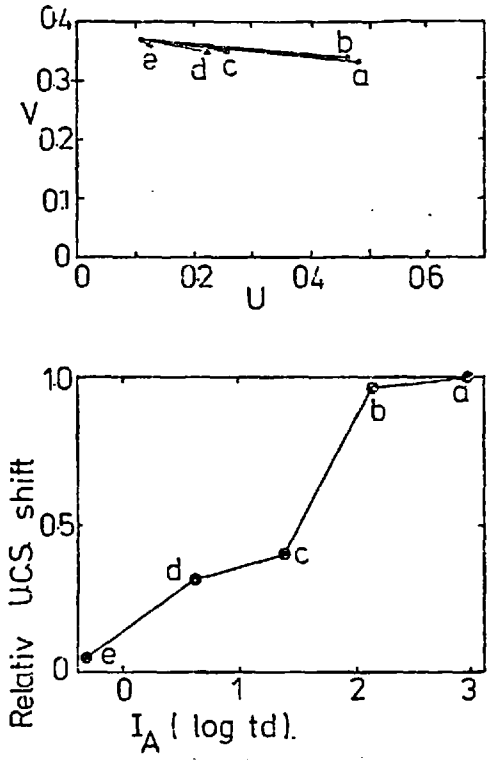

FIGURE 4.11 c & d Data of figures 4.11a,b replotted for CIE-UCS diagram.

The data were again transformed to the 1960 CIE-UCS system, and data appear in figure 4.11c. The relative shift magnitude on the CIE-UCS diagram also increases monotonically with the illumination level of the adaptation stimulus (figure 4.11d).

Average data for the temporal decay of the grating-induced hue shift following cessation of adaptation are plotted in figure 4.12. The data are averaged from five sets of measurements, each taken after five minutes of adaptation to a grating stimulus of wavelength 656 nm and spatial periodicity 5.6 cycles deg^{-1}, and refer to a 560 nm test stimulus. It can be seen that following cessation of adaptation, the colour match changes from that measured in the fully light-adapted state to that measured for the non-adapted state and reaches the latter after about one minute.

The possibility was considered that the colour shifts, which were obtained with spatially structured stimuli, might be due to a reduction in the efficiency of the grating adaptation fields, compared with that of the uniform adaptation fields. Reduction in the efficiency of the adaptation field was simulated

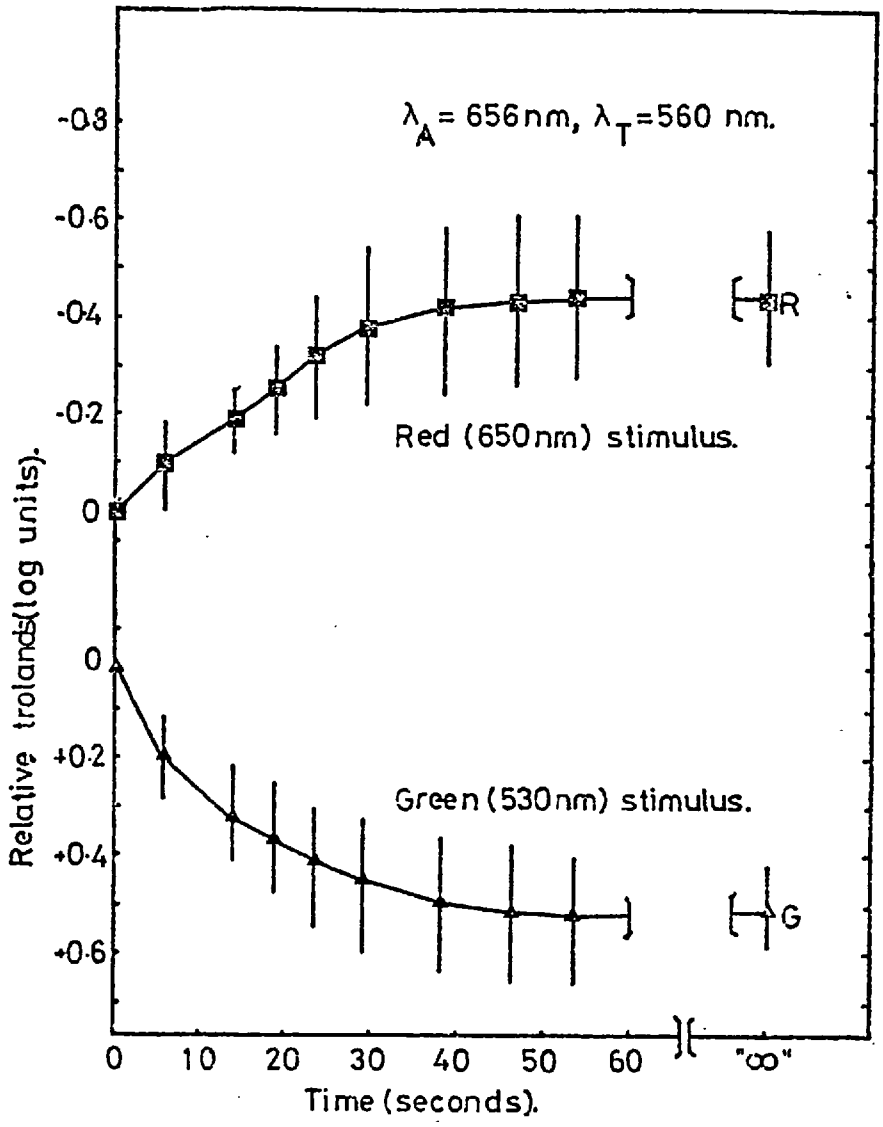

FIGURE 4.12 Recovery of colour match following grating adaptation.

by reducing the illumination level of the lower half of a uniform adaptation field (figure 2.9a) by 0.8 log units relative to that of the top half. Measurements were made with this asymmetric adaptation stimulus and were compared with the measurements made under adaptation to a uniform stimulus with equal illumination levels in the upper and lower halves (figure 2.9a). The results of this differential adaptation experiment are shown in figure 4.13 for observer BN, and it can be seen that for different wavelengths

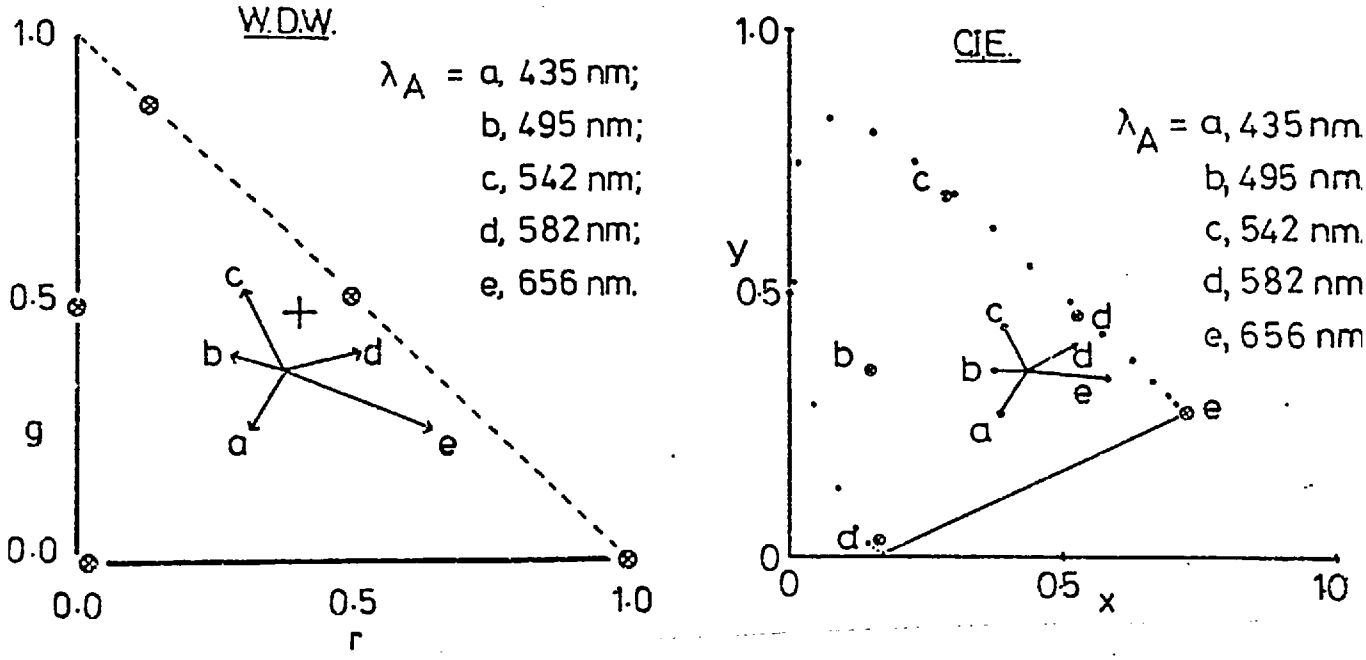

FIGURE 4.13 Chromaticity plots of hue shifts resulting from reduced illumination level in the lower half of the adaptation field.

of the adaptation field, the direction of change in chromaticity of the probe field is towards the chromaticity point corresponding to the adaptation stimulus. Thus, the effect of reducing the illumination level of the lower half of the adaptation stimulus stimulates, qualitatively, the effect of presenting a grating stimulus in the lower half of the adaptation field. It is therefore possible that the colour shifts which have been measured are a result of the reduced adapting efficiency of the grating stimulus, relative to that of a spatially uniform stimulus of the same average illumination level. It is important to note, however, that by reducing the illumination level of the spatially uniform adaptation stimulus, the adaptation at receptor level is reduced, whereas in all previous experiments, great care was taken to ensure that the space-average illumination level of the grating

half of the adaptation field was equal to that of the uniform field.

2. Spatially Structured Probe Stimulus

Adaptation experiments were also performed using the spatially structured probe stimulus (figure 2.8c) in the form of a grating of spatial periodicity equal to 5.1 cycles/degree. The data of figure 4.14 were obtained when the adaptation and test-field wavelengths were 656 nm and 582 nm respectively. The chromaticity shifts are in the same general direction, and there is no substantial difference in shift magnitude (as measured by

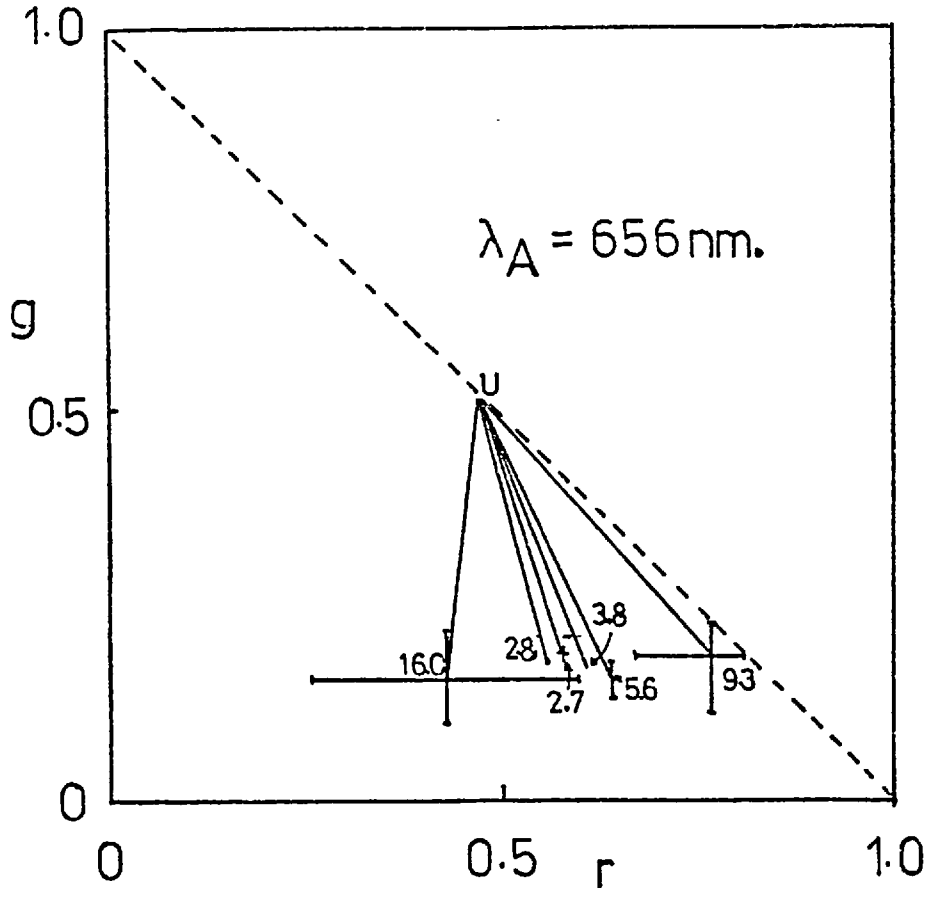

FIGURE 4.14 Colour shifts. The figures on the diagram are the spatial periodicities of the adaptation grating (cycles/degree).

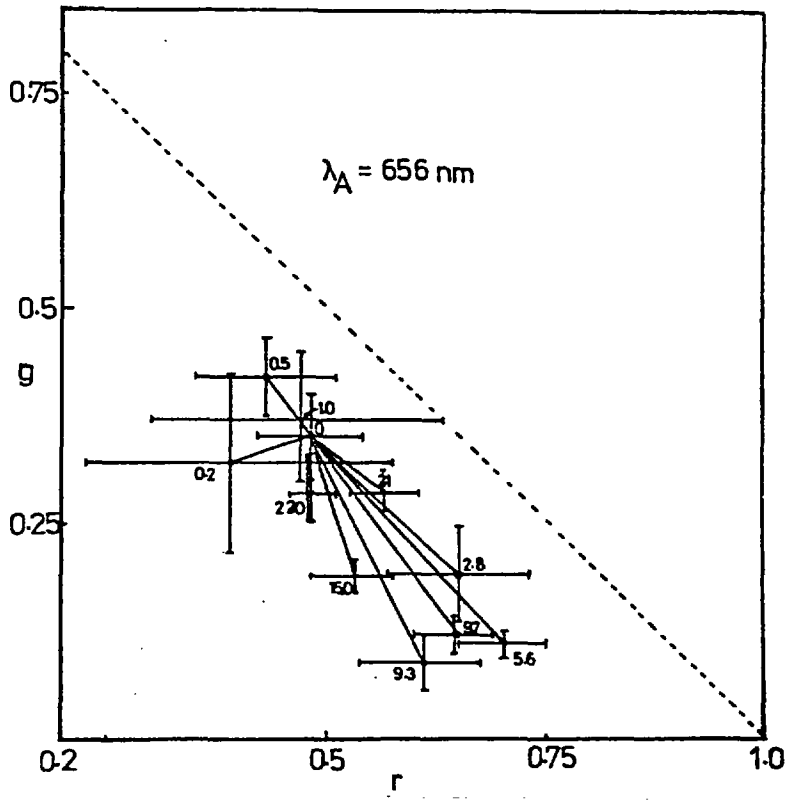

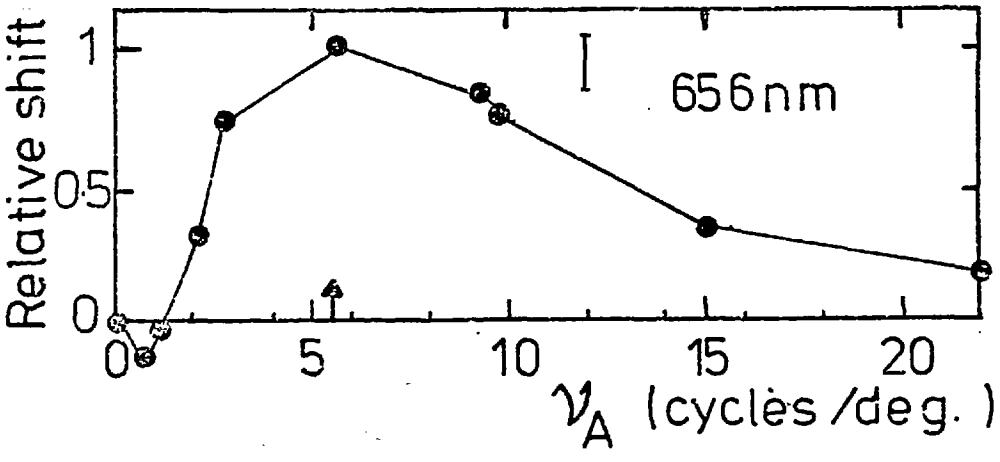

FIGURE 4.15 Colour shift data on WDW chromaticity diagram (a) and plot of relative shift magnitude versus spatial periodicity (b).

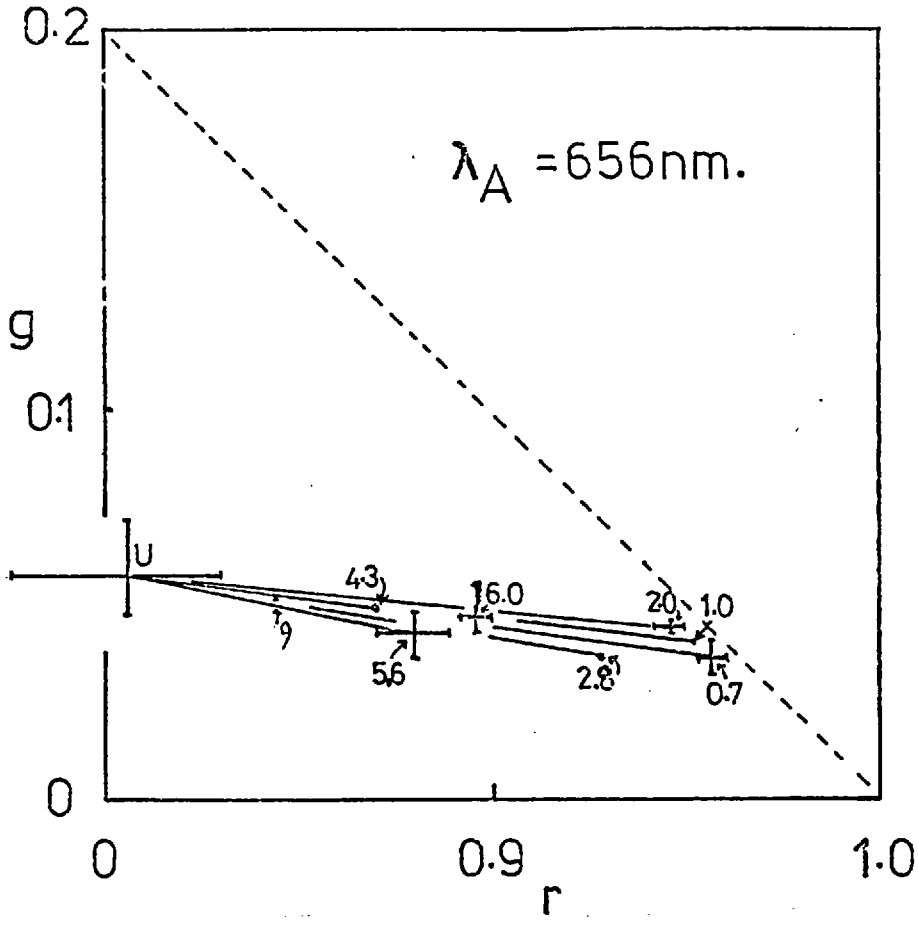

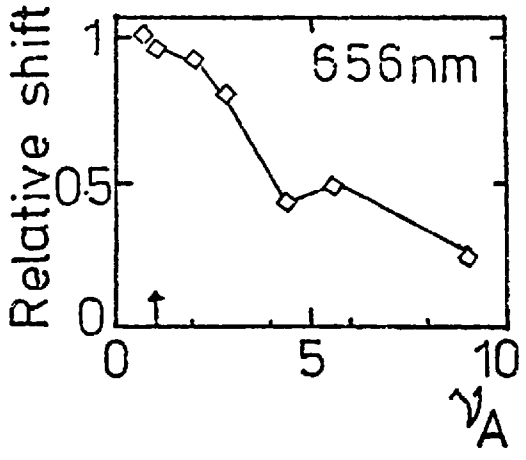

FIGURE 4.16 Colour shifts obtained for a grating probe stimulus of periodicity equal to 1 cycles deg^{-1}.

the lengths of the arrows representing the hue shifts) for different spatial periodicities of the grating adaptation field. Further measurements were made with test and desaturating wavelengths of 582 nm and 460 nm respectively. These data are shown in figure 4.15. The lengths of the hue-shift arrows were taken as a measure of the hue-shift magnitudes, and are plotted in figure 4.15b against the grating spatial periodicity. It is seen that there is a broad 'tuning' of the shift magnitude: the effect peaks at around 5.6 cycles deg^{-1} (shown by the arrow on the abscissa). When the spatial periodicity of the probe field was altered to 1 cycle deg^{-1}, and the test and desaturating wavelengths to 530 nm and 460 nm respectively, the data shown in figure 4.16 were obtained. Again, the shift magnitude is maximum when the spatial periodicity of the probe and adaptation stimuli coincide.

The following experiments were performed using a 5.6 cycles/ degree grating pattern in the probe field (figure 2.8c). The colour-matching data which were obtained using this probe field,

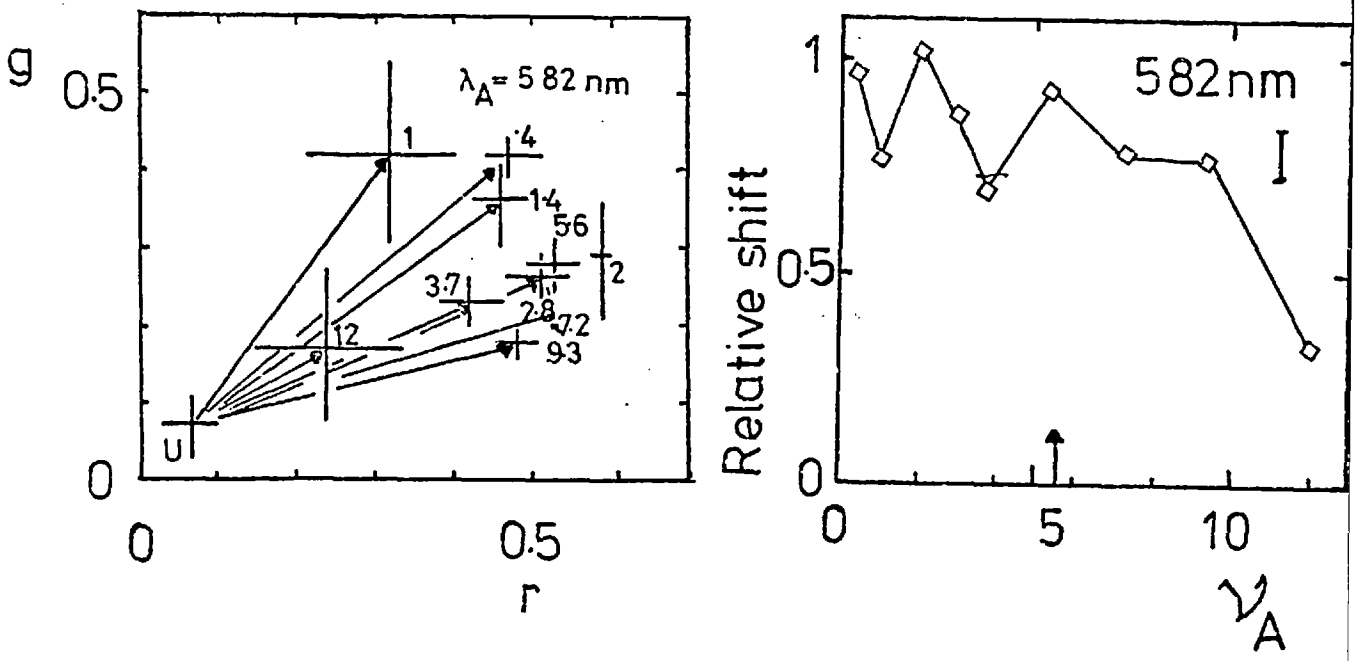

FIGURE 4.17 Colour shifts obtained using a probe grating of periodicity equal to 5.6 cycles deg^{-1}.

and for adaptation, test and desaturating wavelengths of 582 nm, 460 nm and 582 nm, respectively are shown in figure 4.17. The shift magnitudes remain at roughly the same value up to a spatial periodicity of 9 cycles/degree, and fall above this value: the shift directions do not vary in a regular fashion with spatial periodicity. The data obtained for an adaptation wavelength of 536 nm are shown in figure 4.18, and it is seen that the maximum shift away from the match obtained under spatially uniform adaptation conditions (u on the diagram) occurs for an adaptation spatial periodicity of 2.7 deg^{-1}, which is half that of the probe grating. In fact, there was virtually no shift when the spatial periodicity of the probe and adaptation gratings coincided (shown by the large arrow on the abscissa). When adaptation wavelengths of 460 nm or 495 nm were employed together with the grating probe

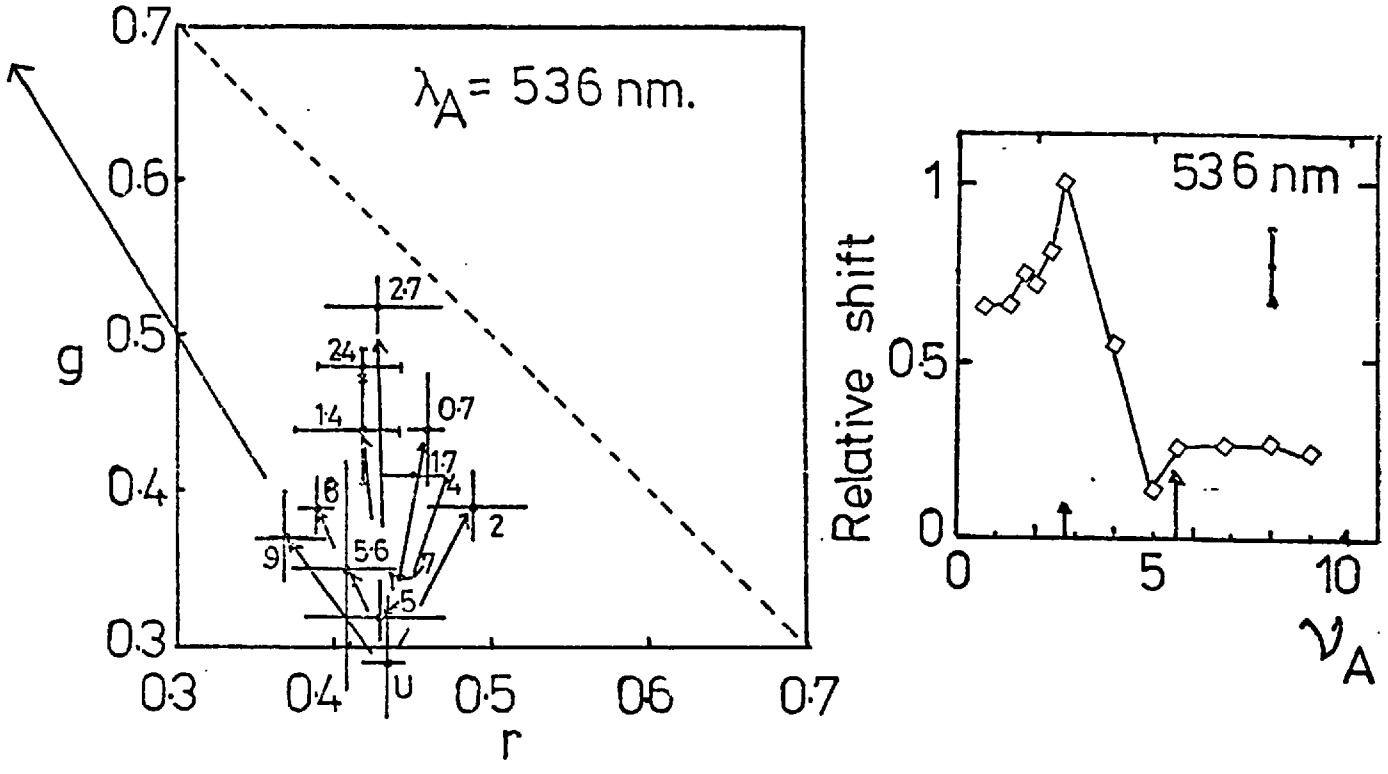

FIGURE 4.18 Colour shifts for a probe grating periodicity of 5.6 cycles deg^{-1}.

stimulus, the chromaticity of the test field remained unchanged for various adaptation spatial frequencies, within error.

A further experiment was undertaken to determine the variation of the hue-shift effect with changes in the relative orientation between the probe grating and the grating in the lower half of the grating adaptation stimulus. The spatial periodicities of the probe and adaptation gratings were both 5.6 cycles deg^{-1}. The adaptation wavelength was 656 nm, and the test and desaturating wavelengths were 530 nm and 460 nm respectively. The shifts in chromaticity were identical for orientations of the adaptation grating of between 0° and 65° measured relative to the vertical (figure 4.19). Larger orientations were not used because of the difference in appearance between the two halves of the probe field following adaptation for large angles of relative orientation: the upper half still appeared as a well-defined grating but the grating

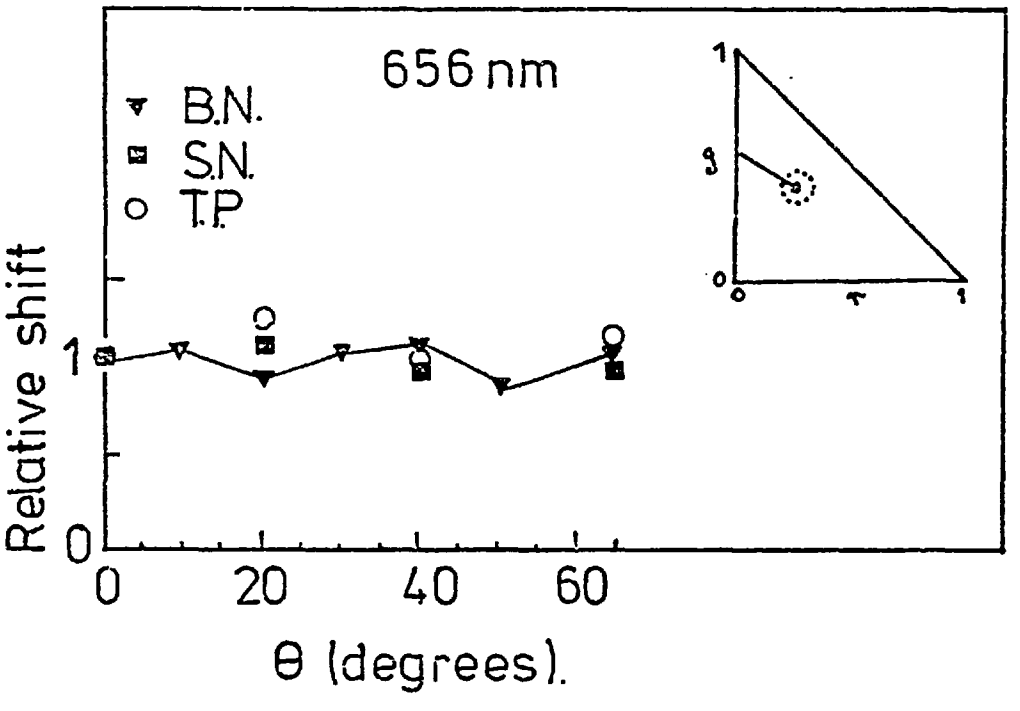

FIGURE 4.19 Dependence of shift magnitude on the relative angle between the probe and adaptation stimulus gratings.

pattern in the lower half was less well-defined and appeared to comprise of horizontal striations of different hue. A similar magnitude of shift was obtained for the same stimulus conditions for observers NS and TP, and again the orientation of the adaptation field had no effect on the shift magnitude or direction. This is illustrated in figure 4.19.

Dichoptic Adaptation Experiment

An experiment was performed using dichoptic presentation of the adaptation and probe stimuli. The colour-matching probe stimulus (figure 2.8a) was presented to the dark-adapted left eye, and the adaptation stimuli (figures 2.9a,b) to the right eye. Colour matches were established firstly with neither eye adapted and with the probe field presented to the left eye. It was found that for adaptation stimuli presented to the right eye, these matches were not disturbed either by a grating adaptation stimulus or by differential light levels in the two halves of a spatially uniform adaptation field.

3. Adaptation to Flickering Lights

The data presented in this section were obtained with the lower half of either the uniform or the grating adaptation stimulus (figure 2.9a,b) flickered with square-wave modulation. The first set of data obtained with flickering adaptation stimuli were measured for the binocular probe stimulus illustrated in figure 2.8b. The 630 nm test field was presented to the right eye, and the trichromatic matching field to the left eye. The adaptation field was presented to the right eye, and the left eye was dark-adapted. The changes of chromaticity which resulted from adaptation to a

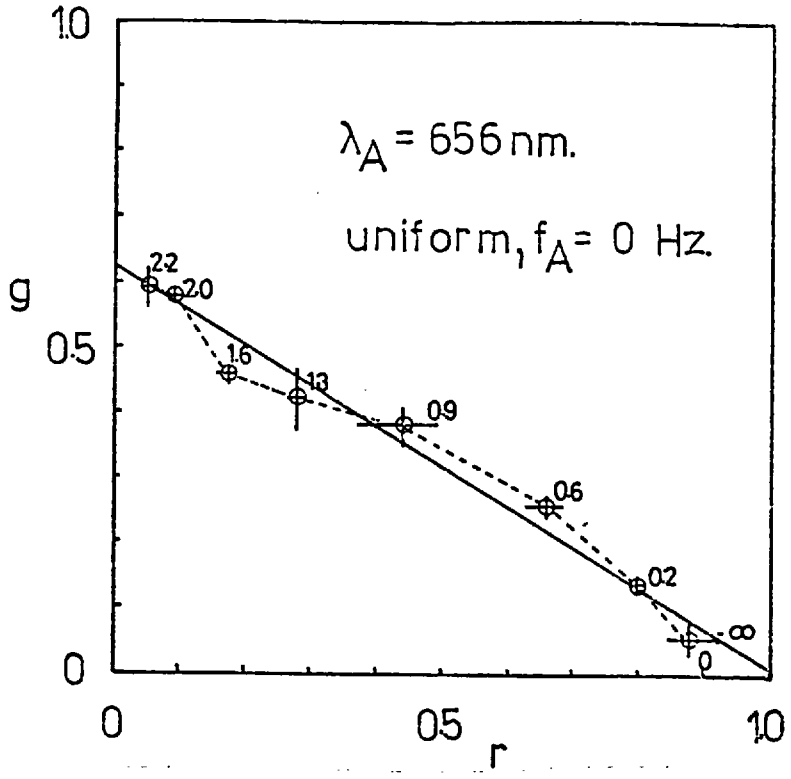

FIGURE 4.20 Hue shifts, for a binocular colour match, induced by adaptation of the right eye to increasing illumination levels of the uniform adaptation stimulus at a wavelength of 656 nm. The numbers alongside data points represent illumination levels in log td - 2 log units.

non-flickered and spatially uniform stimulus (figure 2.9a) are shown in the chromaticity diagram of figure 4.20. The highest adaptation illumination level used was about 4.2 log trolands, and the numbers alongside the chromaticity points represent the relative illumination levels of the adaptation stimulus (in log trolands). The experiment was repeated, again with spatially uniform adaptation fields, but the lower halves of the adaptation fields were flickered at rates of 1.3 Hz, 10 Hz and 30 Hz. The chromaticity co-ordinates measured for each of these frequencies are plotted on separate diagrams (figures 4.21 - 4.23), and the relative adaptation illumination level is given next to each point. The chromaticity points for the flickering adaptation lights are joined by broken lines: the points obtained with the non-flickering adaptation field (figure 4.20) are replotted on

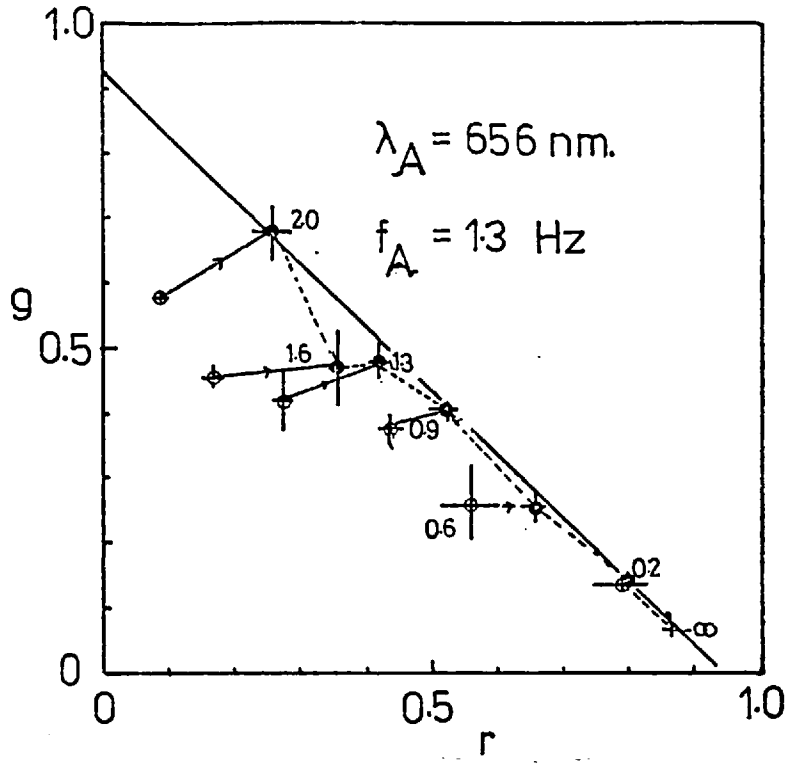

FIGURE 4.21

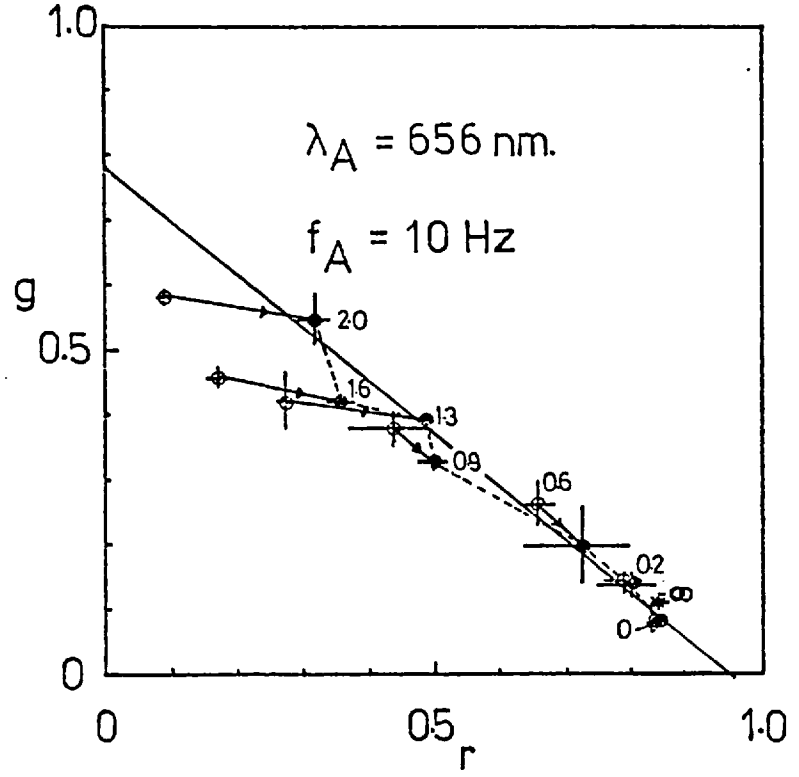

FIGURE 4.22

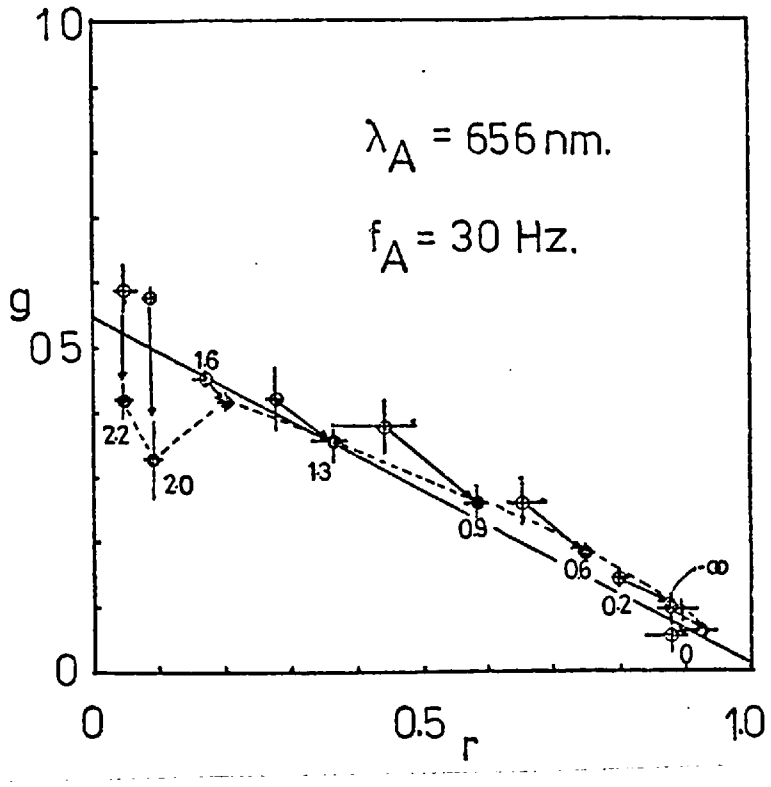

FIGURE 4.23 Hue shifts using binocular matching.

each diagram. Each arrow on these diagrams is drawn from the chromaticity point obtained under adaptation to a non flickering stimulus at a certain illumination level, to the point obtained under adaptation to the flickering stimulus with the same average illumination level. The length and direction of each arrow is a measure of the colour shift introduced by the temporal modulation of the flickering field. At low illumination levels, the shifts of chromaticity are small and mainly towards the red. At higher levels of illumination the chromaticity shifts are larger and the direction of shift depends strongly on the flicker frequency. Straight lines were drawn by eye through the chromaticity points obtained for each rate of flicker, and these are represented by the continuous lines in figures 4.20 - 4.23: the data points and these lines are shown together in figure 3.24. Note that the departures from straight lines are not large

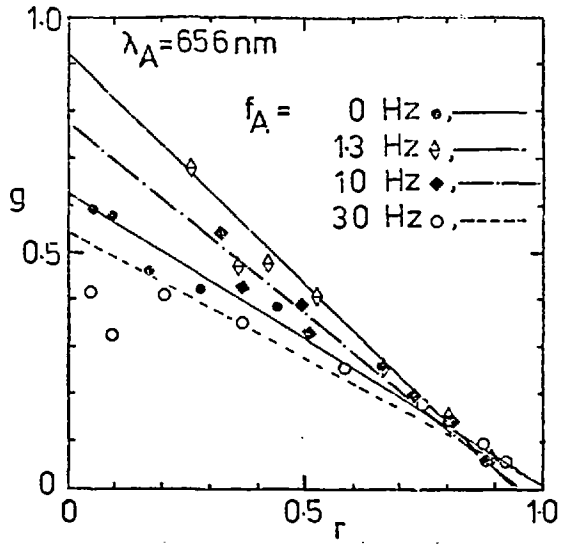

FIGURE 4.24 Data from figures 4.21 - 4.23 replotted.

execept at the highest illumination levels for f_A = 30 Hz (figure 4.23).

The straight lines drawn through the data points of figures 4.20 to 4.23 pass through the chromaticity point (r,g) = (1,0) within error. If a straight line passing through the point (1,0) intersects the axis r = 0 at g_1 (figure 4.25), the equation of the line is

$$g = g_1(1 - r) \qquad (4.1)$$

Since r + g + b = 1 (from equation 1.1), equation (4.1) yields

$$g/b = g_1/(1 - g_1) \qquad (4.2)$$

Thus, since the data of figure 4.24 obey equation (4.2) for each flicker frequency, the ratio of g/b is constant for each frequency of flicker of the adaptation stimulus, as its illuminance is varied. The values of g_1 for flicker frequencies of 1.3 Hz, 10 Hz and 30 Hz were 0.92, 0.78 and 0.54 respectively (figure 4.23). Hence g_1 decreases with

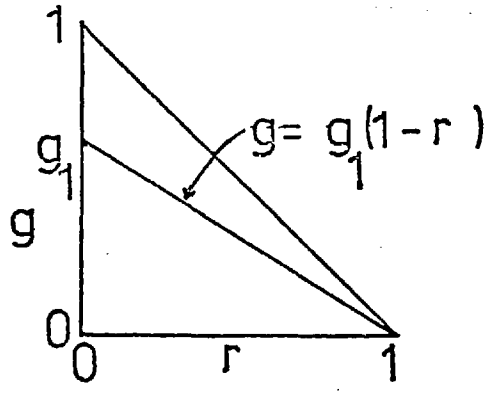

FIGURE 4.25 (See text)

increasing flicker frequency, and so does g/b (from equation 4.2). In these binocular experiments only the half of the probe field in the right eye was light adapted, so that an increase in g/b results from an increase in the adaptation of the blue-sensitive mechanism relative to that of the green-sensitive mechanism. Hence the adaptation of the blue-sensitive mechanism relative to that of the green-sensitive mechanism is greatest at low flicker frequencies (1.3 Hz) and decreases as the flicker frequency increases. This is consistent with the low frequency response of the blue system (Brindley, du Croz and Rushton, 1966).

Large colour-shifts resulted from the use of binocular matching methods, as would be expected from the different states of light-adaptation of the two eyes (figure 4.20). In general, the large colour-shifts caused by light-adaptation do not occur for the monocular colour-matching method that was used to study the effects of adaptation to spatially structured stimuli. All remaining experiments were, therefore, performed monoptically, using the monoptic matching probe field (figure 2.8a).

Firstly, the effect of flicker frequency was investigated for a number of test-stimulus and adaptation-stimulus wavelengths at a single level of retinal illumination. The data shown in figure 4.26 were obtained when the lower half of the uniform adaptation field was flickered: the adaptation wavelength was 530 nm and the test and desaturating wavelengths were 570 nm and 460 nm respectively. The point marked 'U' represents the match made for adaptation to spatially uniform and non-flickered adaptation stimuli. The other points represent the matches made when the lower half-field of the adaptation stimulus was flickered, while the average illumination level remained constant and equal to that of the

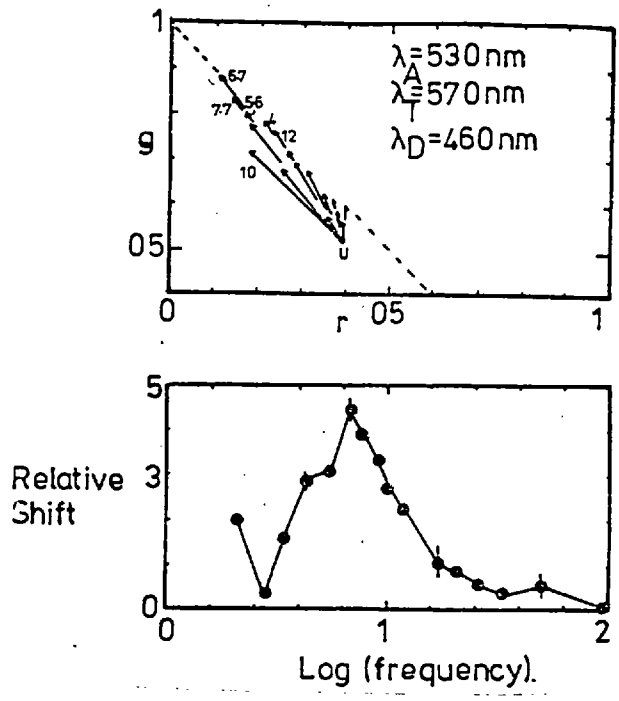

FIGURE 4.26 Hue shifts for spatially uniform adaptation stimulus and monoptic colour-matching.

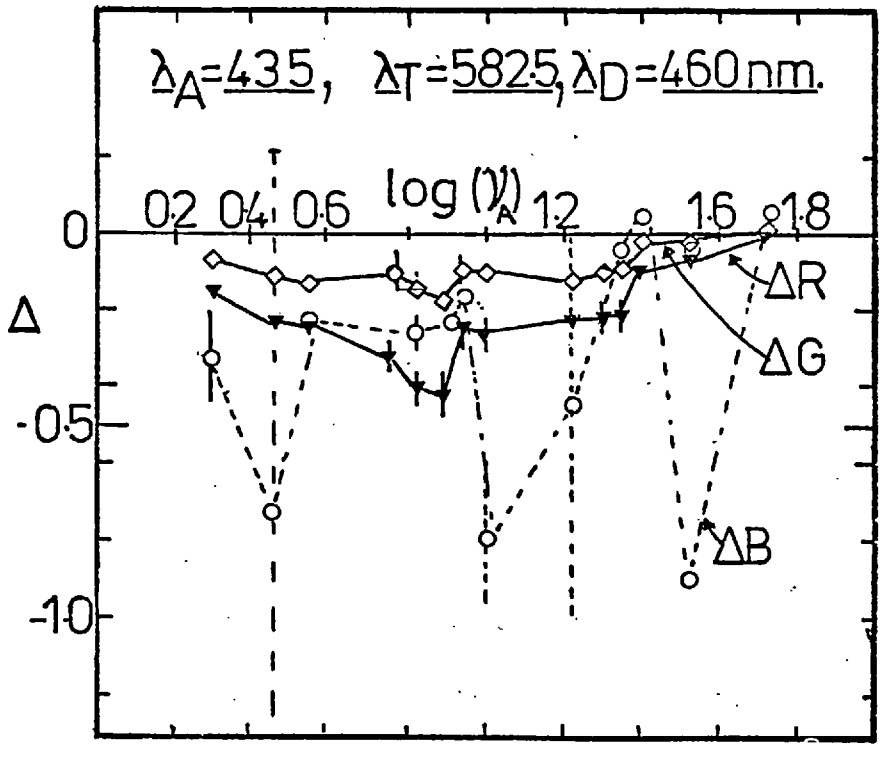

FIGURE 4.27 Δ (relative log trolands) versus log ν_A (Hz)

upper half-field. The flicker frequency is indicated alongside the chromaticity points. The distances between the point 'U' and the other points were again taken as a qualitative measure of the magnitude of the shifts, and are plotted in the lower half of figure 4.26 against the log of the flicker frequency. The maximum hue shift occurred for a flicker-frequency of about 6 Hz (log $f_A \simeq 0.8$). The experiment was repeated for an adaptation wavelength of 435 nm. In this case, the chromaticity shifts were small and the direction of shift varied considerably, although it was mainly towards the chromaticity point (r,g) = (0,1). The ΔR, ΔG and ΔB values, representing the differences in the amounts of the R, G and B matching stimuli for steady and flickering adaptation stimuli, are plotted against the logarithm of the flicker frequency in figure 4.27. It is seen that ΔR and ΔG are minimum at flicker frequencies at around 6.8 Hz (log $f_A \simeq 0.8 - 0.9$).

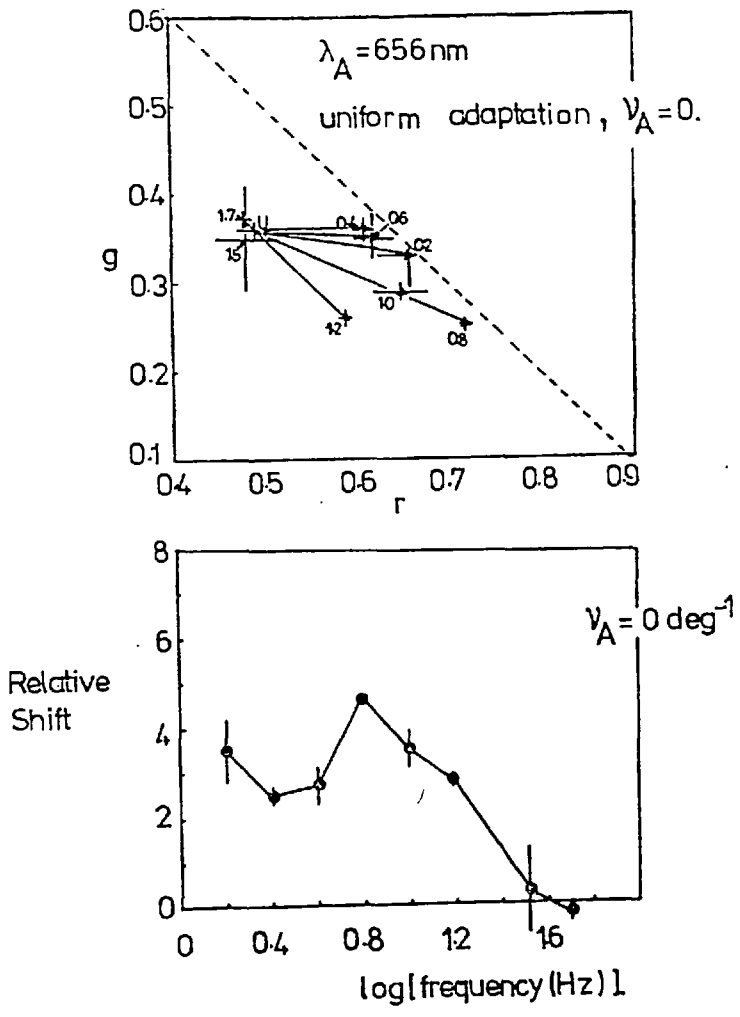

FIGURE 4.28 Hue shifts for flickered adaptation stimulus.

The wavelengths of the adaptation and comparison stimuli were changed to 656 nm and 582 nm respectively, and the hue shifts were recorded for a number of flicker frequencies. These data are shown in figure 4.28 and it can be seen from the plot of the relative shift magnitude versus log

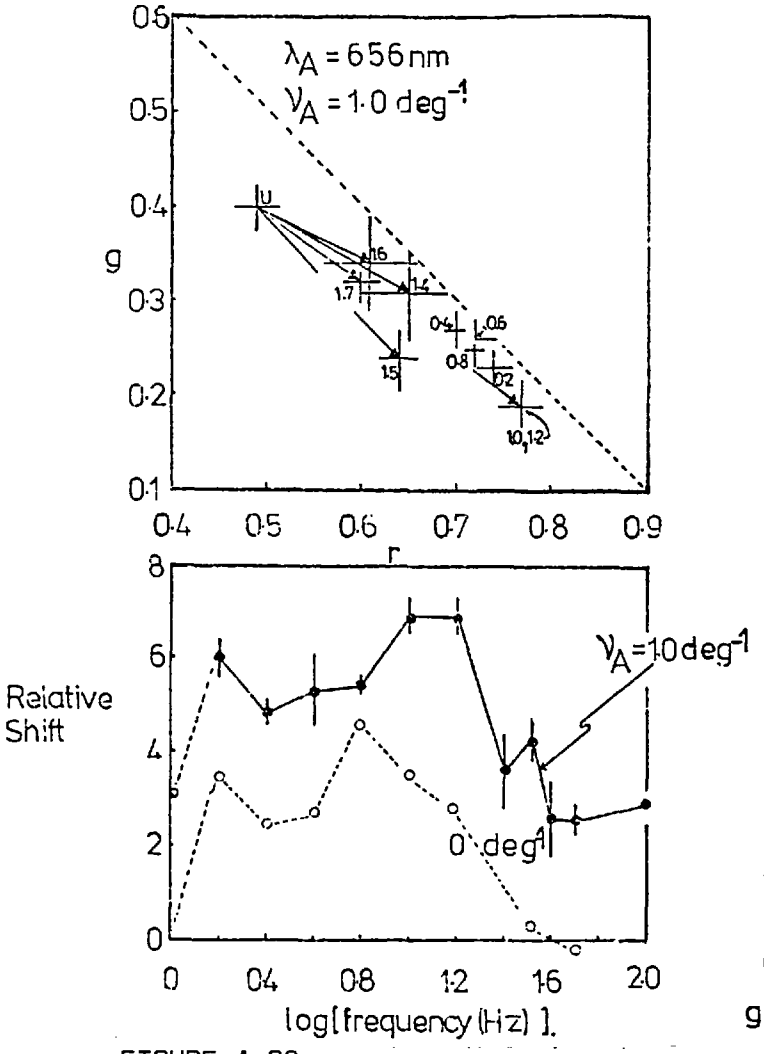

FIGURE 4.29

and temporally modulated adaptation fields were obtained by flikcering the grating stimulus. The results appear in figures 4.29 - 4.32. The relative shifts shown by solid lines in the lower half of each diagram are superimposed (dotted) on the lower half of the next diagram for comparison

frequency. (lower half of figure 4.28) that the effect peaks at 6 Hz (log f = 0.8). (The numbers alongside the arrowheads on the chromaticity diagram are the log of the flicker frequencies).

The uniform adaptation stimulus was replaced by the grating stimulus (figure 2.9b), and data for spatially

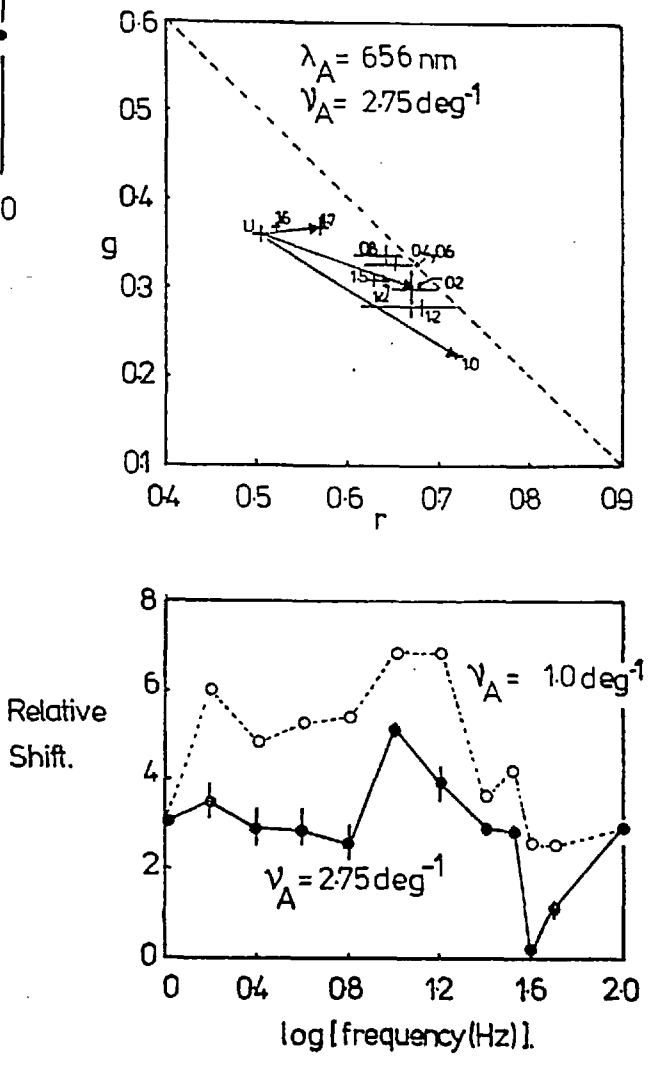

FIGURE 4.30

purposes. These curves of relative shift versus log frequency are replotted in figure 4.33.

The following points should be noted:-

1. Each curve in figure 4.33 has a peak at around log f_A = 1, and minima above and below this flicker frequency.

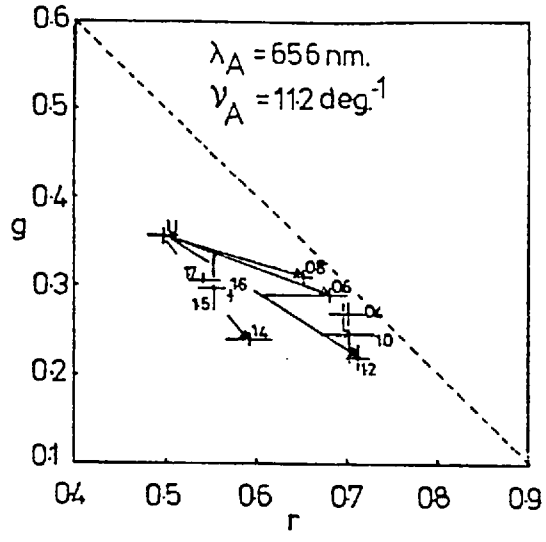

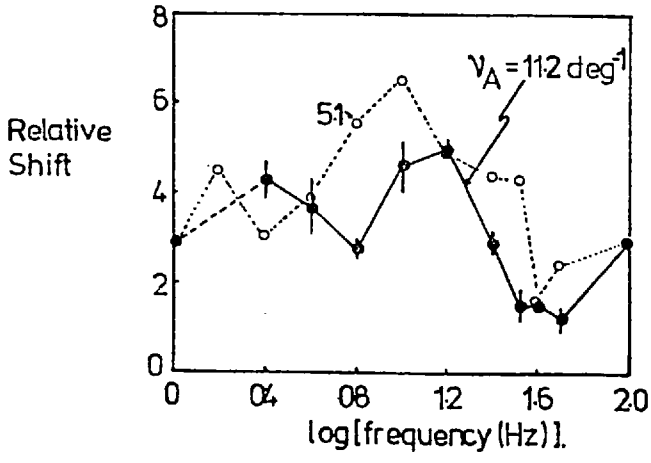

FIGURE 4.32 (See text).

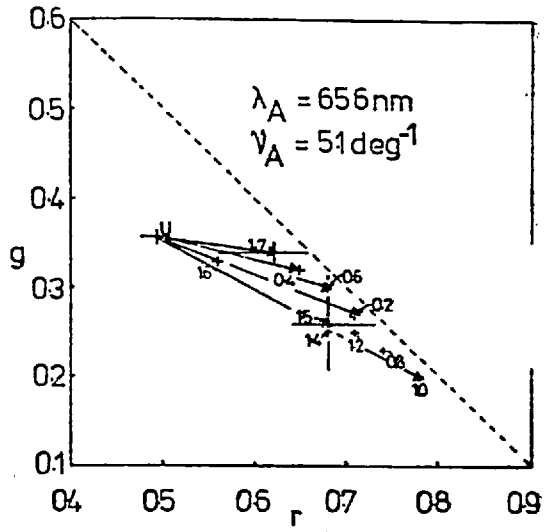

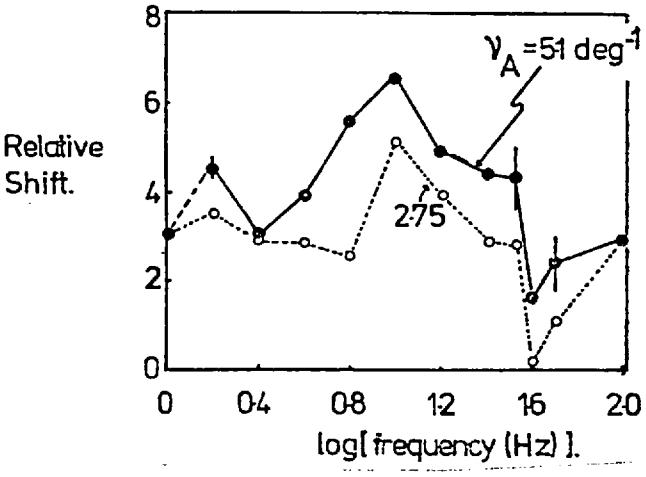

FIGURE 4.31

2. The largest shifts occur for a spatial periodicity (ν_A) of 1.0 cycle deg^{-1}.

3. The shifts are all in the same general direction on the chromaticity diagram (figures 4.28a - 4.32a).

4. The maximum shift for a spatially uniform field ($\nu_A \rightarrow 0$ cycles deg^{-1}) occurs at the lowest

temporal frequency (log f_A = 0.8) at which any curve peaks.

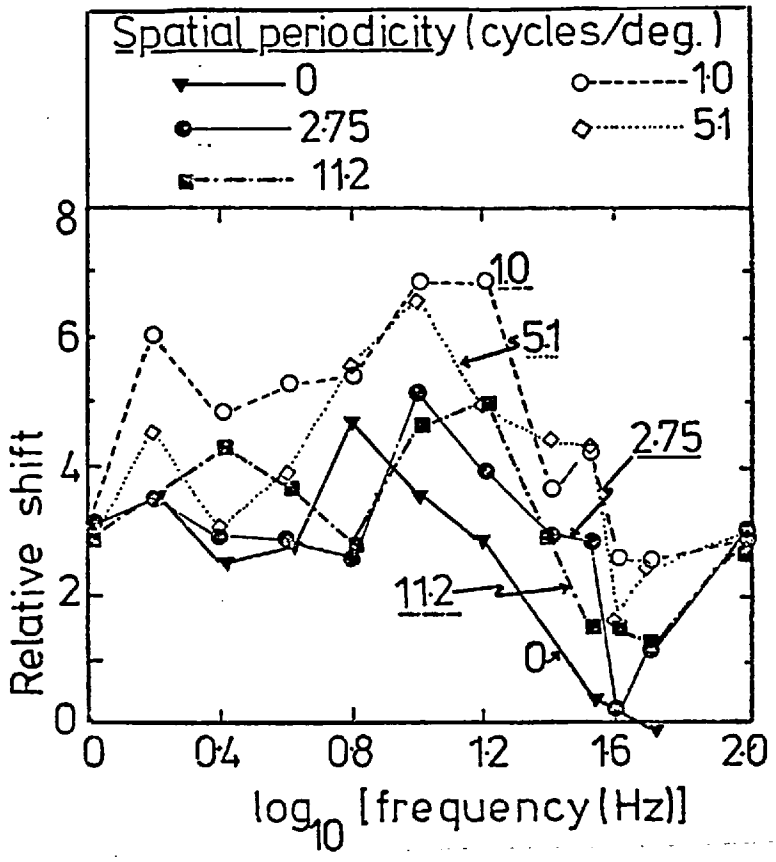

FIGURE 4.33 Data replotted from figures 4.28 - 4.32.

4.4 Discussion

The principal experimental results of the colour-shift experiment are as follows.

1. Adaptation to grating stimuli produced shifts in the chromaticity co-ordinates of matches established with a spatially uniform probe stimulus (figure 2.8a). These colour-shifts occurred even through the illumination levels of the adaptation stimuli were well below those (10^4 td) which cause breakdown of foveal colour matches attributed to bleaching of visual photopigments (Wright, 1936; Brindley, 1953; figures 4.1 - 4.8, 4.11).

2. The direction of shift of chromaticity on the WDW chromaticity

diagram was in most cases towards the chromaticity point in the diagram corresponding to the adaptation stimulus (figures 4.1 - 4.8). The colour shifts were largest for red adaptation stimuli (figures 4.6, 4.7) and least for the blue adaptation stimuli (figures 4.1 to 4.3). The colour shift remains substantially unchanged if the spatial periodicity of the adaptation grating is increased, except that it falls to zero as the acuity limit of the grating is approached (figure 4.9). The magnitude of the colour shift increases monotonically as the illumination level of the adaptation field is raised (figure 4.11), and falls off exponentially over a period of about one minute, following a five-minute adaptation period (figure 4.1). Conversion of these data to co-ordinates on the 1960 CIE-UCS chromaticity diagram does not significantly modify these conclusions (figures 4.9b, c; 4.11c,d).

3. Changes in chromaticity similar to those caused by grating adaptation could be induced by reducing the illumination level of the lower half of the uniform adaptation stimulus (figure 2.9a) by 0.8 log units (figure 4.13).

4. Shifts in chromaticity obtained using the structured probe stimulus (figure 2.8c) were also directed mainly towards the points representing the adaptation stimuli on the WDW chromaticity diagram (figures 4.14 and 4.18). The dependence of the magnitude of these shifts on the spatial periodicity of the adaptation grating was sometimes not marked (figures 4.14, 4.17). However, in contrast with the results obtained with a uniform probe field (figure 2.8a), there was a marked dependence of the shift magnitude on the spatial periodicity of the adaptation grating stimulus for some combinations of adaptation and comparison wavelengths. In the case of the

spatially uniform probe field, the magnitude of the shift decreased monotonically above a spatial periodicity of 10 cycles/degree (figure 4.9), whereas there as a maximum in the shift magnitude measured using the grating probe stimulus, either when the spatial frequencies of the probe grating pattern coincided with that of the adaptation stimulus (figures 4.15 and 4.16), or at a lower spatial frequency (figure 4.18).

5. For experiments employing grating patterns in both the probe and adaptation stimuli, the colour shift was found to be independent of the relative orientation of the probe and adaptation gratings over a range from 0^{o} to 65^{o} (figure 4.19).

6. No interocular transferred effect was obtained for structural adaptation stimuli presented to the right eye, with colour matches established in the left eye (dichoptic adaptation experiment).

7. Colour shifts were also obtained when the lower half of the uniform adaptation stimulus (figure 2.9a) was flickered. The data points obtained by binocular matching for various illumination levels of the flickering stimulus lie on a straight line for each flicker rate (figures 4.20 - 4.23). The slope of these lines ($\delta r/\delta g$) increases as the flicker frequency is raised (figure 4.24).

8. When the colour shifts are measured by monocular matching, there is a strong dependence of the magnitude of the colour shifts on the flicker frequency of the uniform adaptation field.

The magnitude of the shifts is greatest for flicker frequencies around 6 - 8 Hz (figures 4.26 - 4.28).

9. The largest relative magnitude of the colour shift occurs

for flicker frequencies in the range 6 - 16 Hz when a grating adaptation stimulus is flickered, and the flicker frequency at which the largest shift occurs depends on the spatial periodicity of the grating pattern (figure 4.33).

The results summarized above demonstrate that colour matches established between two halves of a horizontally-divided bipartite matching field can be disturbed by adapting the retinal area on which one half of the colour-matching field falls to a spatially and/or temporally modulated adaptation field, even through the retinal area on which the other matching half-field falls is adapted to a uniform field of the same mean illumination level. Possible causes of these effects are now examined and it is argued that they must arise from post-receptoral adaptation events.

1. Choice of Representation in the Chromaticity Chart and its Influence on Interpretation

It can be argued that in order to obtain better comparison between two distances across the chromaticity chart, all the data should be plotted in a uniformly-scaled chromaticity diagram such as the 1960 CIE-UCS diagram. The transformation was made in two cases, and it was shown that the magnitude of the chromaticity changes induced by adaptation to different spatial periodicities and different illumination levels are similar in both the r-g and the u-v chromaticity diagrams (figures 4.9a,b; 4.11a,c). Note, however, that the CIE-UCS diagram relates to foveal vision (or 10^{o} vision), not specifically to parafoveal vision, and the colorimetric non-linearity of parafoveal vision invalidates application

of linear transformations.

2. Directions of Chromaticity Shifts and the Cause

The directions of chromaticity shifts caused by the grating adaptation stimulus (figure 4.9b) were in most cases towards the chromaticity point representing the adaptation stimulus colour (figures 4.1 - 4.8), and the directions of these chromaticity changes could be simulated by reducing the illumination level of the lower half of the uniform adaptation field by 0.8 log units (figure 4.13). A reduction in the illumination level of the lower half-field results in reduced light-adaptation of this half-field. The shifts in chromaticity obtained with the grating stimuli could therefore be attributed to the reduced efficiency of such stimuli in causing adaptation at some point in the visual system. The average illumination levels of the upper and lower halves of the grating stimulus (figure 2.9a) were equal, so that the colour-shifts were not caused by a change in the average state of light-adaptation of the photoreceptors (see 4, 5 and 6 below).

The colour-shift induced by the grating pattern increases monotonically with the adaptation illumination level, and falls exponentially over a period of a minute after the cessation of adaptation (point 2, above). Wright (1946, chapter 20) obtained hue-shifts arising from chromatic adaptation which exhibited similar characteristics to those observed in this study. Wright used a binocular matching technique to measure the hue-shifts which result following adaptation of only one eye to spatially uniform coloured stimuli. These colour shifts were measured relative to the dark-adapted state, and their magnitudes usually increased linearly with intensity and decayed exponentially to zero within 1 - 2

minutes. However, the effects which he measured were caused by the differential light-adaptation of the two eyes. The grating-induced colour shifts are not caused by differential light-adaptation of the different areas of the retina, but might arise from the transmission of the signals, generated by uniform and grating stimuli, along different neural pathways.

3. Temporal Factors Induced by the Combination of Eye Movements and Spatial Structure

The fact that the colour-shift measured with a spatially uniform probe stimulus remains substantially unchanged as the spatial frequency of the adaptation grating stimulus is varied except when the grating acuity limit is approached (figures 4.9a,c), suggests that the colour-shifts may be caused partly by the light flicker at the receptors, which in turn is caused by the action of scanning a fixation line above the grating pattern (figure 2.9b).

Indeed, colour shifts were also obtained when the lower half of the uniform adaptation stimulus (figure 2.9a) was flickered (results 6 and 7 above), so that flickered light does change the state of adaptation induced by spatially uniform light of the same average illumination level.

The action of scanning the eye across a grating effectively yields temporal flicker at the photoreceptors because the receptors are moved from light to dark regions during scanning. Assuming that the scanning rate was not influenced by the spatial structure - it was attempted to scan all stimuli at the same rate - then the higher the spatial periodicity of the grating, the greater the effective flicker frequency introduced by the scanning. Now

temporal flicker of an unstructured adaptation field gives a marked peak of chromaticity shift magnitude for a single frequency around 7 Hz (figures 4.24 - 4.28) for adaptation wavelengths of 435 nm, 530 nm and 650 nm. Thus, if the effects of grating adaptation were due to the associated temporal flicker effects caused by eye-movements, there should be a well-defined temporal-frequency range, for each spatial frequency, equivalent to 7 Hz temporal flicker which gives the biggest effect. This conclusion assumes a constant rate of scan, and although this was attempted, some variation in the scan rate cannot be excluded. None the less, experimentally it is found that the shift magnitude is almost independent of spatial frequency up to cut-off (figure 4.9a), which argues strongly against a purely temporal explanation of the colour-shifts.

When spatial modulation was superimposed on adaptation gratings with different temporal frequencies, there was no regular change in the shift magnitudes as the spatial frequency was altered, for any one temporal flicker frequency (figure 4.33). The hue shifts obtained using the spatially unstructured stimulus (spatial periodicity = 0 cycles/degree, figure 4.33), show that temporal modulation alone can cause hue-shifts. However, this does not contradict the conclusion, stated in the previous paragraph, that the hue shifts found for grating adaptation stimuli are not caused only by the temporal modulation resulting from visual scanning of the grating. Indeed, hue shifts were obtained for temporally and spatially modulated adaptation stimuli which exceeded in magnitude the maximum hue shift obtained for a spatially uniform flickered stimulus (figure 4.33). This result implies that the colour shifts were influenced by the spatial structure of the grating adaptation stimuli in addition to being influenced by the temporal modulation.

4. Time Reciprocity in Photoreceptors as a Factor

An economical explanation of the colour shifts caused by flickering stimuli is that there is a failure of time-intensity reciprocity. Complete summation of light is found only for events occuring within a 'critical duration' (Bloch, 1885; Blondell and Rey, 1911), which varies with stimulus size, wavelength, luminance and retinal location (e.g. Battersby and Shuckman, 1970). Van der Horst and Muis (1969) found hue shifts associated with flickering stimuli, and Nilsson and Nelson (1971) and Nilsson (1972) also reported on hue shifts produced by intermittent stimuli. Wasserman and Kong (1975) showed that failure of intensity-time reciprocity can be partly attributed to receptor reciprocity failure in certain instances. It is shown next, however, that the colour-shift data presented in this chapter cannot be attributed to differential average light-adaptation of receptors by uniform and flickered light of the same average illuminance.

The data of figure 4.13 indicate that the hue shifts obtained with grating adaptation fields (that is, adaptation fields with grating patterns in the lower half-field) can be simulated by reducing the illumination level of the lower half-field of a uniform adaptation stimulus. The question therefore arises, whether the process of equating the average illumination levels of an asymmetric adaptation stimulus is sufficient to ensure equal states of receptoral adaptation in the areas of retina illuminated by the two half-fields.

Now the effect of scanning a grating is to illuminate the receptors intermittently, at a rate determined by eye-movements and the grating spatial frequency. The consequence of intermittent illumination, arising from grating or flickered stimuli, on the

bleaching of visual photopigments can be calculated from the kinetics of their bleaching and regeneration (Campbell and Rushton, 1955; Rushton and Henry, 1968). This calculation was performed for a number of illumination levels and flicker frequencies assuming square-wave modulation of the light illumination level, using the equations and cone pigment kinetics given in Appendix D. The fractions of unbleached pigment which remain following adaptation to temporally uniform and to flickering light, f_o and f respectively were calculated: it was assumed that the eye was initially dark-adapted ($f = f_o = 1.0$), and the amount of bleaching following two minutes of adaptation was calculated. The ratio f/f_o is plotted in figure 4.34 as a function of adaptation intensity (in log (td)) for flicker frequencies of 0.05 Hz and 0.5 Hz. It is seen that f/f_o is very close to 1.0 for intensities below 4.5 log td and flicker frequencies above 0.5 Hz. Such a flicker rate would be achieved at receptor level by scanning a grating with bar widths of 1^o at a rate of 2^o $second^{-1}$. This is slow compared to the rates which were used to scan the adaptation fields, and most gratings used had spatial frequencies well above 0.5 cycles deg^{-1}. Thus the flicker frequency of the light which resulted from the action of scanning the grating always exceeded 0.5 Hz. Also, hue shifts were found when the uniform adaptation stimulus was

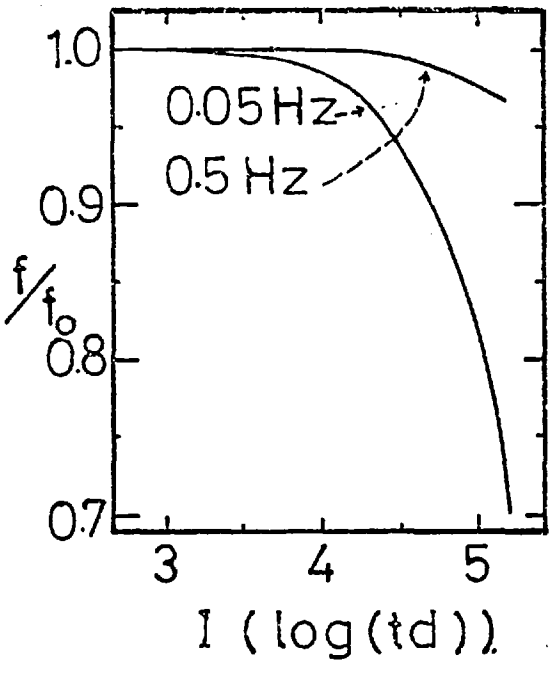

FIGURE 4.34 Ratio f/f_o versus adaptation intensity (log td).

flickered at rates far exceeding 0.5 Hz. Thus the amount of receptoral adaptation, imposed by the top and bottom halves of the adaptation stimuli which were used, was very nearly equal ($f/f_o \simeq 1$). This agrees with the data of Mote, Riopèlle and Meyer (1950) who showed that the dark-adaptation threshold curve following adaptation to intermittent light (2 Hz to 0.35 Hz) was the same as that following adaptation to a constant stimulus of the same time-averaged radiant flux, over an adaptation illumination level range of 2.6 log units. Since the receptoral adaptation was always the same in both halves of the adaptation field, the colour shifts could not have been caused by differential receptoral adaptation of the two areas.

5. The Contribution of Rod Signals to Colour Shifts

Colour matches are disturbed at low levels of illumination because of the influence of rod signals. The present work employed colour-matching stimuli presented to the parafovea, and so the effect of rod involvement must be considered. The effect of an increase in rod participation in a trichromatic colour match is to shift the match towards a desaturated white, represented by a point near the centre of the chromaticity diagram (Clarke, 1962; Stabell and Stabell, 1973). In the present data there is a tendency for this kind of change in chromaticity to occur at low illumination levels (figure 4.11a, point e), but the shifts in chromaticity are generally in directions away from the centre of the WDW diagram (figures 4.1 - 4.8). Thus rod participation cannot explain the major trends in the colour-shift data.

6. Pigment Bleaching by Adaptation

Although the effect on the receptors of the grating or flickering adaptation fields was likely to be the same in the top and bottom half-fields, pigment bleaching itself is known to alter colour matches (Wright, 1936; Brindley, 1953). Three facts make it unlikely that this caused any of the shifts observed. First, the fraction f, of unbleached pigment remaining after two minutes of light adaptation is shown as a function of light illumination level (in log td) in figure 4.35. (These values were calculated using the equations in Appendix D). The magnitude of f at 3.5 log td is about 0.9. The colour shift expected at this level of bleaching is relatively low (as will be seen in chapter 5). Moreover, Brindley (1953) found that the amount of red needed in the matches always increased with bleaching and the amount of green decreased, so that the colour shifts were always towards the red. In the present experiments the colour shifts occurred in various directions across the chromaticity chart, so that in general they cannot be attributed to pigment bleaching. Third, it was shown in the previous subsection that bleaching of visual photopigments was the same in the top and bottom halves of the grating or flickering adaptation fields. These fields had the same average illumination level as those of the reference uniform adaptation

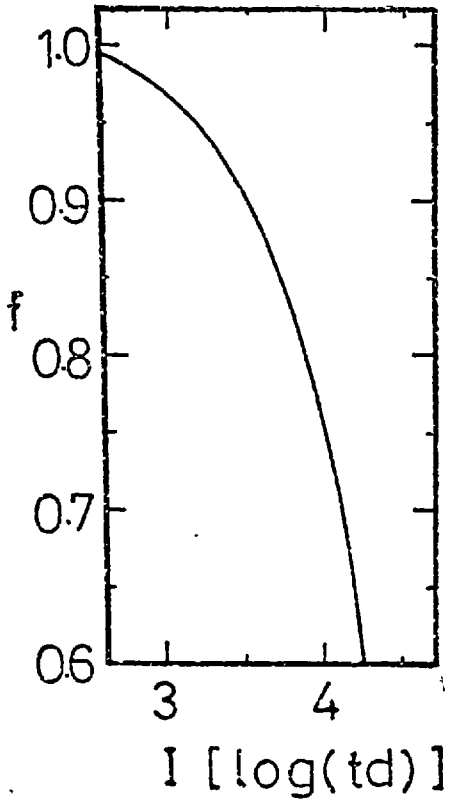

FIGURE 4.35 Fraction f of unbleached pigment versus I (log td).

fields, so that bleaching for all four adapting half-fields was equal. Consequently, no colour shift due to bleaching would be expected when one adaptation field is exchanged for the other, although there might be a slight shift toward the red compared to the dark-adapted state.

It has been demonstrated in the previous three subsections that the colour shifts produced by spatially and temporally modulated stimuli are not caused by differential adaptation of receptors, by rod involvement or by pigment bleaching. Thus it is proposed that the colour shifts occur central to the receptors.

7. Central Mechanisms which may Contribute to Colour Shifts

A number of factors influencing photoreceptor function which could lead to the observed colour shifts have been examined, and rejected as primary causes. In this section, the characteristics of other known post-receptoral adaptation phenomena are compared to those of the colour shift phenomenon in order to identify possible contributory mechanisms.

The contrast threshold elevation effect has characteristics similar to those of the colour-shift effect, and also occurs central to the receptors becuase it is transferred interocularly. (See section 1A.4). The threshold elevation of a grating probe stimulus caused by adaptation to a second grating stimulus is measured with respect to the elevation caused by a uniform field with the same mean illuminance as the second (adaptation) grating stimulus, so that the threshold elevation data also cannot be attributed to differential light-adaptation . The colour shift and contrast threshold elevation effects are compared below.

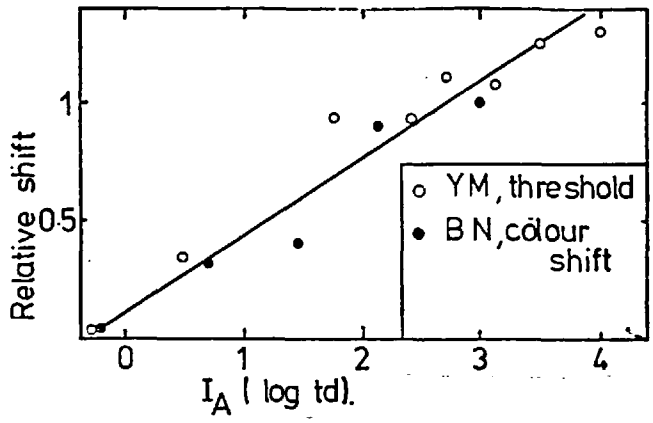

FIGURE 4.36 Relative colour-shift (BN) and contrast threshold elevation effect (YM, Maudarbocus and Ruddock, 1973) versus adaptation illumination level.

1. The magnitudes of the two effects increase with adaptation illuminance. The relative threshold elevation obtained interocularly by Maudarbocus and Ruddock (1973b) using probe and adaptation grating stimuli with sinusoidal luminance profiles of spatial periodicity 6.1 cycles/ degree, is shown in figure 4.36 (open circles) as a function of the adaptation illumination level. The colour-shift data of figure 4.11c are replotted on the same diagram (filled circles, figure 4.36), and it is seen that the magnitudes of the two effects both increase in the same manner with adaptation illumination level.

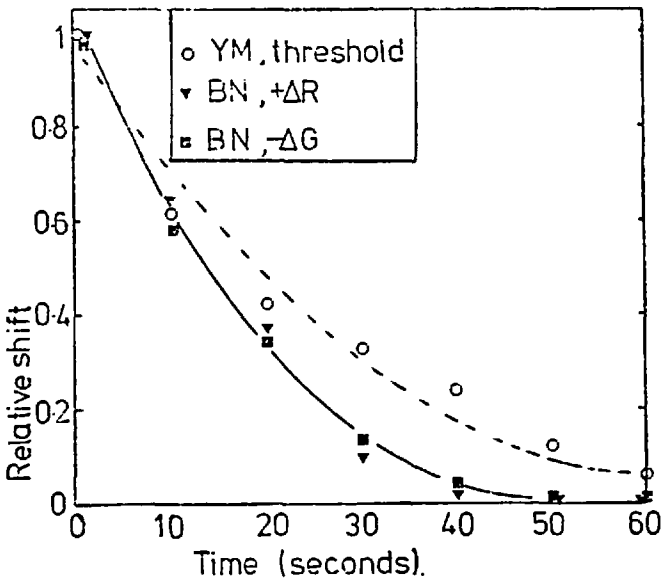

FIGURE 4.37 Relative contrast elevation effect (°), and colour shifts (+ΔR, -ΔG) versus time following cessation of adaptation.

2. The colour-shift and threshold-elevation effects also have similar decay time-constants. The relative contrast threshold elevation following cessation of the adaptation stimulus is shown in figure 4.37 (open circles, YM; from Maudarbocus, 1973). The relative values of ΔR and -ΔG following

cessation of adaptation (figure 4.12) are also plotted in figure 4.37 (solid symbols). The two effects follow similar time-courses of decay. The contrast threshold elevation effect is transferred interocularly (e.g. YM, figure 4.36) and is neural in origin. The similarity between the two effects indicates that the colour-shift effect is neural in origin, and is related to the contrast threshold elevation effect.

3. The contrast threshold elevation effect is maximum when the spatial periodicities of the probe and adaptation grating patterns are equal, and falls off as the spatial periodicities of the two stimuli become increasingly dissimilar. Similar behaviour was found for the colour-shift effect for some adaptation wavelengths (figures 4.15, 4.16). For other cases, however, no tuning of the colour shift with spatial frequency was observed (figure 4.17) and in one case the maximum effect occurred when the periodicity of the adaptation grating was twice that of the probe grating pattern (figure 4.18). The colour shift effect is not transferred interocularly, unlike the contrast threshold elevation effect. Further, the colour-shift magnitude is independent of the relative angle between the probe and adaptation grating patterns (figure 4.19), whereas the orientation selectivity of the contrast threshold elevation effect and other interocularly transferred effects is 13° - 17° (Campbell and Kulikowski, 1966; Blakemore and Nachmias, 1971; Maudarbocus and Ruddock, 1973b). The colour-shifts do not therefore, possess some important response characteristics associated with the adaptation of the orientation and width-sensitive cortical neurones described by Hubel and Wiesel (1968).

Maudarbocus and Ruddock (1973a,b; 1974) used sinusoidal

grating probe and adaptation stimuli with different wavelengths, and showed that the monocular contrast threshold elevation effect was strongly wavelength-dependent, but that the binocular effect was virtually independent of the test and adaptation wavelengths. (The wavelength dependence has been a matter of dispute - May, 1972; Maudarbocus and Ruddock, 1974; Timney, Gentry, Skowbo and Morant, 1976.) Therefore the colour-shift effect may be related to the wavelength-dependent contrast threshold elevation effect observed for monoptic viewing conditions..

The lack of orientation selectivity of the colour-shift effect suggests that it is associated with neural mechanisms possessing circular symmetry. The lack of binocular transfer further suggests that these mechanisms are located in the retina, or LGN. Such mechanisms might conceivably be attributed to ganglion cell behaviour, and adaptation of these cells with temporally or spatially modulated stimuli might lead to changes in the receptive field organisation of the colour-coded ganglion cells (figure 1.9), giving rise to the shifts in colour matches. There are several physiologically distinct classes of ganglion cells in the parafoveal region of the primate retina (e.g. De Monasterio and Gouras, 1975). The different classes have different receptive-field sizes, temporal responses and colour responses, and some respond only to moving stimuli. It is likely that the grating stimuli and the flickered (but spatially uniform) stimuli excite the different classes of ganglion cell to different extents.

4.5 Conclusions

The experiments in this chapter have demonstrated that metameric colour-matches established between two fields can be disturbed by

adapting the portion of the retina covered by the one field to uniform light, and by adapting the retinal area covered by the other field to square-wave spatially and/or temporally modulated light, with the same mean illuminance and the same wavelength as the uniform adaptation light. The colour shifts caused by grating adaptation stimuli which were measured with a spatially uniform colour-matching probe stimulus were wavelength dependent (figures 4.1 - 4.7), increased monotonically with adaptation illuminance (figure 4.11), were independent of the spatial periodicity of the adaptation stimulus up to a value of 10 cycles/degree (figure 4.12), and decayed within a minute after the cessation of adaptation. The colour-shifts measured with a grating probe stimulus depended on the adaptation grating periodicity (figures 4.14 - 4.18), and the maximum effect sometimes occurred when the periodicities of the probe and adaptation grating patterns were equal. Colour shifts were also induced by flickered stimuli, when the spatially uniform probe stimulus was used: these shifts depended on the illumination level of the adaptation stimulus (figures 4.20 - 4.23), on the temporal flicker rate and wavelength of the adaptation field and on the spatial periodicity of the adaptation grating pattern (figures 4.26 - 4.33). It was shown that the colour shifts were not caused by differential light-bleaching of the two halves of the retina (section 4.4.4), or by pigment bleaching itself (section 4.4.3), or by rod activity (section 4.4.6).

The colour-shift effect and the contrast elevation effect behaved similarly as the illumination level of the adaptation stimulus was raised (figure 4.36), and following cessation of adaptation (figure 4.37). However, they differ in that the colour-shift effect is not transferred interocularly, and is

independent of the relative orientation of the probe and adaptation grating stimuli whereas the contrast threshold elevation effect is transferred interocularly and is orientation-dependent. It is concluded that the colour-shift effect may be related to the monocular wavelength-dependent contrast threshold elevation effect (Maudarbocus and Ruddock,1974) and that it is possible that the colour-shifts result from adaptation at the ganglion-cell layer.

CHAPTER 5

A Study of Anomalous Trichromacy

5.1 Introduction

Several differences between the colour vision responses of normal and anomalous trichromats were noted in section 1B.5. For example, the mixture of red and green lights which matches a yellow test light (the Rayleigh match) for a deuteranomalous subject appears too green to normal subjects and that for a protanomalous subject appears too red. Anomalous trichromats (or 'anomals') also suffer decreased hue discrimination compared to normals (Nelson, 1938; McKeon and Wright, 1940), and their spectral sensitivity curves differ in shape from the average sensitivity curve for normals (that is, observers with normal colour vision): the most marked difference is a reduction in relative spectral sensitivity for long-wavelength stimuli observed for protanomals. Observer variations in spectral sensitivity functions for normal subjects is sufficient mask differences between curves of individual trichromats, other than the reduced red sensitivity of protanomals (Wright, 1946, chapter 25).

A number of hypotheses have been proposed to account for the differences between anomalous trichromatic and normal colour vision. The most common hypothesis is that in protanomals an 'abnormal' photopigment replaces the long-wavelength pigment (Rushton's 'erythrolabe') of normal colour vision, and that correspondingly, in deuteranomals an abnormal pigment replaces the green absorbing photopigment ('chlorolabe') of normal colour vision. In each case, the other two photopigments are considered to be normal (Walls and Matthews, 1952; Hurvich and Jameson,

1956; Wald, 1966; Alpern and Torii, 1968b; Mitchell and Rushton, 1971b; Rushton, Powell and White, 1973; Pokorny, Smith and Katz, 1973; Piantanida and Sperling, 1973a,b; Macleod and Hayhoe, 1974; Ruddock and Naghshineh, 1974; Hurvich and Jameson, 1974; Rushton, 1975; Alpern and Moeller, 1977; Pokorny and Smith, 1977; Nunn and Ruddock, 1977, in print). Implicit in most of these theories is the assumption that the abnormal pigment replacing a normal one in cones of one class comprises a single molecular species. Walls and Matthews (1952, p. 157), however, proposed that the abnormal pigment in deuteranomaly consists of a mixture of (normal) chlorolabe and erythrolabe. Ruddock and Naghshineh (1974) suggested that the abnormal pigments of both protanomaly and deuteranomaly consist of such mixtures. In hypotheses based on a single abnormal pigment, the range of red/green energy ratios required by different anomalous subjects to establish the Rayleigh match (figure 1.10) is interpreted as corresponding to a range of different anomalous pigments. In the hypothesis based on pigment mixtures (Ruddock and Naghshineh, 1974) this variation is explained by a range of erythrolabe/chlorolabe mixture ratios. A further hypothesis of anomalous trichromacy is that light entering the outer segments of cones of one class first pass through the visual pigment contained in another class of cone: such a situation could be contrived by changing the refractive index of (say) the outer segments of cones of one class, or by raising the outer segments of cones of one class vertically with respect to those of another class.

Other explanations of anomalous trichromacy are less convincing. For example, the differences between the Rayleigh matches of normals and anomals are not caused by differences in

the non-photolabile eye media transmission, since the transmission of the ocular media of anomals and normals is very similar (Alpern and Torii, 1968a; Alpern, Bastian, Pugh and Gras, 1976; Alpern and Moeller, 1977). Also, anomalous trichromacy cannot be explained entirely by differences in the optical densities of erythrolabe and chlorolabe as the wavelengths of the maximum sensitivivies of normal and anomalous pigments differ (e.g. Mitchell and Rushton, 1971b). The hypothesis that anomalous trichromacy is a consequence of neural 'fusion' of cone signals (Ingling and Drum, 1973) is not a tenable explanation of anomalous trichromacy. Neural fusion of cone signals can account for the colour-matching properties of dichromats (Aitken, 1873; Leber, 1873, Fick, 1879, Le Grand, 1968, 1969), although Rushton's (1965a) densitometric evidence suggests that dichromats possess only one photopigment absorbing light mainly at wavelengths longer than 500 nm (see however, Hurvich, 1972; Le Grand, 1972), and this fact cannot be accounted for by neural fusion. Now neural fusion of cone and rod signals does occur in normal extrafoveal vision and results in colour-vision changes at low illumination levels (Hunt, 1952; Clarke, 1960). Again, Burton and Ruddock (1972) showed that (dichromatic) 'small-field' foveal colour matches can be modified by adjacent, non-overlapping adaptation fields. This result shows that neural fusion can affect even foveal colour matches under certain circumstances. If it is accepted, however, that foveal colour matches established by anomals and by normals using reasonably-sized fields (>30') are determined by only three pigments (e.g. Mitchell and Rushton, 1971b),it follows that neural fusion alone cannot account for anomalous trichromacy.

It has already been mentioned that the parafoveal colour-

matching properties and relative spectral sensitivity curves of normal observers vary appreciably at mesopic illumination levels (e.g. section 1B.2) and that foveal colour matches also change at very high illumination levels due to bleaching of visual pigments and the consequent narrowing of pigment absorption spectra (section 1B.4; Wright, 1936; Brindley, 1953, 1955). Reduction in the effective optical density of pigments can also be affected by decentring the point of entry of a narrow light beam into the eye relative to the optical axis of the eye (Stiles, 1937, 1939; Brindley, 1953; Walraven and Bouman, 1960; Enoch and Stiles, 1961), or by parafoveal presentation of photopic stimuli (e.g. Pokorny, Smith and Starr, 1976). In the present study, the relative spectral sensitivity curves and colour-matching properties of normal and anomalous trichromats were measured foveally and parafoveally at a number of illumination levels, and bleaching experiments were performed to measure the effect of altering the pigment optical densities. The various models of anomalous trichromacy are discussed in the light of these observations.

The experiments and related analysis which have been performed are listed below.

1. The foveal and parafoveal luminosity curves of one normal, one deuteranomalous and one protanomalous trichromat were measured by flicker photometry using a white-light reference source. The curves of the normal and protanomal were measured at successively lower illumination levels of the white light reference. The relative spectral sensitivity curves of the anomalous observers were also measured while the observers were

adapted to monochromatic lights of illumination levels sufficiently high to bleach photopigments to a measurable extent.

2. The colour matches of two anomalous trichromats were measured at mesopic and scotopic illumination levels, using a foveal matching stimulus and a parafoveal test stimulus.

3. The colour matches of a number of normals, protanomals and deuteranomals were measured following adaptation to successively higher illumination levels of a bleaching field. Measurements were made foveally and parafoveally, and the test stimulus wavelength was 582 nm.

4. The colour matches of several normal and anomalous trichromats were measured using a series of monochromatic test stimuli with wavelength between 540 nm and 640 nm. Measurements were made for both foveal and parafoveal viewing of stimuli.

5. The effects on normal colour matches of pigment bleaching by adaptation at high illumination levels are calculated, and the probable range of optical densities of the red-green pigments of normal vision thereby estimated. Several models of anomalous trichromacy are examined theoretically, and the changes of colour matches induced by adaptation to light at high illumination levels are calculated for these models. Finally, the experimental results and theoretical calculations are compared in order to see which model of anomalous trichromacy best describes the experimental data.

5.2 Selection of Observers

A survey was made of about five hundred people (mostly males

at Imperial College) using the Ishihara plates (5th ed.), viewed under normal daylight conditions. People who made two or more errors in identifying the numerals on these plates were asked to establish Rayleigh matches on the Wright colorimeter (Wright, 1946). These matches were recorded, and also examined visually by two normal trichromats. Observers who made consistent matches which appeared distinctly too red or too green to the two colour-normals were selected for further study. Each observer was also requested to match a red (650 nm) stimulus against a green (530 nm) and a yellow one (580 nm). This test for dichromatic vision revealed two deuteranopes and one protanope. No attempt was made to assess the ratios of colour anomals to normals because of the mixed ethnic origins of people in the survey. Most observers were in their early twenties. When necessary, refractive errors were corrected by means of appropriate spectacle lenses.

5.3 Procedure

Flicker-fusion measurements were made by rotating the magnesium oxide-coated 90^{o} sectored disc located at the point DS in figure 2.6. Light from the spectrum W1 was obscured, and only one of the prisms at W2 was used to reflect near-monochromatic light into the probe field. This light filled the $1^{o} \times 1^{o}$ upper half of the probe field, and was alternated with white light from the source S1 reflected by the sectored disc DS. An achromatic collimating lens was placed in front of S1 to increase the illumination level of white light. The illumination level of the near-monochromatic light was adjusted by the observer in order to reduce the perceived brightness flicker to a minimum or zero. The observer made four to seven settings of minimum flicker

illumination level for each of a series of near-monochromatic light stimuli. The average of these settings was determined, and used to calculate spectral sensitivity curves. A dim red fixation point was provided 6^{o} above the $1^{o} \times 1^{o}$ photometric field used for parafoveal measurements, and four red points at the corners of the field aided foveal measurements. The flickering probe field was presented for intervals of 1 - 2 seconds, and was cycled with light or dark background fields (10^{o} in diameter) in the order: 20 sec light (or dark) adaptation, 5 sec dark adaptation, 2 sec probe field presentation (figure 2.10). The wavelength of the adaptation field was either 471 nm or 551 nm. (The probe field became invisible following adaptation to bright red lights.)

A limited number of colour-matching determinations were made at low illumination levels. More extensive colour-matching measurements were performed, for a number of normal and anomalous trichromatic observers, in which adaptation to high illumination level lights was employed in order to induce significant pigment bleaching.

Colour-matching sessions involving parafoveal stimulus presentation commenced with a half-hour dark-adaptation period. The test and matching halves of the probe field used for these measurements were squares of side 2^{o} and were presented on a dark background. The matching half-field contained a mixture of the red (650 nm), green (530 nm) and blue (460 nm) matching stimuli of the WDW system: it was presented for 0.5 seconds every 6 - 20 seconds and was located between four dim fixation points. The test half-field was presented simultaneously with the matching half-field and was located 4^{o} below it. The matches were made for a number of wavelengths of the test stimulus,

and this stimulus was presented at a series of successively lower illumination levels. The colour matches were plotted on the foveal WDW chromaticity diagram for each observer. For experiments in which high illumination level adaptation stimuli were employed, the $1^{o} \times 2^{o}$ test and matching fields of figure 2.10 were used. The upper half of the probe field (fig. 2.10) constituted the matching stimulus and the lower half the test stimulus. For most of the experiments the wavelength of the near-monochromatic test stimulus was 582 nm, which appears as yellow to colour-normal observers. This yellow test field was set at a retinal illumination level of about 3 log trolands and was located 3^{o} to the left of the centre of a circular adaptation field of 10^{o} diameter (fig. 2.10). Each observation session was preceded by a dark-adaptation period of 15 minutes. The observer then adapted to the circular uniform background field for three minutes, following which the background and probe stimuli were presented cyclically as shown in the lower half of figure 2.10 (q.v.). The 6 second period of darkness following each presentation of the adaptation field was necessary to reduce the effects of after-images. The observer adjusted the matching field during the periods of adaptation and the cycle was continued until a satisfactory match was obtained. Four or five matches were established for each illumination level of the adaptation field and each observer made a series of matches, starting in the dark-adapted state and proceeding to the higher illumination levels of the adaptation field. For parafoveal measurements observers looked at a fixation point (figure 2.10) such that the probe field was presented 6^{o} nasally.

Further colour-matching measurements were made in the absence of an adaptation field, using either a circular 1^{o}

bipartite colour-matching field, or an annular one (i.d. = 5^{o}, o.d, = 10^{o}). These fields were divided horizontally, and the stimulus beam entered the eye axially. The wavelength of the test half of each field (the lower half-field) was varied between 540 nm and 640 nm.

5.4 Flicker Sensitivity Data

The aim of the work presented in this section was to measure the relative spectral sensitivity curves of normal and anomalous trichromats under various conditions to see how the curves differ, and later to examine whether the differences are consistent with one of the various models of anomalous trichromacy. The relative spectral sensitivity curves of a normal, a protanomal and a deuteranomal were accordingly measured both foveally and parafoveally using the method of minimum (or zero) flicker. The flicker-fusion sensitivity curves were measured in the total absence of adaptation fields, and also in the dark immediately after adaptation to a bleaching light stimulus.

i) Data Measured for the Dark-Adapted State

The flicker-fusion relative sensitivity curves in figures 5.1 to 5.5 were measured in the absence of adaptation fields for a normal (JB, figures 5.1, 5.2), a protanomal (RF, figures 5.3, 5.4) and a deuteranomal (BR, figure 5.5). The flicker-frequency used in the determination of each of these curves is shown in the inset at the top of each figure, together with the approximate illumination level (in log td.) of the reference white light reflected from the rotating sector DS (figure 2.6).

At the lower illumination levels of the reference light the flicker-fusion frequency fell below 20 Hz even for foveal determinations, and measurements were made at the highest flicker frequencies for which flicker could still be perceived by each observer. Even so, parafoveal flicker-fusion was obtained for the normal BR and the protanomal RF over a wide range of illumination levels of the near-monochromatic lights: the upper and lower limits of this range were determined separately and are shown by the downward- and upward-facing brackets respectively in figures 5.2 and 5.4.

The relative spectral sensitivity curves which were measured foveally for the colour-normal JB are plotted in figure 5.1. These curves were measured at successively lower illumination levels of the white reference light (2, 1.2 and 0.4 log td.), at the flicker-frequencies indicated. The continuous curve (marked 'normal') at the bottom of figure 5.1 is the standard sensitivity curve for normal observers (V_λ, from Wyszecki and Stiles, 1967, p. 240). The spectral curve obtained at the

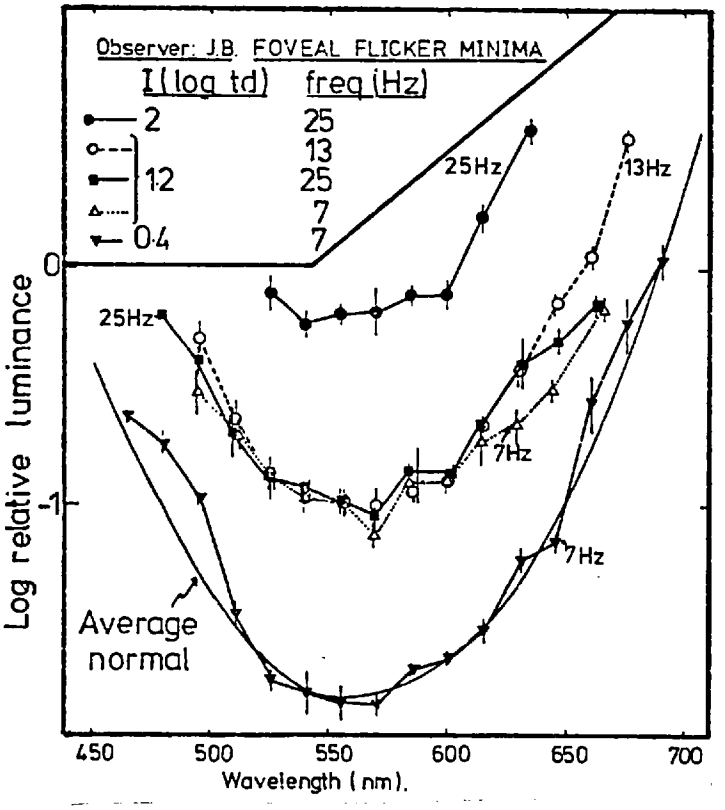

FIG. 5.1 Foveal relative spectral sensitivity curves measured for JB, a normal trichromat. The curve labelled 'normal' is the CIE V_λ curve.

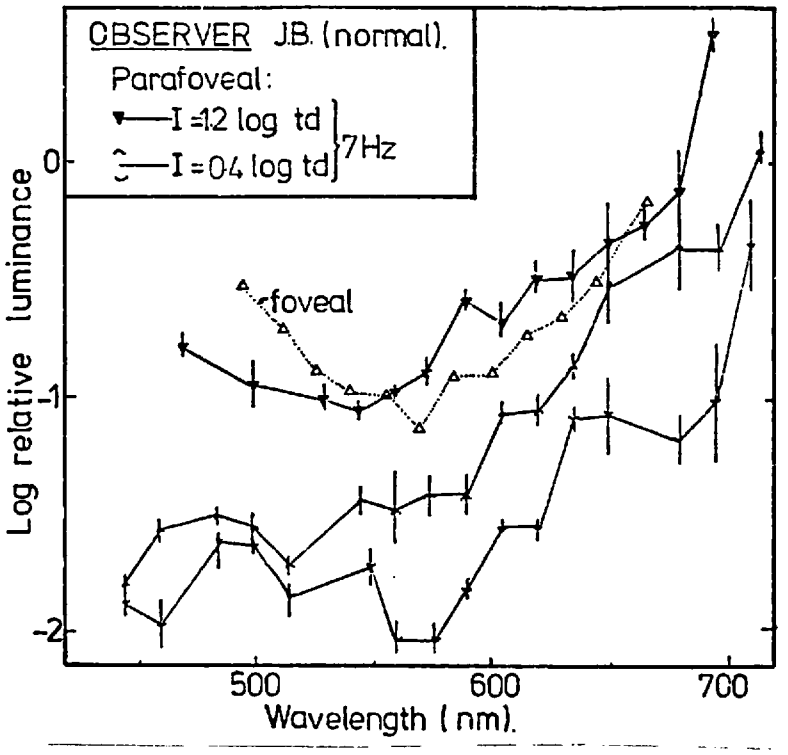

FIG. 5.2 Parafoveal relative spectral sensitivity curves for the normal JB

highest illumination level (2 log td.) is narrower in bandwidth than the other curves. The curve obtained using a flicker frequency of 13 Hz, with an illumination level of the reference light of 1.2 log td., has the same shape as that measured at the lower illumination level of 0.4 log td (figure 5.1). The other two sets of foveal data measured at 1.2 log td. show relatively higher sensitivities at wavelengths above 630 nm. The lower spectral curve (figure 5.1) follows the normal V_λ curve except at wavelengths below 500 nm. All of the relative sensitivity curves in figure 5.1 lie within the limits of the foveal sensitivity curves measured for 53 normal observers by Gibson and Tyndall (1923; see Wyszecki and Stiles, 1967, p. 403). The two relative spectral sensitivity curves

obtained parafoveally for the colour normal JB are shown in figure 5.2: the foveal curve corresponding to the upper parafoveal curve in figure 5.2 is redrawn (broken) on the same diagram. The parafoveal curves are wider in bandwidth than the foveal curve, and the upper curve has a minimum at shorter wavelengths than that of the foveal curve.

The relative spectral sensitivity data obtained for three illumination levels of the white reference light for the protanomal RF are shown in figures 5.3 and 5.4: in these figures the solid curves were obtained for foveal viewing conditions and the broken curves for parafoveal viewing.

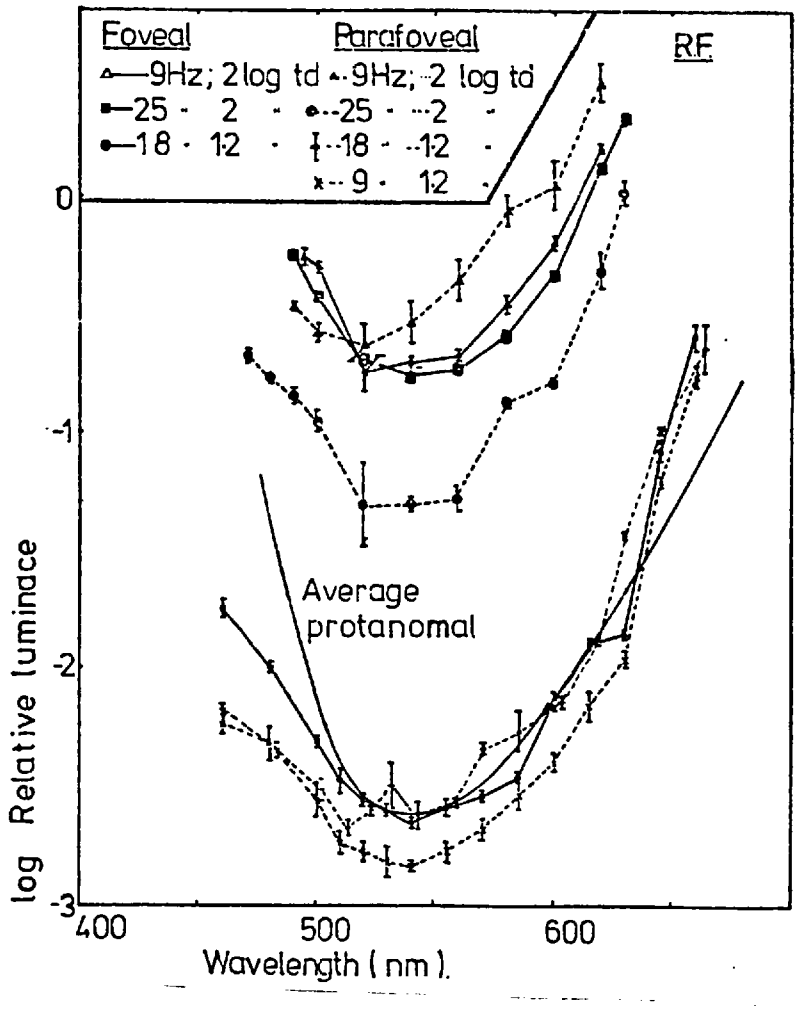

FIG. 5.3 Foveal and parafoveal relative spectral sensitivity curves for the protanomal RF, and the mean protanomalous curve from McKeon and Wright (1940)

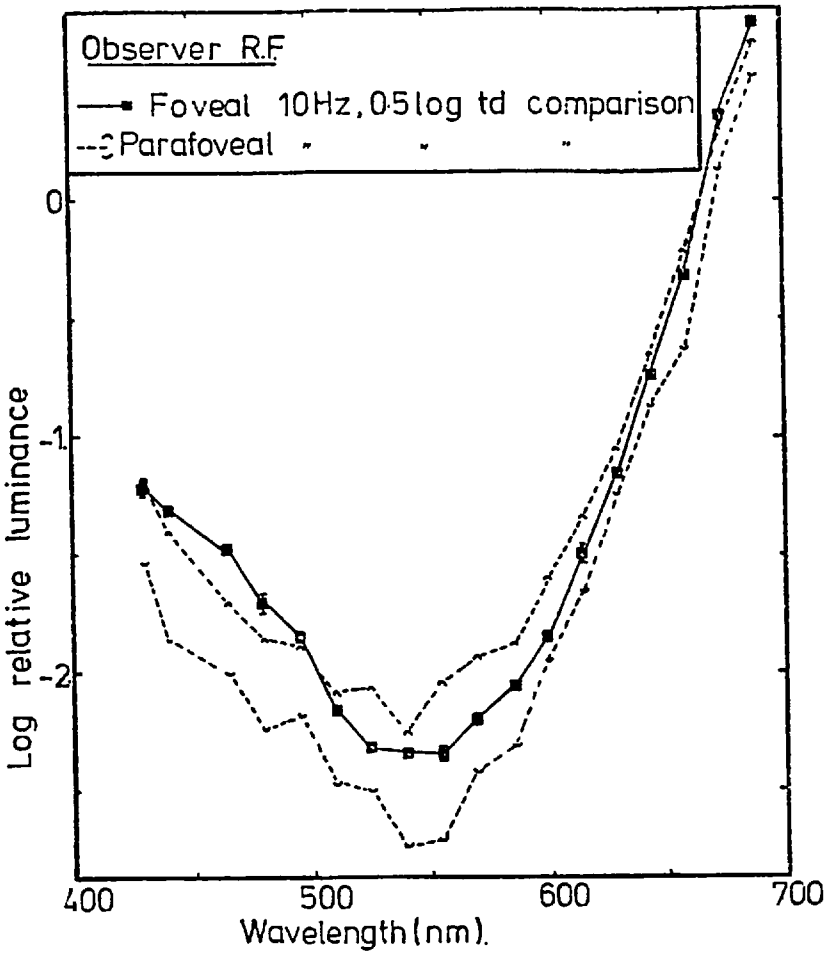

FIG. 5.4 Flicker-fusion spectral sensitivity curves for RF, a protanomal

The continuous spectral curve in figure 5.3 (marked 'average protanomalous') is the mean relative spectral sensitivity curve published by McKeon and Wright (1940) for 11 protanomals (Wyszecki and Stiles, 1967, p. 403). The spectral sensitivity curves measured foveally for RF (solid curves, figure 5.3) have minima around 540 nm. There are small differences in shape between the curves even when these are measured at the same illumination level of the white reference source (e.g. upper two solid curves, figure 5.3), and they follow the mean spectral curve for protanomals (at the bottom of figure 5.3) at wavelengths above about 500 nm. There are large differences in shape between

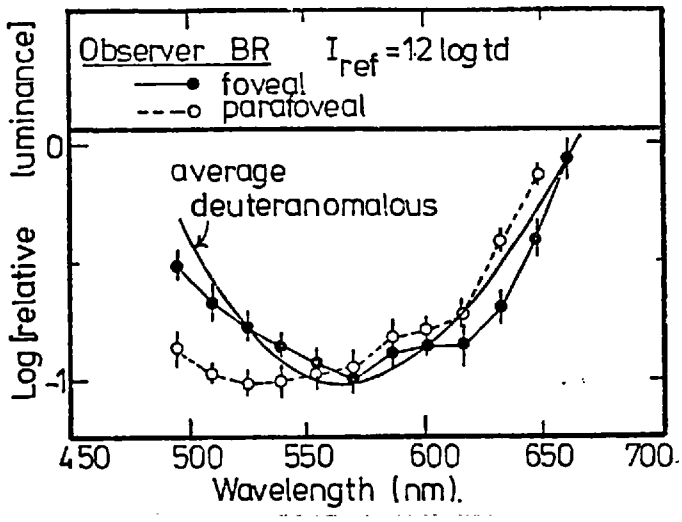

FIG. 5.5 Relative spectral sensitivity curves for the deuteranomal BR, and the mean curve for deuteranomals (Wright, 1946)

the parafoveal spectral curves of figure 5.3: these parafoveal spectral curves have minima between 500 nm and 540 nm - that is, at shorter wavelengths than the minima of the corresponding foveal curves.

The foveal and parafoveal relative spectral sensitivity curves which were obtained for the deuteranomal BR are shown in figure 5.5. (The illumination level of the reference white stimulus was 1.2 log td for both curves.) The smoothly-connected curve is the mean spectral sensitivity curve given by Wright (1946) for deuteranomalous observers: the curve measured foveally for BR matches this curve in mean spectral sensitivity. The parafoveal curve possesses a minimum at shorter wavelengths than that of the foveal curve (about 510 nm for the parafoveal curve compared to 560 nm for the foveal curve).

ii) Spectral Sensitivity Measurements made under Adaptation to Bleaching Lights

The foveal and parafoveal relative spectral sensitivity curves measured for the normal JB, the protanomal RF and the deuteranomal BR are plotted in figures 5.6 - 5.8 (solid curves refer to foveal determinations, broken curves indicate parafoveal measurements). The curves obtained for different flicker frequencies have been displaced vertically by arbitrary amounts for clarity. Again, the flicker frequencies and illumination level of the white reference light used for the determination of each curve are indicated in the insets above the diagrams. The illumination level of the bleaching light (of wavelength 471 nm or 551 nm, indicated on the figures) was about 3.7 log td in each case, in order to cause significant bleaching of the photopigments (e.g. figure 4.35).

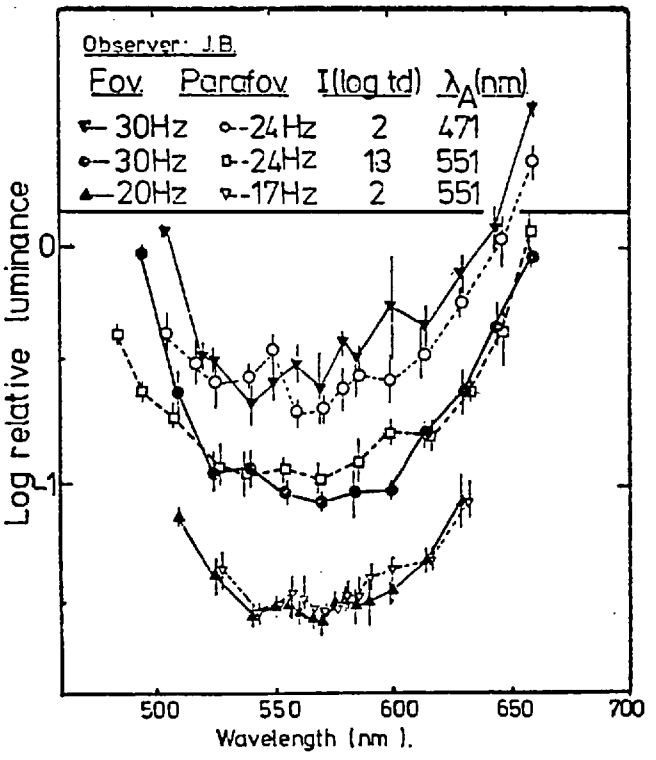

FIG. 5.6 Relative spectral sensitivities in the light adapted state for the colour normal JB.

The foveal spectral curves and the corresponding parafoveal curves

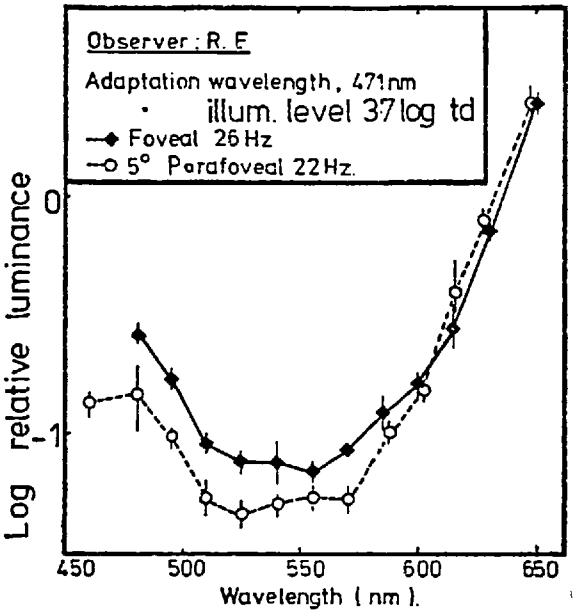

FIG. 5.7 Spectral sensitivity curves for the light-adapted protanomal RF.

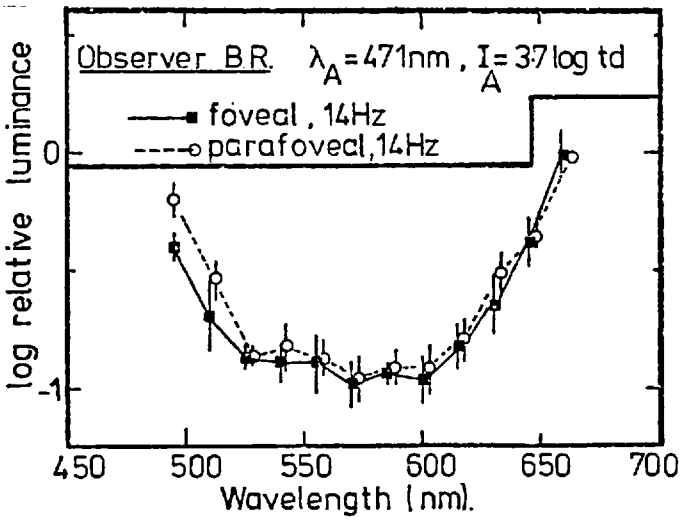

FIG. 5.8 Deuteranomalous light-adapted spectral sensitivities for the fovea and parafovea.

obtained under adaptation to the bleaching light are similar in the case of the normal (figure 5.6) and deuteranomal (figure 5.8), apart from small differences at short wavelengths (≤520 nm). The minimum in the foveal spectral curve of the protanomal occurs at somewhat longer wavelengths than that in the parafoveal spectral curve.

The foveal relative spectral sensitivity curves measured for the dark-adapted state are replotted for the three observers in figure 5.9 (from figures 5.1, 5.3 and 5.5). Alongside these curves are plotted

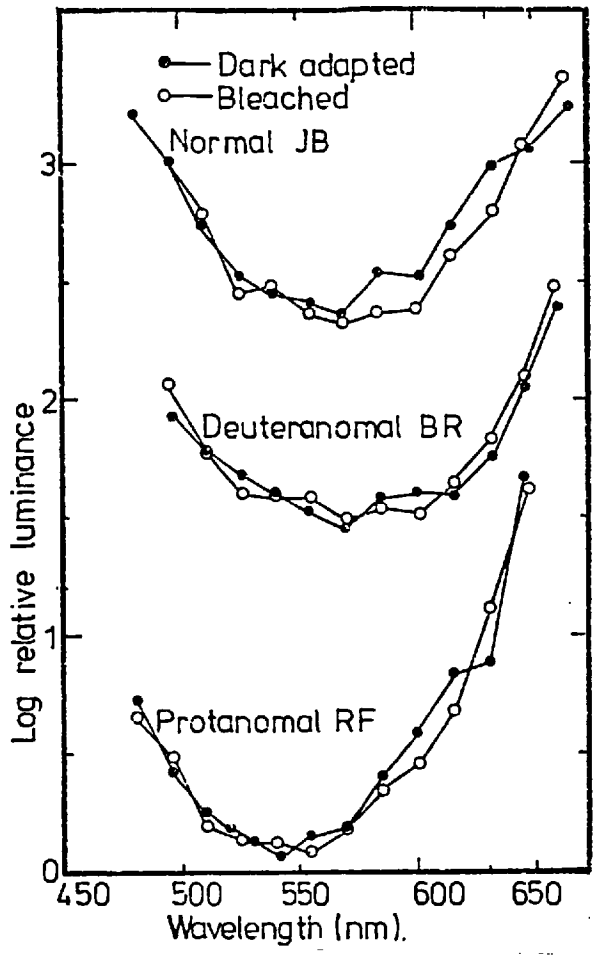

FIG. 5.9 Relative spectral sensitivity curves for the normal, protanomal and deuteranomal in the dark-adapted and bleached states.

the corresponding foveal spectral curves obtained for each observer under adaptation to bleaching light of wavelength 471 nm and illumination level 3.7 log td. (from figures 5.6 - 5.8). The two foveal spectral sensivitity curves obtained for each observer are similar in each case, and there are no systematic differences between the two foveal curves obtained in the presence and in the absence of the 471 nm bleaching light, for each observer.

5.5 Colour-Match Changes at Low Illumination Levels

A plot of the colour-matches made by the deteranomal BR for a test stimulus presented 4^{o} from the central fovea, is given in the WDW foveal chromaticity diagram of figure 5.10. The trivariant matching field was presented foveally, and for each spectral test stimulus measurements were made at a series

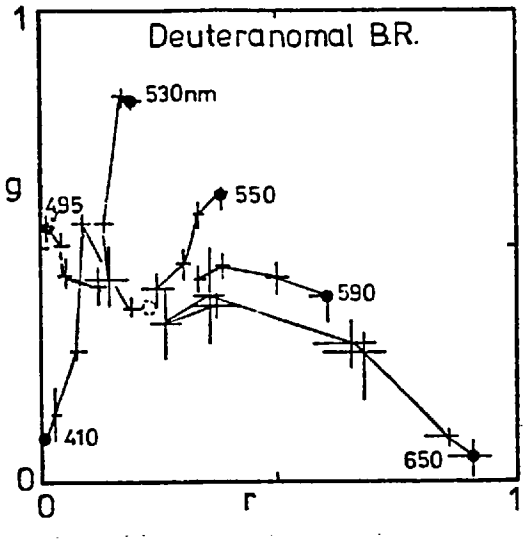

FIG. 5.10 Parafoveal colour matches made at mesopic light levels by the deuteranomal BR.

of illumination levels. The illumination level of the test stimulus was initially 10 - 30 td at each wavelength, and was decreased successively in steps of about 0.5 log units. The results show that the saturation level of all test stimuli decreases as the illumination level is lowered, and the chromaticities of all test stimuli coalesce to the same area on the chromaticity diagram. The results are similar to those found for normal observers by Hunt (1952) and Clarke (1960).

The corresponding colour-matching data for the protanomal RF became very erratic at low illumination levels owing to a reduction in his due discrimination. For RF the colour saturation of a 650 nm parafoveal test stimulus decreased as its illumination level was lowered, but the errors in colour-matching were almost as large as the shifts of chromaticity. RF's hue discrimination between wavelengths of 480 nm and 600 nm was insufficient at low illumination levels to enable satisfactory measurements of the chromaticity of the test stimulus. A few measurements made with a further protanomal, RL, indicated that he too suffered a severely reduced hue discrimination ability at low illumination levels.

5.6 Colour-Match Changes Caused by Bleaching Lights

In this section foveal colour matches, made after adaptation to spatially uniform bleaching lights of various illumination levels, are presented. The sequence of presentation of the adaptation and probe fields which was used is shown in figure 2.10, together with the spatial configuration of the stimuli. Both normal and anomalous trichromats took part in this study: the results obtained for colour-normal observers using a 582 nm test field are presented first.

i) Shifts in Rayleigh Matches of Colour Normals Induced by Light Adaptation

The log of the relative amounts of red and green matching stimuli used in the foveal Rayleigh matches by normal observers are plotted against the log of the adaptation illumination level (in trolands) in figure 5.11. The ordinates of each graph were chosen such that the values of log R and log G are zero at the highest adaptation illumination level used in each case. The upper three graphs in figure 5.11 refer to foveal vision, and the lower one refers to parafoveal vision (figure 2.6). The data were measured using the Wright red (650 nm) and green (530 nm) colour-matching stimuli, and a 590 nm bleaching stimulus. The significant points of these data are as follows.

First, it can be seen from figure 5.11 that the amount of the red stimulus needed in the colour-matches increases with the illumination level of the adaptation stimulus, that the amount of the green stimulus generally decreases as the adaptation illumination level is raised (i.e. the mixture becomes redder at high illumination levels), and that the changes in the amounts

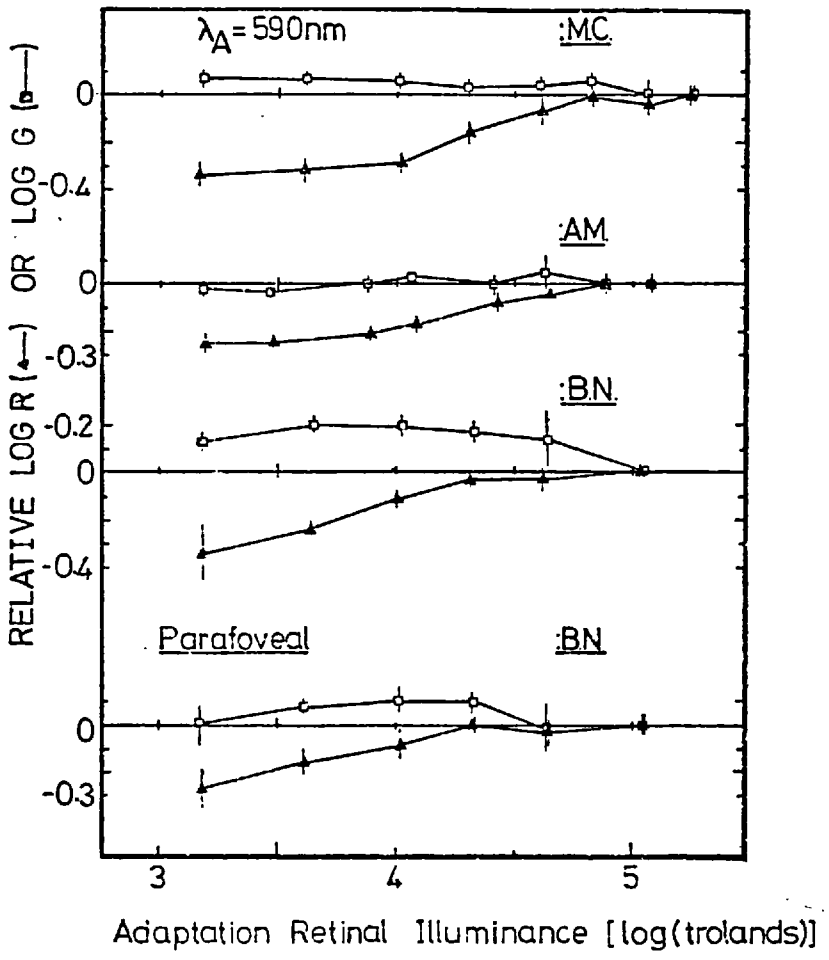

FIG. 5.11 Changes in the amounts of the red and green matching stimuli (in log units) versus the illumination level of the adaptation stimulus (λ_A = 590 nm) for three colour-normal observers.

of the red stimulus are larger.

Second, the shifts in the log R and log G values obtained parafoveally for BN (bottom of figure 5.11) are in the same direction as those obtained foveally, although they are smaller in magnitude.

Measurements of the two end points of the range of adaptation illumination levels were made for a further nine colour-normal observers. Their average Rayleigh matches were determined in the dark-adapted state, and also while they were adapted to a

590 nm stimulus at an illumination level of 5 log td. The measurements were made foveally and parafoveally (figure 2.6), and the corresponding data of MC, AM and BN (figure 5.11) were added to these in order to obtain the average values for 12 colour-normals. The means of the log R and log G values were adjusted to be zero for the bleached foveal state (I_A = 5 log td).

TABLE 5.1: Average R, G values of 12 colour-normals

Measurement	log R (Δ log R)	log G (Δ log G)
foveal, dark-adapted	0.0 (0.04)	0.0 (0.05)
foveal, adapted to 5 log td, λ_A = 590 nm	-0.30 (0.09)	0.05 (0.09)
parafoveal, dark-adapted	-0.12 (0.03)	0.02 (0.05)

The average data appear in Table 5.1, together with the standard deviations of the mean of the individual log R and log G values. The average log R and log G values for the parafoveal dark-adapted state (-0.12 and 0.02 respectively), are closer to those of the adapted foveal state (log R = 0; log G = 0) than the average values measured for the dark-adapted foveal state. A measure of the variation of the Rayleigh matches of colour normals is given by the standard deviations of the mean log R and log G values (Δ log R and Δ log G, Table 5.1): these values are least (about 0.4) for the measurements of the parafovea and the bleached fovea. The variation of the log R and log G values for the dark-adapted state is double this

value (Δ log R = Δ log G = 0.09).

ii) Shifts in Rayleigh Matches of Anomalous Trichromats Caused by Bleaching

As with the normal subjects, Rayleigh matches were established by deuteranomalous and by protanomalous observers for various illumination levels of the bleaching light. The test and matching stimuli were the same as those employed for the measurements with normal subjects described in the previous section, and the field configuration used is shown in figure 2.6.

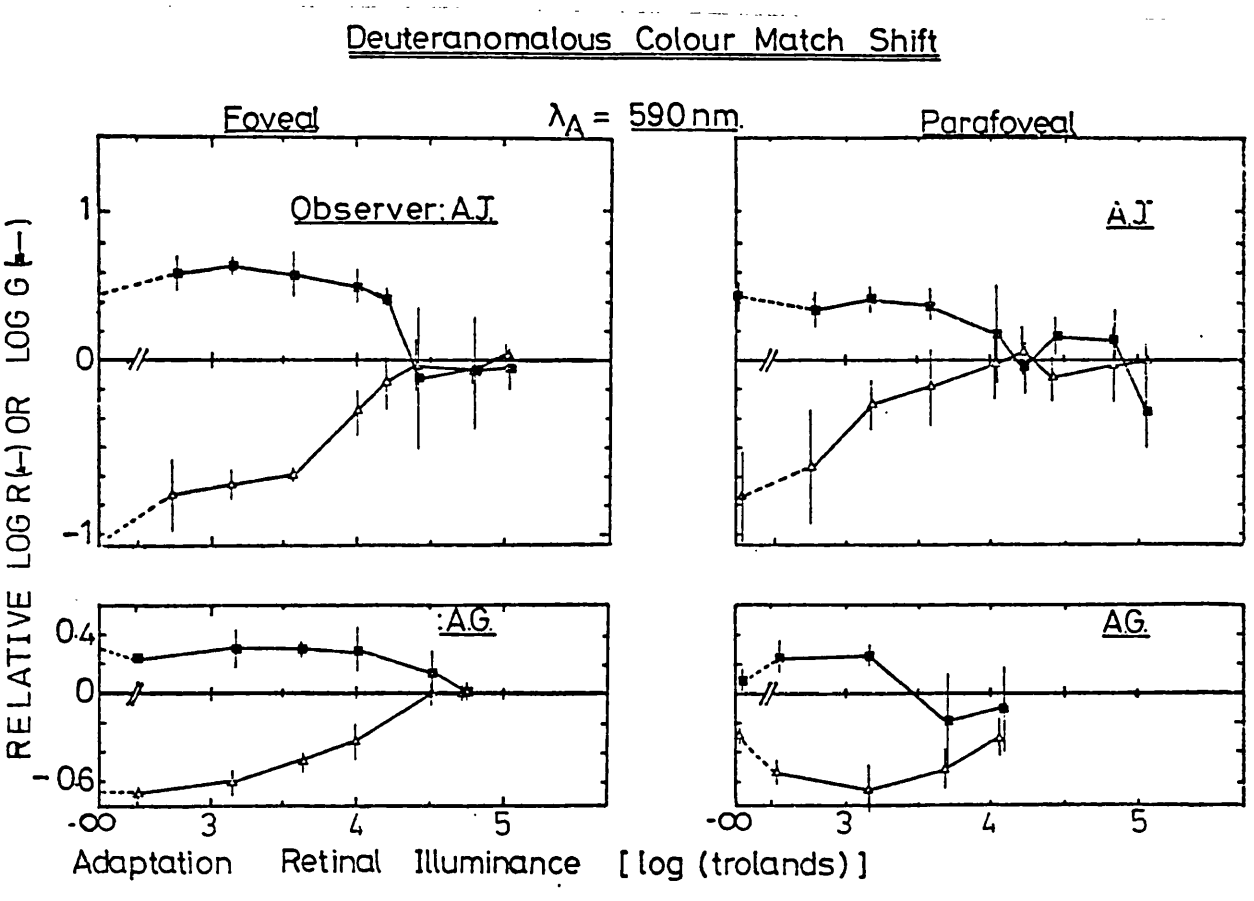

FIG. 5.12 Plots of Δ log R and Δ log G (with scales chosen such that Δ log R = 0, log G = 0 for the average normal adapted to 5 log td light) against adaptation illumination level for two deuteranomals.

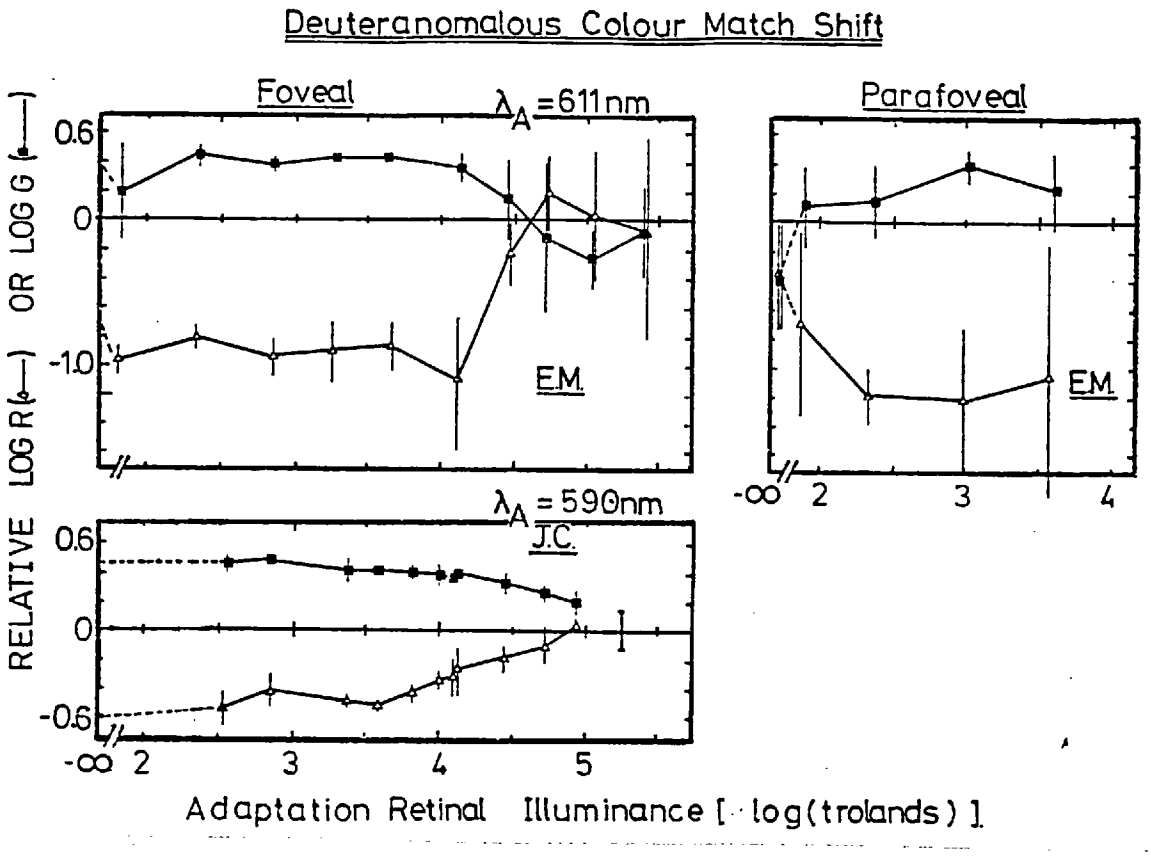

FIG. 5.13 Deuteranomalous Rayleigh match shifts following adaptation to bleaching lights (see caption to fig. 5.12).

The results obtained for the deuteranomalous observers are plotted in figures 5.12 - 5.15. The wavelength of the bleaching light (λ_A) used for the deuteranomals was 590 nm or 611 nm. The zero of the ordinate axis in each case was chosen to coincide with the average log R and log G values calculated for the twelve colour-normal observers (Table 5.1) from the measurements made following high intensity bleaching. The value log G - log R (= log G/R) for each deuteranomal is largest in the dark-adapted state ($I_A \rightarrow -\infty$) and is least at high illumination levels ($I_A \rightarrow 5$ log td), so that the colour matches are 'greener' (need more green light in the matching field) for the dark-adapted state. Also, the dark-adapted foveal values of log G/R for the

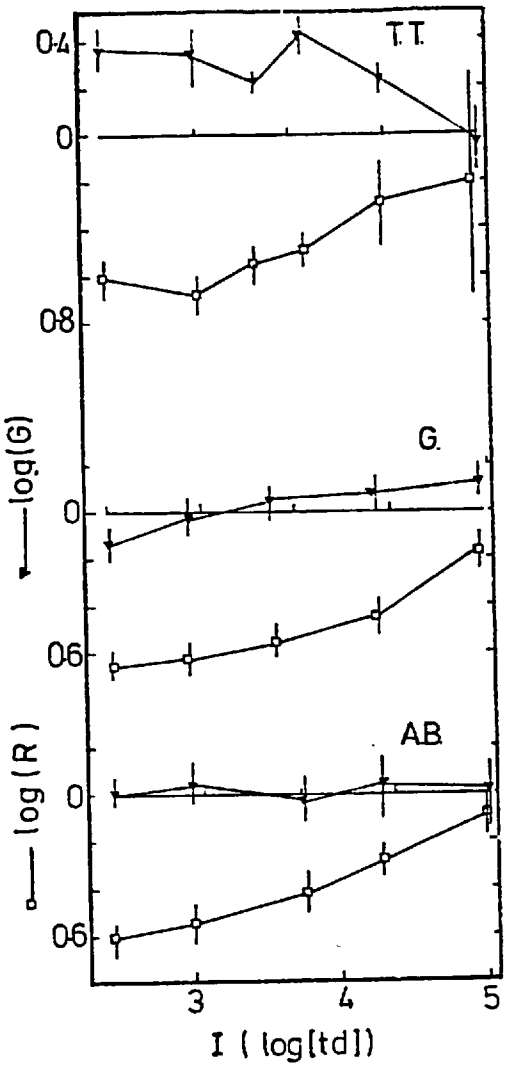

FIG. 5.14 Deuteranomalous foveal Rayleigh match shifts (see fig. 5.12)

deuteranomals (0.6 < log G/R < 1.4) are larger than those of the colour-normals (0.3 < log G/R < 0.6), so that the dark-adapted colour matches of the deuteranomals are greener than those of colour-normals. The most important point about the data of figures 5.12 - 5.15 is that the log R and log G values approach zero as the illumination level of the bleaching light is raised: i.e. for a bleaching light of illumination level 5 log td, the colour matches of deuter-anomalous observers approach the average match established by colour-normal observers under the same conditions. The values of log R and log G are equal to zero (within error) for the highest illumination levels for the foveal measurements of seven of the eight deuteranomalous observers (the exception being observer G, figure 5.14).

The log R and log G values measured for the dark-adapted parafoveas of the deuteranomals are closer to zero than the foveal values (figures 5.13, 5.14). The parafoveal colour-matches of AJ and AG approach the average colour-normal match at high illumination levels of bleaching light (figure 5.12),

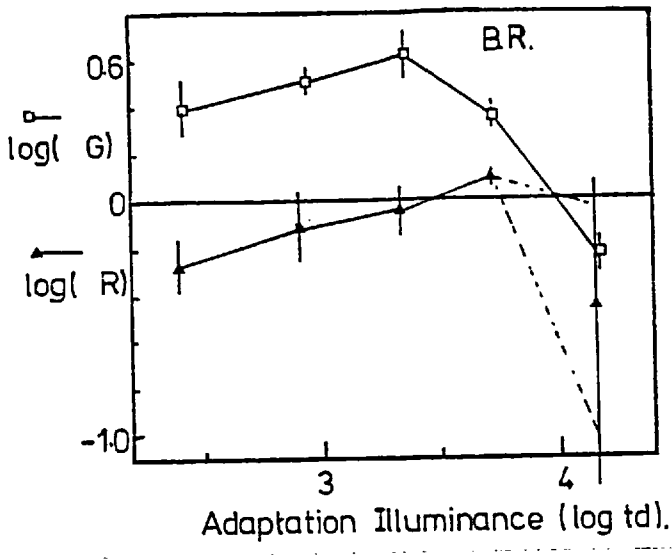

FIG. 5.15 Rayleigh match shift for the deuteranomal BR (see caption to fig. 5.12)

but the parafoveal Rayleigh matches of EM diverge from those of the colour normal up to an illumination level of bleaching light of 3 log td (figure 5.13). EM and AG were unable to make parafoveal colour-matches at higher illumination levels of the bleaching light, as the probe stimulus became too dim.

The Rayleigh colour-matches of three protanomalous observers are shown in figure 5.16. The ordinate scales are again adjusted so that log R = log G = 0 corresponds to the average 'bleached fovea' colour match obtained for twelve normals (Table 5.1). The wavelength of the adaptation stimulus was 530 nm, since it was found that the errors in matching increased with illumination level for longer-wavelength bleaching lights. (The converse was true for the deuteranomal AJ: preliminary measurements showed that his matching errors were greater for short-wavelength (530 nm) bleaching lights than for long-wavelength lights (590 nm).) The probe stimulus became invisible to the protanomalous observers RF and WW at relatively low illumination levels of the bleaching light, so that their matches could not be measured at the highest illumination levels. The values of log G/R for the dark-adapted matches of the

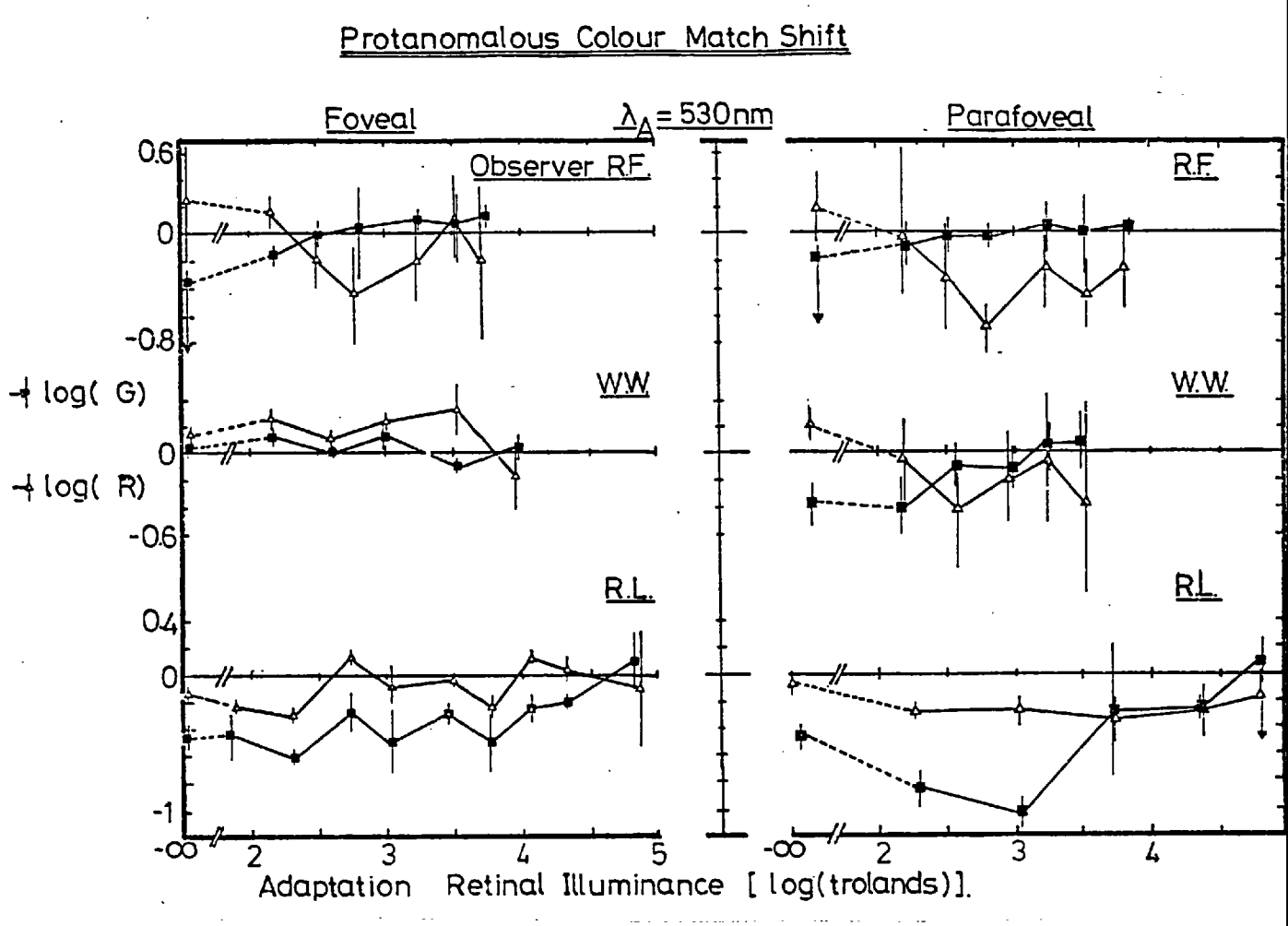

FIG. 5.16 Rayleigh-match shifts for three protanomals (see caption to figure 5.12)

protanomals are all negative (figure 5.16), so that these matches are redder (i.e. log R/G > 0) than the matches made by colour-normals under adaptation to 5 log td light. The colour-matches of the three protanomals again approach the average colour-match of the light-adapted normals as the illumination level of the adaptation stimulus is raised. This is most clearly seen for the matches made by RL.

A further, extreme protanomalous, observer AH made successive dark-adapted Rayleigh matches which differed markedly in the ratio of the amounts of the red and green matching stimuli (Δ log R, Δ log G $\geqslant$ 2 log units). His matching was dichromatic even for low illumination levels of a 590 nm adaptation stimulus,

and his matching errors did not decrease when the wavelength of the adaptation stimulus was changed to 530 nm. However, when the wavelength of the bleaching light was changed to 495 nm or 471 nm, his matching errors (Δ log R, Δ log G) decreased to ± 0.2 at high adaptation illumination levels ($\sim$4 log td). AH found colour-matching under these conditions difficult as he was unable to name the colours of the two halves of the probe field, or to predict whether the (R/G) ratio should be increased or decreased to obtain a match. The matching was eventually accomplished by having the experimenter (the author) change the amounts of R and G independently by small amounts in a staircase fashion. When this method was used for the dark-adapted state, AH again accepted a wide range of R/G values (at equal brightness) for the match point. The matches made by AH at high adaptation illumination levels ($\sim$4 log td) were protanomalous $((\log R/G_{AH} - \log R/G_{\text{average normal}}) = 0.3 \pm 0.2)$, and he was unable to make matches at higher illumination levels owing to the low apparent brightness of the probe field.

5.7 Differences between Normal and Anomalous Trichromatic Colour Matching established for the Non-Adapted Fovea and Parafovea

Values of log (red matching coefficient/green matching coefficient) (log R/G) obtained from colour-matches made with a 1° circular bipartite colour-matching field viewed foveally, and with an annular bipartite field provided with a central fixation spot (figure 5.17), are shown in figure 5.18 for a normal, a protanomal and a deuteranomal. The data of log R/G on the left of figure 5.18 are for foveal viewing, and those on the right for parafoveal colour matching. Values of curves for the normal were derived from the data of Pitt (1944, see section 5.8) for the red-sensitive and green-sensitive mechanisms of normal colour vision, assuming peak optical densities of the two pigments of 0.7 and 0.1 respectively for foveal viewing and 0.42 and 0.06 respectively for extrafoveal viewing. The choice of optical densities is justified in a later section (section 5.8). The calculated values agree well with the

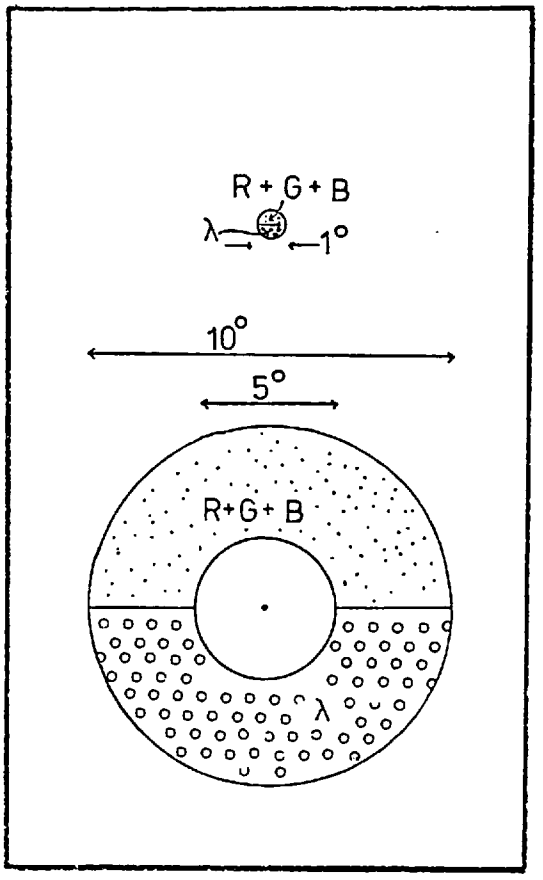

FIG. 5.17 Foveal 1° circular and parafoveal annular colour-matching fields.

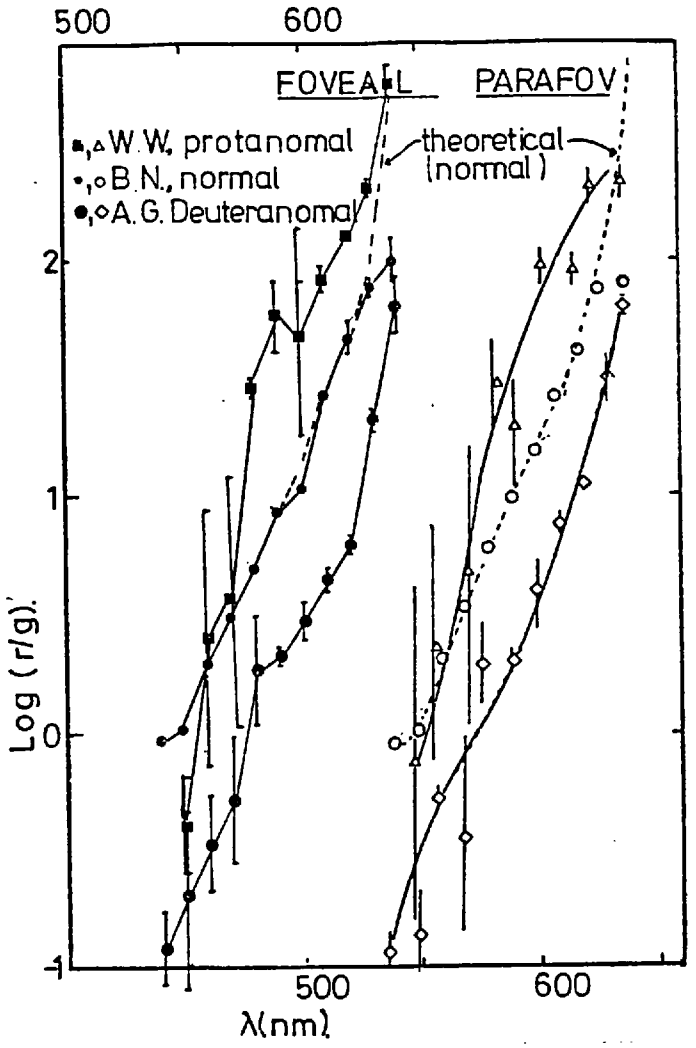

FIG. 5.18 Experimentally determined colour-matching log R/G values (solid curves) for the dark-adapted foveas (left-hand side) and parafoveas (right-hand side) of three trichromats. The broken curves are theoretical curves derived from Pitt's (1944) spectral sensitivity curves for normal vision (see text).

foveal and para-foveal data for the normal matches except in the far red, where stray light effects in the green matching stimulus make precise estimates of log R/G difficult. The data points obtained for the anomals are somewhat closer to those of the normal observer for the parafoveal matching, compared to the foveal data. The values of log (R/G) for different classes of trichromat are not the same for parafoveal vision, except at short wavelengths where the errors of matching make firm conclusions difficult.

5.8 Theoretical Calculations of Colour Matches Predicted by Models of Anomalous Trichromacy: I. Calculations based on Erythrolabe/Chlorolabe Mixtures

Several models of anomalous trichromacy were mentioned in section 5.1. Four of these are depicted schematically in figure 5.19. At the top left of this diagram a pair of schematic cones represents the two classes of 'red' and 'green' cone types of normal vision: the outer segments are filled with pigments α and β. In the 'anomalous pigment' model of anomalous trichromacy (A, figure 5.19) the single anomalous pigments α" or β" replace the normal α or β pigments respectively. (The case for which both pigments are anomalous in the same observer, α" and β", is not shown). In the 'pigment mixture' model (B, figure 5.19) the anomalous pigments (α', β') result from mixtures of the pigments of normal vision (α + β). It has already been argued that the neural-fusion model (C, figure 5.19) cannot account for the

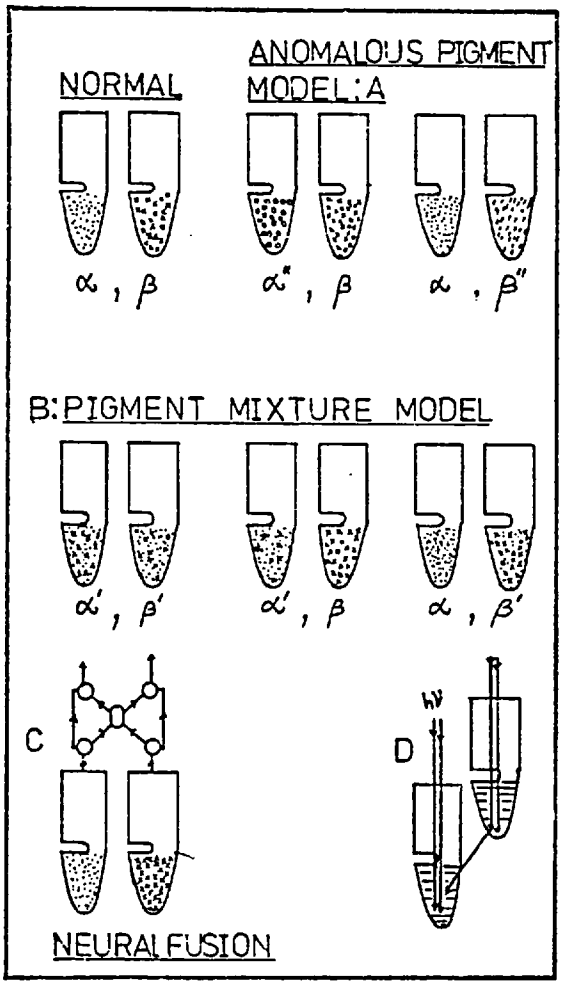

FIG. 5.19 Schematic diagram of four models of anomalous trichromacy.

colour-matching properties of anomalous trichromats. Lastly, it is proposed that optical shielding of one pigment type by the other type (D, figure 5.19) offers a plausible explanation for the Rayleigh-match shifts observed for anomals. In the following sections the models A, B and D are examined theoretically, and the colour matches predicted for such models are shown. The pigment-mixture model (B) is discussed in this section: the assumptions which were made in calculating colour matches of both normals and anomals are given first.

5.8.1 Assumptions

1) The colour-matching properties of normal and anomalous trichromats will be considered only for wavelengths exceeding 500 nm. In the calculations of colour matches, the effect of the blue mechanism is neglected, and this is a good approximation for wavelengths greater than 520 nm owing to the insensitivity of the blue mechanisms at these wavelengths, e.g. Stiles (1946). Absorption curves of the visual photopigments are not corrected for the absorption of the optical media of the eye. Deviations from the true pigment absorption curves will not be large, however, as the non-photolabile optical media absorb most strongly at wavelengths below 500 nm (e.g. figures 1.2, 1.3).

2) Normal colour vision in the red-green region of the spectrum is mediated by two classes of cone which are distinguished by the absorption spectrum (α_λ or β_λ) of the visual pigment (α or β respectively) contained within the cones of each class (Marks, Dobelle and MacNichol, 1964; Brown and Wald, 1964). Further, the absorption spectra

α_λ and β_λ determine the spectral sensitivities of the red and green mechanisms of normal colour vision, and their spectral sensitivities determine the colour-matching properties of the normal (for test wavelengths > 520 nm). Normal (red-green) colour vision will be denoted (α,β) to indicate the visual pigments which are responsible for red-green vision.

3) The sensitivity curves for the red-green colour mechanisms derived by Pitt (1944) determine the absorption spectra α_λ and β_λ for the normal. These data were derived from colour-matching experiments and were for this reason chosen in preference to the increment threshold spectral sensitivity curves measured by Stiles (Stiles, 1946) for moderate levels of background field illumination, and by Brindley (1953) for very high levels of adaptation illumination. Indeed, these threshold measurements are inherently less precise than colour-matching methods (Stiles 1946; Rodieck, 1973), although the relative sensitivity curves derived by all three methods are similar. (The colour matches of individual observers are not correctly predicted by the Stiles (1946) π-mechanisms (e.g. Wyszecki and Stiles, 1967), although Estevez and Cavonius (1976) have recently shown that colour matches of individual observers could be predicted by linear combinations of their own π-mechanisms - π_1 (or π_3), π_4 and π_5.) The precision with which absorption spectra can be determined using objective methods such as fundus reflectometry (Mitchell and Rushton, 1971a) and single-cone measurements (Marks, Dobelle and MacNichol, 1964; Brown and Wald, 1964), is also lower than that of colour-matching determinations, although again the curves obtained by these methods agree qualitatively with the data of Pitt (1944).

4) It is proposed that anomalous trichromacy is the result of the occurrence of a mixture of the normal α and β pigments in those cones which in normal colour vision contain either the red or the green photopigment. The pigment mixture contained in cones (of anomals) which in normals hold only the α pigment will be designated α'; pigment mixtures in the cones of the other class (containing the β pigment in normals) will be labelled β'. The fraction (in terms of molecule numbers) of 'normal' pigment in the mixture (i.e. the pigment which in normals is native to that class of cone: α in the α' mixture and β in the β' mixture) is denoted f in each case (so that the fraction of the other pigment in the mixture is (1 - f)). Thus, the colour matcing in the case of anomalous trichromacy denoted by (α,β'), for example, will be determined by the absorption spectra of the α pigment and of the mixture of the α and β pigments (β'). The other possible cases of anomalous trichromacy are (α',β) and (α',β') (fig. 5.19).

5) The physical dimensions of the cones which contain the red and green photopigments of normal colour vision, and of the mixtures of these pigments in anomalous trichromats, are assumed to be the same for a given retinal location. Marc and Sperling (1977) have recently mapped the distribution of the red, green and blue cone types of primates using the light-stimulated reduction of nitroblue tetrazolium chloride. No systematic morphological differences were found between difference cone types of the retina (Sperling, private communication). It is therefore likely that the physical dimensions of neighbouring

'red' and 'green' cones are the same for the colour-normal, and probable that the same is true for anomalous trichromatcs.

6) Beer's law (Beer, 1852) is assumed to hold for visual pigments and for mixtures of these pigments. This law has been shown to be true in many cases of light absorption, although exceptions have been demonstrated which were caused by light scatter or inhomogeneities of solutions (Hardy and Young, 1948; Williams and Clapper, 1975).

5.8.2 Calculation of Absorption Spectra

The optical density $D_\lambda(\alpha)$ and the extinction coefficient α^*_λ for the pigment are related at the wavelength λ by the equation

$$D_\lambda(\alpha) = \alpha^*_\lambda c_\alpha \ell_\alpha , \qquad (5.1)$$

where c_α and ℓ_α are the concentration of the α pigment and the light path through it respectively. A similar equation can be written for the β_λ pigment of normal vision.

The optical densities of pigment mixtures are additive (Beer's law, assumption 6 above), so that the optical density of the β' pigment mixture (figure 5.21 and point 3, above) is:

$$D_\lambda(\beta') = f\beta^*_\lambda \ell_\beta c_\beta + (1 - f)\alpha^*_\lambda \ell_\beta c_\beta$$

$$= f\beta^*_\lambda \ell_\beta c_\beta + (1 - f)\alpha^*_\lambda \ell_\alpha c_\alpha . c_\beta / c_\alpha$$

$$= fD_\lambda(\beta) + (1 - f)D_\lambda(\alpha)c_\beta / c_\alpha , \qquad (5.2)$$

where β^*_λ is the extinction coefficient of the β pigment.

At this point one of two alternative assumptions are made with regard to the pigments of normal vision. The two assumptions are a) that the concentrations of pigments in the cones of the normal are equal ($c_\alpha = c_\beta$), or b) that their peak absorptions in the dark-adapted state are equal ($\alpha_{max} = \beta_{max}$). The first assumption yields, from equation 5.2:

$$D_\lambda(\beta') = fD_\lambda(\beta) + (1 - f)D_\lambda(\alpha) \qquad (5.3)$$

The second assumption leads to the equation

$$D_\lambda(\beta') = fD_\lambda(\beta) + (1 - f)D_\lambda(\alpha)D_{max}(\beta)/D_{max}(\alpha), \qquad (5.4)$$

from equations 5.1 and 5.2. ($D_{max}(\beta)$, or $D_m(\beta)$, and $D_{max}(\alpha)$, or $D_m(\alpha)$, are the peak optical densities of the α and β pigments respectively in the dark-adapted state.)

The absorption spectrum of β' can then be calculated from Beer's law:

$$\beta'_\lambda = 1 - 10^{-D_\lambda(\beta')} \qquad (5.5)$$

A similar relation holds for α'_λ, so that the absorption spectra of anomalous trichromacy may be calculated, subject to the assumptions stated above.

5.8.3 Colour Match Calculations

Colour-matches are determined by the pigment absorption spectra (assumption 1, above), so that the absorption spectra

derived from the above equations can be used to calculate colour-match data. A colour match between a unit amount of the colour C_λ and the red and green colour-matching stimuli (R and G respectively) is given by

$$(C_\lambda) \equiv R(R) + G(G) \tag{5.6}$$

Hence

$$\left.\begin{aligned} \alpha_\lambda &= R\alpha_R + G\alpha_G \\ \text{and}\quad \beta_\lambda &= R\beta_R + G\beta_G \end{aligned}\right\} \tag{5.7}$$

where the subscripts R and G denote the wavelengths of the red and green matching stimuli respectively. Solution of equations 5.7 yields

$$\left.\begin{aligned} R &= (\alpha_\lambda\beta_G - \alpha_G\beta_\lambda)/(\alpha_R\beta_G - \alpha_G\beta_R) \\ \text{and} \\ G &= (\alpha_R\beta_\lambda - \alpha_\lambda\beta_R)/(\alpha_R\beta_G - \alpha_G\beta_R) \end{aligned}\right\} \tag{5.8}$$

5.8.4 Changes in Colour Matches Induced by Bleaching

The absorption spectra of visual pigments will change if the pigment optical density is reduced, for example, by light bleaching. Before the kinetics of the bleaching process are discussed, the colour matches of trichromats following extreme conditions of bleaching by light are evaluated.

Consider first the (α',β) case of anomalous trichromacy. At extremely high levels of light illumination, the optical

densities of all pigments will be very low, so that the absorption spectrum of the pigment mixture α' in the bleached state is related to the corresponding optical density by:

$$\alpha_\lambda'^{b} = 1 - 10^{-D_\lambda(\alpha'^{b})}$$

$$= 1 - e^{-2.303D_\lambda(\alpha'^{b})}$$

$$\simeq 2.303D_\lambda(\alpha'^{b}), \qquad (5.9)$$

where the superscript "b" refers to the bleached state. Thus

$$\alpha_\lambda'^{b} = 2.303(f^b\alpha_\lambda^b\ell_\alpha c_\alpha^b + (1 - f)\alpha_\beta^b\ell_\beta^b c_\beta^b\, c_\alpha/c_\beta)$$

$$= d\,\alpha_\lambda^b + e\beta_\lambda^b, \qquad (5.10)$$

where d and e are constants (from the equation for α' corresponding to equation 5.2). The colour match for a unit amount of colour C (at wavelength λ) is

$$(C) \equiv R^b(R) + G^b(G)$$

for the bleached state. This corresponds to two equations given by

$$\left.\begin{aligned} \alpha_\lambda'^{b} &= R^b\alpha_R'^{b} + G^b\alpha_G'^{b} \\ \beta_\lambda^b &= R^b\beta_R^b + G^b\beta_G^b \end{aligned}\right\} \qquad (5.11)$$

Combining equations 5.10 and 5.11 yields:

$$\left.\begin{aligned} d\alpha_\lambda^b + e\beta_\lambda^b &= R^b(d\alpha_R^b + e\beta_R^b) + G^b(d\alpha_G + e\beta_G^b) \\ \beta_\lambda^b &= R^b\beta_R^b + G^b\beta_G^b \end{aligned}\right\} \quad (5.12)$$

Equations 5.12 may be solved to give equation 5.13:

$$\left.\begin{aligned} R^b &= (\alpha_\lambda^b\beta_G^b - \alpha_G^b\beta_\lambda^b)/F \\ G^b &= (\alpha_R^b\beta_\lambda^b - \alpha_\lambda^b\beta_R^b)/F \\ \text{where} \quad F &= \alpha_R^b\beta_G^b - \alpha_G^b\beta_R^b \end{aligned}\right\} \quad (5.13)$$

As yet, no assumption has been made about which of the sensitivity curves derived by Pitt are represented by the α_λ and β_λ absorption spectra. Thus, because of the symmetry between α and β in the above equations, the colour matches of the (α,β') system are also given by equations 5.13, under extreme conditions of bleaching. But these equations (equations 5.13) are precisely the colour-matching equations for normal vision in the bleached state (equations 5.8 with superscripts b added to α and β). Hence, under extreme conditions of bleaching the colour-matches are the same for the (α,β) and the (α',β) and (α,β') systems.

This result is, however, generally <u>not</u> true for the (α',β') case of anomalous trichromacy. Consider, for instance, the case where the fraction of the α pigment is the same in both clases of cone (so that <u>all</u> red-green cones contain the same pigment mixture). The colour-matching in the red-green part of the spectrum will

then be essentially monochromatic for all illumination levels of bleaching light, since the absorption spectra of the mixed pigments contained within the two classes of cone will always be the same.

5.8.5 Kinetics of Light-Induced Pigment Bleaching

Pigment bleaching and regeneration are governed by the light illumination level and the concentration of the pigment, and the equation describing the rate of bleaching is given by:

$$-dc_t/dt = \int \gamma_\lambda j_\lambda I_\lambda d\lambda - k(c_{max} - c_t) \qquad (5.14)$$

(from Dartnall, 1957). In this equation c_{max} and c_t are the concentrations of the pigment per unit area (molecules cm^{-2}) in the dark-adapted state (c_{max}) and at time t after the onset of the light (c_t): the illumination level of the light at wavelength λ is I_λ (quanta cm^{-2} s^{-2}). γ_λ is the quantum efficiency of the pigment, and j_λ is the fraction of the flux absorbed by the visual pigment. In the presence of photoproducts which absorb light,

$$j_\lambda = \frac{D_\lambda}{D_\lambda + D'_\lambda} (1 - 10^{-D_\lambda + D'_\lambda}) \qquad (5.15)$$

where D_λ and D'_λ are the optical densities of the pigment and the photoproduct respectively. However, the photoproducts of visual pigments do not absorb light significantly at wavelengths above 500 nm (Dartnall, 1957), so that equation 5.15 reduces to

$$j_\lambda \simeq 1 - 10^{-D\lambda} \qquad (5.16)$$

for $\lambda > 500$ nm.

If the pigment concentration at equilibrium is c_e, then $dc_e/dt = 0$ and, from equations 5.14 and 5.16, the percentage of pigment bleached at equilibrium ($P_e = 100\,(1 - c_e/c_{max})$) is:

$$P_e = \int 100\gamma_\lambda I_\lambda (1 - 10^{-De,\lambda})/kc_{max}\,d\lambda \qquad (5.17)$$

Unfortunately, the time-course of the bleaching experiments of section 5.6 (figure 2.6) were such that true equilibrium would never be achieved, so that, espectially at high illumination levels, the above equation would not describe the bleaching. From equations 5.1, 5.14 and 5.16,

$$\frac{-dc_\alpha}{dt} = \int \gamma_\lambda (1 - e^{-2.303c_\alpha \ell_\alpha \alpha^*_\lambda, t}) I_\lambda d\lambda - k(c_{\alpha,max} - c_{\alpha,t}) \qquad (5.18)$$

for the α pigment. (Strictly $c_\alpha = pc'_\alpha$ and $I_\lambda = I'_\lambda/p$, where p is the light funnelling factor for the cone, c'_α and I_λ are the actual pigment concentration and light level and c_α and I'_λ are the effective concentration and light level for the pigment which are measured objectively.)

An exact solution of equation 5.18 could not be found. In the case where $D_\lambda(\alpha) << 1$, 5.18 becomes

$$\frac{-dc_\alpha}{dt} = \int \gamma_\lambda (2.303c_\alpha \ell_\alpha \alpha^*_\lambda) I_\lambda d\lambda - k(c_{\alpha,max} - c_{\alpha,t}) \qquad (5.19a)$$

$$\text{i.e. } \frac{dh}{dt} = -hIP + (1 - h)/\tau \qquad (5.19b)$$

where h ($= c/c_{max}$) is the fraction of unbleached pigment at time

t, P is the effective Naperian photosensitivity to axial rays, I is the effective integrated illumination level of light and τ is the time constant of regeneration of the photopigment. This is equation D1 of appendix D and its solution is given by equation D3. The values of h were computed for various average light illumination levels (I) from equation 5.19b, assuming that the eye was first fully dark-adapted and then subjected to three minutes of adaptation to a repeated cycle of 20 sec light- and 7 sec dark-adaptation (as in figure 2.10). The computed values of h are plotted against the average illumination level I in figure 5.20. These data are only strictly correct for D << 1, but give a qualitative idea of the bleaching process for larger values of D. In the case of the mixed pigments which were proposed for anomalous trichromacy, the bleaching kinetics become even more complicated. An extreme case may be assumed for the mixed pigments model to simplify the calculation, namely that the fractions f of the α and β pigments (see assumption 4, above) in the α' and β' mixtures respectively are small (f << 1). In such cases, the action of light on the mixture will affect mainly the pigment present in large amounts (fraction 1 - f), and the bleaching kinetics of the dominant pigment will also be described approximately by the

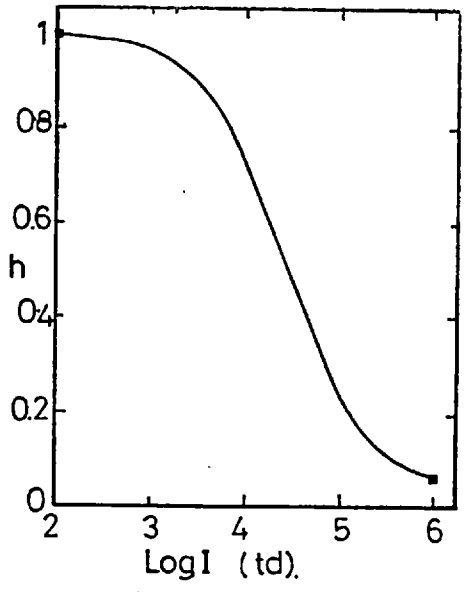

FIG. 5.20 Computed values of h (fraction of unbleached pigment) as a function of adaptation illumination level (assuming a light/dark cycle of 20 sec/7 sec).

data of figure 5.20. The colour matches resulting from bleaching can be calculated in all cases by substituting the calculated absorption spectra data in equations 5.13.

5.8.6 Calculation of Wavelength Discrimination Curves

Wavelength discrimination curves may be calculated from the spectral sensitivity curves using the line-element theory of Stiles (1946). The shapes of the absorption spectra of the visual pigments derived as outlined in section 5.8.2 above were used to define the relative spectral-sensitivities of the colour mechanisms. The maximum absolute sensitivities of the two colour mechanisms were assumed to be the same as those measured by Stiles (1946), as these values are not given by Pitt (1944).

If the effect of the blue mechanism is ignored, Stiles' equation 23 (Stiles, 1946) reduces to

$$\frac{\delta s^2}{\delta \lambda^2} = \left[(C_r^2 - 1)R' + C_g^2 G'\right]^2 \left[\frac{R}{\rho}\ \xi(R)\right]^2 + \left[C_r^2 R' + (C_g^2 - 1)G'\right]^2 \left[\frac{G}{\gamma}\ \xi(G)\right]^2 \qquad (5.20)$$

In this equation δs is the line element,

$$C_r^2 = \left[\frac{R}{\rho}\ \xi(R)\right]^2/\chi\ , \qquad C_g^2 = \left[\frac{G}{\gamma}\ \xi(G)\right]^2/\chi\ ,$$

$$\chi = \left[\frac{R}{\rho}\ \xi(R)\right]^2 + \left[\frac{G}{\gamma}\ \xi(G)\right]^2\ ,$$

$$\left.\begin{aligned} R' &= \frac{1}{R}\ \frac{dR_\lambda}{d\lambda} \\ G' &= \frac{1}{R}\ \frac{dG_\lambda}{d\lambda} \end{aligned}\right\} \qquad (5.21)$$

(where R_λ and G_λ are the spectral sensitivities of the red and green mechanisms);

$$\left.\begin{aligned} \text{and} \quad \xi(R) &= [9R/(1 + 9R)] \\ \text{and} \quad \xi(G) &= [9G/(1 + 9G)] \end{aligned}\right\} \qquad (5.22)$$

are the increment threshold curves of the red and green mechanisms. ρ and γ are constants ($\rho = 1.278$, $\gamma = 1.646$), and

$$\left.\begin{aligned} R &= I_\lambda R_\lambda \\ G &= I_\lambda G_\lambda \end{aligned}\right\} \qquad (5.23)$$

The values of R_λ and G_λ were chosen to match the 'red' and 'green' sensitivity curves of Stiles (1946) at their peaks, so that $R_{\lambda = 580\ nm} = 1.702 \times 10^3$ and $G_\lambda = 1.421 \times 10^3$ ($ergs^{-1}$. seconds). I_λ is the illumination level of the light of wavelength λ which is used for the discrimination experiments.

Equation 5.20 may be further simplified to:

$$\delta s^2/\delta\lambda^2 = a_r^2\, b_g^2 (G' - R')^2/(a_r^2 + b_g^2) \qquad (5.24)$$

where $a_r = (1/\rho)\xi(R)$ and $b_g = (1/\gamma)\xi(G)$.

5.8.7 Evaluation of I_λ

The calculations of the wavelength-discrimination curves were made assuming $I_\lambda = 80$ trolands, which is the illumination level of light used by Wright and co-workers (Wright, 1946) in their study

of the wavelength discrimination of normal and anomalous trichromats. A troland is defined as the retinal illumination level when a field of luminance 1 cd m^{-2} is observed by an eye with an entrance pupil of 1 mm^2. Therefore 80 td ≡ 80 x 10^{-6} lm sterad.$^{-1}$, and for an entrance pupil of 2 mm diameter, 80 td ≡ 80 x 1.4073 x 10^{-5} erg deg^{-2} at a wavelength of 555 nm (for V_λ = 1.0, from conversion data in Wyszecki and Stiles, 1967). The value of I_λ which was used in the calculations, corresponding to an illumination level of 80 td was

$$I_\lambda = 1.4073 \times 10^{-5} \times 80 \times \frac{1}{V\lambda} \times \frac{555}{\lambda} \qquad (5.25)$$

where the factor 555/λ was used to convert I_λ to relative quanta sec^{-1}.

The equations in the above sections were used to calculate the absorption spectra for normals and for the pigment-mixture models of anomalous trichromacy. These curves were numerically fitted using sixth-order Tchebychev polynomials in order that the slopes of the curves (equations 5.21) could be found from derivatives. These curves were used to predict the colour-matching and wavelength discrimination curves for observers under a variety of conditions. The results of these calculations appear below (section 5.9).

5.9 Predictions of the Pigment-Mixture Model

5.9.1 Previous Estimates of Pigment Optical Densities

Previous estimates of photopigment optical densities which were based on psychophysical measurements have ranged between 0.2

and 1.6 (e.g. Brindley, 1953; Enoch and Stiles, 1961; Walraven, 1963; Miller, 1972). Until recently, however, microspectrophotometric measurements (Marks, Dobelle and MacNichol, 1964; Brown and Wald, 1964) and objective ophthalmoscopic investigations (Rushton, 1963a, 1965a,b,c) have yielded values of 0.01 to 0.06 for pigment optical densities, and there were strong objections to the high values predicted by subjective measurements (Stiles, 1960; Wright, 1964; Ingling, 1969). These objective measurements of pigment densities underestimate the true value because of stray light effects (Brindley, 1970), so that they do not refute subjective measurements. Recent microspectrophotometric measurements of the pigments of monkeys (Bowmaker, Dartnall, Lythgoe and Mollon, 1977) and other vertebrates (Dunn, 1969; Liebman, 1969) have indicated that rod and cone pigment optical densities are 0.013 - 0.015 μm^{-1} *in situ*. These measurements meet the previous objections to high estimates of optical densities, since the foveal cone outer segment length is 36 - 40 μm for man and 42 - 67 μm for other primates (Polyak, 1941; Dowling, 1965): thus effective pigment optical densities of up to 0.7 are now predicted on the basis of objective measurements. No objective measurement of pigment optical density has yet been made, however, which fully accounts for *in vivo* light scatter and light funnelling, so that the measurements which have been made can only be regarded as estimates of the true values.

The few objective measurements of the pigment optical densities which have been made for primates have yielded similar values for erythrolabe (the 'red-absorbing pigment') and chlorolabe (the 'green-absorbing pigment'). The effective *in vivo* optical density of erythrolabe (including light scatter and

funnelling) may not be equal to that of chlorolabe, however, and the ratio of the optical densities of erythrolabe and chlorolabe may vary from observer to observer. Estimates of peak optical densities based on subjective experiments also do not give independent values for erythrolabe and chlorolabe: i.e. the experimental data can be explained by assuming that the optical densities of erythrolabe and chlorolabe are equal, or that the optical density of one is greater than that of the other (e.g. Brindley, 1970). In this section the predicted colour-match shifts resulting from reductions in pigment optical densities are considered for cases where the peak optical densities of erythrolabe and chlorolabe are equal, and also for several cases when they are not.

5.9.2 The Relative Ease of Bleaching Erythrolabe and Chlorolabe

Brindley (1953, 1955) assumed for his bleaching studies that erythrolabe is substantially more photolabile than chlorolabe, but admitted later (Brindley, 1970) that it was possible that both pigments might be equally photolabile. In fact, Rushton and Henry (1968) showed by means of ophthalmic densitometry that erythrolabe and chlorolabe in normals are equally photolabile, i.e. their photosensitivities (P, equation A2 in appendix A) are about equal. It is assumed in the following calculations that erythrolabe and chlorolabe are equally photolabile in all normal observers. For these calculations, the α_λ and β_λ pigments of figure 5.19 are identified as erythrolabe and chlorolabe respectively and the sensitivity of the 'red' and 'green' mechanisms (corresponding to α_λ and β_λ) of Pitt (1944) are used for defining the erythrolabe and chlorolabe spectral

sensitivities. The data of Pitt are listed in Table 5.2 as α_λ and β_λ on a quantum basis.

Table 5.2 Pitt (α,β) sensitivity curve data.

λ	α_λ	β_λ	λ	α_λ	β_λ
500	2.64	6.02	590	10.45	6.15
510	4.59	9.72	600	9.45	4.01
520	6.45	12.06	610	8.26	2.30
530	7.67	13.46	620	6.63	1.22
540	8.99	13.76	630	5.09	0.73
550	9.88	13.35	640	3.71	0.34
560	10.45	12.17	650	2.19	0.18
570	10.82	10.61	660	1.43	0.001
580	10.87	8.46			

5.9.3 Examples of Changes in Pigment Absorption Spectra and Colour Matching following Bleaching

The following two examples demonstrate the changes which occur in the pigment absorption spectra of erythrolabe and chlorolabe (α_λ and β_λ), and the changes predicted in the Rayleigh match, following bleaching of the pigments.

a) Changes in pigment absorption spectra

The normalized absorption spectra α_λ and β_λ derived from the data of Pitt (1944) are shown in figure 5.21 (filled and open circles, respectively). The narrowing of the predicted normalized absorption spectra following two successive ten-fold

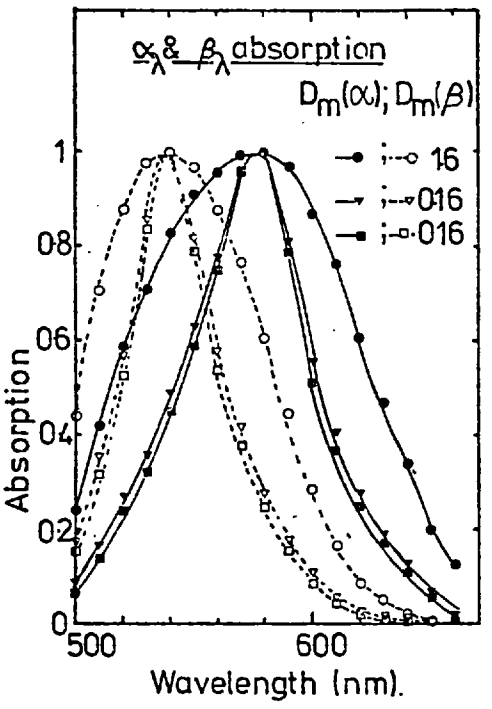

FIG. 5.21 The Pitt (1944) α_λ and β_λ spectral sensitivities before (●,○) and after bleaching; assuming initial peak optical densities of 1.6.

decreases in peak optical density of each pigment is illustrated on the same diagram. These narrow curves were calculated assuming initial peak optical densities of $D_m(\alpha) = D_m(\beta) = 1.6$. This high value of optical density was chosen in this example to show clearly the changes in absorption spectra resulting from reductions in optical density: the changes resulting for lower initial peak optical densities would be smaller.

b) The Rayleigh match changes

The ratios of the amounts of the Wright red (R, 650 nm) and green (G, 530 nm) colour matching primaries needed to match a 580 nm stimulus were calculated for the α and β pigments of normal vision. For all but one of these calculations, the highest peak optical density deduced by Brindley (1953) for erythrolabe was assumed for both pigments: $D_m(\alpha) = D_m(\beta) = 1.0$. These values were chosen arbitrarily to illustrate the direction of the Rayleigh match shift following bleaching. Calculations employing both smaller and larger values of $D_m(\alpha)$ and $D_m(\beta)$ showed that the direction of the shifts is unaltered, but that the magnitudes of the shifts increase, with the magnitude of the assumed initial optical densities. The Rayleigh match ratios

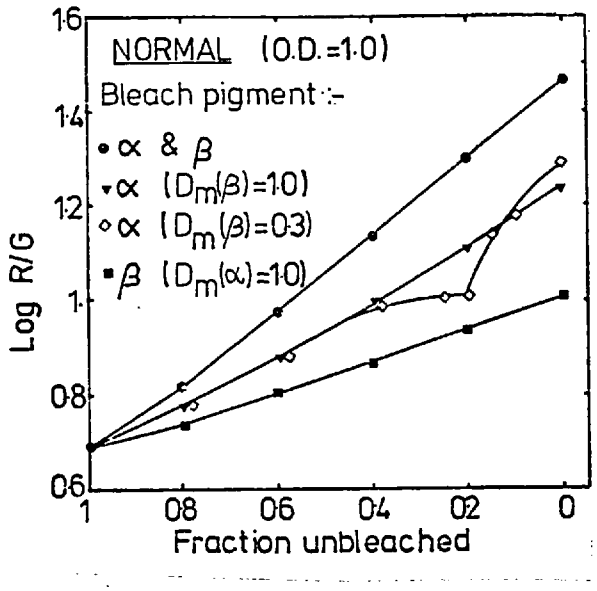

FIG. 5.22 Values of log R/G versus the fraction of unbleached pigment, assuming various values of pigment optical density.

R/G are plotted in figure 5.22 against the fraction of unbleached pigment. It can be seen that the effect of progressively reducing the optical density of either the α pigment only (inverted triangles for $D_m(\beta)$ = 1.0, open squares for $D_m(\beta)$ = 0.3 in fig. 5.22), or only the β pigment (filled squares, figure 5.22), or of both (circles, fig. 5.22) is to increase the predicted R/G ratio in the Rayleigh match. These results illustrate the fact that the direction of change of the Rayleigh colour-match ratio R/G following bleaching can be predicted assuming that either α, or β, or α and β are bleached by light. The magnitudes of predicted changes can be altered by altering the assumed initial values of $D_m(\alpha)$ and $D_m(\beta)$, so that it is difficult to determine the relative photolability of α and β from subjective measurements using a single bleaching light. As stated above, however, ophthalmoscopic measurements indicate that α and β are equally bleachable by light.

5.9.4 The Probable Range of Peak Optical Densities of α and β

In order to find the range of peak optical densities (for the dark-adapted state for normal observers) which are consistent with the changes in the Rayleigh match, R/G, measured for normal

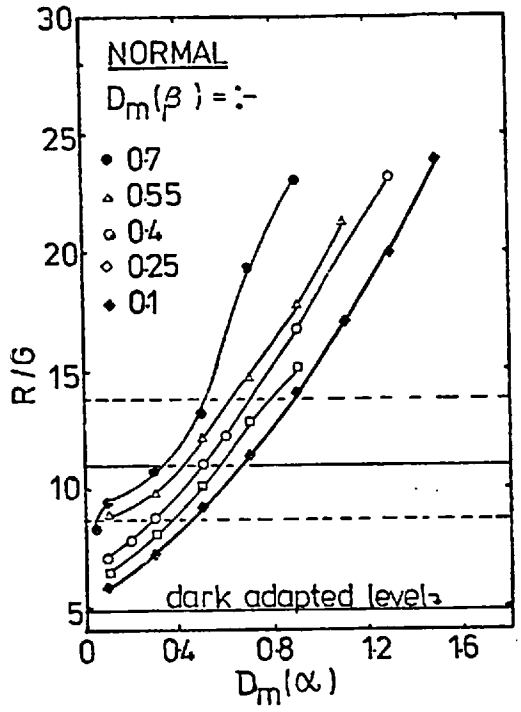

FIG. 5.23 Values of R/G predicted for normals following pigment bleaching, which result for various values of $D_m(\alpha)$ and $D_m(\beta)$.

observers (Table 5.1), a range of peak optical densities of the α and β pigments was first assumed. The R/G ratios were calculated for the highly bleached state (taken as the point where the peak optical densities of the α and β pigments are 1/10 of their original, dark-adapted values). The calculated shifts are shown in figure 5.23. The R/G ratio predicted for normals in the dark-adapted state on the basis of Pitt's (1944) data is equal to 4.91, regardless of the assumed peak optical density. The R/G ratios for the bleached state are plotted against the maximum assumed values of $D_\lambda(\alpha)$ ($D_m(\alpha)$), for a number of $D_m(\beta)$ values.

Experimentally, it was found that the average shift of log R/G for a test wavelength of 580 nm was Δ log R/G = 0.30 + 0.05 = 0.35 (section 5.6.1). This change in R/G is indicated by the solid horizontal line in figure 5.23. The broken lines indicate the range of log R/G which was found for normal observers (from section 5.6.1).

It can be seen from figure 5.23 that there are values of $D_m(\alpha)$ and $D_m(\beta)$ which yield the experimental values of log R/G and that the range of appropriate values of the optical densities

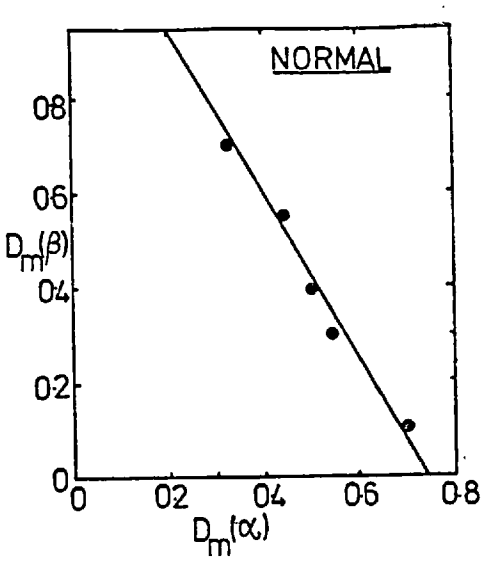

FIG. 5.24 The range of $D_m(\alpha)$, $D_m(\beta)$ values which give rise to Rayleigh match shifts of Δ log R/G = 0.35, following bleaching (from fig. 5.23).

(up to about 1.0) are not inconsistent with the more recent objective measurements (Bowmaker et al., 1977). Combinations of $D_m(\alpha)$ and $D_m(\beta)$ which yield particular shifts in the Rayleigh match can be derived from this diagram. If it is assumed that a particular normal observer (with absorption spectra of the unbleached pigments α_λ and β_λ given in Table 5.2) shows a colour-match shift upon full bleaching which is equal to that of the average, i.e. Δ log R/G = 0.35, then the possible combinations of $D_m(\alpha)$ and $D_m(\beta)$ which would give rise to this shift are shown in figure 5.24 (derived from figure 5.23 for Δ log R/G = 0.35). This range of combinations of $D_m(\alpha)$ and $D_m(\beta)$ will be used in further computations of the effects of chromatic adaptation on anomalous trichromatic Rayleigh matches.

5.9.5 Colour Matches Predicted for Normal and Anomalous Trichromats

a) Predictions based on $D_m(\alpha) = D_m(\beta)$

It is assumed in this section that the peak optical densities of the α and β pigments of normal vision are equal, $D_m(\alpha) = D_m(\beta)$. In this case, equation 5.4 becomes identical to equation 5.3, so that equation 5.3, together with a similar equation for α', can be used to derive the optical densities of the α' and β' pigment

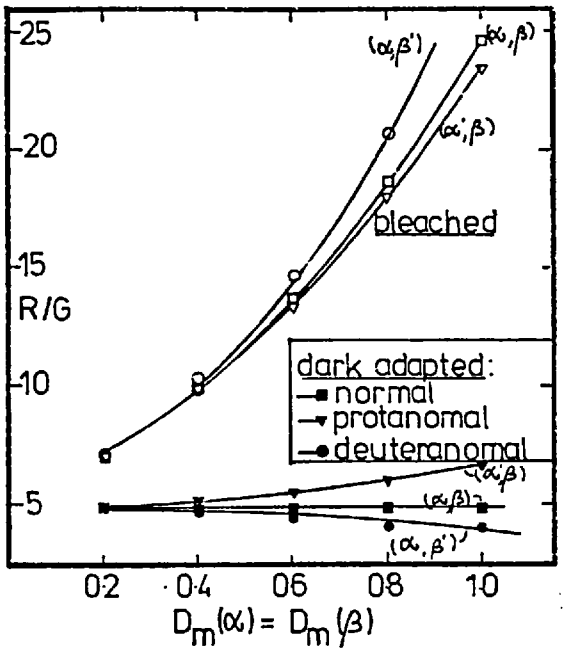

FIG. 5.25 Plot of the R/G ratios, predicted for trichromats assuming $D_m(\alpha) = D_m(\beta)$, versus the peak optical density ($D_m(\alpha)$)

mixtures in the model of anomalous trichromacy based on mixtures of α and β (figure 5.19). The predicted ratios of the red and green matching stimuli, R/G, required for a match against a 580 nm test stimulus are shown in figure 5.25 for the (dark-adapted) normal ((α,β)) and anomalous trichromatic ((α',β) and (α,β')) observers, for a number of peak optical densities of $D_m(\alpha)$ and $D_m(\beta)$ from 0.2 to 1.0 (lower three curves). The R/G ratio for the dark-adapted normal remains constant when the assumed peak optical densities are altered. The R/G ratio for the (α,β') case of dark-adapted anomal is always smaller than that of the normal, corresponding to a deuteranomalous Rayleigh match. The fraction of β pigment in the β' mixture was 0.1 (f = 0.1 in equation 5.3): larger fractions of β in the mixture

resulted in R/G ratios closer to those of the normal. The fraction of α pigment in the α' mixture in the (α',β) case of anomalous trichromacy was 0.1, and in this instance protanomalous matches result (figure 5.25, $R/G_{(\alpha',\beta)} > R/G_{(\alpha,\beta)}$). The upper three curves of figure 5.25 correspond to the R/G ratios predicted for the Rayleigh matches, following a reduction of optical density (corresponding to bleaching, for example) of all pigments to 0.1 of their dark-adapted values. The R/G ratio increases in all cases (the red and green stimulus mixture matching the 580 nm stimulus becomes redder), and the magnitude of the R/G increase rises monotonically with the assumed peak optical density of the pigments α and β.

Log R/G ratios predicted for the dark-adapted state of the (α',β) and (α,β') anomals differ from that of the normal by at most 0.1 log units, at pigment densities of 1.0 (figure 5.25). The fraction of α and β in the α' and β' mixtures was chosen to be 0.1 for the anomals. This fraction (0.1) represents an extreme case: larger fractions of α and β in the α' and β' mixtures result in still smaller differences between the three lower R/G curves in figure 5.25. The differences between the logarithms of the R/G ratios of normals and anomals often exceed 0.4 (e.g. figures 5.38 - 5.40). The model of anomalous trichromacy based on pigment mixtures for which $D_m(\alpha) = D_m(\beta)$ is, therefore, incapable of predicting even the dark-adapted colour matches of anomals for pigment densities less than 1.0. This value of pigment density is, however, greater than the value predicted earlier (from bleaching experiments with normal observers): the data of figure 5.24 indicate that, if the peak optical densities of α and β are equal for the average normal

observer, the value of the peak optical density is $D_m(\alpha)$ = 0.46 = $D_m(\beta)$. (If the restriction of equal peak optical densities, $D_m(\alpha) = D_m(\beta)$, does not hold, however, the individual values of either $D_m(\alpha)$ or of $D_m(\beta)$ may exceed 0.46 (figure 5.24)).

b) Colour Matches Predicted for Anomalous Trichromats using equation 5.3, assuming $D_m(\alpha) \neq D_m(\beta)$

Equation 5.3 relates the optical density of the β' pigment mixture to those of the individual normal pigments in the mixture, and is based on the assumption that the concentrations (moles/unit volume) of these pigments in neighbouring cones of the normal eye are equal: $c_\alpha = c_\beta$. To simplify the calculation of pigment kinetics (section 5.8.5), only extreme cases of the α' and β' pigment mixtures are considered, for which the ratio of the amounts of the α and β pigments in the mixtures is 0.9 or 0.1 (f = 0.1 in equation 5.3). The R/G matching ratios predicted for a match against a 580 nm test stimulus (using the Wright red R (650 nm) and green G (530 nm) primaries) are shown on the left of figure 5.26. On the left half of fig. 5.26, the R/G ratios are plotted against $D_m(\alpha)$, and for each value of $D_m(\alpha)$ the corresponding $D_m(\beta)$ was derived from figure 5.24 in order that the values remain consistent with bleaching data for the average normal (section 5.6.1). The values of R/G obtained for the normal (α,β), and anomalous (α',β) and (α,β') cases are shown.

The data are shown here for the unbleached state, so that the R/G ratio does not change for the normal case with variation in $D_m(\alpha)$. In the case of the anomalous trichromatic data, values of R/G which are greater or less than those of the normal (corresponding

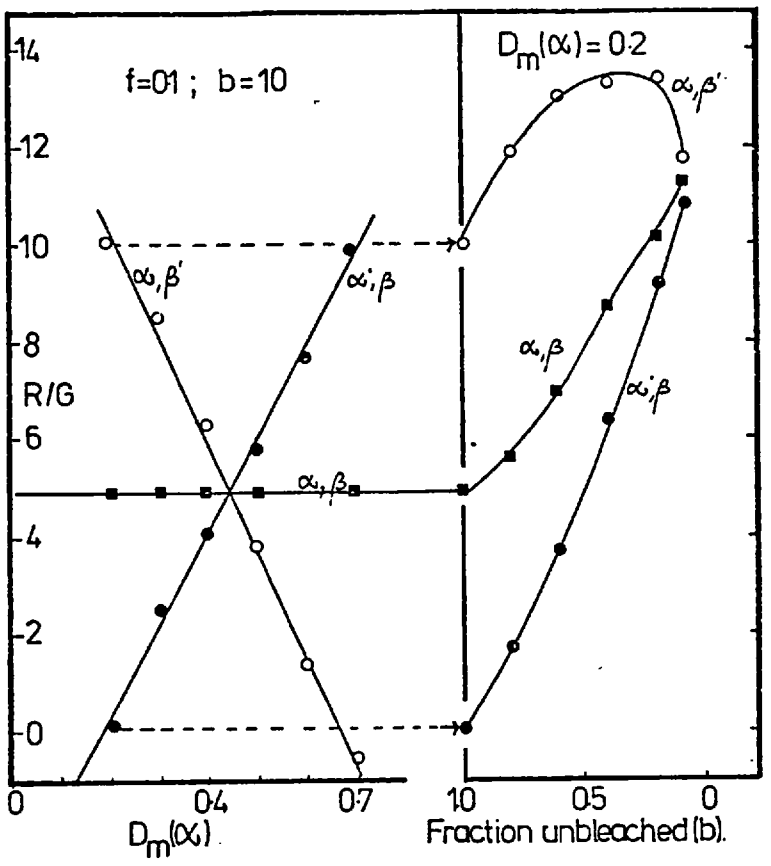

FIG. 5.26 Left: Plot of R/G versus $D_m(\alpha)$. Right: Plot of R/G versus the fraction of unbleached pigment assuming $D_m(\alpha) = 0.1$. In both cases the data were based on equation 5.3.

to protanomaly and deuteranomaly respectively) can be obtained for either the (α',β) or (α,β') cases by suitable choice of $D_m(\alpha)$ (and $D_m(\beta)$). In the following two examples values of $D_m(\alpha) = 0.7$ and 0.2 are used and the behaviour of the colour-matching is predicted from these values for different optical densities of the pigments.

1. $D_m(\alpha) = 0.2$

In the case that $D_m(\alpha) = 0.2$, the values used for $D_m(\beta)$ was 0.95 (derived from figure 5.24). The way in which R/G varies, for a 580 nm test stimulus, with bleaching of the

pigment is shown on the right of figure 5.26. The abscissa values for this half of the figure are the fractions (b) by which the pigment optical densities are decreased from the unbleached values (i.e. b is the fraction of unbleached pigment). (In the case of mixed pigments, the pigment present initially at low concentration is assumed not to be bleached). The relationship between the abscissa values (b) and the illumination level of light which bleaches the pigments to a corresponding extent can be obtained (approximately) from figure 5.20. In this example, the 'pigment mixture' model of anomalous trichromacy predicts that the (α',β) system yields deuteranomalous matches, the (α,β') system protanomalous matches, and that the matches of these two systems and that of the normal (α,β) system would converge at high levels of illumination ($b \rightarrow 0$).

2. $\underline{D_m(\alpha) = 0.7}$

For this example ($D_m(\alpha) = 0.7$, $D_m(\beta) = 0.1$ from figure 5.24), the calculated R/G ratios for the unbleached state are shown on the left half of figure 5.27 for test wavelengths between 500 nm and 640 nm, for the (α,β), (α',β) and (α,β') systems. On the right of figure 5.27 the R/G ratio is plotted against the fraction of unbleached pigment (b) for a match against a 580 nm test stimulus. In this case the (α',β) system yields protanomalous matches, and the (α,β') system deuteranomalous matches, and again the R/G values converge for the three systems at low values of b.

In the above two sets of calculations, values of $D_m(\alpha)$ of 0.2 and 0.7 were chosen as examples (figures 5.26, 5.27). Similar calculations have been performed for several other

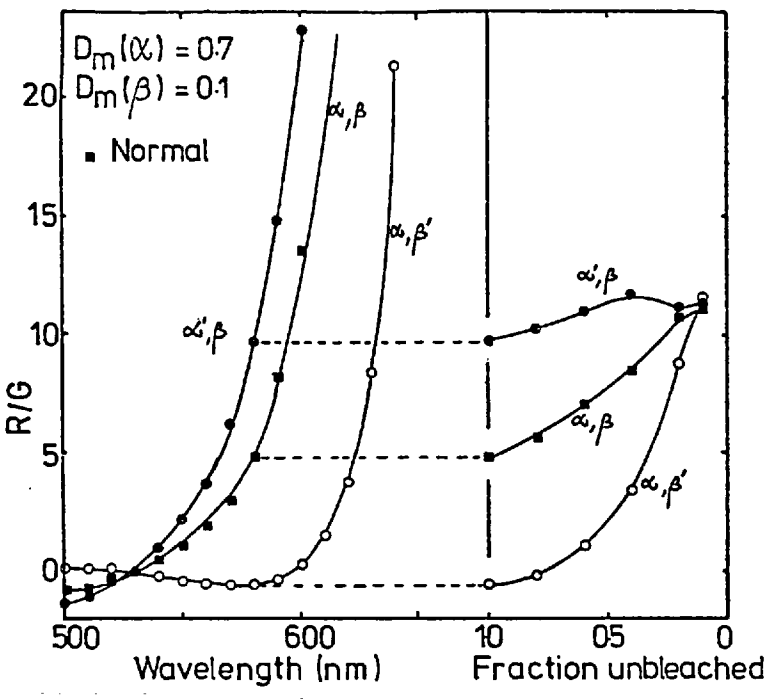

FIG. 5.27 Plots of R/G versus a) test wavelength and b) the fraction of unbleached pigment for a test wavelength of 580 nm. (Based on equation 5.3).

values of $D_m(\alpha)$ and $D_m(\beta)$, obtained from 5.24). The shifts in R/G resulting from bleaching of the photopigments were similar to those of figures 5.26 or 5.27, and the R/G ratios of all trichromats always converged at small values of b (the unbleached pigment fraction). It will be shown later that the reductions in optical density can be related to bleaching of pigments caused by light (section 5.11), and that the predicted changes in R/G resulting from bleaching can be found, which follow the changes measured for anomals by suitable choice of the variables $D_m(\alpha)$, $D_m(\beta)$ and f (e.g. $D_m(\alpha) = 0.2$, figure 5.39, $D_m(\alpha) = 0.2$, figure 5.40).

Having analysed colour matching on the basis of the assumption of equal pigment concentrations ($c_\alpha = c_\beta$) in normals which yields equation 5.3, the alternative assumption, namely that the peak absorbances of normal pigments are equal ($\alpha_{max} = \beta_{max}$), which yields equation 5.4 is examined in the following section.

c) Predictions of Colour Matches based on the Model of Equation 5.4

In this section calculations of the Rayleigh colour matches of anomalous trichromats are made assuming that the peak absorbances of the two pigments (α and β) in normals are equal ($\alpha_{max} = \beta_{max}$, equation 5.4), and again it is assumed that anomalous trichromacy is caused by mixtures of normal pigments in single cones. The predicted Rayleigh matches of the anomals are calculated for the dark adapted state and for various amounts of bleaching.

The R/G values which are predicted for the anomalous trichromatic Rayleigh matches in this case are shown in figure 5.28 for the unadapted state (for the (α',β) system on the left of fig.

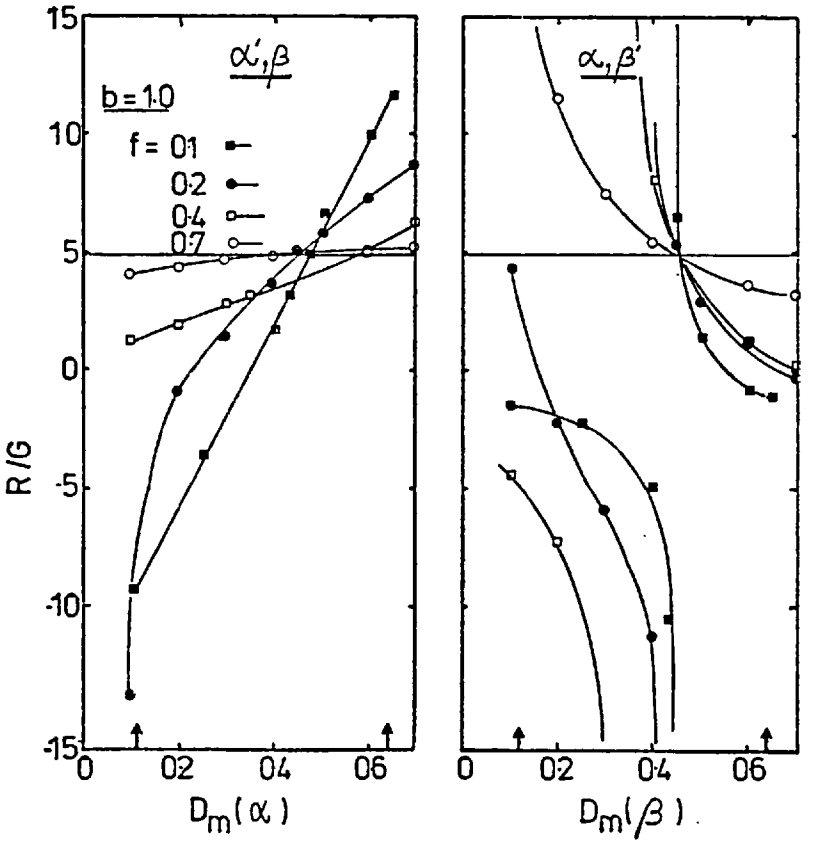

FIG. 5.28 Plots of R/G versus $D_m(\alpha)$ for the (α',β) and (α,β') systems (based on eqn. 5.4), for four values of f. The pigments are assumed to be unbleached (b = 1.0).

5.28, and for (α, β') on the right), for four values of f (f = 0.1, 0.2, 0.4 and 0.7 in equation 5.4). The values of R/G are plotted against $D_m(\alpha)$, the assumed value of peak optical density of normal erythrolabe: the value of $D_m(\beta)$ corresponding to each $D_m(\alpha)$ value was found from figure 5.24. The system (α,β) is represented by the horizontal lines at R/G = 4.91 (as in figure 5.26), and again the (α',β) and (α,β') systems can produce protanomalous or deuteranomalous matches by suitable choice of $D_m(\alpha)$. However, the behaviour of the R/G ratio for the (α',β) and (α,β') systems is asymptotic. The R/G values obtained for f = 0.1, 0.2, 0.4 and 0.7 (equation 5.4) are shown in figure 5.28, and it is seen that the asymptotic behaviour of the (α,β') system occurs for all these values, but that it occurs at different values of $D_m(\alpha)$ as f is changed. Two examples are given below of shifts in R/G ratios which result from reductions in pigment optical densities. For these examples f = 0.1 (eqn 5.4) and $D_m(\alpha)$ = 0.1 or 0.65 (marked by arrows on the abscissa of figure 5.28).

1. $\underline{D_m(\alpha) = 0.1}$

In this first example $D_m(\alpha)$ = 0.1 and $D_m(\beta)$ = 1.0 (from figure 5.24). The R/G values predicted for the three systems are shown as a function of test wavelength on the left of figure 5.29, and as a function of the fraction of unbleached pigment b (λ_{test} = 580 nm) on the right.

The variation of R/G with wavelength for the (α,β') system is regular above 510 nm, but the corresponding curve for the (α',β) system changes irregularly with wavelength. The behaviour of the (α',β) system during bleaching ($b \rightarrow 0$) is monotonic, whereas the (α,β') system exhibits asymptotic behaviour at

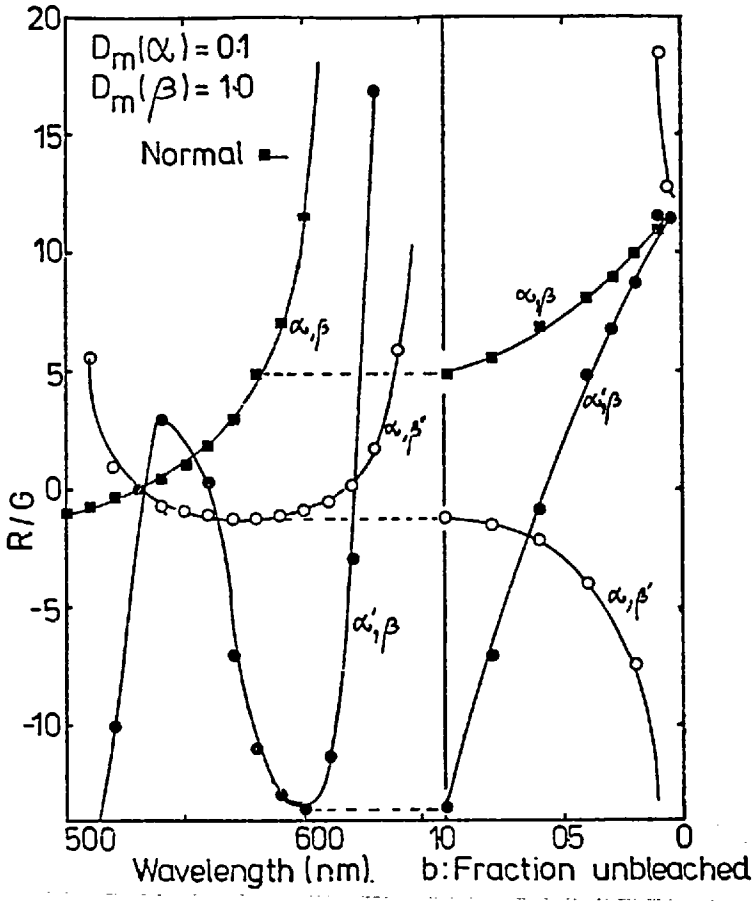

FIG. 5.29 Plots of R/G versus a) test wavelength and b) the fraction of unbleached pigment. Calculations were based on equation 5.4.

b = 0.1. The R/G ratio of the (α,β') system initially diverges from the R/G ratio for the normal, but the R/G values of all three systems converge at low values of b. An important point to note is that many of the predicted R/G values are negative, indicating that a colour-match would be obtained only if one of the two matching stimuli were to be added to the test stimulus. This result would not normally be expected, and might explain why a few anomalous trichromats were unable to match a red or green stimulus against a yellow (and so were not dichromats), and yet experienced difficulty in making Rayleigh matches and never seemed fully happy with the matches (personal observation). These observers were unfortunately not available for further study after the above calculations on the model had been performed. Negative values of R/G do not, however, account for the data which <u>have</u> been measured (e.g. figure 5.39, 5.40).

2. $D_m(\alpha) = 0.65$

The R/G curves for $D_m(\alpha) = 0.65$ (and $D_m(\beta) = 0.1$), corresponding to those of figure 5.24 for the above example, are shown in figure 5.30. The curves in this example are more regular than those of the previous example, and here protanomalous and deuteranomalous matches are produced by the (α', β) and (α, β') systems respectively. The R/G ratios of all three systems (one normal and two anomalous cases) converge upon bleaching (fig. 5.30, $b \rightarrow 0$). The initial and final values of R/G for the (α', β) system before and after complete bleaching are not very different, and matches made by such a protanomalous observer would vary little upon bleaching. The fourth curve drawn on

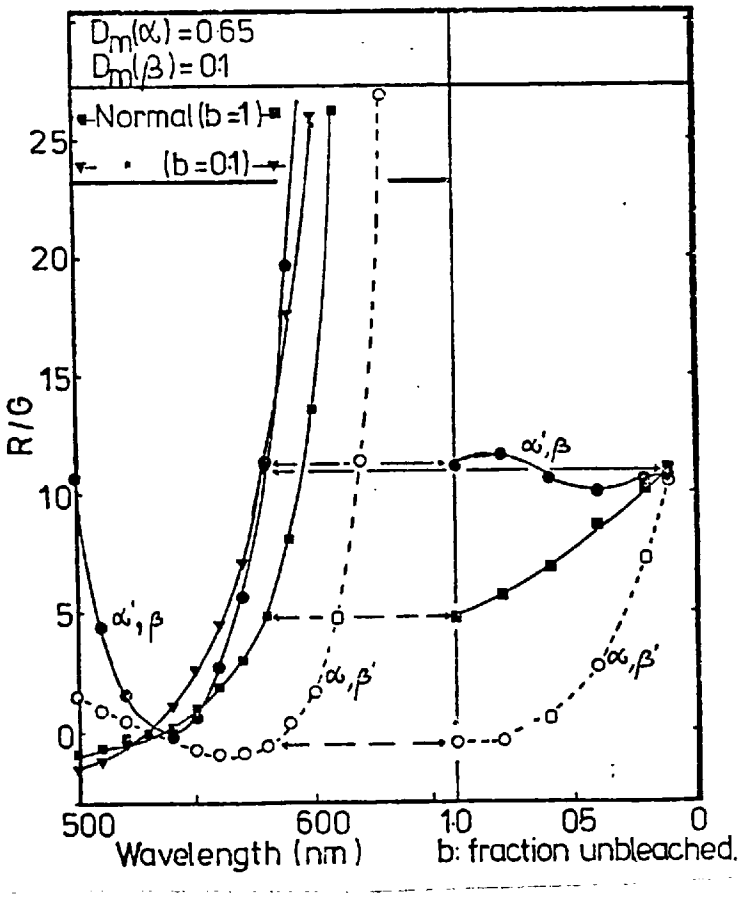

FIG. 5.30 Plots of R/G versus wavelength and versus the fraction of unbleached pigment b for $D_m(\alpha) = 0.65$, $D_m(\beta) = 0.1$ (based on eqn. 5.4).

the left of figure 5.30 corresponds to the matches made by the normal (α,β) in the adapted state (b = 0.1), and it is seen that the curve follows closely that of the (α',β) anomalous trichromat.

Calculations of R/G have been performed using other values of $D_m(\alpha)$ (figure 5.28), and the changes in R/G following reductions of optical density were qualitatively similar to those of figure 5.29 or 5.30. It is shown in the discussion that the predicted changes in R/G resulting from reductions in optical density (i.e. from bleaching) can be used to explain the form of the changes which have been measured for protanomals ($D_m(\alpha)$ = 0.1, figure 5.39) and deuteranomals ($D_m(\alpha)$ = 0.4, figure 5.40).

5.9.6 Wavelength Discrimination Curves

Wavelength-discrimination curves were calculated for monochromatic test stimuli using Stiles' line-element theory (Stiles, 1946; section 5.8.6). The calculations were made for normal observers using Pitt's (1944) data for the spectral sensitivities (α_λ, β_λ) of normals, and for several hypothetical anomalous observers whose pigment absorption spectra are predicted by the pigment mixture model ($\alpha'_\lambda,\beta_\lambda$) and ($\alpha_\lambda,\beta'_\lambda$), figure 5.19). The line-element δs (equation 5.20) was set at 0.02 for all the calculations, as this resulted in the best fit of the theoretical and experimental curves for normal observers.

The results of the calculations for a normal observer are shown in figure 5.31 for the pigments in the dark-adapted state (b = 1.0; b is the fraction of unbleached pigment) and bleached state (b = 0.1) (assuming $D_m(\alpha)$ = 0.7, $D_m(\beta)$ = 0.1). The

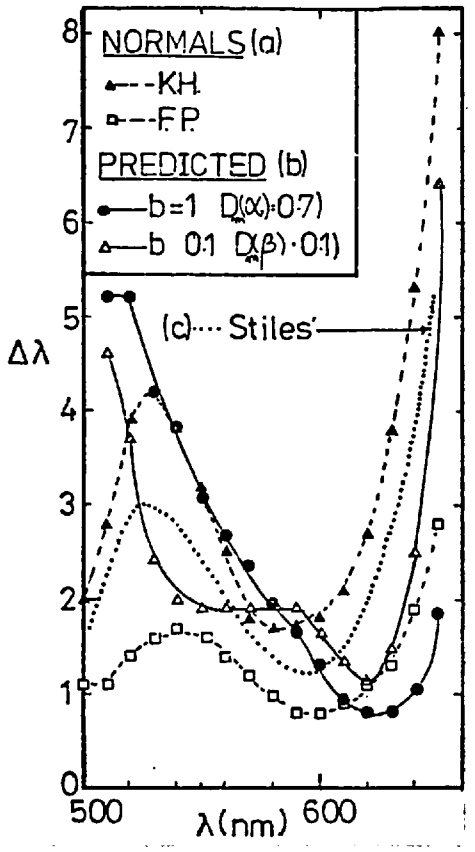

FIG. 5.31 Wavelength discrimination curves for normals a) measured by Wright and Pitt (1934), KH, FP), b) predicted on the basis of the Pitt (1944) spectral sensitivities and c) predicted by Stiles (1946) on the basis of his increment-threshold sensitivity curves.

wavelength-discrimination curves measured by Wright and Pitt (1934; Wright, 1946) for two normal observers (KH and FP) are shown on the same diagram, together with the curve predicted for normals by Stiles (1946). The effect of the blue cone mechanism was neglected in the calculation of the discrimination curves (equation 5.24), so that it is to be expected that the predicted curves are inaccurate for wavelengths below about 530 nm. The predicted wavelength-discrimination curve for the dark-adapted normal observer (b = 1.0, fig. 5.31) has the same shape, qualitatively, as the experimentally-determined curves (KH, FP), but the minimum in the predicted curve occurs at longer wavelengths (620 nm) than those of the experimental curves (600 nm). In this respect the wavelength discrimination curve predicted by Stiles (Stiles, 1946), which is shown dotted in figure 5.31, provides a better fit to the experimental data of Wright and Pitt (1934).

The wavelength discrimination curves, predicted for anomalous trichromats of the 'pigment-mixture' model are shown in figures

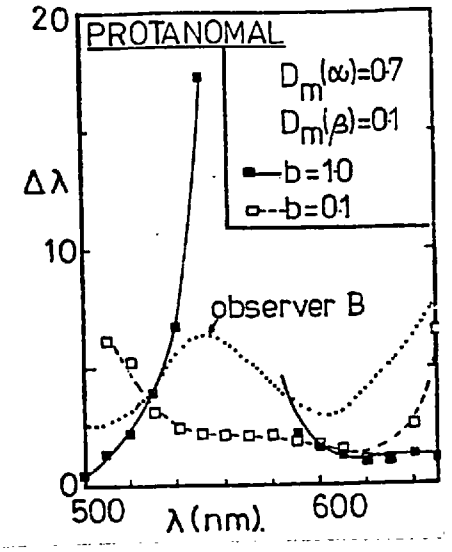

FIG. 5.32 Wavelength-discrimination curves predicted for protanomals (based on the model of eqn. 5.3), and the curve measured by McKeon & Wright (1940), observer B.

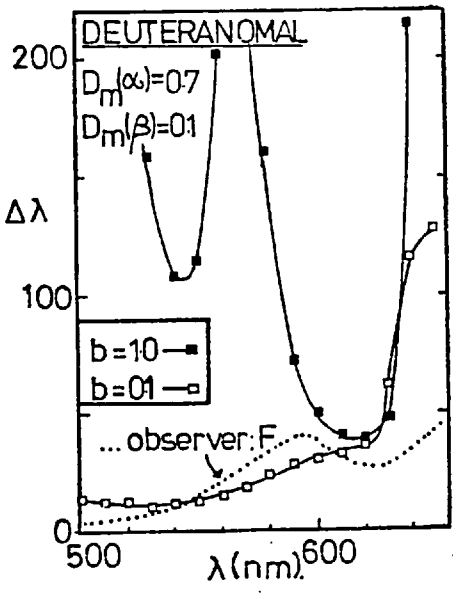

FIG. 5.33 Wavelength-discrimination curves for deuteranomals: precited and measured (observer F, Wright, 1946).

5.32 - 5.35, together with the wavelength discrimination curves measured for some anomals by Wright and co-workers (Wright, 1946). The predicted data for the first two figures (figs. 5.32, 5.33) were calculated on the assumption of section 5.9.5b that $c_\alpha = c_\beta$ (using equations 5.3 and 5.20). The value of $D_m(\alpha)$ used in these calculations was 0.7 ($D_m(\beta)$ = 0.1): the colour matches calculated for this value of $D_m(\alpha)$ are shown in figure 5.27. The wavelength discrimination curves for the protanomalous case are shown in figure 5.32 and those for the deuteranomalous case in figure 5.33 (both for the dark-adapted and bleached conditions, for which the values of the fraction of unbleached pigment is b = 1.0 and b = 0.1 respectively). The theoretical data for the third and fourth figures (figures 5.34, 5.35) were

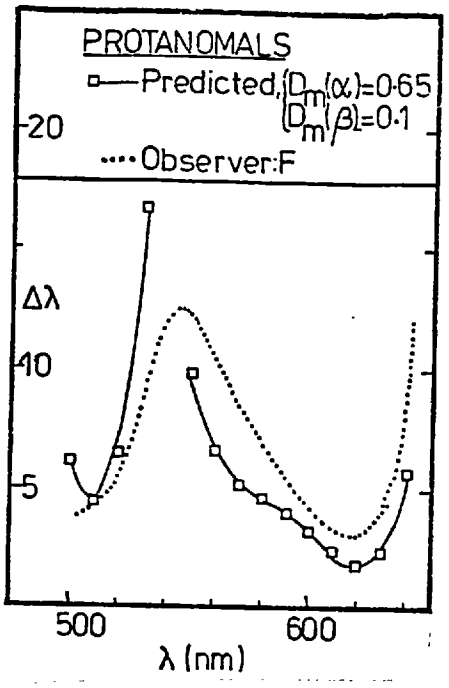

FIG. 5.34 Predicted and measured wavelength-discrimination for protanomals (see text for details)

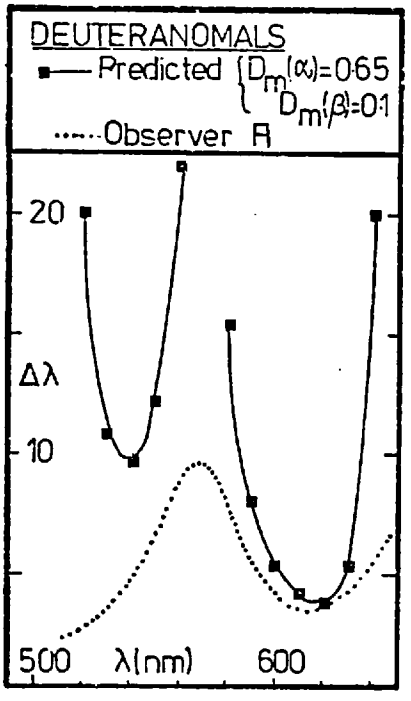

FIG. 5.35 Predicted and measured discrimination curves for deuteranomals (see text for details).

calculated on the assumption that the peak absorbances of erythrolabe and chlorolabe are equal ($\alpha_{max} = \beta_{max}$ - see equation 5.4 and section 5.9.5c). The predicted wavelength discrimination curves of figures 5.34 and 5.35 were calculated assuming that $D_m(\alpha) = 0.65$, $D_m(\beta) = 0.1$: the colour matches predicted for this system appear in figure 5.30. Some wavelength discrimination curves measured by Wright and co-workers (Wright, 1946, chapter 25) are reproduced in figures 5.32 - 5.35 (for protanomal B, fig. 5.32, deuteranomal F, fig. 5.33, protanomal F, figure 5.34 and deuteranomal A, figure 5.35).

The theoretical and experimentally-measured curves in figures 5.32 - 5.35 have two major features in common. (Again, the theoretical curves

should be ignored for $\lambda \leq 530$ nm, as the blue mechanism was ignored in the wavelength-discrimination calculations.) First, the wavelength discrimination curves have a minimum (corresponding to a minimum in the wavelength-discrimination step) at wavelengths around 610 - 620 nm in figures 5.33, 5.34 and 5.35. (The curve of the protanomalous observer B in figure 5.32 shows a minimum at around 600 nm, whereas the theoretical curve falls to a minimum at 600 nm, but stays at the same value at longer wavlengths.) Second, the calculated wavelength discrimination curves of figures 5.32, 5.34 and 5.35 have very pronounced maxima at wavelengths corresponding to maxima in the experimental curves. (The maximum in the calculated curve for the dark-adapted deuteranomal of figure 5.33 occurs at shorter wavelengths (570 nm) than that in the experimental curve (590 nm)).

Note that the amplitude of the wavelength-discrimination step at the minima of the theoretical curves can be the same as that for normals ($\sim$ 2 nm, figure 5.32) or much larger (40 nm, figure 5.33), and that correspondingly large variations are found for anomals (figures 5.32 - 5.35, Wright, 1946, chapter 25). In addition, the predicted wavelength discrimination for the anomalous model improved following bleaching, especially at wavelengths around 550 nm ($b = 0.1$, figures 5.32, 5.33).

5.10 Theoretical Calculations of Colour Matches Predicted by Models of Anomalous Trichromacy: II. Anomalous Pigment and Light Shielding Models

In this section the models of anomalous trichromacy, involving anomalous pigments (model A, figure 5.19) and light-shielding (model D), are considered.

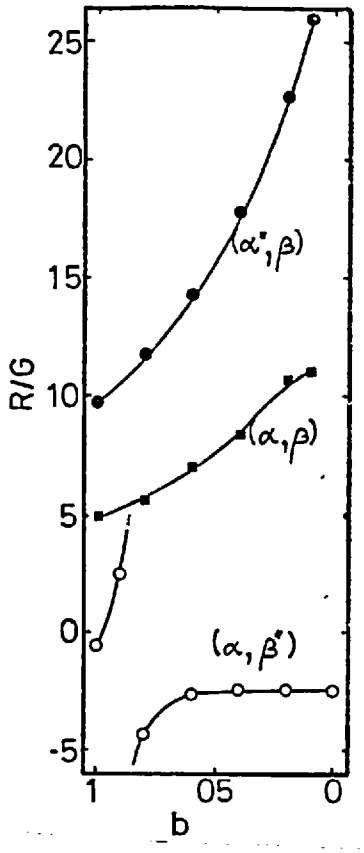

FIG. 5.36 R/G values for the anomalous pigment model, plotted against the fraction b of unbleached pigment. Note that the matches do not converge with those of the normal (α,β) system.

Rayleigh colour-matches predicted in the case of anomalous pigments (model A) will in general differ from those of colour-normals. This is demonstrated for one particular case in figure 5.36. In this diagram the R/G ratios predicted for normals (α,β) and for model A anomals (α",β) and (α,β") are plotted against b, the fraction of unbleached pigment. The peak optical densities in this case were $D_m(\alpha,\alpha") = 0.65$, $D_m(\beta,\beta") = 0.1$. The absorption spectra assumed for the anomalous pigments α" and β" were the same in shape in the dark-adapted state as the ones used for the pigment-mixture model (f = 0.1, equation 5.3), as these latter curves predict realistic values of R/G for anomals in the dark-adapted state. It is seen that for this example the Rayleigh matches of the anomals (α",β) and (α,β") do not converge with those of the normal (α,β) at high illumination levels. In general the R/G ratios predicted for anomals and normals on the basis of single abnormal pigments α" and β" will not converge at high illumination levels of bleaching light (Alpern, 1977, in print). Colour matches predicted by the pigment-shielding model (model D, figure 5.22) will also differ in general from the normal colour match under the same conditions. Consider the extreme (and

physiologically unlikely) case where all the light reaching the β pigment (say) first passes through the α pigment. (Let this be represented by $\alpha_\lambda \rightarrow \beta_\lambda$). The illumination level of light following traverses through each pigment will be successively $I_o(1 - \alpha_\lambda)$ and $I_o(1 - \alpha_\lambda)(1 - \beta_\lambda)$ for an incident illumination level of I_o. The effective absorption spectrum of the underlying β pigment ($\beta_{eff,\lambda}$) is given by the difference of these factors divided by I_o:

$$\beta_{eff,\lambda} = (1 - \alpha_\lambda)\beta_\lambda \qquad (5.26)$$

A similar equation can be written for the case where all the light reaching the α pigment is filtered by β_λ ($\beta_\lambda \rightarrow \alpha_\lambda$). It can be shown by substitution of equation 5.26 in equations 5.8 that in general the R/G ratio for the Rayleigh match in this model will differ from that of normals (for which observers it is assumed that no shielding of visual pigments occurs except for self-screening in individual cones). This is demonstrated in the following example.

Equation 5.26 was used to calculate the predicted Rayleigh matches (R/G) for various peak optical densities of D(α) and D(β), and for decreasing values of b (≤ 1) corresponding to reductions in the optical densities given by b.D(α), b.D (β) (b is the fraction of unbleached pigment). The results of these calculations are shown in figure 5.37. In this diagram the predicted R/G ratios are shown for an average normal observer ($D_m(\alpha) = 0.7$, $D_m(\beta) = 0.1$), and for anomalous trichromats based on the inter-cone pigment shielding model (model D, figure 5.19) plotted against the fraction of unbleached pigment b. It

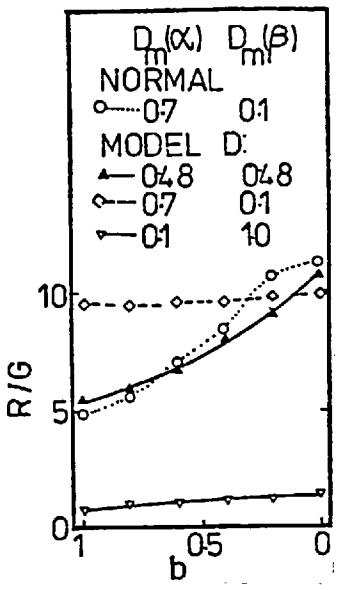

FIG. 5.37 Inter-cone light-shielding model.

is seen that the matches of normals and of the anomals based on model D will in general differ, even at the highest illumination levels of light. This conclusion has been reached for the case where all the light reaching one pigment is filtered by the other pigment. In the case of incomplete shielding of one pigment by the other (which is physiologically more likely than total shielding), the equation for the effective absorption spectrum of the partially-shielded pigment will contain a term like that on the right of equation 5.26, and again the resulting colour matches will differ from that of the normal for all levels of bleaching illumination.

5.11 Discussion

The results of the experimental measurements of normal and anomalous trichromats, and of the calculations of colour matches predicted by three models of anomalous trichromacy, are summarized below.

i) Summary of Results

1) Foveal flicker-fusion relative-energy curves measured in the dark-adapted state for a normal, a protanomal and a deuteranomal agree with published data for each type of observer (figures 5.1, 5.3 and 5.5). The corresponding parafoveal spectral curves possess minima at shorter wavelengths than those of the foveal curves

(figures 5.2 - 5.5). There were differences in shape between the foveal curves of the normal (figure 5.1) and also between those of the protanomal (figure 5.3) which resulted from changes in the flicker-frequency. The foveal and corresponding parafoveal spectral curves obtained for each observer under adaptation to bleaching stimuli were similar (figures 5.6 - 5.8). The foveal spectral curves obtained under light-adapted conditions (λ_A = 471nm, I_A = 3.7 log td) for each observer (the normal, protanomal and deuteranomal) were also similar to the spectral curves measured for the dark-adapted foveas (figure 5.9).

2) Colour-matching measurements made with the deuteranomal BR showed that an extrafoveally presented test light became desaturated with respect to foveal matching stimuli as the illumination level was lowered to scotopic levels (figure 5.10). The colour of stimuli at six different wavelengths approached the same desaturated white at the lowest illumination levels used. Extrafoveal test stimuli became desaturated for the protanomal RF as the illumination level was lowered, but his hue discrimination was very poor at low light illumination levels.

3) The Rayleigh colour-matches of normal observers became more protanomalous at high illumination levels of adapting lights (figure 5.11, table 5.1). The foveal and parafoveal Rayleigh matches of 12 colour normals approached a common log R/G value at high illumination levels, and the colour match shift was largest for the foveal measurements (table 5.1). The Rayleigh-match shifts caused by bleaching were measured for 8 deuteranomals and the values were larger in magnitude than those for the normals (figures 5.12 - 5.15, compared with figure 5.11). The matches

made by the deuteranomals approached the average normal match at an adaptation illumination level of 590 nm light of 5 log td. The colour shifts measured for two deuteranomals in the parafovea were less than those at the fovea (figure 5.12). The foveal and parafoveal colour matches of three protanomals approached the average colour-normal match at high illumination levels of 530 nm adaptation light (figure 5.16). The foveal colour match shifts observed for protanomals were less than those of deuteranomals. An extreme protanomal was able to make colour-matches with increased precision when subjected to bleaching by 471 nm light.

4) Foveal colour matches for a normal observer were adequately predicted by Pitt's (1944) data (figure 5.18), and the parafoveal data were fitted between 540 - 640 nm assuming an effective pigment optical density in the parafovea of 60% of that at the fovea (for $D_m(\alpha) = 0.7$, $D_m(\beta) = 0.1$, fig. 5.18). The parafoveal matches of a deuteranomal and a protanomal were slightly closer to those of the normal, compared with the matches made at the fovea.

5) The average shift of the Rayleigh match of normal observers was used to evaluate the possible values of the maximum optical densities of the red- and green-sensitive photopigments of normal foveal vision (figure 5.23). A range of $D_m(\alpha)$ and $D_m(\beta)$ values was found which could fit these data (figure 5.24).

6) A model of anomalous trichromacy based on mixtures (α', and β') of normal long- and medium-wavelength pigments (α and β) was analysed. According to this model (figure 5.19), pigment mixtures occur in one or both classes of cone which normally contain

only one pigment (α or β). For two types of anomalous trichromat corresponding to the models, (α',β) and (α,β'), the predicted colour-matches approach the colour matches of normals at low pigment densities (equation 5.13). If, in the model, it is assumed that $D_m(\alpha) = D_m(\beta)$, the dark-adapted R/G ratios obtained with realistic estimates of the peak optical densities do not differ significantly from those of the normal system (α,β) (figure 5.25). Thus a model in which $D_m(\alpha) = D_m(\beta)$ can not account for anomals whose log R/G ratios differ from that of normals by more than 0.1. If it is assumed, however, either that the normal pigment concentrations are equal ($c_\alpha = c_\beta$), or that their maximum absorptions are equal ($\alpha_m = \beta_m$), realistic R/G ratios are predicted for anomals in both the (α',β) and (α,β') cases: in each case either protanomaly or deuteranomaly can be produced, depending on the ratio of the amounts of the α and β in the pigment mixtures α' and β' (e.g. figures 5.26, 5.28). The R/G matching ratios are usually well-behaved a) as wavelength is varied and b) as photopigment optical density is varied (e.g. figs. 5.26, 5.27, 5.30), but asymptotic behaviour was obtained on occasion, with negative R/G values occurring for test wavelengths between 500 nm and 600 nm (figure 5.29). It is argued that colour matches of the (α',β') system would generally not approach those of the normal at low pigment densities (section 5.8.4).

7) Calculations of the long-wavelength discrimination curves for anomalous vision of the pigment-mixture model predict a maximum discrimination at wavelengths above 600 nm and a severely reduced discrimination below about 560 nm in most cases (e.g. figure 5.32 - 5.35). The predicted discrimination of

anomals is as good as, or worse than, that of normals (figures 5.31 - 5.35), but the predicted discrimination curve for normals does not fit precisely the curves measured for normals by Pitt and Wright (Wright, 1946), or the theoretical curve predicted by Stiles (1946; figure 5.31).

8) It was demonstrated that in general the colour matches of anomalous trichromats predicted by the 'anomalous pigment' and inter-cone screening models (models A and D, figure 5.19) would not converge to the matches obtained for normal subjects following adaptation to lights of high illumination level.

In the discussion which follows, these experimental data are examined in turn, and are compared with the results predicted by the various models of anomalous trichromacy proposed in the introduction (figure 5.19).

ii) Flicker-Frequency Relative Spectral Sensitivity Curves

The relative spectral sensitivity curves were measured for normal and anomalous trichromats (section 5.4) in order to see whether differences between the curves for each observer could be correlated with differences in pigment optical density for foveal and parafoveal measurements, and for foveal measurements in the dark-adapted and bleached states. It is intended to show in this section that the flicker-fusion measurements do not provide a good method for testing the various models of anomalous trichromacy.

Comparison of the two foveal relative spectral sensitivity curves obtained for the normal observer JB (figure 5.9) under dark-adapted and bleached conditions (I_A = 3.7 log td) reveals

that there is no systematic difference between the relative spectral sensitivities in the two states of adaptation. The same is true of the pairs of relative spectral sensitivity curves measured for the protanomal and the deuteranomal (figure 5.9) which were obtained under dark-adapted and bleached conditions. It would be expected that one effect of pigment bleaching would be to reduce the spectral bandwidth of the relative spectral sensitivity curves, as this occurs for the individual pigment spectral sensitivity curves (figure 5.21). Even if peak optical densities of 1.6 are assumed for foveal erythrolabe and chlorolabe, however (and such high optical densities are unlikely for normals - figure 5.24), the maximum change in the relative spectral sensitivity curves of either pigment which would result from complete bleaching would be about 0.4 log units (figure 5.21). Lower values of peak optical densities in the dark-adapted fovea would result in smaller changes in relative spectral sensitivity following bleaching. Also, the interpretation of these curves is complicated by the fact that their shapes depend not only on the pigment absorption spectra, but also on the relative sensitivities of the colour mechanisms to flickered light (which in turn depend on the relative distributions of the cone types), and on the relative phase-lag of the signals in the colour mechanisms (e.g. Wagner and Boynton, 1972). In fact, the measured shapes of the relative spectral sensitivity curves varied with the illumination level of the reference stimulus and the flicker-frequency (figures 5.1 - 5.6) by as much as 0.4 log units. Spectral sensitivity predictions based on relative spectral sensitivity curves are, therefore, difficult to use as evidence for or against any particular model

of anomalous trichromacy involving altered pigment extinction spectra.

Likewise differences between the relative spectral sensitivity curves measured foveally and parafoveally for each observer cannot be used to measure the differences between the foveal and parafoveal pigment optical densities, especially because of the effects of macular pigment, and of the rods at low illumination levels, in the parafovea (figures 5.2 - 5.7).

iii) Dark-Adapted Parafoveal Colour Matching

Test stimuli presented parafoveally to colour normals become desaturated at mesopic light levels, and all stimuli approach the same desaturated white colour at scotopic levels (Hunt, 1952; Clarke, 1960). Similar results were found for the deuteranomal BR - this is shown for the parafoveal data in figure 5.10 which are plotted in his foveal chromaticity chart. Parafoveal colour matches became less saturated at low illumination levels for the protanomal RF. The hue discrimination of RF and that of a second protanomal RF were severely reduced at low illumination levels, however, so that the parafoveal colour matches could not be measured at such illumination levels. Even at moderate illumination levels, protanomals normally suffer a loss of hue discrimination compared to normals for wavelengths below 570 nm (Wright, 1946). Again, Thompson and Trezona (1951) measured a very marked hue discrimination loss for a protanomal for wavelengths between 480 nm and 580 nm at low illumination levels, so that the loss of hue discrimination of RF and RL was not unexpected.

Rod vision is mediated by the single photopigment rhodopsin,

so that the collapse of parafoveal vision to a single colour is to be expected for illumination levels at which the rod threshold is below that of the cones. The evidence for colour normals (Hunt, 1952; Clarke, 1960, 1963) and the deuteranomal BR (figure 5.10) is that the colorimetric response of the rods is equivalent to a 'white' colour represented by a point near the centre of the foveal chromaticity chart of each observer. The initial desaturation of parafoveal test stimuli measured for the protanomal RF as the illumination level was lowered indicate that, for this observer, the rod system also contributes a desaturated component to colours at low illumination levels. A similar conclusion was reached by Ruddock (1971) in the cases of a tritanope, one protanope and a deuteranope, so that it is likely that the contribution of the rod mechanism to colour vision at scotopic illumination levels is similar for normal and all classes of red-green defective colour vision.

iv) Colour Matches Following Adaptation to High Illumination Levels

The convergence of Rayleigh colour matches made by normal observers adapted to light at high illumination levels (figure 5.11, table 5.1) indicate that the bleached erythrolabe and chlorolabe pigments are identical in different normal observers. Observer differences in Rayleigh matches made at low illumination levels can be partly attributed to observer variations in the optical densities of these pigments in the dark-adapted eye. The log R/G values for the foveal matches of three normal observers are replotted against the illumination level of bleaching light

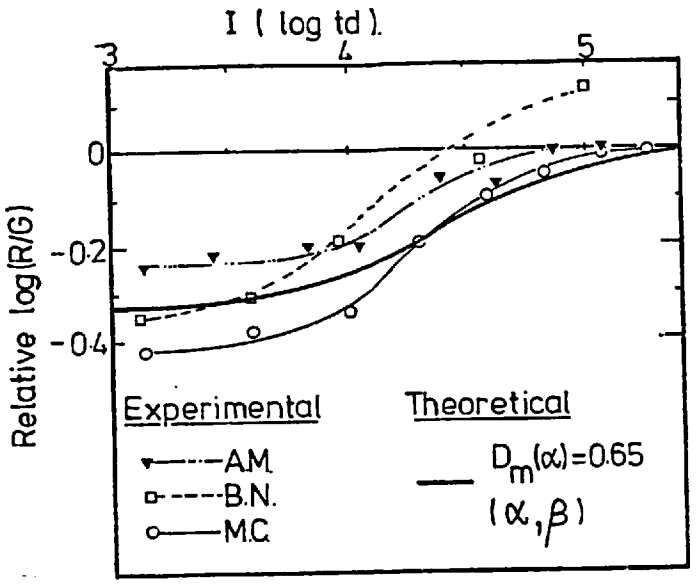

FIG. 5.38 Normal log (R/G) shifts caused by bleaching, using bleaching light of illumination level I (log td).

in figure 5.38 (data from figure 5.11), together with the matches predicted for normals. (The predicted curve was obtained from figure 5.30 ($D_m(\alpha)$ = 0.65, $D_m(\beta)$ = 0.10) and from the kinetics-of-bleaching curve in figure 5.20). It can be seen from figure 5.38 that the theoretical data agrees qualitatively with the experimental data. It has already been mentioned that the high optical densities of visual pigments which are necessary to produce the colour-match shifts are consistent with the results of other psychophysical experiments (e.g. Brindley, 1953, 1955; Enoch and Stiles, 1961; Walraven and Bouman 1960; Miller, 1972) and objective measurements (e.g. Dunn, 1969; Liebman, 1969; Bowmaker et al., 1977).

The log R/G values obtained foveally and parafoveally for 7 deuteranomals and 3 protanomals (figures 5.12 - 5.16 are replotted in figures 5.39 and 5.40. Some log R/G values predicted for deuteranomals and protanomals by the pigment-mixture model of anomalous trichromacy are plotted on the same diagrams. The data were derived from the rate-of-bleaching

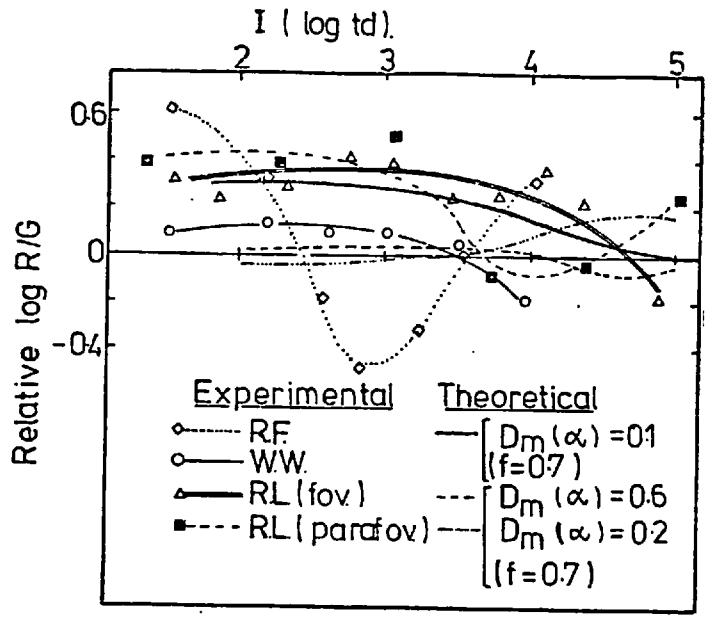

FIG. 5.39 Log R/G values for protanomals, and predicted shifts.

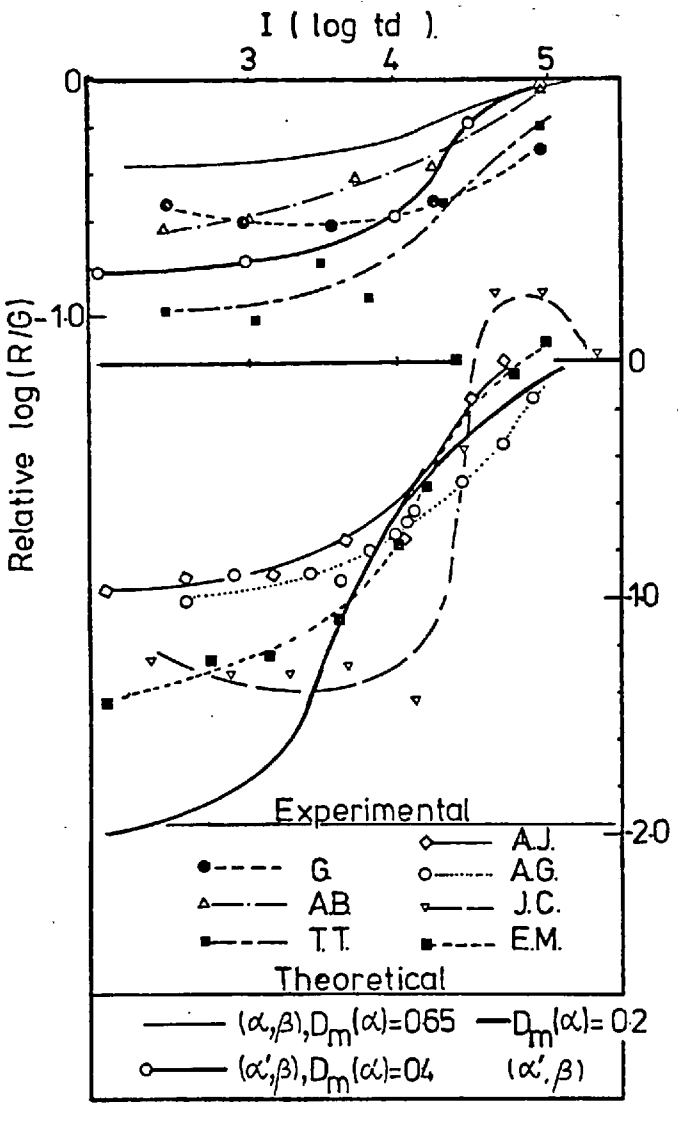

FIG. 5.40 Deuteranomalous Rayleigh match shift, and predicted shifts.

data in figure 5.20 and the predicted Rayleigh matches (λ_{test} = 580 nm) given in figs. 5.26, 5.27 and 5.30. The theoretical data shown are mostly for extreme ratios of pigment amounts in the pigment mixtures (i.e. ratios of 9/1 or 1/0; f = 0.1, equations 5.3, 5.4), and smaller colour shifts would be obtained for higher values of f. It is seen clearly from these diagrams (figures 5.38 - 5.40) that the colour matches of normals and anomals approach the same R/G value at higher illumination levels, and that the colour-matching can be explained by the pigment-mixture model of trichromacy.

v) Parafoveal Colour Matches

The small differences between the foveal and parafoveal matches of a normal trichromat were predicted by assuming that the pigments in the shorter parafoveal cones had, on average, an optical density of 0.6 times that at the fovea (figure 5.18), in agreement with the findings of Pokorny and Smith (1973) and Alpern (in print). The colour shifts measured for a protanomal and a deuteranomal under identical stimulus conditions were small. This result does not contradict the predictions of the pigment-mixture model of anomalous trichromacy, as the colour match changes predicted by this model for a decrease in optical density of 0.4 (to 0.6 of the foveal value) would in many cases be insignificant (e.g. figures 5.26, 5.30).

vi) Wavelength-Discrimination Data

The wavelength-discrimination curves predicted for normal observers at long wavelengths had minima at longer wavelengths than those measured by Pitt and Wright (Wright, 1946) and predicted by Stiles (Stiles, 1946) (figure 5.31). Now Stiles used his π-mechanism curves to evaluate the hue discrimination curves for normals, whereas in this study, the Pitt (1944) sensitivity curves were used. Also, the wavelength-discrimination curves predicted using Stiles' line-element theory are very sensitive to the slopes of the pigment absorption spectra (R' and G' in equation 5.24). Differences between the methods of curve-fitting (between data points for absorption spectra) used by Stiles and in this study may well have caused most of the differences between the predicted hue-discrimination curves (fig. 5.31).

The wavelength-discrimination predicted in this study for the anomals was generally worse than that found for normals, and in most cases the predicted discrimination was best above 600 nm, and worst below 560 nm (figures 5.32 - 5.35). The data agree qualitatively with those measured for anomals (figures 5.32 - 5.35; Nelson, 1938; McKeon and Wright, 1940). Quantitative comparison between the theoretical and experimental discrimination curves is complicated by the fact that discrimination often differs on the long- and short-wavelength sides of a test wavelength, and this is marked for protanomals (Thompson and Trezona, 1951). Published data usually refer to the average of the short- and long-wavelength discriminations, and the Stiles line-element theory does not differentiate between the two cases.

The improvement of the discrimination of the extreme protanomal following bleaching (λ_A = 471 nm) can be explained by the pigment-mixture model of anomalous trichromacy. If the fraction of one pigment type (α or β) present in both long-wavelength cone types is predominant, the shapes of the absorption spectra of the two long-wavelength mechanisms will be very similar, so that hue-discrimination will be poor. Then, if the dominant pigment is preferentially bleached by chromatic light, the spectral sensitivities of the two long-wavelength mechanisms will become increasingly dissimilar as the relative proportion of the least concentrated pigment increases, and hue discrimination will improve (e.g. figures 5.32, 5.33). Hue discrimination is expected to decrease at very high illumination levels owing to a loss in sensitivity of the colour mechanisms, explaining the increase of discrimination of some anomals at moderate illumination levels (figs. 5.12, 5.16), followed by a subsequent decrease in

discrimination.

Walls and Matthews (1952) mention that Trendelenberg (1943) used short-duration white-light bleaches on extreme anomalous trichromats in order to improve their discrimination: the improvement in the precision of setting R/G in the Rayleigh match was marked. This agrees with the results found for the extreme anomal mentioned in section 5.6.

vii) The Relative Merits of the Models of Anomalous Trichromacy

It was demonstrated that the log R/G ratios for the anomalous pigment and pigment screening models of anomalous trichromacy (figure 5.19) would in general differ from those of the normal at all illumination levels of bleaching light (e.g. figures 5.36, 5.37). Therefore these models of anomalous trichromacy are unable to explain the fact that normal and anomalous trichromatic Rayleigh matches converge at high illumination levels (figures 5.39, 5.40). The pigment mixture model is unable to predict the dark-adapted Rayleigh matches of anomals when it is assumed that the data of Pitt (1944, table 5.2) refer to equal optical densities of α and β (figure 5.25). In contrast, when it is assumed either that the erythrolabe and chlorolabe concentrations are equal ($c_\alpha = c_\beta$), or that their maximum absorptions are equal ($\alpha_m = \beta_m$), the colour-matching behaviour of normals and anomals can be predicted at all illumination levels (figures 5.38 - 5.40).

5.12 Conclusion

In this study of anomalous trichromacy, flicker-fusion and colour-matching measurements were made with normal and anomalous trichromats. The resulting data were compared with the predicted behaviour of several models of anomalous trichromacy (fig. 5.19) in order to find a model which is consistent with the measured behaviour of anomalous trichromatic vision.

The anomalous-pigment and inter-cone light-shielding models predict Rayleigh matches which differ, in general, from the matches of normals at all illumination levels (figures 5.36, 5.37). In contrast, the pigment-mixture model was able to predict the convergence of Rayleigh matches of normals and anomals (figures 5.38 - 5.40). In addition, the wavelength-discrimination behaviour of anomals was qualitatively predicted by the pigment-mixture model (figures 5.32 - 5.35), and the improvement of the discrimination of extreme anomals following bleaching was also explained. Further, dichromatic vision can be predicted as an extension of the pigment-mixture model in which all red-green cone types contain the same single pigment or pigment mixture. (This latter model was proposed by Rushton (1958a,b) for deuteranopic vision). Therefore, the pigment-mixture model of anomalous trichromacy provides a reasonable description of anomalous trichromacy.

CHAPTER 6

SUMMARY AND CONCLUSIONS

In this thesis, established psychophysical methods have been applied to the analysis of three different phenomena, all of which involve some degree of interaction between the different spectral mechanisms active in human vision. Studies of the metacontrast effect (chapter 3) were concerned with lateral interaction effects through which cones influence threshold detection by the rod photoreceptors. The instability of colour matches for observers under adaptation to spatially structured stimuli was described and analysed (chapter 4) and colour-matching methods were also applied as part of an experimental and theoretical study of red-green anomalous trichromacy (chapter 5).

In the metacontrast study (chapter 3) it was found that both rod and cone mechanisms contributed to the relative spectral sensitivity functions for masking (figures 3.15 - 3.23a), even though preliminary experiments had established that the probe stimulus (λ = 495 nm) excited only the rod mechanism over a range of suprathreshold illumination levels (pages 81 - 89). Three separate arguments were employed to show that the masking effects were not caused by scattered light (section 3.7, page 114), and it is concluded that lateral rod-cone interactions occur in metacontrast masking. Masking experiments performed with a red probe stimulus demonstrated cone-cone lateral interactions (page 123). A model for the lateral rod-rod and cone-rod interactions was proposed (this is shown schematically in figure

3.47). The essential feature of this model is suppression by cone signals arising from the mask stimulus of rod signals elicited both by the probe and mask stimuli.

Data obtained from masking experiments employing a red background field and annular mask stimuli, and from experiments with rotating 'windmill' mask stimuli are consistent with this model. The red background fields reduce the magnitude of the cone signals elicited by the mask stimulus, and this leads to a decrease in the masking of rod signals evoked by the mask stimulus. The observed effect is, therefore, a relative increase in the sensitivity to masking of the rod signals evoked by short wavelength probe stimuli (figures 3.32, 3.33). Changes in the speed of rotation of the windmill mask stimulus resulted in changes in the short-wavelength relative spectral sensitivity of masking (figures 3.39, 3.40), because of differences in the relative stimulation of the cone mechanism of the different rotational speeds of the windmill stimulus (page 126).

The time-course of the metacontrast masking effect (figure 3.20) was found to be consistent with an 80 msec delay of rod signals relative to cone signals, and reaction time experiments gave independent confirmation of this 80 msec delay (figure 3.38, and pages 123 - 124).

Masking effects measured monoptically differed from those measured dichoptically in that masking was induced monoptically by both annular and uniform stimulus fields (figures 3.30, 3.31), whereas dichoptically it could only be induced using annular mask stimuli (pages 104, 105). Dichoptic transfer implies that the masking effects observed with annular stimuli occur in

cortical cells (probably the simple cells described by Hubel and Wiesel, 1968). Other differences between monoptic and dichoptic masking functions are found in the action spectra (figures 3.15, 3.17, 3.29, section 3.8) and in the temporal characteristics (figures 3.35, 3.37). It was concluded that there is both a central site and a peripheral site at which masking occurs, and that these sites are differently organized (page 129). Subsequent to the experiments reported in this thesis, rod-cone interaction in metacontrast was confirmed for monoptic (Foster, 1976) and dichoptic presentation (Foster and Mason, 1977).

The aim of the colour matching experiments described in chapter 4 was to quantify and to analyse the changes in colour matches induced by adaptation to spatially structured (grating) stimuli. Changes in colour matches were demonstrated for a number of adaptation and test stimulus wavelengths. In the experiments, the upper half of the adaptation stimulus was spatially uniform and the lower half contained a vertical square-wave grating, and the two halves of the adaptation field were of the same average illumination. The chromaticity shifts induced by the grating stimulus were in most cases towards the chromaticity point corresponding to the adaptation stimulus (figures 4.1 - 4.8). Similar changes in chromaticity were observed when the lower half of the adaptation stimulus was uniform but 0.8 log units dimmer than the upper half (figure 4.13). This result implies that the grating stimulus is less effective at adapting the units responsible for the colour-match changes than a uniform stimulus of the same average illumination level. The changes in chromaticity obtained for

adaptation stimuli which had either uniform or grating patterns in the lower half, and for which the lower half was flickered, led to the conclusion that spatial structure and temporal flicker in the adaptation stimulus both give rise to colour shifts (page 176). The action of scanning a grating therefore gives rise to colour shifts both because of the grating structure, and because of the temporal flicker imposed by the scanning action.

It was demonstrated that the colour shifts were caused neither by reciprocity failure in the receptors (pages 177 - 179), nor by rod intrusion (page 179), nor by pigment bleaching (pages 180 - 181). The characteristics of the chromaticity changes induced by adaptation to spatially structured stimuli are in some respects similar to those of the contrast threshold elevation effect (Gilinsky, 1968; Pantle and Sekuler, 1968; Blakemore and Campbell, 1968, 1969). The magnitudes of the two effects increase in the same manner with adaptation illumination level (figure 4.36), and decrease at the same rate following cessation of adaptation (figure 4.37). The contrast threshold elevation effect is maximum when the spatial periodicities of the probe and adaptation grating patterns are equal, but this was true of the colour-shift magnitude only in selected instances (compare 4.15, 4.16 with 4.17, 4.18). Further, the magnitude of the colour shift effect was found to be independent of the relative angle between the probe and adaptation stimulus gratings,whereas the contrast threshold elevation effect is highly orientation specific (Blakemore and Campbell, 1969). Maudarbocus and Ruddock (1973a,b, 1974) showed that the monocular contrast

threshold elevation effect was wavelength-dependent, but that the binocular contrast threshold elevation effect was virtually independent of stimulus wavelength. Similarly, the colour shifts induced by grating adaptation could only be induced monocularly.

From the experimental data reviewed above, it was concluded that the colour shifts induced by grating and flicker adaptation occur neither at the receptor level, nor at the level of binocularly-driven cortical cells, although they do have features in common with the contrast threshold elevation effect. It was concluded that the colour shifts may be attributable to ganglion cell activity (page 184).

In the study of anomalous trichromacy, two experimental techniques were used to compare the characteristics of red-green anomalous trichromats with those of normal colour-vision, namely flicker-fusion relative spectral sensitivity measurements and colour-matching. It was shown that measurements of the flicker-fusion relative spectral sensitivity curves, both with and without chromatic adaptation, were not sufficiently precise to allow estimates of the effects of bleaching on pigment optical densities (figures 5.1 - 5.9).

It was established that for a normal, a protanomalous and a deuteranomalous observer the maxima in the dark-adapted parafoveal relative spectral sensitivity occurred at shorter wavelengths than for measurements at the fovea. In addition, parafoveal stimuli for the two anomals become desaturated with respect to the foveal matching stimuli at mesopic illumination levels (although the hue-discrimination ability of the protanomal was drastically reduced at low illumination levels), in agreement with the results found for normals by Hunt (1952)

and Clarke (1960). It is deduced that the rods behave normally in red-green anomalous trichromats.

Rayleigh colour-matches were measured following adaptation to spatially uniform stimuli, at a series of successively higher adaptation illumination levels. Measurements were made for 12 subjects with normal colour vision, for eight deuteranomals and for three protanomals. It was found that the red/green ratios for the Rayleigh matches of these different classes of observer converge to the same value at high adaptation illumination levels (around 5 log td) (figures 5.38 - 5.40).

Calculations were made for several alternative models of anomalous trichromacy (figure 5.19). It was demonstrated that, in general, the anomalous-pigment model and the 'inter-cone light shielding' models of figure 5.19 predict that Rayleigh matches for anomalous trichromats should differ from the normal match at all adaptation illumination levels (figures 5.36, 5.37). A theory of anomalous trichromacy based on mixtures of erythrolabe and chlorolabe in single cones (Ruddock and Naghshineh, 1974) was shown to be compatible with the convergence of the Rayleigh matches of normals and anomals at high illumination levels of adaptation stimuli. In this model, it is assumed that normal erythrolabe (α) and chlorolabe (β) occur in either class of the red-green cones of normal vision. For the configurations presented in this thesis, it was assumed that the absorption spectra of erythrolabe (α_λ) and chlorolabe (β_λ) are described, respectively, by Pitt's (1944) red and green spectral sensitivity functions. The ranges of pigment optical densities which give correct predictions for adaptation changes in the normal Rayleigh match (figure 5.24) were computed and then used in the calculations of

the colour-matches for anomals. The required range of optical densities (0.1 - 1.0) is compatible with recent objective measurements of primate pigment optical densities (Dunn, 1969; Liebman, 1969; Bowmaker et al., 1977). It was found that the colour matches of anomals and normals do not in general converge if pigment mixtures occur in cones of both long-wavelength classes (the (α',β') model), or if it is assumed that the optical densities of chlorolabe and erythrolabe are equal (figure 5.25).

The convergence of anomalous and normal colour matches at high adaptation illumination levels is predicted, however, if it is assumed that pigment mixtures occur in only one class of red-green cone ((α',β) or (α,β')), and that either the concentrations of α and β are equal in the dark-adapted normal, $c_\alpha = c_\beta$, or that their peak absorbances are equal, $\alpha_m = \beta_m$. In either case, the changes in the Rayleigh match with change in adaptation illumination level can be predicted (figures 5.38 - 5.40).

The wavelength-discrimination curves for normal subjects predicted on the basis of Pitt's (1944) sensitivity data for α_λ and β_λ and the Stiles line-element theory (Stiles, 1946) agree qualitatively with the measured values of Wright and Pitt (1934), although the agreement is not as good as that found by Stiles (1946) using his increment-threshold spectral data for α_λ and β_λ (figure 5.31). The wavelength-discrimination curves predicted for anomalous subjects from the Stiles (1946) line-element theory and the (α',β) and (α,β') models of anomalous trichromacy are compatible with those measured for protanomaly and deuteranomaly respectively (Wright, 1946; figures 5.32 - 5.35). In addition, the size of the wavelength discrimination step predicted for

anomalous vision decreases for high adaptation illumination levels (figures 5.32, 5.33), and this behaviour was observed in the wavelength discrimination data of an extreme protanomalous subject. Trendelenberg (1943) has also published data showing that anomalous wavelength discrimination is improved following adaptation to strong bleaching lights.

Finally, the small differences between colour matches established foveally and parafoveally for normal and anomalous trichromatic subjects can be interpreted as evidence that the optical density of photopigments in parafoveal cones is some 0.6 times that at the fovea (figure 5.18), as has been inferred from other measurements (Pokorny, Smith and Starr, 1976).

In conclusion, the aims of this study as stated in the introduction (chapter 1) and at the beginning of each chapter (chapters 3, 4 and 5) have been accomplished. Thus rod-cone interaction has been shown to occur in metacontrast and the mechanisms of this interaction have been studied; the causes of the chromaticity-shifts induced by grating adaptation stimuli have been established and the probable site of the shifts has been identified, and it has been shown that the pigment-mixture model of anomalous trichromacy is compatible with the observed colour-match changes which occur under adaptation at illumination levels that cause significant bleaching. Future refinements of objective methods of measuring pigment optical densities are needed to demonstrate conclusively the presence of normal erythrolabe and normal chlorolabe in single cones of anomalous trichromats.

APPENDICES (A - E)

Appendix A: The stabilized lamp power supply

A schematic circuit diagram of the stabilized lamp power supply which was used for the source S on the metacontrast apparatus (figure 2.1) and for the lamp S_5 on the colorimeter (figure 3.7) is shown in figure A1. The operation of this circuit is described in this appendix.

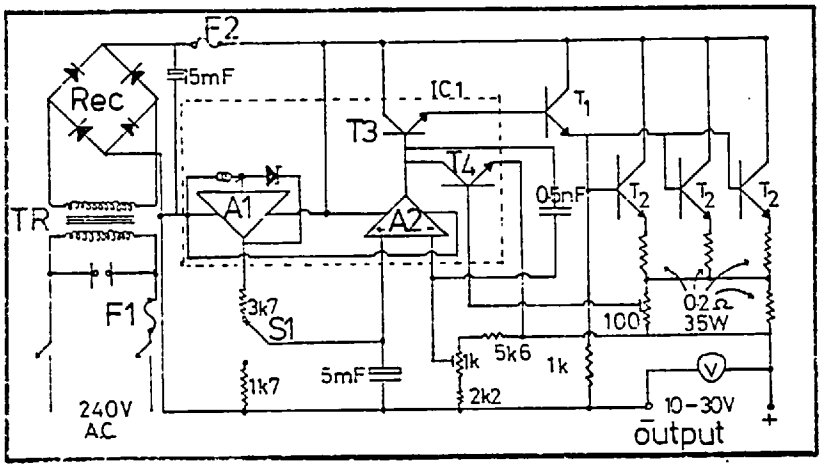

FIG. A1 Stabilized lamp power supply

The 240 V A.C. mains current is fed into the conventional transformer (Tr)/full-wave-rectifier (Rec)/15 mF capacitor circuit which provides an unstabilized D.C. voltage (30 V) at its output. Fuses F1 and F2 provide protection to the mains circuit and the D.C. circuit. The integrated circuit (inside the broken rectangle) stabilizes the final output voltage and limits the output current of the power supply in the following manner.

The zener diode in the feedback loop of the amplifier A1 controls the voltage applied to the non-inverting input of

amplifier A2 (via switch S1). The amplifier A2 in turn controls the power supply output voltage at the emitters of the output power transistors T2, via the transistors T3, and T1, and the three transistors T2 connected in parallel. A fraction of the power supply output voltage, the magnitude of which is determined by the series 5.6 kΩ resistor/1 kΩ potentiometer/2.2 kΩ resistor chain, is fed to the inverting input of the amplifier A2 (negative feedback). Now the output voltage of the amplifier A2 (and hence, that of the power supply) is proportional to the difference between the voltage applied to its non-inverting input and the negative of the voltage applied to its inverting input. Because of the negative feedback chain (T3, T1, and the T2 transistors) from the output of amplifier A2 to its inverting input, the amplifier A2 seeks to maintain its inverting input at the same voltage as that at its non-inverting input. This non-inverting input voltage is controlled by the zener diode and amplifier A1, so that the power supply output voltage is controlled by the zener diode: the output voltage value can be preset using the 1 kΩ potentiometer.

Current limiting of the power supply is controlled by transistor T4 as follows. The voltage across the 100 Ω preset potentiometer is proportional to the output current, and the fraction of this voltage which is fed to the base of the transistor T4 is adjusted (by adjusting the 100 Ω potentiometer) such that the transistor T3 is switched fully 'on' by transistor T4 when the output current exceeds 10 amps. Thus, before the output can exceed 10 amps, transistors T4 and T3 reduce the output voltage to limit the output current to only 10 amps.

The switch S1 is used to avoid rapid voltage changes at

the output of the power supply (to prevent lamp damage) in the following manner. When the contact of switch S1 is switched to the 1.7 kΩ resistor, the output voltage of the power supply decreases exponentially to zero because of the discharge circuit (the 5 mF capacitor and 1.7 kΩ resistor with time constant τ = 8.5 sec) at the non-inverting input of amplifier A2. Similarly, when the switch S1 is switched back to the position shown in figure A1, the output voltage rises exponentially to its final value at a rate determined by the 3.7 kΩ resistor and the 5 mF capacitor circuit (τ = 18.5 s).

The components of the power supply circuit were chosen to allow a power output in excess of 200 W, and the output voltage and limiting currents were set at 23.00 V and 10 A.

Appendix B: Transformation between the CIE and WDW coordinate systems

The primary matching stimuli of the WDW co-ordinate system are the red (R, 650 nm), green (G, 530 nm) and blue (B, 460 nm) colours. The following equation defines the relationship between the R, G and B colours of the WDW system and the X, Y and Z primaries of the CIE system, for 10^{o} viewing conditions:

$$\begin{bmatrix} X \\ Y \\ Z \end{bmatrix} = \begin{bmatrix} 0.7634 & -0.5872 & 0.0281 \\ -0.2021 & 1.4637 & -0.0701 \\ -0.1173 & 0.0057 & 1.7992 \end{bmatrix} \begin{bmatrix} R \\ G \\ B \end{bmatrix} = A^{*} \begin{bmatrix} R \\ G \\ B \end{bmatrix} \qquad (B1)$$

The CIE x, y, z chromaticity co-ordinates of a particular colour can therefore be converted to the WDW r, g, b chromaticity

co-ordinate using B2:

$$\begin{bmatrix} r \\ g \\ b \end{bmatrix} = aA \begin{bmatrix} x \\ y \\ z \end{bmatrix} \qquad \text{(B2)}$$

where 'a' is a normalizing constant and A is the transpose of matrix A* (Wyszecki and Stiles, page 236). The inverse matrix A^{-1} can be used to transform from the WDW to the CIE co-ordinate systems:

$$\begin{bmatrix} x \\ y \\ z \end{bmatrix} = dA^{-1} \begin{bmatrix} r \\ g \\ b \end{bmatrix} \qquad \text{(B3)}$$

where 'd' is a normalizing constant.

Appendix C: Estimation of Scattered Light

In this appendix the illumination level of scattered light at the centre of the masking stimulus (figure 2.5) is estimated from data of Fry and Alpern (1953).

Fry and Alpern (1953) measured the effective veiling luminance B_e on a central test rectangular stimulus produced by two outer rectangular stimuli of the configuration illustrated in figure C(a). The general formula which they found relating B_e to the luminance B_c of the outer two stimuli was

$$B_e = kB_c/\theta^n \quad . \qquad \text{(C1)}$$

where k = 0.00545, n = 2.5, and θ is the angular separation between the rectangular bars (figure C(a)). It is expected that the illumination level of the scattered light produced by the outer rectangular stimuli of figure C(b) on the 23' disc stimulus (shown to scale in figure C(b)) is not greater than that measured for the rectangular test stimulus of figure C(a) (since the separation between the test and inducing stimuli in figure C(b) is greater than that of the stimuli in figure C(a)). Now equation C1 was derived from data obtained for values of θ between 0.75° and 4.5°, so that it holds for the stimulus configurations of figures C(a) and C(b) where θ = 0.75 . For this value of θ, equation C1 yields

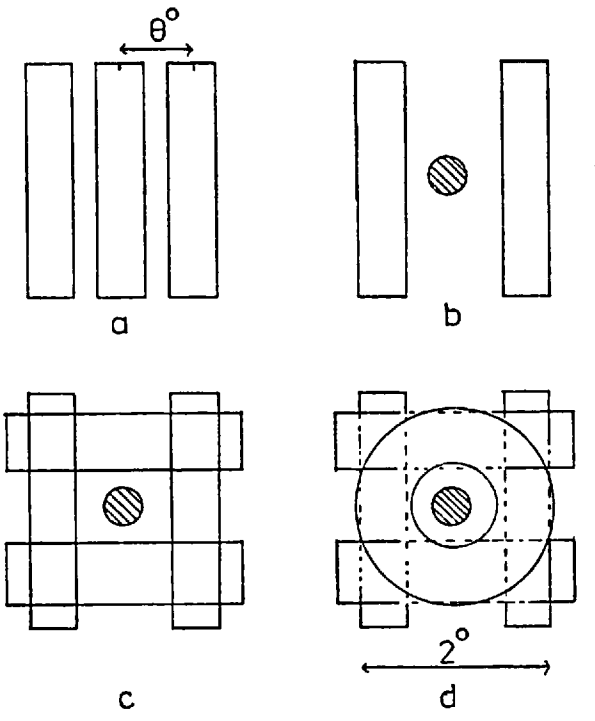

FIG. C(a-d) Glare stimuli of Alpern and Fry (1953) and metacontrast stimuli (to scale, the scale is indicated by the 2° arrow).

$$\log_{10}B_e = \log_{10}B_c - 1.94 \qquad (C2)$$

If a second pair of rectangular veiling sources are placed at right angles to the first (figure C(c)), the total veiling glare

illuminance at the centre should be doubled, and

$$\log_{10}B_e = \log_{10}B_c - 1.64 \qquad (C3)$$

The dimensions of the veiling stimulus of figure C(c) are very similar to those of the mask stimulus used for most of the metacontrast measurements. This is illustrated in figure C(d). Thus, to a first approximation, equation C3 might be expected to yield a reasonable estimate of the equivalent veiling glare produced by the annular mask of figure C(d) on the circular probe stimulus at its centre. Since the illuminance of a stimulus is proportional to its radiance, equation C3 can be rewritten in terms of the annular stimulus radiance P_A, and of the equivalent veiling radiance P_e produced at its centre:

$$\log_{10}P_e \simeq \log P_A - 1.6. \qquad (C4)$$

Fry and Alpern (1953) found that they could account for the veiling effect of the outer rectangles of figure C(a) in terms of scattered light. The ages of their two observers are not given, although Ruddock (1964) has shown that ocular scatter increases with age. Thus a third assumption is necessary: it is assumed that the ocular scatter of observer BN is not markedly greater than that for the two observers used by Fry and Alpern (1953). Hence, the field radiance incident on the probe stimulus area due to light scattered by the annular stimulus of figure C(d) is at least 1.6 log units less than that of the annular stimulus. This is true for white light, but scatter may be greater at short wavelengths of monochromatic

mask stimuli (e.g. figure 1.2).

Appendix D: Pigment Kinetics

Campbell and Rushton (1955) used reflex densitometry to study the time course of *in vivo* bleaching and regeneration of visual photopigments. The reaction kinetics of these photopigments are described by first-order equations, indicating that the kinetics are rate-limited by one reaction in the forward direction and by one reaction in the reverse direction. The rate-limiting step in regeneration appears to depend on the availability of 11-cis retinol (Rushton and Henry, 1968).

If h is the fraction of unbleached photopigment at time t, and P is the effective naperian photosensitivity to axial rays, then

$$\frac{dh}{dt} = (1 - h)/\tau - hIP \qquad (D1)$$

describes the rate of change of h. I is the illumination level of bleaching light (in trolands), and τ is the time-constant of pigment regeneration in the absence of light. At equilibrium dh/dt = 0, whence

$$h = 1/(1 + IP\tau) = 1/(1 + I/I_o) \qquad (D2)$$

$I_o = (P\tau)^{-1}$ corresponds to the illumination level which at equilibrium bleaches half of the visual photopigments. For the normal rod photopigment I_o = 40 000 and τ = 360 s (Campbell and Rushton, 1955), and for a cone mixture in the normal fovea, I_o = 20 000 and τ = 120 s (Rushton and Henry, 1968).

Integration of D1 yields, successively:

$$\int_{h_1}^{h_2} dh/[h(IP + 1/\tau) - 1/\tau] = -\int_{t_1}^{t_2} dt$$

and

$$[1/(IP + 1/\tau)]\ln[h(IP + 1/\tau) - 1/\tau] \Big|_{h_1}^{h_2} = -t_2$$

if $t_1 = 0$. Thus

$$h_2 = (h_1 - 1/a\tau)e^{-at} + 1/a\tau \qquad (D3)$$

where $a = IP + 1/\tau$.

Equation D3 can be used to evaluate h following any time course of light- and dark-adaptation.

Appendix E: Computer Programmes

This appendix contains a brief description of the computer programmes which were written to produce stimulus patterns and to compute meaningful results from experimental data.

1. Stimulus Pattern Generation

Several FORTRAN programmes were written to allow circular or linear patterns to be produced on the face of a high-resolution C.R.T. screen of a remote graphics terminal attached to the University of London Computer network. The C.R.T. screen was photographed automatically by a 35 mm camera, and the resulting negative pictures were used as stimuli. The resolution

of the C.R.T. screen/negative system was at least 80 lines mm^{-1}, and the optical density difference between the exposed and unexposed areas of the film was about 1.7 log units. The images used for the metacontrast stimuli (e.g. fig. 2.5) were copied onto high contrast film for which the optical density difference between light and dark areas was at least 3 log units.

2. Data Evaluation

A Tektronix model 31 calculator was programmed to accept as input the experimental data read off scales attached to wedges on the colorimeter (figure 2.6), or printed out by the DVM/printer of the metacontrast apparatus (figure 2.3). The calibration data for the wedges and stimulus illumination levels were stored in the calculator memory, and these data were updated following each recalibration of the stimulus illumination levels. The calculator was programmed to evaluate the average of a number of data points, and to print the average relative illumination level of the experimental settings as well as the standard deviation of the average. In addition, in the case of colorimetric determinations, the average WDW chromaticity was evaluated for each colour match. A further programme was written to convert the WDW chromaticities to the CIE chromaticity system (see appendix B).

The Tektronix calculator was also programmed to calculate the pigment-bleaching kinetics for figures 4.34, 4.35 and 5.20.

3. Calculations of Pigment Absorption Spectra and Colour Matching and Wavelength Discrimination Curves

A Hewlett Packard calculator (HP series 9800) attached to a

magnetic tape reader and an XY plotter was used in the calculations of pigment absorption spectra, colour matches and wavelength discrimination step size in chapter 5 (sections 5.8 - 5.10). The programmes written for the HP calculator were interactive in order to allow rapid changes of the variable parameters in the programmes (such as peak optical densities $D_m(\alpha)$, $D_m(\beta)$, the fraction f of pigments in the pigment-mixture model of anomalous trichromacy (equations 5.3, 5.4), the fraction of unbleached pigment, b and the Stiles line-element, δs (equation 5.24)).

For the calculations of the wavelength-discrimination curves (section 5.9.6) the spectral sensitivity curves were calculated at 10 nm intervals, and these points were fitted using sixth-order Tchebychev polynomials. The polynomial coefficients were calculated to ten significant figures to

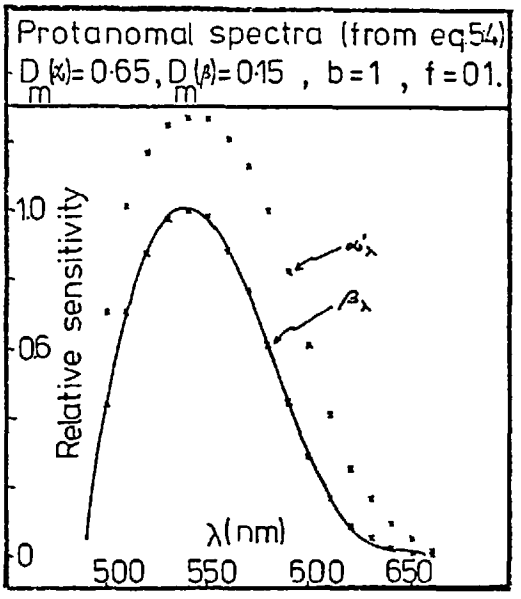

FIG. E1

maintain accuracy. The XY plotter was programmed to draw these spectral sensitivity curves. The plot in figure E1 illustrates the agreement which was obtained between action spectra computed for discrete wavelengths (crosses, figure E1, calculated for a particular example as detailed in the figure) and the continuous curve derived from these data using Tchebychev polynomials.

BIBLIOGRAPHY

The bibliography is indexed according to the Harvard system. The numbers at the end of each reference (between the slashes, /) are the numbers of the pages on which the reference is mentioned.

ABNEY, Sir W. de W. (1913), Researches in colour vision and the trichromatic theory, Longmans: London. /34/

AITKEN, J. (1873), "On colour and colour sensation", Trans. R. Scott. Soc. Arts, 8, 375 - 418. /189/

ALEXANDER, K.R. (1974), "Sensitization by annular surrounds: the effect of test stimulus size", Vision Res., 14, 1107 - 1113. /39/

ALPERN, M. (1952), "Metacontrast: Historical Introduction", Am. J. Optom., 29, 631 - 646. /40/

ALPERN, M. (1953), "Metacontrast", J. Opt. Soc. Amer., 43, 648 - 657. /40/

ALPERN, M. (1965), "Rod-cone independence in the after-flash effect", J. Physiol. (Lond.) 176, 462 - 472. /40, 129, 135/

ALPERN, M. (1977), "The stability of colour matching", in print. /253, 267/

ALPERN, M., BASTIAN, B., PUGH, E.N. Jr. and GRAS, W. (1976), "Altered ocular pigments, photostable and labile: Two causes of deuteranomalous trichromacy", Mod. Probl. Ophth., 17, 273 - 291. /189/

ALPERN, M., LEE, G.B. and SPIVEY, B.E. (1965), "π_1 cone monochromatism", Arch. Opthal., N.Y., 74, 334 - 337.

ALPERN, M. and MOELLER, J. (1977), "The red and green cone visual pigments of deuteranomalous trichromacy", J. Physiol., 226, 647 - 675. /188, 189/

ALPERN, M. and PUGH, E.N. Jr. (1977), "Variation in the action spectrum of erythrolabe among deuteranopes", J. Physiol., 266, 613 - 646.

ALPERN, M. and RUSHTON, W.A.H. (1965), "The specificity of the cone interaction in the after-flash effect", J. Physiol. 176, 473 - 482. /40/

ALPERN, M. and RUSHTON, W.A.H. (1967), "The nature of rise in threshold produced by contrast-flashes", J. Physiol. (Lond.), 189, 519 - 534. /40/

ALPERN, M., RUSHTON, W.A.H. and TORII, S. (1969), "Encoding of nerve signals from retinal rods", Nature (Lond.), 223, 1171 - 1172. /40/

ALPERN, M., RUSHTON, W.A.H. and TORII, S. (1970a),"The size of rod signals", J. Physiol., 206, 193 - 208. /40, 114/

ALPERN, M., RUSHTON, W.A.H. and TORII, S. (1970b), "The attenuation of rod signals by backgrounds", J. Physiol., 206, 209 - 227. /40, 114/

ALPERN, M., RUSHTON, W.A.H. and TORII, S. (1970c), "The attenuation of rod signals by bleachings", J. Physiol. (Lond.), 207, 449 - 461. /40/

ALPERN, M., RUSHTON, W.A.H. and TORII, S. (1970d), "Signals from cones", J. Physiol. (Lond.), 207, 463 - 475. /40/

ALPERN, M. and TORII, S. (1968a), "Prereceptor colour vision distortions in protanomalous trichromacy", J. Physiol., 198, 549 - 560. /189/

ALPERN, M. and TORII, S. (1968b), "The luminosity curve of the protanomalous fovea", J. Gen. Physiol., 52, 717 - 732. /188/

ALPERN, M. and WAKE, T. (1977), "Cone pigments in human deutan colour vision defects", J. Physiol., 266, 595 - 612.

ANDREWS, D.P. and HAMMOND, P. (1970a), "Suprathreshold spectral properties of single optic tract fibres in cat, under mesopic adaptation: cone-rod interaction", J. Physiol., 209, 83 - 101. /130/

ANDREWS, D.P. and HAMMOND, P. (1970b), "Mesopic increment threshold spectral sensitivity of single optic tract fibres in the cat: cone-rod interaction", J. Physiol., 209, 65 - 82. /130/

ARDEN, G.B. and WEALE, R.A. (1934), "Nervous mechanisms and dark adaptation", J. Physiol.,(Lond.), 125, 417 - 426. /38, 72, 74, 133/

AUERBACH, E. and WALD, G. (1954), "Identification of a violet receptor in human colour vision", Science, 120, 401 - 405. /37/

BAGRASH, F.M., KERR, L.G. and THOMAS, J.P. (1971), "Patterns of spatial integration in the detection of compound visual stimuli", Vision Res., 11, 635 - 645. /39/

BARLOW, H.B. and ANDREWS, D.P., "The site at which rhodopsin bleaching raises the scotopic threshold", Vision Res., 13, 903 - 908. /131/

BARLOW, H.B., BLAKEMORE, C.B. and PETTIGREW, J.D. (1967), "The neural mechanism of binocular depth discrimination", J. Physiol. 193, 327 - 342. /32/

BARTLETT, J.R. and DOTY, R.W. (Sr.) (1974), "Response of units in striate cortex of squirrel monkeys to visual and electrical stimuli", J. Neurophysiol., 37, 621 - 641. /32/

BATTERSBY, W.S. and SHUCKMAN, H. (1970), "The time course of temporal summation", Vision Res., 10, 263 - 273. /177/

BATTERSBY, W.S. and WAGMAN, I.H. (1962), "Neural limitations of visual excitability. IV: spatial determinants of retrochiasmal interaction", Am. J. Physiol., 203 (2), 359 - 365. /41, 129/

BAYLOR, D.A. and FUORTES, M.G.F. (1970), "Electrical responses of single cones in the retina of the turtle", J. Physiol., 207, 77 - 92. /26/

BAYLOR, D.A., FUORTES, M.G.F. and O'BRYAN, P.M. (1971), "Receptive fields of cones in the retina of the turtle", J. Physiol., 214, 265 - 294. /26/

BEER, A. (1852), "Bestimmung der Absorption des rothen Lichts in farbigen Flüssigkeiten", Ann. Phys. Chem., 86, 78. /220/

BLAKEMORE, C. and CAMPBELL, F.W. (1968), "Adaptation to spatial stimuli", J. Physiol. 200, 11 - 13. /41, 134, chapter 6/

BLAKEMORE, C. and CAMPBELL, F.W. (1969), "On the existence of neurons in the human visual system selectively sensitive to the orientation and size of retinal images", J. Physiol., 203, 257 - 260. /41, 134, chapter 6/

BLAKEMORE, C. and NACHMIAS, J. (1971), "The orientation specificity of two visual after-effects", J. Physiol., 213, 157 -174. /183/

BLASIE, J.K. and WORTHINGTON, C.R. (1969), "Planar liquid-like arrangement of photopigment molecules in frog retinal receptor disk membranes", J. Molec. Biol., 39, 417 - 439. /15/

BLASIE, J.K., WORTHINGTON, C.R. and DEWEY, M.M. (1969), "Molecular localization of frog retinal receptor photopigment by electron microscopy and low-angle x-ray diffraction", J. Molec. Biol., 39, 407 - 416. /15/

BLICK, D. and MacLEOD, D.I.A. (1974), "Rod threshold; influence of neighbouring cones", Paper presented to the Assoc. Res. Vis. Ophthal., Sarasota, Fla. /71/

BLOCH, A.M. (1885), "Expériences sur la vision", C.r. séanc. Soc. Biol. (Paris), 37, 493 - 495. /177/

BLONDEL, A.M. and REY, J. (1911), "Sur la perception des lumières brèves à la limite de leur portée", J. Phys., 1, 530 - 550. /177/

BOETTNER, E.A. (1967), Spectral transmission of the eye, University of Michigan, Contract AF41 (609) - 2966. USAF School of Aerospace Medicine. /14/

BOLES, J. (1971), "Colour and contour detection by cells representing the fovea in monkey striate cortex", Abstracts of First Annual Meeting, Society Neuroscience, Washington D.C., 127. /33/

BONIN, G.N.V., CAROL, H.W. and McCULLOCH, W.S. (1942), "The functional organisation of the occipital lobe", Biol. Symp., 7, 165 - 192. /24/

BORNSHEIN, H. (1951), "Die absolute Lichtswelle des menschlicheren Auges. Eine experimentell-varianganalytische Kritik ihrer subjektiven Bestimmungs-methoden", v. Graef. Arch. Ophthal., 151, 446 - 475. /36/

BORKOFF, A. (1964), "Localization of slow potential responses in the Necturus retina", Vision Res., 4, 627 - 635. /26/

BOWMAKER, J.K., DARTNALL, H.J.A., LYTHGOE, J.N. and MOLLON, J.D. (1977), "The visual pigment of rods and cones in the Rhesus monkey Macaca mulatta", Manuscript in preparation. /231, 237, 263, chapter 6/

BOYNTON, R.M., DAS, S.R. and GARDINER, J. (1966), "Interactions between visual mechanisms revealed by mixing conditioning fields", J. Opt. Soc. Amer., 56, 1775 - 1780. /37/

BRIDGEMAN, B. (1971), "Metacontrast and lateral inhibition", Psychol. Review, 78, 528 - 539. /131/

BRIOGEMAN, B. (1975), "Correlates of metacontrast in single cells of the cat visual system", Vision Res., 15, 91 - 100. /131/

BRINDLEY, G.S. (1953), "The effects on colour vision of adaptation to very bright lights", J. Physiol., 122, 332 - 350. /34, 37, 136, 170, 180, 190, 218, 231, 232, 234, 263/

BRINDLEY, G.S. (1954), "The summation areas of the human colour-receptive mechanisms at increment threshold", J. Physiol. 124, 400 - 408. /38/

BRINDLEY, G.S. (1955), "A photochemical reaction in the human retina", Proc. Phys. Soc., 68B, 862 - 870. /190, 233, 263/

BRINDLEY, G.S. (1957), "Two theorems in colour vision", Quant. J. exp. Psychol., 9, 101 - 104. /34/

BRINDLEY, G.S. (1970), Physiology of the retina and Visual Pathway, Monographs of the Physiol. Soc., Ed. Davson, H., Greenfield, A.D.M., Whittam, R. and Brindley, G.S. Edward Arnold (Publ.) Lond: Camelot Press. /32, 39, 113, 231, 232/

BRINDLEY, G.S., DU CROZ, J.J. and RUSHTON, W.A.H. (1966), "The flicker fusion frequency of the blue-sensitive mechanism of colour vision", J. Physiol., (Lond.), 183, 497 - 500. /38, 165/

BRINDLEY, G.S. and LEWIN, W.S. (1968), "The sensations produced by electrical stimulation of the visual cortex", J. Physiol. (Lond.), 196, 479 - 493. /20/

BROWN, K.T. and MURAKAMI, M. (1968), "Rapid effects of light and dark adaptation upon the receptive field organization of S-potentials and late receptor potentials", Vision Res., 8, 1145 - 1171. /27/

BROWN, P.K. and WALD, G. (1963), "Visual pigments in human and monkey retinas", Nature, 200, 37 - 43. /15, 16, 17, 18/

BROWN, P.K. and WALD, G. (1964), "Visual pigments in single rods and cones of the human retina", Science 144, 45 - 52. /17, 44, 217, 218, 231/

BURTON, G.J. and RUDDOCK, K.H. (1972), "A lateral light adaptation effect in human vision", Vision Res., 12, 347 - 352. /19, 189/

CAMPBELL, F.W. and KULIKOWSKI, J.J. (1966), "Orientation selectivity of the human visual system", J. Physiol., 187, 437 - 445. /183/

CAMPBELL, F.W. and RUSHTON, W.A.H. (1955), "Measurement of the scotopic pigment in the living human eye", J. Physiol., 130, 131 - 147. /178, Appendix D/

CHAN, R.Y., and NAKA, K.-I. (1976), "The amacrine cell", Vision Res., 16, 1119 - 1129. /28/

CHOUDHURY, B.P., WHITTERIDGE, D. and WILSON, M.E. (1965), "The function of the collosal connections of the visual cortex", Quant. J. Exp. Physiol., 50, 214 - 219. /24/

CLARK, B., JOHNSON, M.L. and OREHER, R.E. (1946), "The effect of sunlight on dark adaptation", Amer. J. Ophthal., 29, 828 - 836. /36/

CLARKE, F.J.J. (1960), "Extra-foveal colour metrics", Optica Acta 7, 355 - 384. /71, 189, 204, 261, 262, chapter 6/

CLARKE, F.J.J. (1962), "Extrafoveal vision and the additivity concept", Die Farbe, 11, 19 - 28. /179/

CLARKE, F.J.J. (1963), "Further studies of extrafoveal colour metrics", Optica Acta, 10, 257 - 284. /34, 262/

COBLE, J.R. and RUSHTON, W.A.H. (1971), "Stiles-Crawford effect and the bleaching of cone pigments", J. Physiol., 217, 231 - 242. /18/

COBLENTZ, W.W. and EMERSON, W.B. (1918), Bull. Bur. Stds., 14, 167.

CONNER, J.D. and MacLEOD, O.I.A. (1977), "Rod photoreceptors detect rapid flicker", Science, 195 (4279), 698 - 699. /37/

COOPER, G.F. and ROBSON, J.G. (1969), "The yellow colour of the lens of man and other primates", J. Physiol. 203, 411 - 417. /13/

COPENHAGEN, H.R. (1975), "Time course of threshold elevation in on-off ganglion cells of Necturus retina: effects of lateral interactions", Vision Res., 15, 573 - 581. /26/

COPENHAGEN, D.R. and OWEN, W.G. (1976), "Functional characteristics of lateral interactions between rods in the retina of the snapping turtle", J. Physiol. 259, 251 - 282. /134/

CRAIK, K.J.W. and VERNON, M.D. (1941), "The nature of dark-adaptation", Brit. J. Psychol., 32, 62 - 81 /133/

CRESCITELLI, F. and DARTNALL, H.J.A. (1953), "Human visual purple", Nature (Lond.), 172, 195 - 197. /16/

DARTNALL, H.J.A. (1957), The visual pigments, London: Methuen. /35, 225/

DAS, S.R. (1964), "Foval sensitivity for a protanope in relation to Stiles' "blue" and "green" mechanisms", J. Opt. Soc. Amer. 54, 839 - 841. /45/

DE MONASTERIO, F.M. and GOURAS, P. (1975), "Functional properties of ganglion cells of the Rhesus monkey retina", J. Physiol., 251, 167 - 195. /28, 29, 31, 184/

DE MONASTERIO, F.M., GOURAS, P. and TOLHURST, D.J. (1975a), "Trichromatic colour opponency in ganglion cells of the Rhesus monkey retina", J. Physiol. 251, 197 - 216. /30/

DE MONASTERIO, F.M., GOURAS, P. and TOLHURST, D.J. (1975b), "Concealed colour opponency in ganglion cells of the Rhesus monkey retina", J. Physiol. 251, 217 - 229. /28/

DE VALOIS, R.L. (1965), "Behavioural and electrophysiological studies of primate vision", In Contributions to sensory physiology, Vol. 1 , ed. Neff, W.D., pp 137 - 178. New York: Academic Press. /30/

DE VALOIS, K.K. (1973), "Black and White: equal but separate", Proceedings of the Spring Meeting of the Association for Research in Vision and Ophthalmology, at Sarasota, Florida, p. 61. /42/

DE VALOIS, K.K. (1977), "Independence of black and white: phase-specific adaptation", Vision Res., 17, 209 - 215. /42/

DE VRIES, H., SPOOR, A. and JEILOF, R. (1953), "Properties of the eye with respect to polarized light", Physica, 19, 419. /15/

DOW, B.M. (1974), "Functional classes of cells and their laminar distribution in monkey visual cortex", J. Neurophysiol., 37, 927 - 946. /33/

DOW, B.M. and GOURAS, P. (1973), "Colour and spatial specificity of single units in Rhesus monkey foveal striate cortex", J. Neurophysiol., 36, 79 - 100. /33/

DOWLING, J.E. (1963), "Neural and photochemical mechanisms of visual adaptation in the rat", J. gen.Physiol. 46, 1287 - 1301. /134/

DOWLING, J.E. (1965), "Foveal receptors of the monkey retina: fine structure", Science 147, 57 - 59. /231/

DOWLING, J.E. and WERBLIN, F.S. (1969), "Organization of retina of the mudpuppy, Necturus maculosus. I. Synaptic structure", J. Neurophysiol., 32, 315 - 338. /21/

DREHER, B., FUKADA, Y. and RODIECK, R.W. (1976), "Identification, classification and anatomical segregation of cells with x-like and y-like properties in the lateral geniculate nucleus of old-world primates", J. Physiol., 258, 433 - 452. /31/

DUNN, R.F. (1969), "The dimensions of rod outer segments related to light absorption in the gecko retina", Vision Res. 9, 603 - 609. /231, 263, chapter 6/

DZN, DE LANGE H. (1954), "Relationship between critical flicker-frequency and a set of low-frequency characteristics of the eye", J. Opt. Soc. Amer., 44, 380 - 389. /126/

DZN, DE LANGE H. (1958), "Research into the dynamic behaviour of the human fovea → Cortex systems with intermittent and modulated light. I. Attenuation characteristics with white and coloured light", J. Opt. Soc. Amer., 48, 777 - 784. /126/

ENOCH, J.M. (1963), "Optical properties of the retinal receptors", J. Opt. Soc. Amer., 53, 71 - 85. /18/

ENOCH, J.M. and STILES, W.S. (1961), "The colour change of monchromatic light with retinal angle of incidence", Optica Acta, 8, 329 - 358. /19, 190, 231, 263/

ENROTH-CUGELL, C., HERTZ, B.G. and LENNIE, P. (1977), "Convergence of rod and cone signals in the cat's retina", J. Physiol. 269, 297 - 318. /130/

ESTÉVEZ, O. and CAVONIUS, C.R. (1977), "Human color perception and Stiles' π mechanisms", Vision Res., 17, 417 - 422. /218/

ESTÉVEZ, O., SPEKREIJSE, H., VAN DEN BERG, T.J.T.P. and CAVONIUS, C.R. (1975), "The spectral sensitivities of isolated human colour mechanisms determined from contrast evoked potential measurements", Vision Res., 15, 1205 - 1212. /33/

FAIN, G.L. (1975), "Interactions of rod and cone signals in the mudpuppy retina", J. Physiol., 252, 735 - 769. /131/

FICK, A. (1879), "Die Lehre von der lichtempfindung", In Handbuch der Physiologie, 3, ed. Hermann, L., pp 139 - 234. Leipzig: Vogel. /189/

FINLAY, B.F., SCHILLER, P.H. and VOLMAN, S.F. (1976), "Quantitative studies of single-cell properties in monkey striate cortex. IV. Cortical cells", J. Neurophysiol. 39, 1352 - 1361. /24/

FIORENTINI, A. and MAZZANTINI, L. (1966), "Neural inhibition in the human fovea: a study of interactions between two live stimuli", Atti. Ford. Georgio Ronchi, 21, 738 - 47. /38/

FLAMANT, FRANCOISE and STILES, W.S. (1948), "The directional and spectral sensitivities of the retinal rods to adapting fields of different wavelengths", J. Physiol. 107, 187 - 202. /18/

FOSTER, D.H., (1968), "The perception of moving, spatially periodic, intensity distributions", Optica Acta, 15, 625 - 626. /95/

FOSTER, D.H. (1976), "Rod-cone interactions in the after-flash effect", Vision Res., 16, 393 - 396. /40, 130, chapter 6/

FOSTER, D.H. and MASON, R.J. (1977), "Interaction between rod and cone systems in dichoptic visual masking", Neuroscience Lett., 4, 39 - 42. /40, 129, chapter 6/

FRUMKES, T.E., SEKULER, M.D., BARRIS, M.C., REISS, E.H. and CHAPULA, L.M. (1973), "Rod-cone interaction in human scotopic vision - 1. Temporal analysis", Vision Res. 13, 1269 - 1282.

FRUMKES, T.E. and TEMME, L.A. (1977), "Rod-cone interaction in human scotopic vision - II. Cones influence rod increment thresholds", Vision Res., 17, 673 - 679. /71/

FRY, G.A. and ALPERN, M. (1953), "The effect of a peripheral glare source upon the apparent brightness of an object", J. Opt. Soc. Amer., 43, 189 - 195. /Appendix C)

GESCHWIND, N. (1965a), "Disconnexion syndromes in animals and man, Part I", Brain, 88 (2), 237 - 294. /20/

GESCHWIND, N. (1965b), "Disconnexion syndromes in animals and man, Part II", Brain, 88 (3), 585 - 644. /20/

GIBSON, K.S. and TYNDALL, E.P.T. (1923), "Visibility of radiant energy", Bull. Bureau of Standards, 19, 131. /197/

GILBERT, C.D. and KELLY, J.P. (1975), "The projection of cells in different layers of the cat's visual cortex", J. Comp. Neurol., 163, 81 - 106. /24/

GILBERT, M. (1950), "Colour perception in parafoveal vision", Proc. Phys. Soc. (London), 63, 83 - 89. /34/

GILINSKY, A.S. (1968), "Orientation-specific effects of patterns of adapting light on visual acuity", J. Opt. Soc. Amer., 58, 13 - 18. /41, 136, chapter 6)/

GLEES, P. (1961), "Terminal degradation and trans-synaptic atrophy in the lateral geniculate body of the monkey", In The Visual System, Ed, Jung and Kornhuber, Berlin: Springer. 104 - 110. /23/

GOLDBERG, M.E. and WURTZ, R.H. (1972), "Activity of superior colliculus in behaving monkey. I. Visual receptive fields of single neurons", J. Neurophysiol., 35, 542 - 559. /31/

GOSE, E.E. (1969), "Introduction to biological and mechanical pattern recognition", In Methodologies of Pattern Recognition, Ed. Watanabe, S. Academic Press, N.Y., 203 - 273. /22/

GOSLINE, C.J., MacLEOD, D.I.A. and RUSHTON, W.A.H. (1976), "The dark adaptation curve of rods measured by their after-image", J. Physiol., 259, 491 - 499. /36, 131/

GOURAS, P. (1967), "The effects of light-adaptation on rod and cone receptive field organization of monkey ganglion cells", J. Physiol., 192, 747 - 760. /30/

GOURAS, P. (1968), "Identification of cone mechanisms in monkey ganglion cells", J. Physiol., 199, 533 - 547. /28, 30/

GOURAS, P., (1969), "Antidromic responses of ortodromically identified ganglion cells", J. Physiol. 204, 407 - 419. /28/

GOURAS, P. (1972), "Colour opponency from fovea to striate cortex", Invest. Ophthal., 11, 427 - 457. /33/

GOURAS, P. (1974), "Opponent-colour cells in different layers of foveal striate cortex", J. Physiol., 238, 583 - 602. /33/

GOURAS, P. and LINK, Krista (1966), "Rod and cone interaction in dark-adapted monkey ganglion cells", J. Physiol. 184, 499 - 510. /30, 130/

GOURAS, P. and PADMOS, P. (1974), "Identification of cone mechanisms in graded potentials of foveal striate cortex", J. Physiol., 238, 569 - 581. /33/

GRABOWSKI, S.R., PINTO, L.H. and PAK, W.L. (1972), "Adaptation in retinal rods of axolotl: intracellular recording", Science, N.Y., 176, 1240 - 1243. /134/

GREEN, D.G. (1968), "The contrast senstivity of the colour mechanisms of the human eye", J. Physiol. 196, 415 - 429. /38/

GREEN, D.G. (1970), "Regional variations in the visual acuity for interference fringes on the retina", J. Physiol., 207, 351 - 356. /38/

GROWNEY, R. (1976), "The function of contour in metacontrast", Vision Res. 16, 253 - 261. /41, 129/

GRÜSSER, O.-J. (1960), "Receptorabhänige Potentiale der Katzenretina und ihre Reaktionen auf Flimmerlicht", Pflügers Arch. Ges. Physiol. 271, 511 - 525. /26/

GUILD, J. (1931), "The colorimetric properties of the spectrum", Phil. Trans., 230 A, 149 - 187. /34/

HAMMOND, P. (1971), "Chromatic sensitivity and spatial organization of cat visual cortical cells: cone-rod interaction", J. Physiol., 213, 475 -494. /130/

HAMMDND, P. (1972), "Chromatic sensitivity and spatial organization of LGN neurone receptive fields in cat: cone-rod interaction", J. Physiol., 225, 391 - 413. /130/

HARDY, A.C. and YOUNG, F.M. (1948), "In defence of Beer's law", J. Opt. Soc. Am., 38, 854. /220/

HARTRIDGE, H. (1947), "The visual perception of fine detail", Phil. Trans., 232, 516 - 617. /18/

HECHT, S., HAIG, C. and CHASE, A.M., (1937), "The influence of light-adaptation on subsequent dark-adaptation of the eye", J. Gen. Physiol., 20, 831. /84, 133/

HECHT, S., HENDLEY, C.D., ROSS, S. and RICHMOND, P.N. (1948), "The effect of exposure to sunlight to night vision", Amer. J. Ophthal., 31, 1573 - 1580. /36/

HOLMES, G. (1918), "Disturbances of vision by cerebral lesions", Brit. J. Ophthal., 2, 353 - 384. /20/

HUBEL, D.H. and WIESEL, T.N. (1960), "Receptive fields of optic nerve fibres in the spider monkey", J. Physiol., 154, 572 - 580. /28, 30/

HUBEL, D.H. and WIESEL, T.N. (1962), "Receptive fields, binocular interaction and functional architecture in the cat's visual cortex", J. Physiol., 160, 105 - 54. /24, 32/

HUBEL, D.H. and T.N. WIESEL (1965), "Receptive fields and functional architecture in two non-striate areas (18 and 19) of the cat", J. Neurophysiol., 30, 1561 - 1573. /24, 32/

HUBEL, D.H. and WIESEL, T.N. (1968), "Receptive fields and functional architecture of monkey striate cortex", J. Physiol., 195, 215 - 243. /24, 31, 32, 33, 132, 183, chapter 6/

HUBEL, D.H. and WIESEL, T.N. (1969), "Anatomical demonstration of columns in the monkey striate cortex", Nature, 221, 747 - 750. /20/

HUBEL, D.H. and WIESEL, T.N. (1970), "Cells sensitive to binocular depth in area 18 of the macaque monkey cortex", Nature (Lond.), 225, 41 - 42. /32/

HUNT, R.W.G., (1952), The reproduction of colour, Fountain Press, England. /189, 204, 261, 262, chapter 6/

HURVICH, L.M. (1972), "Colour vision deficiencies", In Handbook of Sensory Physiology, Vol. VII/4, ed. Jameson D. & Hurvich, L.M., p. 607, Berlin, Heidelberg, New York: Springer. /189/

HURVICH, L.M. and JAMESDN, D. (1974), "Evaluation of single pigment shifts in anomalous color vision", Colour Vision Deficiencies II. Int. Symp., Edinburgh, 1973. Mod. Probl. Dphthal., 13, 200 - 209 (Karger, Basel, 1974). /188/

HURVICH, L.M. and JAMESDN, D. (1956), "Theoretical analysis of anomalous trichromatic color vision", J. Dpt. Soc. Amer., 46, 1075 - 1089. /187/

INGLING, C.R. (1969), "A tetrachromatic hypothesis for human colour vision", Vision Res., 9, 1131 - 1148. /231/

INGLING, C.R. Jr. and DRUM, B.A. (1973), "How neural adaptation changes chromaticity co-ordinates", J. Dpt. Soc. Amer., 63, 369 - 373. /189/

INGLING, C.R. Jr., LEWIS, A.L., LDDSE, D.R. and MYERS, K.J. (1977 , "Cones change rod sensitivity", Vision Res., 17, 555 - 563. /71/

JONES, E.G. and PDWELL, T.P.S. (1970), "An anatomical study of converging sensory pathways within the cerebral cortex of the monkey", Brain, 93, 793 - 820. /24/

JONES, R.M. and TULUNAY-KEESEY, V. (1975), "Local retinal adaptation and spatial frequency channels", Vision Res., 15, 1239 - 1244. /137/

KAHNEMANN, D. (1968), "Method, findings, and theory in studies of visual masking", Psychol. Bull., 70, 404 - 425. /40, 131/

KANEKO, A. (1970, "Physiological and morphological identification of horizontal, bipolar and amacrine cells in goldfish retina", J. Physiol., 207, 623 - 633. /26, 27/

KELLY, J.P. and VAN ESSEN, D.C. (1974), "Cell structure and function in the visual cortex of the cat", J. Physiol., (Lond.), 238, 515 - 547. /32/

KOLB, H. (1970), "Organization of the outer plexiform layer of the primate retina: electron microscopy of Golgi-impregnated neurons", Phil. Trans. R. Soc. B , 258, 261 - 283. /21, 27/

KOLERS, P.A. and ROSNER, B. (1960), "On visual masking (metacontrast): Dichoptic observation", Amer. J. Psychol., 73, 2 - 21. /41, 129/

KÖNIG, A. (1894), "Über den menschlichen Sehpurpur und seine Bedeutung für das Sehen", S.B. Akad. Wiss. Berlin, 577 - 598. /19/

KÖNIG, A. and DIETERICI, C. (1886), "Die Grundempfindungen und ihre Intensitäts — Vertheilung im Spectrum", S.B. Akad. Wiss. Berlin, 805 - 829. /34/

KRAUSKOPF, J. and MOLLEN, J.D. (1971), "The independence of the temporal integration properties of individual chromatic mechanisms in the human eye", J. Physiol., 219, 611 - 623. /38, 124/

LAMB, T.D., (1976), "Spatial properties of horizontal cell responses in the turtle retina", J. Physiol., 263, 239 - 255. /27, 134/

LATCH, M. and LENNIE, P. (1977), "Rod-cone interaction in light adaptation", J. Physiol., 269, 517 - 534. /71/

LEBER, T. (1873), "Uber die Theorie der Farbenblindheit und ueber die Art und Wiese, der untersuchung von Farbenblinen entnommene einwaerde gegen die Young-Helmholtz theorie sich mit derselben verlingen lassen", Klin, Mbl. Augenheilk., 11, 467 - 473. /189/

LEE, R.H., FINCH, E.M. and POUNDS, G.A. (1945), "Periodic fluctuations in the dark adapted threshold", Amer. J. Physiol., 143, 6 - 10. /36/

LEFTON, L.A. (1973), "Metacontrast: A review", Perception & Psychophys. 13, 161 - 171. /40/

LE GRAND, Y. (1968), Light, Colour and Vision, 2nd edn., pp. 488. London: Chapman and Hall Ltd. /189/

LE GRAND, Y. (1969), "Photopigments des cônes humains", Documenta. Ophthal., 26, 257 - 263. /189/

LE GRAND, Y. (1972), "About the photopigments of colour vision", Mod. Probl. Ophthal. 11, 186 - 192. /189/

LE GROS GLARK, W.E. (1959), "The anatomy of cortical vision", Trans. Opthal. Soc. U.K., 79, 455 - 461. /20, 23/

LE GROS CLARK, W.E. and PENMAN, G.G. (1934), "The projection of the retina in the laternal geniculate body", Proc. Roy. Soc., 114 B, 291 - 313. /23/

LENNIE, P., HERTZ, B.G. and ENROTH-CUGELL, C. (1976), "Saturation of rod pools in cat", Vision Res., 16, 935 - 940. /134/

LENNIE, P. and MacLEOD, D.I.A. (1973), "Background configurations and rod threshold", J. Physiol., (Lond.), 233, 143 - 156. /39, 71/

LEVAY, S., HUBEL, D.H. and WIESEL, T.N. (1975), "The pattern of ocular dominance columns in macaque visual cortex revealed by a reduced silver stain", J. Comp. Neurol., 159, 559 - 576. /24/

LEIBMAN, P.A. (1969), "Microspectrophotometry of retinal cells", Annals. New York. Acad. Sci., 157, 250 - 264. /231, 263, chapter 6/

LEIBMAN, P.A. (1972), "Microspectrophotometry (MSP) of photoreceptors", In Handbook of Sensory Physiology, ed. Dartnall, H.J.A. Berlin: Springer-Verlag. /17/

MacLEOD, D.I.A. (1972), "Rods cancel cones in flicker", Nature, Lond., 235, 173 - 174. /71/

MacLEOD, D.I.A. and HAYHOE, M. (1974), "Three pigments in normal and anomalous colour vision", J. Opt. Soc. Amer., 64, 92 - 99. /189/

McCANN, J.J. (1972), "Rod-cone interactions: different colour sensations from identical stimuli", Science, 176, 1255 - 1257. /71/

McCANN, J.J. And BENTON, J.L. (1969), "Interaction of the long-wavelength cones and rods to produce colour sensations", J. Opt. Soc. Amer., 59, 103 - 107, /71/

McCREE, K.J. (1960), "Small-field tritanopia and the effect of voluntary fixation", Optica Acta, 7, 317 - 323. /19/

McCULLOCH, W.S. (1965), Embodiments of Mind, M.I.T. Press, 67 - 71. /20/

McKEE, Suzanne P. and WESTHEIMER, G. (1970), "Specificity of cone mechanisms in lateral interaction", J. Physiol., 206, 117 - 128. /39/

McKEON, W.M. and WRIGHT, W.D. (1940), "The characteristics of protanomalous vision", Proc. Phys. Soc., 52, 464 - 479. /187, 198, 199, 250, 266/

MAKOUS, W. and BOOTHE, R. (1974), "Cones block signals from rods", Vision Res., 14, 285 - 293. /71, 85/

MARC, R.E. and SPERLING, H.J. (1977), "Chromatic organization of primate cones", Science, 196, 454 - 456. /219/

MARKS, W.B. (1965), "Visual pigments of single gold-fish cones", J. Physiol., 178, 14 - 32. /26/

MARKS, W.B., DOBELLE, W.H. and MacNICHOL, E.F. Jr. (1964), "Visual pigments of single primate cones", Science, 143, 1181 - 1183. /17, 44, 217, 218, 231/

MARROCCO, R.T. (1972), "Responses of monkey optic tract fibres to monochromatic lights", Vision Res., 12, 1167 - 1174. /28/

MARROCCO, R.T., (1976), "Sustained and transient cells in the monkey lateral geniculate nucleus: Conduction velocities and response properties", J. Neurophysiol., 39, 340 - 353. /31/

MAUDARBOCUS, A.Y. (1973), Response characteristics of the human visual system in the detection of spatially periodic stimuli , PhD thesis, University of London. /71/

MAUDARBOCUS, A.Y. and RUDDOCK, K.H. (1973a), "The influence of wavelength on visual adaptation to spatially periodic stimuli", Vision Res., 13, 993 - 998. /42, 183, chapter 6/

MAUDARBOCUS, A.Y. and RUDDOCK, K.H. (1973b), "Non-linearity of visual signals in relation to shape-sensitive adaptation responses", Vision Res. 13, 1713 - 1737. /182, 183, chapter 6/

MAUDARBOCUS, A.Y. and RUDDOCK, K.H. (1974), "Comments on "Adaptation to pairs of coloured gratings: inhibition between colour-specific spatial detectors in the human visual system?" by C.R. Sharpe", Vision Res., 14, 1485 - 1487. /42, 183, 185, 186, chapter 6/

MAY, J.G. (1972), "Chromatic adaptation of orientation and size-specific visual processes in man", Vision Res., 12, 1509 - 1517. /42, 184/

MILLER, S.S. (1972), "Psychophysical estimates of visual pigment densities in red-green dichromats", J. Physiol., 223, 89 - 107. /231, 263/

MINKOWSKI, M. (1920), "Über den Verlaug, die Endigung und die zentrale Repräsentation von gekreutzen und ungekreutzen Sehnerverfassern bie einigen Säugetieren und beim Menschen", Schweiz. Arch. Neurol. Psychiatr., 6, 201 - 252. /23/

MITCHELL, D.E. and RUSHTON, W.A.H. (1971a), "Visual pigments in dichromats", Vision Res., 11, 1033 - 1044. /44, 218/

MITCHELL, D.E. and RUSHTON, W.A.H. (1971b), "The red-green pigments of normal vision", Vision Res., 11, 1045 - 56. /44, 45, 188, 189/

MOHLER, C.W. and WURTZ, R.H. (1976), "Organization of monkey superior colliculus: Intermediate layer cells discharging before eye movements", J. Neurophysiol., 39, 722 - 744. /24/

MOHLER, C.W. and WURTZ, R.H. (1977), "Role of striate cortex and superior colliculus of saccadic eye movements in monkeys", J. Neurophysiol., 40, 74 - 94. /24/

MOLLON, J.O. and KRAUSKOPF, J., "Reaction time as a measure of the temporal response properties of individual colour mechanisms", Vision Res., 13, 27 - 40. /38/

MORELAND, J.O. and CRUZ, A. (1959), "Colour perception and the peripheral retina", Optica Acta, 6 (2), 117 - 151. /34/

MOTE, F.A., RIOPELLE, A.J. and MEYER, O.R. (1950), "The effect of intermittent preadapting light upon subsequent dark adaptation in the human eye", J. Opt. Soc. Am., 40, 584 - 588. /179/

NAKA, K.-I. (1977), "Functional organization of catfish retina", J. Neurophysiol., 40, 26 - 43. /27, 28/

NAKA, K.-I. and RUSHTON, W.A.H. (1966a), "S-potentials from colour units in the retina of fish (cyprinidae)", J. Physiol., 185, 536 - 555. /27/

NAKA, K.-I. and RUSHTON, W.A.H. (1966b), "An attempt to analyse colour reception by electrophysiology", J. Physiol., 185, 556 - 586. /27/

NAKA, K.-I. and RUSHTON, W.A.H. (1967), "The generation and spread of S-potentials in fish (cyprinidae)", J. Physiol., 192, 437 - 461. /27, 134/

NAYLOR, E.J. and STANWORTH, A. (1954), "Retinal pigment and the Haidinger effect", J. Physiol., (Lond.), 124, 543. /15/

NELSON, J.H. (1938), "Anomalous trichromatism and its relation to normal trichromatism", Proc. Phys. Soc. (Lond.), 50, 661. /43, 187, 266/

NELSON, R. (1977), "Cat cones have rod input: A comparison of the receptor properties of cones and horizontal cell bodies in the retina of the cat", J. Comp. Neurol., 172, 109 - 136. /131/

NELSON, R., KÖLB, H., FAMIGLIETTI. E.V. Jr. and GOURAS, P. (1976), "Neural responses in the rod and cone systems of the cat retina: intracellular records and procion stains", Invest. Ophthal., 15, 946 - 953. /131/

NELSON, R., LÜTZOW, A.V., KÖLB, H. and GOURAS, P., (1975), "Horizontal cells in cat retina with independent dendritic systems", Science, 189, 137 - 139. /27, 131/

NIEMEYER, G. and GOURAS, P. (1973), "Rod and cone signals in S-potentials of the isolated perfused cat eye", Vision Res., 13, 1603 - 1612. /27, 131/

NIKARA, T., BISHOP, P.O. and PETTIGREW, J.O. (1968), "Analysis of retinal correspondence by studying receptive fields of binocular single units in cat striate cortex", Expl. Brain Res., 6, 353 - 372. /32/

NILSSON, T.H. (1972), "Effects of pulse duration and pulse rate on hue of monochromatic stimuli", Vision Res., 12, 1907 - 1922. /177/

NILSSON, T.H. and NELSON, T.M. (1971), "Hue shifts produced by intermittent stimulation", Vision Res., 11, 697 - 712. /177/

NUNN, B.J. (1977), "Influence of spatial structure of adaptation fields on parafoveal colour matches", Color research and application, 2, 171 - 177. /137/

OGOEN, T.E. and MILLER, R.F. (1966), "Studies of the optic nerve of the Rhesus monkey: nerve fibre spectrum and physiological properties", Vision Res., 6, 485 - 506. /22, 30/

ORLOV, O.Y. and MAKSIMOVA, E.M. (1965), "S-potential sources as excitation pools", Vision Res., 5, 573 - 582. /27/

ØSTERBERG, G. (1935), "Topography of the layer of rods and cones in the human retina", Acta Ophthal., suppl. 6, 1 - 103. /19/

PADMOS, P. and NORREN, D.V. (1973), "Increment spectral sensitivity and colour discrimination in the primate, studied by means of graded potentials from the striate cortex", Vision Res., 15, 1103 - 1113. /31, 33/

PANTLE, A. and SEKULER, R. (1968), "Size detection mechanisms in human vision", Science, N.Y., 162, 1146 - 1148. /41,136, chapter 6/

PENMAN, G.C. (1934), "The representation of the areas of the retina in the lateral geniculate body", Trans. Dphthal. Soc. U.K., 54, 232 - 270. /20/

PIANTANIDA, T.P. and SPERLING, H.G. (1973a), "Isolation of a third chromatic mechanism in the protanomalous observer", Vision Res., 13, 2033 - 2047. /188/

PIANTANIDA, T.P. and SPERLING, H.G. (1973b), "Isolation of a third chromatic mechanism in the deuteranomalous observer", Vision Res., 13, 2049 - 2058. /188/

PIRENNE, M.H. (1962), "Directional sensitivity of the rods and cones", In The Eye, Vol. 2, ed. Davson, H., pp. 31 - 63. New York: Academic Press. /18/

PIRENNE, M.H. (1967), Vision and the eye, Lond.: Chapman and Hall. /19/

PITT, F.H.G. (1935), "Characteristics of dichromat vision with an appendix on anomalous trichromatic vision", Med. Res. Council Special Report, No. 200, 5 - 58. /37/

PITT, F.H.G. (1944), "The nature of trichromatic and dichromatic vision", Proc. Roy. Soc. B,(Lond), 132, 101 - 117. /214, 215, 218, 228, 232, 233, 234, 236, 248, 257, 265, 267, chapter 6/

POGGIO, G.B., BAKER, F.H., LAMARRE, Y. and SANSEVERINO, E.R. (1969), "Afferent inhibition at input to visual cortex of the cat", J. Neurophysiol., 32, 916 - 929. /131/

POKORNY, J. and SMITH, V.C. (1977), "Evaluation of single pigment shift model of anomalous trichromacy", J. Opt. Soc. Amer., 67, 1196 - 1209. /188/

POKORNY, J., SMITH, V.C. and KATZ, I. (1973), "Derivation of the photopigment absorption spectra in anomalous trichromats", J. Opt. Soc. Amer., 63, 232 - 237. /188/

POKORNY, J., SMITH, V.C. and STARR, S.J. (1976), "Variability of colour mixture data. II. The effect of viewing field size on the unit co-ordinates", Vision Res., 16, 1095 - 1098. /190, chapter 6/

POLYAK, S.L. (1941), The retina, Chicago: Univ. Chicago Press. /14, 231/

POTTS, A.M., HODGES, D., SHELMAN, C.B., FRITZ, K.J., LEVY, N.S. and MANGNALL, Y. (1972a), Invest. Ophthal., 11, 980 - 988: (1972b), Invest. Ophthal., 11, 989 - 1002. /22/

PUGH, E.N. Jr. (1976), "The nature of the π_1 colour mechanism of W.S. Stiles", J. Physiol., 257, 713 - 747. /37/

RAVIOLA, E. and GIULA, N.B. (1973), "Gap junctions between photoreceptor cells in the vertebrate retina", Proc. Natn. Acad. Sci., U.S.A., 70, 1677 - 1681. /131/

REGAN, D. (1975), "Recent advances in electrical recording from the human brain", Nature, 253, 401 - 407. /33/

RIPPS, H., and WEALE, R.A. (1964), "On seeing red", J. Opt. Soc. Amer., 54, 272 - 273. /18, 19/

RIPPS, H. and WEALE, R.A. (1965), "Directional properties of cone pigments", J. Opt. Soc. Amer., 55, 205 - 206. /18, 19/

RODIECK, R.W. (1973), The Vertebrate Retina. W.H. Freeman & Co: San Francisco. /18, 26, 37, 218/

RODIECK, R.W. and RUSHTON, W.A.H. (1976a), "Isolation of rod and cone contributions to cat ganglion cells by a method of light exchange", J. Physiol., 254, 759 - 773. /30, 130/

RODIECK, R.W. and RUSHTON, W.A.H. (1976b), "Cancellation of rod signals by cones, and cone signals in the cat retina", J. Physiol., 254, 775 - 785. /30/

RUDDOCK, K.H. (1963), "Evidence for macular pigmentation from colour matching data", Vision Res., 3, 417 - 429. /15, 44/

RUDDOCK, K.H. (1964), The effect of age upon colour matching and colour discrimination, PhD thesis, University of London. /Appendix B/

RUDDOCK, K.H. (1971), "Parafoveal colour vision responses of four dichromats", Vision Res., 11, 143 - 156. /262/

RUDDOCK, K.H. (1975), "Visual form perception", Contemp. Phys., 16, 317 - 348. /23/

RUDDDCK, K.H. and NAGHSHINEH, S. (1974), "Mechanisms of red-green anomalous trichromacy: hypothesis and analysis", Mod. Problems Ophthal., 13, 210 - 214. /47, 188, chapter 6/

RUSHTON, W.A.H. (1956), "The difference spectrum and the photosensitivity of rhodopsin in the living eye", J. Physiol., 134, 11 - 29. /16/

RUSHTON, W.A.H. (1958a), "The cone pigments of the human fovea in colour blind and normal", In Visual problems of colour, pp. 71 - 101. National Physical Laboratory Symposium, No. 8. London: H.M. Stationery Office. /17, 268/

RUSHTDN, W.A.H. (1958b), "Kinetics of cone pigments measured objectively on the living human fovea", Ann. N.Y. Acad. Sci., 74 (Art. 2), 291 - 204. /2 - 68/

RUSHTON, W.A.H. (1963a), "A cone pigment in the protanope", J. Physiol., 168, 345 - 359. /17, 44, 231/

RUSHTON, W.A.H. (1963b), "The density of chlorolabe in the foveal cones of the protanope", J. Physiol., 168, 360 - 373. /17, 44/

RUSHTON, W.A.H. (1963c), "Cone pigment kinetics in the protanope", J. Physiol., 168, 374 - 388. /17/

RUSHTON, W.A.H. (1965a), "A foveal pigment in the deuteranope", J. Physiol., 176, 24 - 37. /16, 17, 44, 189, 231/

RUSHTON, W.A.H. (1965b), "Cone pigment kinetics in the deuteranope", J. Physiol., 176, 38 - 45. /17, 44, 231/

RUSHTON, W.A.H. (1965c), "Stray light and the measurement of mixed pigments in the retina", J. Physiol., 176, 46 - 55. /17, 231/

RUSHTON, W.A.H. (1975), "Visual pigments and colour blindness", Scient. Amer., 232, 64 - 74. /188/

RUSHTON, W.A.H. and COHEN, R.D. (1954), "Visual purple level and the course of dark-adaptation", Nature, (Lond.), 173, 301 - 302. /133/

RUSHTON, W.A.H., FULTON, A.B. and BAKER, H.D., "Dark adaptation and the rate of pigment regeneration", Vision Res., 9, 1473 - 1479. /134/

RUSHTON, W.A.H. and HENRY, G.H. (1968), "Bleaching and regeneration of cone pigments in man", Vision Res., 8, 617 - 631. /36, 178, 232, appendix D/

RUSHTON, W.A.H. and POWELL, D.S. (1971), "The dark adaptation of rods", J. Phys., 218, 101. /134/

RUSHTON, W.A.H. and POWELL, D.S. (1972), "The Rhodopsin content and the visual threshold of human rods", Vision Res., 12, 1073 - 1081. /134/

RUSHTON, W.A.H., POWELL, D.S. and WHITE, K.D. (1973a), "Anomalous pigments in the eyes of the red-green colour blind", Nature (Lond.), 243, 167 - 168. /45/

RUSHTON, W.A.H., POWELL, D.S. and WHITE, K.D. (1973b), "Pigments in anomalous trichromats", Vision Res., 13, 2017 - 2031. /45/

RUSHTON, W.A.H. and WESTHEIMER, G. (1962), "The effect upon the rod threshold of bleaching neighbouring rods", J. Physiol., 164, 318 - 329. /133/

SCHILLER, P.H. (1965), "Monoptic and dichoptic visual masking by patterns and flashes", Perceptual and Motor Skills, 1, 193 - 199. /41/

SCHILLER, P.H., FINLAY, B.L. and VOLMAN, S.F. (1976a), "Quantitative studies of single-cell properties in monkey striate cortex. I. Spatiotemporal organization of receptive fields", J. Neurophysiol., 39, 1288 - 1319. /31/

SCHILLER, P.H., FINLAY, B.L. and VOLMAN, S.F. (1976b), "Quantitative studies of single-cell properties in monkey striate cortex: II. Orientation specificity and ocular dominance", J. Neurophysiol., 39, 1320 - 1333. /31/

SCHILLER, P.H., FINLAY, B.L. and VOLMAN, S.F. (1976c), "Quantitative studies of single-cell properties in monkey striate cortex. III. Spatial frequency", J. Neurophysiol., 39, 1334 - 1351. /31/

SCHILLER, P.H. and KOERNER, F. (1971), "Discharge characteristics of single units in superior colliculus of the alert Rhesus monkey", J. Neurophysiol., 34, 920 - 936. /31/

SCHILLER, P.H., STRYKER, M., CYNADER, M. and BERMAN, N. (1974), "Response characteristics of single cells in the monkey superior colliculus following ablation or cooling of visual cortex", J. Neurophysiol., 37, 181 - 194. /24, 31/

SCHILLER, P.H. and WIENER, M. (1963), "Monoptic and dichoptic visual masking", J. exp. Psychol., 66, 386 - 393. /41/

SCHWARTZ, E.A. (1973), "Responses of single rods in the retina of the turtle", J. Physiol., 232, 503 - 514. /134/

SCHWARTZ, E.A. (1975a), "Rod-rod interaction in the retina of the turtle", J. Physiol., 246, 617 - 638. /26, 134/

SCHWARTZ, E.A. (1975b), "Cones excite rods in the retina of the turtle, J. Physiol., 246, 639 - 651. /26, 131/

SEKULER, R.W. (1965), "Spatial and temporal determinants of visual backward masking", J. Exp. Psychol., 70 (4), 401 - 406. /41, 129/

SHCHADRIN, V.E. and BOUGARD, M.M. (1971), "A new type of lateral interaction in the human visual system", Vision Res., 11, 241-249. /39/

SPALDING, J.M.K. (1952a), "Wounds of the visual pathway. I. The visual radiation", J. Neurol., 15, 99 - 107. /20/

SPALDING, J.M.K. (1952b), "Wounds of the visual pathway. II. The striate cortex", J. Neurol., 15, 169 - 183. /20/

SPERLING, H.G. and HARWERTH, R.S. (1971), "Red-green cone interactions in the increment-threshold spectral sensitivity of primates", Science, N.Y., 172, 180 - 184./33/

STABELL, U. and STABELL, B. (1973), "Chromatic rod activity at mesopic intensities", Vision Res., 13, 2255 - 2260. /71, 108, 179/

STABELL, B. and STABELL, U. (1974), "Chromatic rod-cone interaction", Vision Res., 14, 1389 - 1392. /71/

STABELL, U. and STABELL, B. (1975a), "Scotopic contrast hues triggered by rod activity", Vision Res., 15, 1115 - 1118. /71, 108/

STABELL, U. and STABELL, B. (1975b), "The effect of rod activity on colour matching functions", Vision Res., 15, 1119 - 1123. /71, 108/

STABELL, B. and STABELL, U. (1976a), "Rod and cone contributions to peripheral colour vision", Vision Res., 16, 1099 - 1104. /71/

STABELL, B. and STABELL, U. (1976b), "Effects of rod activity on color threshold", Vision Res., 16, 1105 - 1110. /71/

STABELL, U. and STABELL, B. (1977), "Wavelength discrimination of peripheral cones and its change with rod intrusion", Vision Res., 17, 423 - 426.

STEINBERG, R.H. (1969a), "Rod and cone contributions to S-potentials from the cat retina", Vision Res., 9, 1319 - 1329. /27, 131/

STEINBERG, R.H. (1969b), "Rod-cone interaction in S-potentials from the cat retina", Vision Res., 9, 1131 - 1344. /27, 131/

STEINBERG, R.H. (1969c), "The rod after-effect in S-potentials from the cat retina", Vision Res., 9, 1345 - 1355. /27, 134/

STIGLER, R. (1910), "Chronophotische Studien über den Umgebungskontrast", Arch. ges. Physiol., 134, 365 - 435. /40/

STILES, W.S. (1937), "The luminous efficiency of monochromatic rays entering the eye pupil at different points and a new colour effect", Proc. Roy. Soc., 123 B, 90 - 118. /190/

STILES, W.S. (1939), "The directional sensitivity of the retina and the spectral sensitivities of the rods and cones", Proc. Roy. Soc. B, 127, 64 - 105. /18, 37, 190/

STILES, W.S. (1946), "A modified Helmholtz line-element in brightness-colour space", Proc. Phys. Soc., 58, 41 - 65. /217, 218, 228, 229, 248, 249, 259, 265, chapter 6/

STILES, W.S. (1949), "Increment thresholds and the mechanisms of colour vision", Documenta Dphthal., 3, 138 - 165. /37, 38/

STILES, W.S. (1953), "Further studies of visual mechanisms by the two-colour threshold method", In: Colloquio sombre problemas opticos de la vision, 1, pp 65 - 103, Union Internationale de Physique pure et appliquée, Madrid. /15, 37, 121/

STILES, W.S. (1955), "The basic data of colour matching", Phys. Soc. Year Book, Physical Society, Lond., 44 - 65. /34/

STILES, W.S. (1959), "Color vision: The approach through increment-threshold sensitivity", Proc. Natl. Acad. Sci. U.S.A., 45, 100 - 114. /37, 121, 125/

STILES, W.S. (1960), "The trichromatic scheme", In Mechanisms of Colour Discrimination, ed. Galifret, Y., 187 - 195. Pergamon Press, New York, London. /231/

STILES, W.S. (1962), "The directional sensitivity of the retina", Ann. Roy. Coll. Surg., 30, 73 - 101. /18/

STILES, W.S. and BURCH, J.M. (1959), "N.P.L. Colour-matching investigation: final report", Optica Acta, 6, 1 - 26. /71/

STILES, W.S. and CRAWFORD, B.H. (1933), "The luminous efficiency of rays entering the pupil at different points", Proc. Roy. Soc. B, 112, 428 - 450. /18, 77/

STURR, J.F. and TELLER, D.Y. (1973), "Sensitization by annular surrounds: dichoptic properties", Vision Res., 13, 909 - 918. /39/

SVAETICHIN, G. and MacNICHOL, E.F.,Jr. (1958), "Retinal mechanisms for chromatic and achromatic vision", Ann. N.Y. Acad. Sci., 74, 385 - 404. /26/

SWETS, J.A. (1973), "The relative operating characteristics in psychology", Science, N.Y., 182, 990 - 1000. /36/

TALBOT, S.A. and MARSHALL, W.H. (1941), "Physiological studies on neural mechanisms of visual localization and discrimination", Amer. J. Ophthal., 24, 1255 - 1263. /20/

TELLER, D.Y. and LINDSAY, B. (1970), "Sensitization by annular surrounds: Individual differences", Vision Res., 10, 1045 - 1055. /39/

TELLER, D.Y., MATTER, C.F. and PHILLIPS, W.D. (1970), "Sensitization by annular surrounds: spatial summation properties", Vision Res., 10, 549 - 561. /39/

TELLER, D.Y., MATTER, C., PHILLIPS, W.D. and ALEXANDER, K. (1971), "Sensitization by annular surrounds: Sensitization and masking", Vision Res., 11, 1445 - 1458. /39/

TEMME, L.A. and FRUMKES, T.E. (1977), "Rod-cone interaction in human scotopic vision - III: Rods influence cone increment thresholds", Vision Res., 17, 681 - 685. /71/

TEUBER, H.-L., BATTERSBY, W.S. and BENDER, M.B. (1960), Visual field defects after penetrating missile wounds of the brain, Cambridge, Mass., Harvard University Press. /20, 22/

THOMAS, J.P., PAOILLA, G.J. and ROURKE, D.L. (1969), "Spatial interactions in identification and detection of compound visual stimuli", Vision Res., 9, 283 - 292. /39/

THOMSON, L.C. and TREZONA, P.W. (1951), "The variations of hue discrimination with change of luminance level", J. Physiol., 114, 98 - 106. /261, 266/

TIMNEY, B.N., GENTRY, T.A., SKOWBO, D. and MORANT, R.B. (1976), "Threshold elevation following adaptation to coloured gratings", Vision Res., 16, 601 - 607. /41, 184/

TOMITA, T. (1965), "Electrophysiological study of the mechanisms subserving colour coding in the fish retina", Cold Spring Harb. Symp. Quant. Biol., 30, 559 - 566. /26/

TOMITA, T., KANEKO, A, MURAKAMI, M. and PAUTLER, E.L. (1967), "Spectral response curves of single cones in the carp", Vision Res., 7, 519 - 531. /26/

TOYODA, J.-I., NOSAKI, H., and TOMITA, T. (1969), "Light-induced resistance changes in single photoreceptors of Necturus and Gekko", Vision Res., 9, 453 - 463. /26/

TRENDELENBURG, W. (1943), Der Gesichtssinn. Grundzüge der physiologischen Optik. (Berlin: Springer). /267, chapter 6/

TREZONA, P.W. (1970), "Rod participation in the "Blue" mechanism and its effect on colour matching", Vision Res., 10, 318 - 332. /71/

TURVEY, M.T. (1973), "On peripheral and central processes in vision: inferences from an information-processing analysis of masking with patterned stimuli", Psychol. Rev., 80, 1 - 52. /131/

UENO, T. (1976), "Luminance-duration relation in reaction-time to spectral stimuli", Vision Res., 16, 721 - 725 /38/

UTTAL, W.R.(1970), "On the physiological basis of masking with dotted visual noise", Perc. Psychophys., 7 (6), 321 - 327. /41, 131/

VAN DER HORST, G.J.C. and MUIS, W. (1969), "Hue shift and brightness enhancement of flickering light", Vision Res., 9, 953 - 963. /177/

VAN ESSEN, D.C. and KELLY, J.P. (1973a), "Correlation of cell shape and function in the visual cortex of the cat", Nature, (Lond.), 241, 403 - 405. /32/

VAN ESSEN, D.C. and KELLY, J.P. (1973b), "Morphological identification of simple, complex and hypercomplex cells in the visual cortex of the cat", Intracellular staining in Neurobiology, ed. Kater, S.B. and Nicholson, C., N.Y.: Springer-Verlag. /32/

VON GRÜNAU, M.W. (1976), "The "Fluttering Heart" and spatio-temporal characteristics of color processing - III. Interactions between the systems of the rods and long-wavelength cones", Vision Res., 16, 397 - 401. /71/

WAGNER, G. and BOYNTON, R.M. (1972),"Comparison of four methods of heterochromatic photometry", J. Opt. Soc. Amer., 62, 1508 - 1515. /260/

WALD, G., (1945), "Human vision and the spectrum", Science, 101, 653 - 658. /72, 84/

WALD, G. (1966), "Defective color vision and its inheritance", Proc. Nat. Acad. Sci. U.S.A., 55, 1347 - 1363./188/

WALD, G. and BROWN, P.K. (1965), "Human color vision and color blindness", Cold Spring Harb. Symp. Quant. Biol., 30, 345 - 359. /17/

WALLS, G.L., (1942), The vertebrate eye and its adaptive radiation, Cranbrook Press, Michigan. /12/

WALLS, G.L. (1953), "The lateral geniculate nucleus and visual histophysiology", Univ. Calif. Public. Physiol., 9, 1 - 100. /23/

WALLS, G.L. and MATTHEWS, R.W. (1952), New means of studying colour blindness and normal foveal color vision, University of California Press, L.A. /187, 188, 267/

WALRAVEN, P.L. (1963), On the mechanisms of colour vision, Institute for perception RVO-TNO, Soesterberg, The Netherlands. /231/

WALRAVEN, P.L. and BOUMAN, M.A. (1960), "Relation between directional sensitivity and spectral response curves in human cone vision", J. Opt. Soc. Amer., 50, 780 - 784. /190, 263/

WALTERS, J.W. (1971), "Scotopic vision at photopic levels", Vision Res., 11, 787 - 798. /71/

WASSERMAN, G.S. and KONG, K.-L. (1975), "Temporal summation in a photoreceptor: Dependence on response magnitude", Vision Res., 15, 1297 - 1299. /177/

WATKINS, R.D. (1969a), "Foveal increment thresholds in normal and deutan observers", Vision Res., 9, 1185 - 1196. /45, 122/

WATKINGS, R.D. (1969b), "Foveal increment thresholds in protan observers", Vision Res., 9, 1197 - 1204. /45/

WEALE, R.A. (1953), "Cone-Monochromatism", J. Physiol., 121, 548 - 569.

WEALE, R.A. (1961), "Notes on the photometric significance of the human crystalline lens", Vision Res., 1, 183 - 191. /18/

WEALE, R.A. (1962a), "Further studies of photo-chemical reactions in living human eyes", Vision Res., 1, 354 - 378. /16/

WEALE, R.A. (1962b), "Photo-chemical changes in the dark-adapting human retina", Vision Res., 2, 25 - 33. /16/

WEALE, R.A. (1967), "On an early stage of rhodopsin regeneration in man", Vision Res., 7, 819 - 827. /16/

WEISSTEIN, N. (1966), "Backward masking and models of perceptual processing", J. exp. Psychol., 72, 232 - 240. /131/

WEISSTEIN, N. (1968), "A Rashevsky-Landahl neural net: Simulation of metacontrast", Psychol. Rev., 75, 494 - 521. /131/

WEISSTEIN, N. (1972), "Metacontrast", In Handbook of Sensory Physiology, ed. Jameson, Dorothea, and Hurvich, Leo M. Springer-Verlag, Berlin. 1st edn., 233 - 272. /40, 131/

WERBLIN, F.S. (1970), "Response of retinal cells to moving spots: Intracellular recording in Necturus maculosus", J. Neurophysiol., 33, 342 - 350. /25, 28/

WERBLIN, F.S. (1973), "The control of sensitivity in the retina", Scientific Amer., Jan. 1973, 71 - 79. /21, 25/

WERBLIN, F.W. and DOWLING, J.E. (1969), "Organization of the retina of the mudpuppy, Necturus maculosus. II. Intracellular recording", J. Neurophysiol., 32, 339 - 355. /25, 27/

WERNER, H. (1935), "Studies on contour: I. Qualitative analyses", Amer. J. Psychol., 47, 40 - 64. /41/

WESTHEIMER, G. (1965), "Spatial interactions in the human retina during scotopic vision", J. Physiol., 181, 881 - 894. /39/

WESTHEIMER, G., (1966), "The Maxwellian View", Vision Res., 6, 669 - 682. /69, 81, 108/

WESTHEIMER, G. (1967), "Spatial interactions in human cone vision", J. Physiol., 190, 139 - 154. /39/

WESTHEIMER, G. (1970), "Rod-cone independence for sensitizing interaction in the human retina", J. Physiol., 206, 109 - 116. /39/

WESTHEIMER, G. and HAUSKA, G. (1975), "Temporal and spatial interference with vernier acuity", Vision Res., 15, 1137 - 1141. /41/

WHITE, C.W. and LORBER, C.M. (1976), "Spatial-frequency specificity in visual masking", Perc. & Psychophys., 19, 281 - 284. /41/

WHITTEN, D.N. and BROWN, K.T. (1973a), "The time course of late receptor potentials from monkey cones and rods", Vision Res., 13, 107 - 135. /131/

WHITTEN, D.N. and BROWN, K.T. (1973b), "Photopic suppression of monkeys rod-receptor potential, apparently by a cone-initiated lateral inhibition", Vision Res., 13, 1629 - 1658. /131/

WIESEL, T.N. and HUBEL, D.H. (1966), "Spatial and chromatic interactions in the lateral geniculate body of the Rhesus monkey", J. Neurophysiol., 29, 1115 - 1156. /30, 31/

WIESEL, T.N., HUBEL, D.H. and LAM, D.M.K. (1974), "Autoradiographic demonstration of ocular-dominance columns in the monkey striate cortex by means of transneuronal transport", Brain Res., 79, 273 - 279. /24/

WILLIAMS, F.C. and CLAPPER, F.R. (1975), "Multiple internal reflections in photographic colour prints", J. Opt. Soc. Amer., 43, 595 - 599. /22D/

WILLMER, E.N. (1946), Retinal structure and colour vision, Cambridge: Cambridge Univ. Press. /19/

WILLMER, E.N. and WRIGHT, W.D. (1945), "Colour sensitivity of the foveal centralis", Nature, (Lond.), 156, 119 - 121. /19/

WRIGHT, W.D. (1927 - 28), " Trichromatic Colorimeter with Spectral Primaries", Trans. Opt. Soc., 29, 225. /58/

WRIGHT, W.D. (1929), "A re-determination of the trichromatic mixture data", Med. Res. Counc. Spec. Rep., 115 B, 49 - 87. /34/

WRIGHT, W.D. (1936), "The breakdown of a colour match with high intensities of adaptation", J. Physiol., 87, 23 - 33. /34, 136, 170, 180, 190/

WRIGHT, W.D. (1946), Researches on Normal and Defective Colour Vision, London: Kimpton. /34, 35, 43, 48, 58, 67, 138, 174, 187, 192, 200, 229, 249 - 252, 259, 261, 265/

WRIGHT, W.D. (1964), "A new look at 37 years of research", Vision Res., 4, 63 - 74. /231/

WRIGHT, W.D. and NELSON, J.H. (1936), "The relation between the apparent intensity of a beam of light and the angle at which the beam strikes the retina", Proc. phys. Soc., 48, 401 - 405.

WRIGHT, W.D. and PITT, F.H.G. (1934), "Hue discrimination in normal colour-vision", Proc. phys. Soc. (Lond.), 46, 459. /249, chapter 6/

WYSZECKI, G. and STILES, W.S. (1967), Color science. Concepts and methods, quantitative data and formulas, New York: John Wiley. /121, 148, 196, 197, 199, 218, 230/

YATES, J.T. (1974), "Chromatic information processing in the foveal projection (Area striata) of unanaesthetized primate", Vision Res., 14, 163 - 173. /33/

YELLOTT, J.I. Jr and WANDELL, B.A. (1976), Colour properties of the contrast flash effect: monoptic vs dichoptic comparisons", Vision Res., 16, 1275 - 1280. /40, 131/

YOUNG, R.W. (1969), "The organization of vertebrate photoreceptor cells", In The retina: Morphology, function and clinical characteristics, ed. Straatsma, B.R., Hall, M.O., Allen, R.A. and Crescitelli, F., 177 - 210. Forum in Medical Sciences, No. 8. Berkley: Univ. Calif. Press. /16/

ZEKI, S.M. (1976), "Colour coding in the superior temporal sulcus of the Rhesus monkey", Proc. Physiol. Soc. J. Physiol., 263, 169 - 170. /24/

Acknowledgements

The work for this thesis was performed with the direct or indirect help of many people.

Dr. K.H. Ruddock suggested the projects, offered advice and encouragement at all times, provided space and equipment for the work and enabled me to attend many local and international conferences; he also pointed out many errors in grammar and fact during his diligent proofreading of the script. Thank you, Keith!

Mr. H. D'Souza, Mr. J. Last and Mr. W.H. Kitchen lent me equipment, and Mr. M. Pimm, Mr. E. Abbott and Mr. C. Cooper helped me in the construction of apparatus.

I was encouraged by friends in the Physics Department including Dr. D. Foster, Dr. G. Burton, Dr. S. Naghshineh, Dr. E. Thoms (nee Wigley), Dr. M. Djamgoz, Mr. J. Barbur, Ms. V. Waterfield, Ms. R. Phillipson, Ms. L. Harwood, and also by the many people who patiently acted as observers, including: Prof. W. Welford, Prof. M. Alpern, Dr. K.H. Ruddock, Dr. D.H. Foster, Mr. J. Barbur, Mr. M.R. Inggs, Mr. A.P. Jarvis, Mr. R. Fletcher, Dr. R. Latham, Mr. E. MacLeod, Dr. A. Gadian, Mr. A. Hughes, Dr. T. Taylor, Mrs. J. Spencer and Dr. S. Naghshineh.

I thank all these people and my parents and family, and I deeply appreciate the National Scholarship awarded by Rhodes University, South Africa, and a scholarship awarded by the Council for Scientific and Industrial Research of South Africa. Lastly, thank you, Lesley, for your patience with my handwriting and your skillful layout of this typescript!

Brian J. Nunn